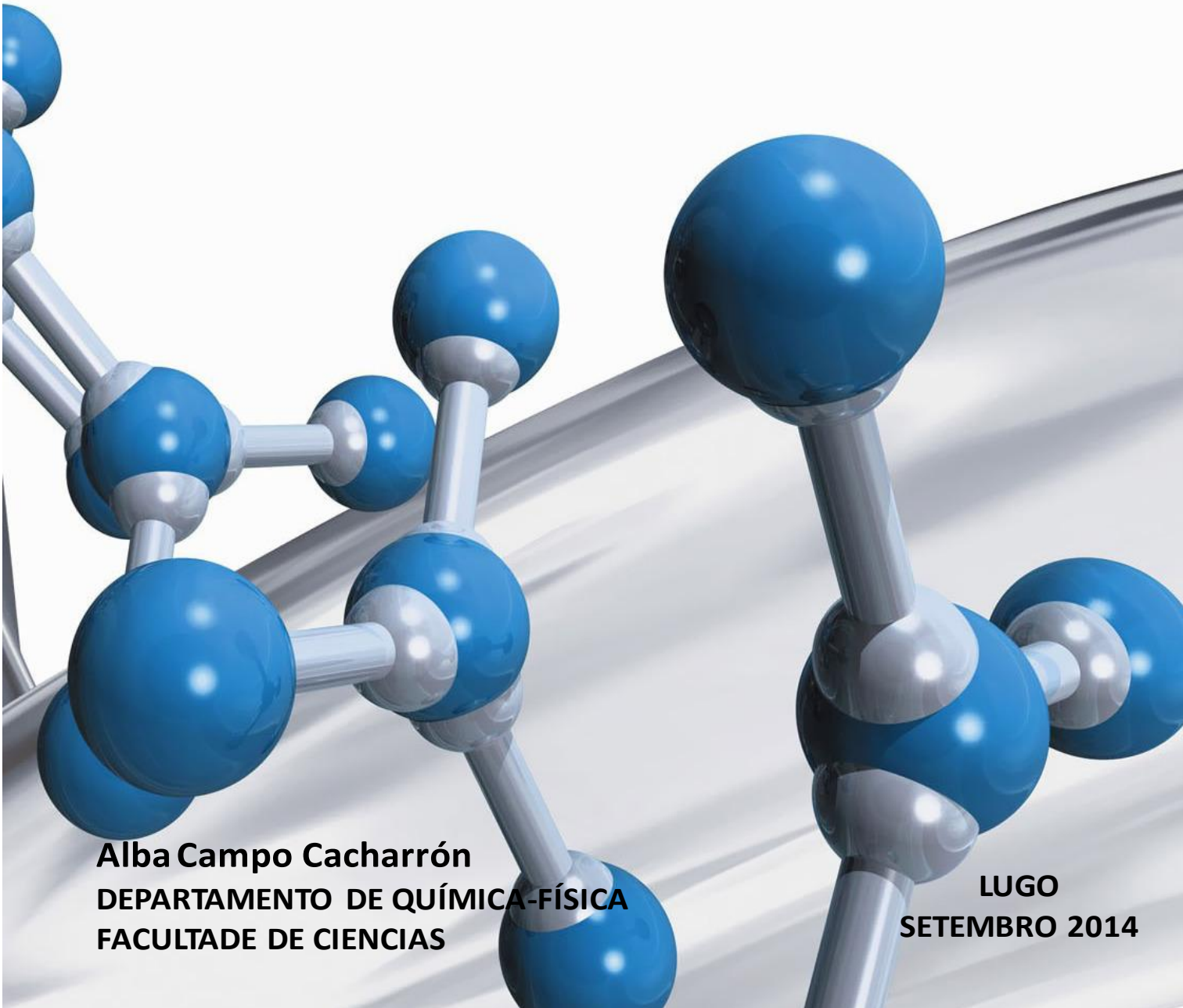
TESE DE DOUTORAMENTO

Programa Ciencia e tecnoloxía química

ON THE INTERACTION BETWEEN IONS AND COMPLEX AROMATIC SYSTEMS:

amino acid side chains, ion channels, and buckybowls



Alba Campo Cacharrón

DEPARTAMENTO DE QUÍMICA-FÍSICA

FACULTADE DE CIENCIAS

LUGO

SETEMBRO 2014

USC
UNIVERSIDADE
DE SANTIAGO
DE COMPOSTELA

TESE DE DOUTORAMENTO

Programa Ciencia e Tecnoloxía Química

On the interaction between ions and complex aromatic systems:

amino acid side chains, ion channels, and buckybowls

Alba Campo Cacharrón

Departamento de Química-Física

Facultade de Ciencias

LUGO, SETEMBRO 2014

USC
UNIVERSIDADE
DE SANTIAGO
DE COMPOSTELA

Autorización dos directores da tese

D. Enrique Manuel Cabaleiro Lago
Profesor/a do Departamento: Química-Física (Lugo)

D. Jesús Rodríguez Otero
Profesor/a do Departamento: Química-Física (CIQUS)

Como Directores da Tese de Doutoramento titulada: "*On the interactions between ions and complex aromatic systems: amino acid side chains, ion channels and buckybowls*".

Presentada por Dna. Alba Campo Cacharrón

Alumna do Programa de Doutoramento en Ciencia e Tecnoloxía Química (D1121)

Autorizan a presentación da tese indicada, considerando que reúne os requisitos esixidos no artigo 34 do regulamento de Estudos de Doutoramento, e que como Director da mesma non incurre nas causas de abstención establecidas na lei 30/1992.

Lugo a 20 Setembro de 2014

Asdo: Enrique M. Cabaleiro Lago

Asdo: Jesús Rodríguez Otero

USC
UNIVERSIDADE
DE SANTIAGO
DE COMPOSTELA

Agradecementos

Quixera facer uns breves agradecementos posto que me gustan máis as demostracións con abrazos que con palabras, e máis, se estas hai que ir buscalas a libros tan pouco apetecibles para ler como este.

En primeiro lugar aos directores de tese, Quique e Jesús. En especial a Quique, que máis que un director é un amigo. Gracias pola túa paciencia, os teus consellos e pola túa preocupación. Fas que todo pareza fácil e sinxelo e sempre poñendo un toque de humor.

A Ortigueira, porque a tese sen esos cafés e crucigramas diarios ben seguro non houbera saído adiante.

A meus pais, polo seu apoio constante, os seus ánimos e sobretodo o seu sacrificio para que eu puidera continuar e acabar esta tese aínda sen contrato. Son o meu exemplo.

A meu irmán, que aínda que non falemos tan a miúdo como deberamos sei que conto co seu apoio incondicional ante calquera das miñas decisións.

A meus tios e primos, porque son a mellor familia que un pode ter, sempre pensando en comer e en xogar o tenis.

As miñas amigas, porque sen elas non sería quen son. Tamén a Raquel, parte fundamental destos anos en Lugo estudiando, porque sei que levo unha amiga para a vida.

A Tamara e a Maritere, por ese duro pero fantástico ano traballando á vez que facía a tese. Polos nosos cotilleos ata altas horas da madrugada, polos chocolates e pola vosa preocupación pola miña vida amorosa. Gracias, porque sei que levo dúas amigas para sempre.

Por último a Miguel, que aínda que foi o último en entrar na miña vida convertiuse nun dos máis importantes, sempre alentándome a estudiar, a mellorar, a emprender, sempre co seu apoio e cariño infinito.

USC
UNIVERSIDADE
DE SANTIAGO
DE COMPOSTELA

INDEX

RESUMEN ..... **I**

1. INTRODUCTION **1**

1.1. Supramolecular Chemistry 3
1.2. Intermolecular Interactions 4
1.3. Interaction involving aromatic systems 9
1.4. Interactions with buckybowls 17
1.5. References 21

2. OBJECTIVES **25**

3. METHODOLOGY **31**

3.1. Interaction Energy 33
3.1.1. Basis Set Superposition Error *34*
3.1.2. Many-body effects *36*
3.2. Wavefunction-based Methods 37
3.2.1. The Hartree-Fock method *37*
3.2.2. Many Body Perturbation Theory (MPn) *39*
3.2.3. Coupled Cluster *41*
3.2.4. Errors in Wavefunction-based Methods *43*
3.2.4.1. Extrapolating to basis limit 45
3.2.4.2. Obtaining benchmarking values 47
3.3. Density Functional Theory Methods 49
3.3.1. Kohn-Sham procedure *50*
3.3.2. Functional types *52*
3.3.3. Dispersion-corrected DFT methods *54*
3.3.3.1. DFT-D2 55
3.3.3.2. DFT-D3 56
3.4. Reducing computational cost 57
3.5. Interaction Energy Partitioning 59
3.5.1. Energy Decomposition Analysis (EDA) Methods *59*
3.5.2. Symmetry-Adapted Perturbation Theory Methods (SAPT) *61*
3.5.2.1. SAPT(DFT) 65
3.6. Electron density analysis 66
3.6.1. NCI index *67*
3.7. Solvation effects 71
3.7.1. Continuum models *72*
3.8. References 75

4. EFFECTS OF MICROHYDRATION ON THE CHARACTERISTICS OF CATION-PHENOL COMPLEXES 81

4.1. INTRODUCTION 83
4.2. COMPUTATIONAL DETAILS 84
4.3. RESULTS 85
4.3.1. Cation···phenol complexes 87
4.3.2. Monohydrated cation···phenol complexes 89
4.3.3. Dihydrated cation···phenol complexes 90
4.3.4. Trihydrated complexes 97
4.3.5. Tetrahydrated clusters 97
4.3.6. Vibrational spectra 100
4.4. CONCLUSIONS 103
4.5. REFERENCES 104

5. INTERACTION OF AROMATIC UNITS OF AMINO ACIDS WITH GUANIDINIUM CATION. THE INTERPLAY OF Π···Π, X-H···Π AND M^+···Π CONTACTS 107

5.1. INTRODUCTION 109
5.2. METHODS 110
5.3. RESULTS 112
5.3.1. Complexes with the same aromatic molecules 112
5.3.2. Complexes with different aromatic molecules 119
5.3.3. Pair energies 126
5.3.4. LMO-EDA analysis 129
5.3.5. Non Covalent Interaction Index (NCI) 132
5.4. CONCLUSIONS 134
5.5. REFERENCES 135

6. A DFT STUDY OF THE INTERACTION BETWEEN MICROHYDRATED ANIONS AND NAPHTHALENDIIMIDES 139

6.1. INTRODUCTION 141
6.2. COMPUTATIONAL DETAILS 145
6.3. RESULTS AND DISCUSSION 146
6.3.1. Complexes with para-diphenylnaphthalendiimide 146
6.3.2. Complexes with naphthalendiimide 151
6.3.3. Microhydrated complexes with naphthalendiimide 154
6.4. CONCLUSIONS 159
6.5. REFERENCES 159

7. INTERACTION BETWEEN ANIONS AND SUBSTITUTED CORANNULENE 163

7.1. INTRODUCTION 165
7.2. COMPUTATIONAL DETAILS 167
7.3. RESULTS 170
7.3.1. Substituted Molecular Bowls 170
7.3.2. Complexes between anions and molecular bowls 173
7.3.2.1. Complexes with pentasubstituted corannulene 173
7.3.2.2. Complexes with decasubstituted corannulene 175
7.3.2.3. Energy decomposition 182
7.3.2.4. Solvent Effect 184
7.4. CONCLUSIONS 185
7.5. REFERENCES 186

8. INTERACTION BETWEEN IONS AND SUBSTITUTED BUCKYBOWLS: A COMPREHENSIVE COMPUTATIONAL STUDY 189

8.1. INTRODUCTION 191
8.2. METHODS 193
8.3. RESULTS 197
8.3.1. Molecular Electrostatic Potentials 197
8.3.2. Method Performance 197
8.3.2.1. Chloride Complexes 197
8.3.2.2. Sodium Complexes 201
8.3.3. Influence of the Bowl 201
8.3.4. SAPT(DFT) Analysis 207
8.4. CONCLUSIONS 212
8.5. REFERENCES 213

9. INTERACTION OF ANIONS WITH SUBSTITUTED BUCKYBOWLS. ANION'S NATURE AND SOLVENT EFFECTS. 217

9.1. INTRODUCTION 219
9.2. COMPUTATIONAL DETAILS 220
9.3. RESULTS 225
9.3.1. Orientation dependence 225
9.3.2. Effect of the approaching line 231
9.3.3. Anion and bowl dependence 231
9.3.4. NCI Analysis 235
9.3.5. SAPT(DFT) Energy Analysis 235
9.3.6. Solvent Effect 240
9.4. CONCLUSIONS 244
9.5. REFERENCES 245

10. CONCLUSIONS 249

APPENDICES 255

APPENDIX A 257
APPENDIX B 259
APPENDIX C 265
APPENDIX D 273

USC
UNIVERSIDADE
DE SANTIAGO
DE COMPOSTELA

Resumen

Esta tesis es el resultado de una serie de trabajos dedicados a profundizar en las características de las interacciones no covalentes, más específicamente aquellas interacciones que involucran a sistemas aromáticos y especies cargadas. Este tipo de interacciones han sido estudiadas de forma teórica utilizando medios computacionales con los que se han realizado predicciones sobre los comportamientos y las características de los complejos. A lo largo de las últimas décadas, la evolución de la investigación ha permitido determinar fehacientemente cuáles son las principales propiedades de estas interacciones, en muchas ocasiones de forma experimental, y cada vez con mayor frecuencia de forma computacional o una combinación de ambas. Sin embargo, estas investigaciones han estado centradas a menudo en los sistemas aromáticos e iones más simples. Es por este motivo que se ha decidido orientar la temática de esta tesis hacia nuevos aspectos de las interacciones ion···π enfocados hacia sistemas más complejos.

Para llevar a cabo este objetivo se han planteado varios trabajos que pueden ser agrupados en dos partes. La primera está centrada en las interacciones catión···π y en el efecto modulador que otras moléculas vecinas pueden tener sobre ellas, como puede ser el caso de las moléculas de disolvente o de otras especies aromáticas que compiten por el contacto con el catión. La segunda parte de esta tesis se centra en las interacciones anión···π, cuyo interés ha surgido en los últimos años aunque el descubrimiento de ambas interacciones se produjese de forma casi simultánea en el tiempo. En este caso las interacciones anión···π se han estudiado en sistemas que presentan contactos entre aniones y sistemas aromáticos relativamente grandes. Para ello se ha seleccionado un canal aniónico sintético mediante el cual se ha podido simular y estudiar el efecto del disolvente sobre el funcionamiento del canal en disoluciones aniónicas acuosas. Seguidamente se ha hecho un amplio estudio sobre otro tipo de sistemas aromáticos extendidos que han despertado interés en los últimos años debido a su superficie curva; los llamados buckybowls o cuencos moleculares. Estos buckybowls presentan multitud de posibilidades debido a que tienen distintas propiedades en sus caras cóncava y convexa, por lo que podrían actuar como receptores altamente selectivos. En consecuencia, se ha estudiado esta capacidad receptora para comprobar las bondades de estos materiales relativamente poco conocidos.

Todos estos trabajos se han llevado a cabo haciendo uso de la batería de métodos que ofrece la química computacional. En los últimos años, se ha propuesto toda una serie de nuevos métodos o modificaciones de los ya existentes, que permiten abordar el estudio de la interacción en sistemas de mayor complejidad ofreciendo resultados de mayor calidad. Parte de estos métodos han sido empleados en esta tesis, entre los que se podría destacar el uso de métodos basados en la teoría del funcional de la densidad (DFT) corregidos empíricamente para describir las interacciones de dispersión, nuevos

funcionales como M06-2X que proporcionan una mejor descripción de las interacciones no covalentes, o variantes de métodos clásicos como MP2, que han sido modificados empíricamente para mejorar su comportamiento. Además, en una buena parte de los trabajos realizados, se han empleado métodos que permiten desglosar la energía de interacción en una serie de contribuciones a las que se puede asignar significado físico. Es de destacar en este sentido el uso del método de perturbación adaptado en simetría SAPT(DFT) como una herramienta fundamental para poder comprender los factores que controlan la interacción. Las características de los métodos y técnicas empleados en los diferentes trabajos se exponen con mayor detalle en el **capítulo 3**, dedicado a metodología.

Las interacciones catión···π están involucradas en mecanismos de reconocimiento molecular y transporte a través de membranas, entre otros, por lo que se puede pensar que este tipo de interacción puede ser empleada como parámetro de diseño de nuevos receptores o ligandos cuya actividad estaría condicionada por este tipo de interacciones. Además, se trata de una interacción de gran relevancia en la estabilidad de las proteínas, ya que algunos aminoácidos contienen especies aromáticas en sus cadenas laterales que pueden interaccionar con cationes en las cadenas laterales de otros aminoácidos o con otros cationes presentes en el medio. En sí misma, la interacción catión···π es una interacción relativamente bien conocida y estudiada, pero no lo es tanto su comportamiento bajo factores modulantes como pueden ser otras moléculas cercanas al contacto catión··· π. Este tipo de fenómenos son considerados en los capítulos 4 y 5.

El **capítulo 4** se centra en los efectos de la microhidratación en las características de los complejos catión···fenol. Se ha estudiado el efecto que tiene la presencia de un número reducido de moléculas de agua en el entorno más próximo sobre la interacción catión··· π, representada a través de complejos formados por fenol y cuatro cationes simples como son K^+, Na^+, Li^+ y Mg^{+2}. La elección del fenol como anillo aromático surge de su característico grupo OH, que le proporciona una segunda zona adecuada para la interacción con cationes junto con la nube π y marca un aspecto diferenciador respecto a los habituales estudios con benceno. Además, el estudio de sistemas conteniendo fenol reviste interés ya que forma parte de la cadena lateral de la tirosina.

Se han obtenido las estructuras más estables mediante la optimización de las geometrías de los complejos, que se hacen crecer mediante una microhidratación paso a paso hasta incluir cuatro moléculas de agua en el complejo. En estos complejos microhidratados se estudia el efecto que el agua ejerce sobre el complejo al competir por el catión con la molécula de fenol. Se observa un delicado balance de fuerzas, asociadas a la interacción del ion con las moléculas neutras y de las moléculas neutras entre sí, que condiciona la estabilidad final de los complejos. Para Li^+ y Mg^{+2}, la interacción del agua y fenol con el catión es mucho más fuerte que la interacción entre las moléculas neutras (agua y fenol) por lo que las estructuras más estables presentan al fenol y las moléculas de agua alrededor del catión. Sin embargo, en los complejos con K^+

y en menor proporción los de Na^+, a medida que se incluyen moléculas de agua, los enlaces de hidrógeno entre agua y fenol o entre moléculas de agua pueden competir con el contacto directo con el catión, por lo que algunas moléculas pueden no contactar directamente con el catión.

Además, se ha obtenido el espectro vibracional de los complejos estudiados, incluyendo hasta cuatro moléculas de agua. Los espectros obtenidos reproducen de forma adecuada las observaciones experimentales disponibles y permiten interpretar el origen de los principales desplazamientos en la posición de las señales. Para los complejos de Li^+ y Mg^{2+} se predice un espectro bastante simple y sólo cuando la cuarta molécula de agua es incluida en el complejo aparecen señales claramente asociadas a enlaces de hidrógeno en los que participa el fenol. En el caso de los complejos con Na^+ y K^+, ya con tres moléculas de agua se aprecia participación del grupo hidroxilo del fenol en la red de enlaces de hidrógeno. Estos resultados ayudan a entender cómo una unidad de fenol interacciona con cationes y cómo la presencia de moléculas de agua cercanas puede afectar en gran medida a las características de la interacción.

Avanzando en el estudio de las interacciones catión···π, en el **capítulo 5** se ha llevado a cabo un estudio sobre la interacción de unidades aromáticas y cationes presentes en las cadenas laterales de aminoácidos. En este caso se pretende estudiar el efecto de una segunda molécula aromática en el entorno inmediato de una interacción catión···π, y cómo puede alterar sus características. Los complejos que se han utilizado para este estudio son estructuras ternarias que contienen dos anillos aromáticos iguales o distintos y un catión. Se ha elegido el catión guanidinio por ser parte de la cadena lateral de la arginina, pero también por su peculiar forma plana que en principio podría favorecer estructuras apiladas. Benceno, fenol e indol se han utilizado como especies aromáticas de tamaño creciente, para poder también determinar el efecto del tamaño del sistema aromático sobre la interacción.

Los complejos adoptan una amplia variedad de estructuras con orientaciones diversas que pueden ser clasificadas aproximadamente en tres grandes grupos: anillos en paralelo (parallel stacked), anillos orientados perpendicularmente entre sí (T-shaped) y anillos a ambos lados del catión (doubly T-shaped). Este último grupo es el que presenta los complejos más estables dado que el catión guanidinio se sitúa en una posición central contactando favorablemente con los dos anillos aromáticos. De forma general la interacción se intensifica a medida que aumenta el tamaño de las moléculas aromáticas, de forma que el guanidinio tiende a coordinar el indol para formar los trímeros más estables. En el caso de los complejos conteniendo fenol e indol, se observa la formación de enlaces de hidrógeno entre especies aromáticas en las estructuras de tipo T-shaped, que contribuyen a una mayor estabilidad de este tipo de complejos. Además, sólo en este tipo de estructuras son apreciables fenómenos cooperativos que contribuyen a una mayor estabilidad de los complejos. Las estructuras paralelas son las

menos estables, y de hecho no se han localizado en complejos con fenol debido a la tendencia de esta especie aromática a interaccionar mediante enlaces de hidrógeno.

En resumen, los trímeros están principalmente condicionados por la intensidad de los contactos catión···π, pero interacciones secundarias entre especies aromáticas puede modular su comportamiento, especialmente cuando se forman enlaces de hidrógeno en complejos con fenol e indol. A pesar de esto, el balance de las diferentes contribuciones a la energía (π···π, X-H···π y M^+···π) es muy delicado dependiendo de la naturaleza y de la orientación relativa de los fragmentos.

El segundo bloque de esta tesis está dedicado al estudio de las interacciones no covalentes donde intervienen especies aromáticas y aniones. Así como las interacciones catión···π han sido estudiadas desde hace tiempo, el campo de las interacciones entre moléculas aromáticas y aniones es de reciente desarrollo. Esto es probablemente debido a que en una primera instancia la interacción entre un anión y una molécula aromática no parece posible debido a la capacidad de donar electrones de ambas especies. Sin embargo, pronto se hizo evidente que este carácter dador podía ser modulable en las moléculas aromáticas a través de la sustitución del anillo con grupos electroatrayentes. Así, se pueden definir las interacciones anión···π como las interacciones favorables entre aniones y sistemas aromáticos deficientes en electrones.

Las interacciones anión···π han cobrado gran relevancia debido a su posible participación en importantes áreas como por ejemplo en bioquímica, ya que el ADN es un polianión y muchos cofactores y sustratos de las enzimas son aniónicos. Además, se han propuesto nuevas aplicaciones empleando este tipo de interacciones para actuar en receptores aniónicos. Por tanto, cuatro capítulos en esta tesis se corresponden con el estudio de la interacción anión···π: uno de ellos dedicado a las características de la interacción en un canal aniónico sintético y otros tres centrados en las características de las interacciones entre especies aromáticas curvas y aniones, principalmente para determinar su posible uso como receptores aniónicos.

El **capítulo 6** está dedicado al primer canal aniónico sintético basado en interacciones anión···π, que ha sido propuesto recientemente. Las posibilidades de este canal y su novedosa estructura compuesta por un motivo geométrico con anillos aromáticos deficientes en electrones repetido a lo largo del canal lo hacen perfecto para el estudio de las interacciones anión···π. Así, se han estudiado complejos formados por modelos simplificados del canal iónico interaccionando con cuatro aniones diferentes (Br^-, Cl^-, F^-, y OH^-) a los que se les han añadido hasta tres moléculas de agua de forma explícita. Los resultados obtenidos muestran que la interacción de las unidades que forman el canal con los aniones es intensa en fase gas, dando lugar a complejos muy estables. Sin embargo, la presencia de un pequeño número de moléculas de agua que pueda acompañar al ion dentro del canal altera de forma significativa las características de los complejos, especialmente los más estables, formados con los aniones más polarizantes.

Los resultados indican que el papel de las moléculas de agua más próximas al anión puede ser relevante en el funcionamiento del canal iónico, disminuyendo los costes asociados a la deshidratación del ión para entrar en el canal. Además, si algunas moléculas entran con el ion en el canal pueden contribuir a facilitar el proceso estableciendo interacciones atractivas con el propio canal iónico.

Una última sección, formada por los tres capítulos finales, está dedicada a las interacciones anión···π en las que participan los sistemas aromáticos curvos llamados buckybowls. Los buckybowls son hidrocarburos aromáticos policíclicos formados por una serie de anillos fusionados de cinco y seis miembros que dan lugar a una estructura curvada en forma de cuenco. La curvatura tiene su origen en la propia estructura de estas moléculas, ya que no es posible formar una estructura plana combinando pentágonos y hexágonos. Este tipo de especies también son denominadas fragmentos de fulerenos, ya que su esqueleto carbonado se corresponde con partes de las estructuras de los fulerenos. Los buckybowls más sencillos que se pueden proyectar sobre el fulereno C_{60} son el coranuleno $C_{20}H_{10}$ (seis anillos hexagonales rodeando un anillo pentagonal central) y el sumaneno $C_{21}H_{12}$ (tres anillos hexagonales y tres pentagonales alternos en torno a un anillo hexagonal central). En esta tesis se considerarán derivados sustituidos de ambas especies. Los buckybowls muestran diferentes propiedades dependiendo de la cara cóncava o convexa en la que tiene lugar la interacción. Tanto sumaneno como coranuleno forman complejos con cationes y metales de transición, fundamentalmente por la cara convexa del bowl. Al igual que otras especies aromáticas, podría ser posible modular las características de estos bowls mediante sustituyentes apropiados, de modo que pudieran coordinar aniones preferentemente por la cara cóncava y actuar como receptores aniónicos. Este aspecto es uno de los objetivos a tratar en la presente tesis.

En el **capítulo 7** se intenta determinar cómo la sustitución de grupos en el borde de los buckybowls afecta a sus propiedades. Concretamente, se trata de determinar si se produce la inversión del potencial electrostático molecular (MEP) de los bowls, pudiendo ser así adecuados para un contacto favorable con aniones. Además, mediante este estudio se ha comprobado qué grupos sustituyentes son los más adecuados para favorecer la interacción buckybowl···anión.

Se ha determinado el potencial electrostático del coranuleno sustituido con 5 o 10 grupos fluoruro, cloruro y nitrilo. La curvatura del coranuleno apenas sufre cambios al ser sustituido, excepto en los derivados decasustituidos con cloruro y nitrilo, en lo que se aprecia una pérdida de curvatura del bowl. Tras comprobar que se consigue la inversión del potencial electrostático (especialmente con CN), se optimizan los complejos formados por dichos buckybowls sustituidos y tres aniones diferentes, Cl^-, Br^- y BF_4^-. En dichos complejos se prueban diferentes regiones para la interacción con los aniones, comprobando así las diferencias energéticas entre complejos formados por las caras cóncava y convexa. Los contactos con el anión situado en la parte cóncava del

bowl son los más estables con energías de coordinación que siguen aproximadamente los valores obtenidos para los MEPs, siendo los más estables aquellos formados por el coranuleno sustituido completamente con 10 grupos CN y el anión cloruro por la cara cóncava. Además, se ha estimado el efecto de varios disolventes empleando modelos de continuo, que muestran importantes pérdidas de estabilidad de los complejos en disolución. Aún así, los resultados animan a seguir investigando este tipo de sistemas, ya que parecen apuntar que los buckybowls sustituidos podrían actuar como receptores de aniones.

El **capítulo 8** está más centrado en aspectos metodológicos. Se ha detectado que la interacción con buckybowls es bastante compleja de describir, y que los distintos métodos de cálculo proporcionan resultados dispares. Como no existen valores de referencia para este tipo de sistemas, en este capítulo se han realizado cálculos con una batería de métodos de diferente nivel, para poder determinar valores de referencia así como para estimar qué métodos de menor coste computacional pueden ofrecer una descripción aceptable de estos sistemas. En este estudio se han considerado complejos con aniones y cationes, para poder establecer una comparación directa de sus características usando los mismos métodos con los mismos buckybowls.

Se han considerado complejos formados por bowls parcialmente sustituidos con CH_3, F y CN basados en coranuleno y sumaneno, e iones Cl^- y Na^+. En el caso del coranuleno se han sustituido cinco átomos de hidrógeno alternos en el borde del bowl. Con sumaneno hay dos posibles sustituciones, una que afecta a los átomos de hidrógeno de los grupos CH de los anillos hexagonales, y otra en la que se sustituyen los átomos de hidrógeno de los grupos CH_2 de los anillos pentagonales. Se han obtenido las energías de interacción de los complejos a lo largo de una línea que pasa por el eje central del buckybowl variando las distancias a las que se sitúan los iones.

Los resultados obtenidos con los diferentes métodos probados muestran un grado de correspondencia variable. Comparando con los valores obtenidos con el método de referencia empleado (MP2.X) se observa que el método SCS-MP2 extrapolado a base completa es el que mejores resultados ofrece a un coste de cálculo razonable, aunque otras opciones de menor coste como el funcional M06-2X también proporcionan una descripción aceptable. En general, el sumaneno interacciona más fuertemente que el coranuleno con ambos iones. Además, en el sumaneno el efecto de la sustitución es más pronunciado en los grupos CH que en los CH_2. De forma general las interacciones siguen el mismo patrón que el observado para los MEPs, aunque pueden apreciarse ligeras desviaciones. Los resultados indican que la naturaleza de la interacción es diferente en complejos catiónicos y aniónicos. Así, la interacción con aniones está controlada por la interacción electrostática con contribuciones significativas de la dispersión, mientras que en los complejos con cationes son las contribuciones de inducción las que desempeñan un papel predominante.

Por último en el **capítulo 9** se estudia el efecto que la naturaleza del anión y la presencia de disolvente ejercen sobre las características de los complejos con buckybowls. Se han considerado una serie de variables y efectos a estudiar tales como: tres tipos de buckybowls sustituidos con grupos nitrilo, uno basado en coranuleno y dos basados en sumaneno; cuatro líneas de aproximación del anión con respecto al bowl; distintas orientaciones de los iones con respecto al bowl; seis aniones diferentes agrupados en pares de distinto tipo: monoatómico (Cl^-, Br^-), trigonal plano (NO_3^-, CO_2H^-) y tetraédrico (BF_4^-, ClO_4^-). Las energías de interacción se han obtenido empleando los métodos SCS-MP2 y M06-2X, tal como sugerían los resultados del capítulo 8.

Los resultados indican que en todos los casos los complejos se forman por la cara cóncava del bowl, siguiendo su eje central. Igualmente, las distintas orientaciones del anión no parecen tener demasiado efecto sobre la interacción, aunque se favorecen orientaciones con el mayor número de regiones negativas orientadas hacia la pared interna del bowl. Los complejos más estables en fase gas son los formados con CO_2H^-, seguidos por los monoatómicos, NO_3^-, y finalmente los tetraédricos como los menos estables. Este comportamiento cambia radicalmente al incorporar el efecto del disolvente. Todos los complejos sufren importantes pérdidas de estabilidad, pero los más afectados son los formados con CO_2H^- que pasan a estar entre los menos estables en disolventes con constantes dieléctricas elevadas. Los complejos más estables en esas condiciones son los formados con Br^-.

Los resultados conjuntos de estos tres trabajos indican que sería plausible que los aniones fueran atrapados por los buckybowls, dando lugar a complejos que podrían ser estables incluso en disolución, abriendo nuevas posibilidades para el diseño de receptores aniónicos basados en este tipo de especies tan atractivas.

USC
UNIVERSIDADE
DE SANTIAGO
DE COMPOSTELA

USC
UNIVERSIDADE
DE SANTIAGO
DE COMPOSTELA

USC
UNIVERSIDADE
DE SANTIAGO
DE COMPOSTELA

1. Introduction

USC
UNIVERSIDADE
DE SANTIAGO
DE COMPOSTELA

1.1. Supramolecular Chemistry

Supramolecular chemistry is a field of science that deals with the relationship between molecular structure and function; it is the chemistry of the noncovalent bond, which forms the basis of highly specific recognition, transport, and regulation events that act in biological processes. Supramolecular chemistry arises from the natural result of the curiosity of humans, who have imitated phenomena of the nature during centuries. This subject was initiated with the pioneering works of Jean-Marie Lehn in 1969 about the idea of molecular recognition and led him to obtain the Nobel Prize in 1987 together with Donald J. Cram and Charles J. Pedersen.[1, 2]

A tentative definition of Supramolecular Chemistry provided by Lehn is the following:[1,3]

> *"Supramolecular chemistry directs to the development of big complex chemical systems from the components that interact between them by means of intermolecular noncovalent forces"*

and has opened a new field where the interest of various disciplines of Chemistry converge, including Organic and Inorganic Chemistry, Physical Chemistry, Biochemistry, Materials Science and Nanotechnology.

As mentioned above, the objective of Supramolecular Chemistry is to form an aggregate or molecular entity constituted by species that are not linked covalently among them, but associated by their geometric or/and electronic affinity; that is, they are molecularly recognized. Three concepts are essential to understand these processes: fixation, recognition and coordination. These concepts were established at the end of XIX century by Paul Ehrlich (1898), Emil Fischer (1894) and Alfred Werner (1893), respectively.[1, 2]

Ehrlich recognized that a molecule cannot act if it does not bind to the neighborhood of others. On the other hand, Fischer introduced the key-lock concept to explain the performance of enzimes. According to this concept, the enzyme selectively recognizes the substrate because it presents a specific geometry in its active site, the same way a key fits with its lock. The better they fit together the more efficient the complexation will be. This recognition is not only geometric; but it also implicates a chemical interaction and a conformational rearrangement thus explaining the notable specificity of enzyme catalysis. This kind of noncovalent interaction can be related to the idea of coordination as introduced by Werner.

Following the same line, Cram was the first one to introduce the terms host-guest.[4, 5] Thus, one supramolecule is obtained from the process in which one molecule acts as receptor (host) and another one as substrate (guest), binding to the first one to obtain a receptor-substrate complex. Normally, the receptor is a big molecule or aggregate, as an

enzyme or macrocycle, with an adequate cavity. The substrate can be an inorganic single ion or a more complex molecule, as for example a hormone or neurotransmitter. As mentioned above, the associations between the receptor and substrate molecules are based on intermolecular interactions that are, in general, weaker than covalent bonds. For this reason, several simultaneous interactions are usually established between the complexation sites of both molecules ensuring the efficiency of the enzyme-substrate interactions, the antigen-antibody interaction, and other important biological functions.[1, 2] In summary, the receptor would be the molecule formed by covalent bonds able to complex the substrate through intermolecular noncovalent interactions allowing the formation of a supramolecule. Related to these host-guest concepts, self-assembly can be defined as the process through which supramolecular species are spontaneously formed from their components. It is present in nature, acting on the DNA structure, the formation of lipid bilayers, and the secondary, tertiary and quaternary conformations of proteins, among other examples. The common factor to all these self-assembly processes is the requirement of chemical and structural complementarity of different components through numerous noncovalent interactions.

Therefore, the key and repetitive feature in all supramolecular compounds is the fact that the union between the various components is done through noncovalent interactions. So, focusing in the forces responsible of the interactions among molecules it can be said that covalent bonds determine the disposition of atoms inside the molecule, but the bonds responsible for the conformation of the molecules or molecular aggregations are the intermolecular interactions. These intermolecular interactions are weaker than covalent bonds described in molecular chemistry, but they play an important role because they modify various molecular properties as the fusion point, boiling point, etc. The weakness of the interaction is crucial in some cases because it allows breaking the system leading to another process as occurs in DNA chain replication, where it is necessary to break the hydrogen bonds joining the DNA strands. In summary, in order to understand supramolecular structures a deep knowledge of noncovalent interactions is imperative.

1.2. Intermolecular Interactions

Though the existence of intermolecular interactions is known since van der Waals proposal of his equation of state for gases, only from the elucidation of the electronic structure of atoms and molecules and the development of the quantum theory it was possible to start understanding the origin of intermolecular forces. It was soon established that the origin of all molecular forces was essentially electromagnetic.[6-8] Although other forces, as magnetic or gravitational, exist, their magnitudes are negligible compared to electrostatic forces.

In order to understand noncovalent interactions it is convenient to make a classification of the intermolecular interactions. There are different ways of classifying intermolecular interactions though any of them is definitive. One of the most intuitive classifications attends to the repulsive or attractive behavior of the interaction. That way, intermolecular interactions can be attractive, making the molecules come together, or repulsive, avoiding the molecules to collapse. This classification is simple but it does not give any hint about the origins and nature of the interactions.

The most popular classification is the one that attends to the range where the interaction is significant and it will be the classification employed in this work because it has a theoretical foundation.[6-8] Thus, intermolecular interactions can be divided into long-range and short-range interactions. The interaction energy of long-range forces varies as a function of R^{-n}, where R is a distance between molecules. On the other hand, short-range forces depend on the distance as $e^{-\sigma R}$. The following scheme summarizes this classification.

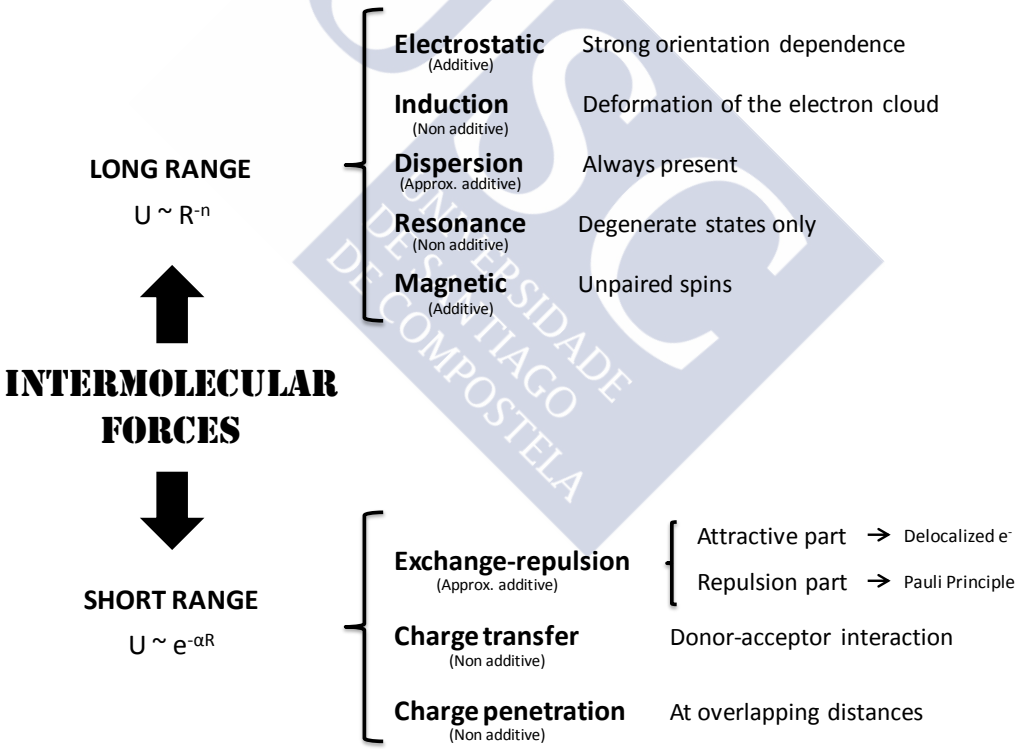


Figure 1.1. Classification of intermolecular interactions depending on the range of the interaction.

As observed in Figure 1.1, the main long-range effects can be classified as coming from three different effects: electrostatic, induction and dispersion. These long-range contributions are the ones that survive at large separations. However, they are still present at short distances, even when the molecules overlap strongly.[6, 7]

Electrostatic interactions are the simplest to understand in general terms: they arise from the straightforward classical interaction between the static charge distributions of the molecules. They are strictly pairwise additive and may be either attractive or repulsive depending on the mutual orientation of the interacting molecules. The electrostatic interaction can be represented as a series of contributions coming from the interaction between the non-zero multipoles of the interacting molecules. The electrostatic effects emerge from the classic interaction between net charges (monopoles) or from distributions of static charges of two molecules (multipoles), not from charge distributions modified by interactions.[6] Theoretically, the development of the multipolar series allows knowing the electrostatic interaction through the sum of the terms of the infinite series of the interactions charge-charge, charge-dipole, dipole-dipole, charge-quadrupole, dipole-quadrupole, etc. Thus, depending on the interacting systems, different number of multipolar expansion terms are employed to define the interaction. For instance, in ionic solids the charge-charge term dominates ($1/R$), in polar fluids, employing a dipole-dipole expression ($1/R^3$) can be a good approximation, and in centre-symmetric molecules (like benzene), quadrupole-quadrupole interaction ($1/R^5$) is a good representation of the electrostatic energy at long-range. In general, the dependence of the interaction energy with the distance for the different multipole-multipole interactions depends as $R^{l1+l2+1}$, being $l1$ and $l2$ the order of the multipoles (0 for monopole, 1 for dipole, 2 for quadrupole, etc.). It has to be indicated that the multipolar approach is only valid when the separation between molecules is large, breaking down at short distances as the overlap between the charge distributions becomes significant.[6]

Although the electronic density of a molecule is hardly compressible, it is quite easily deformed (polarizable). Inductive forces arise from the deformation of the charge distribution of a molecule caused by an external electric field generated by neighboring molecules.[6] When one of the interacting molecules presents a permanent electric moment induction interactions are always present, although their relative importance can decrease if the electrostatic contribution is large. As the induction energy is the result of a distortion in a charge distribution as answer to an external field, it is always negative for the molecules in their ground electronic states. Also, it is non-additive because the interaction between two molecules is affected by the presence of the other ones. In the interaction between a dipolar and an apolar molecule, the electric field of the polar molecule distorts the electronic charge distribution of the apolar molecule, generating an induced dipolar moment in it. Then, this induced dipole moment interacts

with the permanent dipole resulting in an attractive force. The interaction shows a $1/R^6$ dependency, allowing classifying this interaction in the long-range category.

Dispersion is an effect that cannot be easily understood in classical terms. The origin of attractive forces between non-polar molecules was a serious problem at the beginning of twentieth century, until 1930, when F. London described them using a second order perturbation theory, pointing to a relationship between these forces and the optic dispersion in gases, and naming these interactions as dispersion forces.[6, 9] They are also named London forces and are the only long-range forces present in all molecular interactions, representing the most important contribution to the interaction except in small polar molecules. The dispersion energy cannot be analyzed in classical terms and has its origin in quantum mechanics, as a consequence of the continuous fluctuation of the charge distribution of molecules due to electron movement. The usual description of this effect assumes that because the electronic density of molecules varies continuously, instantaneous electric moments are generated which can induce an electric moment in a second molecule. Between the induced multipole of the second molecule and the inductor of the first one an attractive force emerges instantaneously named dispersion force. In fact, dispersion arises because the motions of the electrons in the two molecules become correlated, in such a way that lower-energy configurations are favored and higher-energy ones disfavored. The average effect is a lowering of the energy, and since the correlation effect becomes stronger as the molecules approach each other the result is an attraction. The dispersion energy can be approximately described as depending on the ionization potentials and polarizabilities of the interacting molecules. Due to the dependence on the polarizability, the size and the molecular shape are the factors which control the relative strength of the dispersion interactions. Therefore, dispersion effects usually increase as the size of the molecule, and its polarizability increase.

Two other secondary effects that can arise at long range can be considered: resonance and magnetic effects. Resonance interactions occur either when at least one of the molecules is in a degenerate state (usually an excited state) or when the molecules are identical and one is in an excited state. Consequently they do not occur between ordinary closed-shell molecules in their ground states. Magnetic interactions that involve nuclei can occur whenever there are nuclei with non-zero spin, which is quite common, but the energies are several orders of magnitude smaller and are hardly of any significance in the context of intermolecular forces.[6]

The interaction energy terms between molecules at long-range can be expressed straightforwardly and accurately in terms of power series in $1/R$, and this description is relatively easy to understand and to manipulate. At short-range, however, the description is complicated by the effects of overlap and exchange, and further contributions arise at distances where the molecular wavefunctions overlap significantly and electron exchange between molecules becomes possible. The most important

contribution to the energy at short range is normally described as exchange-repulsion. It can be thought of as comprising two effects: an attractive part, arising because the electrons become free to move over both molecules rather than just one, increasing the uncertainty in their positions and so allowing the energy to decrease, and a repulsive part arising because the wavefunction has to adapt to maintain the Pauli antisymmetry requirement that electrons of the same spin cannot be in the same place and this costs energy. When the electronic clouds of two molecules are close enough to overlap, Pauli's exclusion principle forbids some electrons to occupy the same region of space, reducing the electronic density in this region. Therefore, the atomic nuclei are partially unshielded, thus repelling each other more intensely. Repulsion normally dominates leading to a destabilizing effect overall, so it is usual to take these effects together.[6, 7]

Moreover two more effects can be considered as short-range forces: charge transfer and charge penetration. On one hand, charge transfer is an effect that can be also considered as part of the induction forces that act as short-range.[6] The charge transfer model was introduced by Mulliken in complexes that have an electron-rich (donor) and an electron-poor (acceptor) component.[10] The acceptor component strongly attracts electrons and therefore these complexes are also known as electron donor-acceptor complexes. On the other hand, charge penetration is an attractive effect of purely electrostatic origin that takes place at electronic distances where the interacting molecules overlap.[6] Conceptually, it can be understood as the attraction experimented by the atomic nuclei partially unshielded of one molecule and the electronic cloud associated to another molecule. As a consequence of this interaction, the multipolar expansion ceases to be valid at short distances. In any case, whereas the terms contributing to long range are commonly accepted, at short-range there are more discrepancies, and depending on the method applied different contributions can be defined. It has to be taken into account that this partitioning is to some extent arbitrary and closely related to the application of perturbation theory to intermolecular interactions.

In the systems object of this work, there is an ion as part of the system. Therefore, it is expected that the interaction will be dominated by the electrostatic interaction between the charge of the ion and the multipole distribution of the other species. However, in the studied systems at least one aromatic species is present, so there will be a polarizable aromatic cloud. Therefore, the combination of a polarizing ion together with a polarizable aromatic cloud is expected to result in important induction effects. Also, in the largest systems dispersion effects can also be of importance.

1.3. Interaction involving aromatic systems

The intermolecular interactions can be very different depending on the nature of the species involved in the interaction. Also, though noncovalent interactions are normally weaker than covalent bonds, there is a wide range of interaction strengths depending on the nature and characteristics of the interacting species.[6, 8] Table 1.1 summarizes several different interaction types and their usual interaction strength. It is worth noting that these strengths are for a single contact, but that the combination of many weak contacts can have deep impact onto the properties of the whole systems, as it is the case of stacking in protein interactions.

Table 1.1. Binding energies and nature of noncovalent interactions.

Interactions	Binding Energy (kcal/mol)	Nature of the Interaction
Ion-Ion	25 – 85	Electrostatic
Ion-Dipole	10 – 50	Electrostatic and induction
Dipole-Dipole	1 – 10	Electrostatic and induction
Hydrogen Bond	1 – 30	Electrostatic (dipole-dipole)
X-H···π	1	Weak hydrogen bond
Cation···π	1 – 20	Electrostatic and induction
π···π Stacking	1 – 10	Weak electrostatic and dispersion
Anion···π	5 – 10	Electrostatic and induction
Lone pair···π	1 – 5	Electrostatic
Halogen Bond	1 – 45	Weak electrostatic
Hydrophobic Effect	< 1	Thermodynamic
van der Waals Forces	< 1	Dispersion

Among the different interaction types in Table 1.1, the goal of this work focuses on studying interactions with participation of aromatic molecules. Interactions with aromatic units are particularly interesting because they are fundamental in many biological processes; for instance, in the protein-ligand recognition and consequently in drug design.[11-13] In fact, most of the X-ray structures of complexes formed by proteins and molecules of smaller size show interactions between amino acid chains and aromatic or heteroaromatic rings of ligands. Also, interactions with aromatic units are important in receptors, neurotransmitters, crystal engineering, protein folding, stacking interactions in DNA and RNA, drug receptors or K^+ channels.[11, 12, 14]

In addition to the mentioned applications, aromatic units are important by their presence in the side chains of the so-called aromatic amino acids.[11, 12, 15, 16] Thus, benzene is found as part of phenylalanine, phenol in tyrosine, indole in tryptophan and imidazole in histidine. The side chain groups described above are displayed in Figure 1.2. Understanding the behavior of these aromatic interactions helps to figure out many biological processes which are essential in the life.

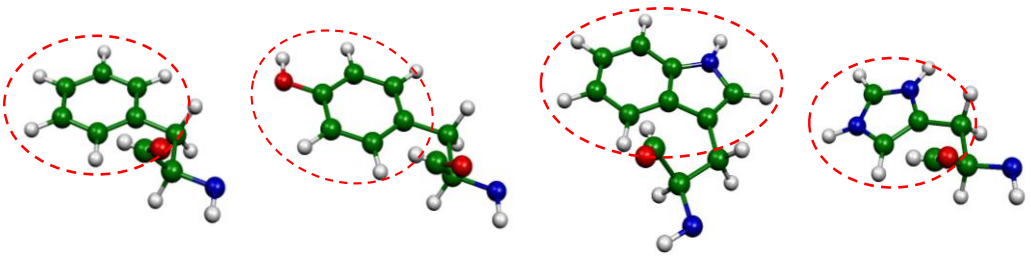


Figure 1.2. Aromatic groups in amino acid side chains.

When aromatic species are present in complex systems, it is usual for the structure to show π···π contacts, XH···π interactions and interactions between ions and the π cloud, being any of these contacts relevant for determining the structural characteristics and energy of the system. Following there is a brief description of these interactions.[13]

X-H···π interactions

This interaction is based on the attraction between X-H groups, normally C-H, N-H or O-H groups, and the π electron cloud of an aromatic ring.[13, 17-21] Normally, the range of distances between the hydrogen atom and the centroid of the ring is 2.4-3.2 Å, larger than the distance in a typical hydrogen bond (around 2 Å).

The C-H···π interaction was first postulated by Tamres in 1952, who noted that dissolving benzene in chloroform was exotermic.[22] Qualitatively, the strength of the C-H···π interaction arises mainly from charge transfer, giving rise to interaction geometries where the CH bond lies directly in line with a *p*-orbital on the ring. O-H···π and N-H···π interactions show similar characteristics and have been frequently recognized as a motif contributing to the stability in different systems. Besides, despite the weakness of these individual contacts, their effects can be additive and in macromolecular systems their influence can be pronounced. This has been show in many cases by Nishio, who has compiled an extensive literature database on C-H··· π interactions and their effects on energetics, reactivity and conformational changes of different species.[17, 23]

Theoretical studies and experimental results in the gas phase seem to indicate that the nature of C-H···π interaction is totally different to conventional hydrogen bonds. While the hydrogen bonds are mainly due to electrostatic interactions, the electrostatic component in the C-H···π interactions is minimum, being dispersion interactions the main cause of formation. Other fundamental difference is the directionality that both interactions exhibit. While the fundamental hydrogen bond feature is its high

directionality due to the electrostatic contribution, the C-H···π interaction does not depend so dramatically on the orientation of the interacting group. Thus, it is frequent to find X-H···π contacts clearly departing from the typical linear arrangement of hydrogen bonds.[17, 19]

π···π interactions (stacking)

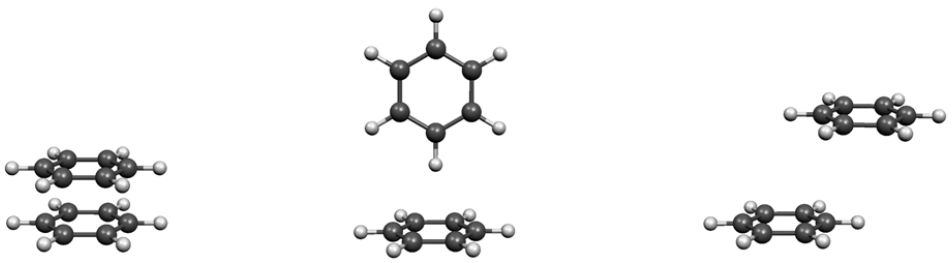
This type of interaction takes place between the π electron clouds of stacked aromatic systems[11-13, 24, 25] Normally, one of the rings is electron-rich, while the other is electron poor, although cases have been described where both rings have the same electron wealth. This corresponds in principle to a weak interaction (bonding energy around 0-10 kcal/mol) but with a global effect of great importance from a biological and supramolecular points of view, as well as in crystallography. π···π interactions, like in benzene dimer, are usually governed by dispersion effects, since these are the unique forces acting in the case of nonpolar molecules (the quadrupole-quadrupole interaction between benzene molecules is weaker).

π···π interactions play an important role in the stabilization of DNA, together with hydrogen bonds, resulting in the stacking of bases pairs and generating its characteristics helicoidal structure.[11, 12] Based on this, a number of intercalating drugs have been designed exploiting π···π stacking interactions. On the other hand, π···π stacking interactions have a lot of applications in Supramolecular Chemistry, especially for host-guest systems. A remarkable case is the one described by Sygula et al., who have synthesized a buckycatcher based on a multitude of conjugated aromatic rings that adopt a concave conformation matching perfectly with a fullerene C_{60} molecule, acting as receptor of this molecule through π···π stacking interactions.[26]

There has been controversy concerning the physical nature of this kind of interaction. In 1990, Hunter and Sanders proposed a simple model based on the competition between the electrostatic and the van der Waals forces to explain the variety of geometries observed for these interactions and to quantitatively predict their interaction energies.[27] These authors postulate the existence of an attractive overlap in van der Waals interactions, which are proportional to the surface contact area between both π systems. This overlap is due to an attraction between the π electronic cloud negatively charged of one of the rings and the σ electronic cloud positively charged from the other. The relative orientation of both rings is determined by electronic repulsions between both π systems negatively charged. For this reason, when an aromatic system is stacked in a parallel way, it is normally observed that the rings are not totally aligned, with one slightly displaced with respect to the other, minimizing the π···π repulsion and maximizing the π···σ attraction. In fact, few examples exist where the aromatic rings are arranged totally overlapping.[28, 29] The most common arrangements are the parallel-displaced and T-shaped dispositions, because π···σ attractions predominate in both. The three dispositions have been usually employed in this kind of complexes to study the

effect of the arrangement on the interaction energy and stability of the complexes. These arrangements are shown in Figure 1.4 with a benzene dimer as example.[24, 25]

It can be observed that in the case of benzene dimer (the most studied π···π interaction), the stacking interactions are competitive with other possible arrangements as the C-H···π interaction in T-shaped structures.[24, 25] This can be observed in Figure 1.4, which shows how both structures are virtually isoenergetic. It is worth mentioning that the strength of these interactions is highly affected by different factors, such as the presence of electron-donor or electron-acceptor substituents in the rings, the existence of heteroatoms forming part of the ring and the degree of annelation of the rings involved in the stacking. Thereby, the higher the number of fused rings, the more favorable the stacking.[13] Regarding substitution effects, it has been shown that the presence of electron-attractor substituents in the ring increases the strength of this kind of interactions since the electronic density of the π cloud of the ring decreases, minimizing the π···π repulsions between the rings. In fact, studies by Sherrill and coworkers have shown that substitution always leads to stronger interaction unregardingly of the donor or acceptor character of the substituents.[30, 31]



Sandwich	T-Shaped	Parallel displaced
-1.81	-2.74	-2.78

Figure 1.4. Types of π···π contacts for benzene dimer with their corresponding interaction energies.

When the stacking is produced between aromatic heterocycles the strength of these interactions increase. The substitution of a carbon atoms of the ring by a nitrogen atom in a six-membered rings (like in pyridine for example) causes a decrease of the electronic π density in the carbon atoms of the ring, which leads to a stabilization of the system and decreases the π···π repulsion forces as mentioned above.[32] In any case, this interpretation of substituent effect has been recently reviewed by Wheeler.[33, 34]

Cation···π interactions

A cation···π interaction arises from the electrostatic interaction of a cation with a face of a π system, as could be a benzene ring and its derivatives or π systems as ethylene. The first evidence of this type of interaction in the gas phase came out from the work by Kebarle in 1981.[35] In a systematic study of ion solvation by various solvents, Kebarle observed that benzene stabilizes K^+ ions better than water in the gas phase. Kebarle proposed that this was a result of the ion interacting with the quadrupole moment of benzene. A molecule with a dipole moment, such as water, experiments a favorable electrostatic interaction with an ion if the ion is positioned near the appropriate end of the dipole. Benzene, of course, has no dipole moment, but it does have a substantial permanent quadrupole moment.[36] A quadrupole can be thought of as two dipoles aligned in such a way so that there is no net dipole. Thus, there is a permanent nonspherical charge distribution in benzene, with regions of relative negative and positive charges. Just as an ion can be attracted to the appropriate end of a dipole, so can an ion experience a favorable interaction with appropriate regions of a quadrupole. This is an electrostatic interaction and does not requires adjustment of the electronic distribution around the ion or the molecule. Importantly, there is no a priori reason to expect that such interactions will be inherently weaker when the molecule contributes a quadrupole rather than a dipole as demonstrated by Reisse and Williams.[37, 38]

Most neurotransmitters have a cationic group that permits them a selective anchorage to their receptors by cation···π interactions.[39-41] The cation···π interaction has important applications in the field of Supramolecular Chemistry. [41-49] Numerous studies have reported the occurrence of cation···π interactions in protein structures and in protein-ligand and protein-DNA complexes.[40, 41, 50, 51] These analyses have revealed the preferential location of amino groups in the area of aromatic rings.[39, 52] This interaction is calculated to be even more stabilizing than an analogous salt bridge, and it is not so strongly attenuated in water.[53] The side-chains of the aromatic amino acid residues, Phe, Tyr and Trp, provide a surface of negative electrostatic potential than can bind to a wide range of cations through a predominantly electrostatic interaction. It has been found that 50% of the Arg residues are in contact with an average of two aromatic side chains. Of particular interest is the interaction of the cationic Arg residue with aromatic side chains. Two limiting geometries are possible, a perpendicular arrangement in which the NH of the Arg points into the face of the aromatic unit, and a parallel or stacked arrangement of the planar guanidinium of Arg and the aromatic moiety. The stacked arrangement is more frequently found, but there seems that this is related to environment effects. Also, series of cation···π interactions involving both Arg and Lys appear in different structures containing several aromatic and cationic side chains from different strands of the protein, intercalated to form an extended array of cation···π interactions.[39, 51, 52] Another remarkable case is the acetylcholine nicotinamide receptor whose mechanism of molecular recognition to their substrate is based only on cation···π

interactions.[40, 54] Furthermore, systems with molecular structures similar to crown ethers, with π systems strategically placed, have shown to be very effective binding places for alkali cations.[41, 55] Additionally, cation···π interactions have also been used to increase the π-face selectively in catalysis in asymmetric catalysis.[41, 56]

The strength of the cation···π interaction has been rationalized on the basis of the strong electrostatic interaction between the positively charged cation and the ring negative molecular electrostatic potential (MEP). Many studies, especially of gas-phase complexes, established that electrostatic interactions play a prominent and usually dominant role in prototypical cation···π interactions.[41, 57, 58] Electrostatic reasoning can also explain variations due to changes in the aromatic ring. The more negative the maximum in electrostatic potential over the center of the aromatic molecule, the stronger the cation···π interaction. In fact, good correlation has been found in many cases between the MEP value and the strength of the cation···π interaction. [41, 59, 60] A clear indication that electrostatics play an important role in cation···π interactions comes from a comparison of simple alkali metals binding to benzene. The observed trend in stability is $Li^+ > Na^+ > K^+ > Rb^+$, the classical electrostatic sequence, and exactly what would be seen if benzene were replaced by Cl^- or if one was comparing hydration energies.[41, 50, 61]

However, this analysis neglects the role played by polarization interaction. The electrostatic contribution does not represent the 100% of the energy of cation···π interactions; in fact, the fraction of the total binding energy that comes from electrostatics varies considerably depending on the aromatic molecule. The "nonelectrostatic" component of the cation···π interaction, sometimes the major component, reflects a combination of effects mostly related to the polarizability of the aromatic unit. Probably the most important of these for simple systems is the interaction of the ion with the induced dipole in the aromatic molecule.[62, 63] As the aromatic species becomes larger it is expected that induction contribution also becomes larger reflecting the increase in polarizability. In fact, studies show that there can be cation···π complexes held by induction contributions, whereas the electrostatic term is repulsive.[64] Induction contributions also explain the presence of off-plane cation···π stabilizing interactions for example in benzene···Na^+ complexes. The location of the cation in the ring plane is destabilized electrostatically, but also shows a stabilizing induction contribution leading to a global attractive (though weak) interaction.[65]

Different studies have been devoted to determine the origins of substitution effects upon the cation···π interaction. Recent studies propose that the origin of the changes has nothing to do with changes in the π cloud but depend on trough-space interaction between the cation and the substituents.[59] These results have been slightly corrected by Quiñonero et al. indicating that induction effects are also responsible of such changes.[66]

In summary, the cation···π interaction is an intense interaction in the gas phase that can frequently appear in systems of interest and basically controlled by electrostatic and induction contributions. However, the presence of solvent or other units near the cation···π contact can modulate significantly the strength of the interactions. It is usually observed a decrease on the interaction strength, but this can also be accompanied by significant structural changes in the geometry of the complex. Solvent molecules compete with the aromatic component for interacting with the cation and, as a consequence, a decreasing of the intensity of the cation···π interaction in the presence of the solvent is normally observed. This led to some controversy regarding the role of cation···π interactions in protein stability. While some studies suggest a relevant contribution another studies estimate that the contribution is insignificant.[15, 41, 53, 58, 61, 67] These differences are normally attributed to the different degree of exposure of the cation···π contact to the solvent. If the contact is buried in a hydrophobic region, it can present an appreciable intensity, while if the contact is exposed to the solvent, it even cannot take place.

Anion···π interactions

While coordination of cations has been object of study one century ago, the coordination of anions has received little attention until short time ago. The advent of synthetic molecules able to coordinate cations and anions was almost simultaneous: in 1967, C. J. Pedersen prepared the first synthetic ligand able to coordinate cations,[68] and only one year after C. H. Park and H. E. Simmons synthesized the first system suitable to coordinate anions which was called “kapatinato” (from kapatinosis, which means swallow in greek).[69] Despite of this almost simultaneous discovery, the area of anion coordination was relatively unexplored in contrast to the cation coordination. The first discovery of the concept anion···π interaction in literature is dated from the year 2000 by Schneider.[2]

From that moment on, various studies were carried out to understand the nature of the interaction between anions and aromatic species.[70-81] The results of those studies demonstrated that, contrary as it could be expected, the intensities of interactions between cations and anions with aromatic species can be of similar magnitude as shown in Table 1.5.

A priori the idea of an interaction between an aromatic ring and an anion will be non-viable due to the electron donor capacity of both molecules, but the electron donor capacity of the aromatic ring can be modulated so, if the aromatic ring is completely substituted with groups which attract electrons, it becomes an electro-deficient aromatic cloud and then an attractive interaction with an anion is possible. Thus, anion···π interactions are described as the favorable noncovalent interactions between electron deficient aromatic systems and an anion.[70, 72]

Table 1.5. Interaction energies of different types of contacts with the π cloud obtained at diverse levels of calculation in kcal/mol.

	ΔE (kcal/mol)
$C_6H_6\cdots C_6H_6$	-2,5
$C_{10}H_8\cdots C_{10}H_8$	-5,7
$C_6H_6\cdots H_2O$	-3,0
$C_6H_5OH\cdots CH_3CN$	-6,6
$C_6H_6\cdots Na^+$	-21,3
$C_6H_6\cdots K^+$	-17,0
$C_6F_6\cdots Cl^-$	-14,0
$C_3N_3H_3\cdots Cl^-$	-6,9

Studies revealed that anion···π interactions are, in general, dominated by the electrostatic and induction contributions.[75, 78] The electrostatic component of the interaction is directly related with the permanent quadrupole moment of the electron-deficient aromatic ring. As indicated in Figure 1.6, the quadrupole of a benzene ring is positive but it can be modulated through the substitution of groups on the rim of the ring. For instance, the quadrupole moment for a benzene ring is -8.45 B while the quadrupole moment for the benzene ring substituted with six fluoride groups is positive by 9.50 B.[70, 72]

Therefore, the presence of electron-withdrawing substituents (halogen, nitro or cyano groups) or nitrogen atoms in the ring (pyridine, triazine, tetrazine, among others) favors the formation of anion···π complexes.

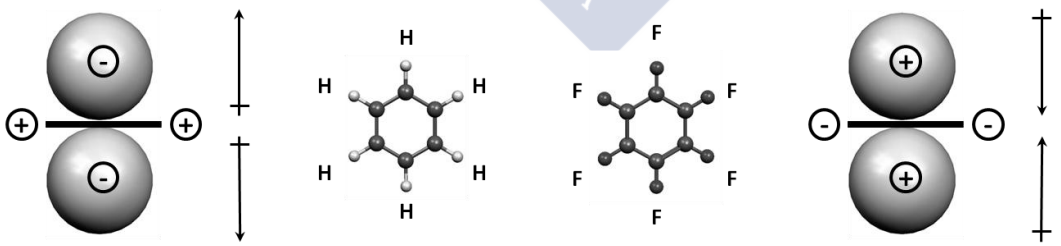


Figure 1.6. Schematic representation of the quadrupole moments of hexafluorobenzene and benzene. Quadrupole moments (Qzz) in Buckingham and molecular polarizabilities parallel to the main symmetry axis ($\alpha_{||}$) in atomic units are given.

A topological analysis of the electrostatic potential in anion···π interactions has demonstrated that there exists a correlation between the MEP value of the aromatic ring and the electrostatic contribution to the anion···π interaction.[70, 72] Thus, the systems with a very positive quadrupole moment give more favorable interactions. Other studies show that for molecules with very positive quadrupole moments the anion···π interaction is dominated basically by the electrostatic term, while for molecules with small quadrupole moments the polarization contribution induced by the anion can be the dominating one. Finally, considering the larger polarizability of anions it has also been found that dispersion contributions tend to be larger in anion···π complexes than in similar cation···π ones.[70, 72]

The properties of the anion are also important for applications of anion···π interactions in Supramolecular Chemistry.[70, 72, 82] Both the electrostatic and polarization contributions to the total interaction energy depend strongly upon the ion-arene distance. Small anions are more polarizing and show short equilibrium distances and, consequently, give rise to stronger interactions. In addition, planar and linear anions such as NO_3^- or N_3^- can also interact with the aromatic ring via π···π stacking.[70, 72, 79]

Finally, a comment must be said on the interplay of the different interactions commented above, all of them involving aromatic species. Different π interactions are very important and omnipresent in a great variety of biological systems, so the study of the mutual influence of different interactions is crucial. The interplay between ion···π and π···π interactions, which can lead to strong cooperativity effects, has been shown. The cooperativity effects can be favorable or unfavorable depending on the nature of the aromatic ring and the sign of the ion.[41, 83-87] The theoretical results on ion···π···π complexes have also been used to explain an unexpected experimental finding regarding the parallel stacking of pentafluorphenyl groups in substituted ferrocenes.[88] Most often, the interactions are not isolated but inserted in long structures where multiple interactions of different type are possible. Thus, it is quite typical to find π···π interactions at the same time as cation···π or X-H···π interactions in many proteins and amino acids. Sometimes, these interactions are combined forming a larger complex where two or more different kinds of interactions are established with simultaneous participation of the aromatic units.[11, 12, 41]

1.4. Interactions with buckybowls

Polycyclic aromatic hydrocarbons (PAH) are a family of hydrocarbon molecules that typically possess a structure formed by a series of fused benzene rings creating a planar structure. In graphene, material with potentialities still to discover, this structural motive extends creating large bidimensional layers. Some of these PAHs constitute important atmospheric contaminants with some implications for human health but, on the other hand, some PAHs have been located in the interstellar medium and postulated as species that could act as basis for the more primitive ways of life.[89]

In 1966 Barth and Lawton presented the first synthesis of the $C_{20}H_{10}$ PAH, called corannulene, that presents a non-planar structure.[90] Contrary to other PAH as helicenes the non-planarity of corannulene is not a consequence of the presence of bulky groups that force the location of part of the fused rings out of the plane. The origin of the non-planarity of corannulene is the proper structure of the carbon rings: corannulene is formed by five benzene rings grouped around a pentagonal central ring. The presence of the five carbon central ring introduces the curvature in the corannulene structure because it is not possible to build a planar layer fusing pentagons and hexagons. According to this, the structure is deformed creating species with bowl shape that, contrary to planar PAH, present two faces, concave and convex, which can exhibit different properties. This is the motivation why these species are denominated molecular bowls, π-bowls or buckybowls.[91]

The relatively recent discovery of buckminsterfullerene and other fullerenes has incremented the interest in buckybowls because they are considered as fullerene fragments and they could be a key piece in the synthesis and design of new species related to fullerenes and carbon nanotubes.[92, 93] There is a complete family of buckybowls that has been identified or synthesized in the laboratory, and it has been observed that though these species frequently share as structural motive their bowl shape, their properties change appreciably with size, curvature and substituents.[91]

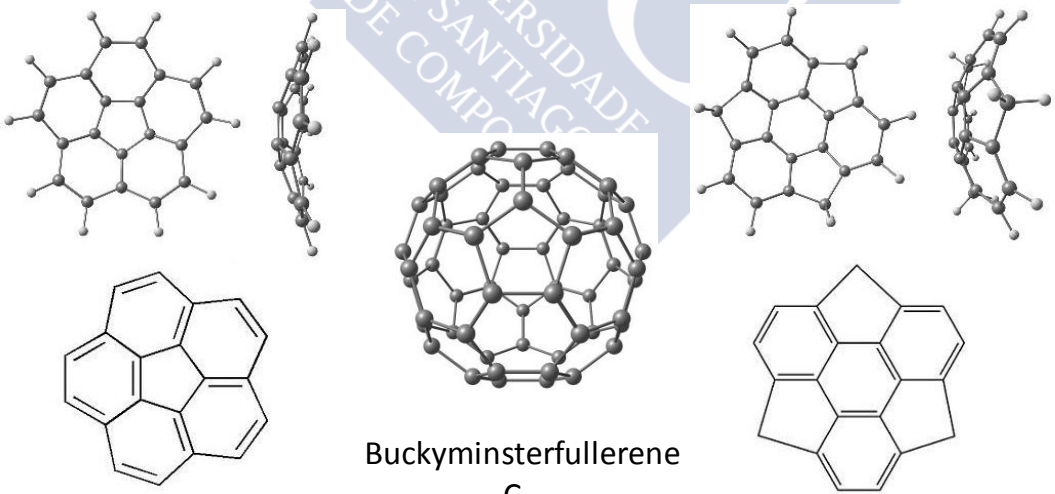


Figure 1.7. Buckyminsterfullerene and the smallest buckybowls related to it.

In any case, this area of study is recently emerging: while corannulene has been synthesized in 1966, the other smallest buckybowl related to C_{60}, denominated sumanene ($C_{21}H_{12}$), has been synthesized so recently as in 2003.[94] Sumanene presents a structure that is formed by a hexagon as the central ring and alternating hexagons and pentagons around it. Due to its recent discovery, relatively few studies which describe properties and characteristics of sumanene are published.[94-99]

These carbon aromatic nanosystems show subtle dependences between their structure, dynamic and properties, so they are a set of materials with great potentialities in a variety of areas. One of the most interesting aspects is the possibility of creating intermolecular complexes of different nature employing one or both faces of the buckybowls, creating supramolecular structures bonded by noncovalent interactions. In this sense, there is a great variety of possibilities in which buckybowls could act as receptors interacting with other buckybowls or fullerenes, transition metals, ions of different nature, etc.[91]

An interesting application of these species is related to a concave-convex interaction between two buckybowls by means of π···π contacts, so they that can be employed as tweezers for catching species of interest, for instance fullerenes. In this case, buckybowls can be used as one of the most efficient buckycatchers, as proposed by Sygula.[26]

Whereas stacking with planar hydrocarbons is limited to the region nearby the bottom of the bowl, the use of curved surfaces allows extending the contact area increasing the interaction. Different modifications of coranulenne and sumanene have been studied as possible fullerene receptors based on π···π interactions, though other effects as C-H···π can also help stabilizing the complex as already shown for sumanene.[100-106]

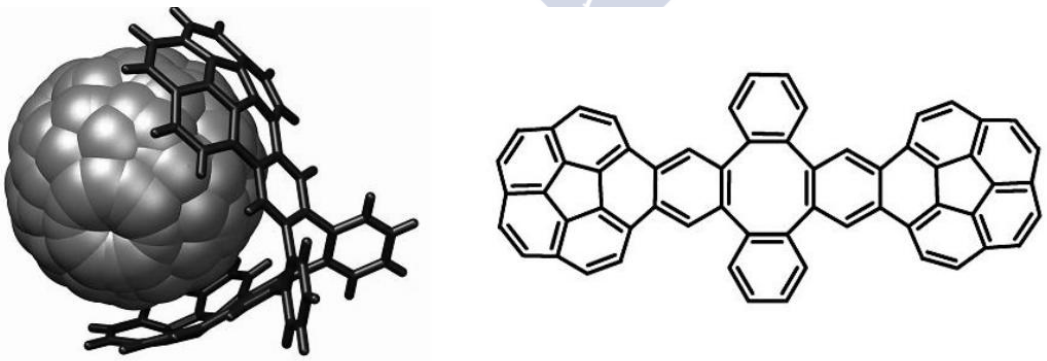


Figure 1.8. Tweezers developed by Sygula et al. to catch fullerenes.

Another interesting aspect of the curved structures of buckybowls comes from having different properties depending on the face, concave or convex, considered. More specifically, it has been shown that corannulene has different molecular electrostatic potential by both faces, being the convex one more negative.[107] Therefore, different complexes of corannulene with cations and transition metals have been synthesized mostly showing coordination by the convex face,[91, 108-116] though there are some cases where coordination has been observed by the concave face of the bowl.[95]

Regarding cation···buckybowl complexes, it becomes clear that the convex face is electrostatically favored, so in order to form more stable complexes by the concave side of the bowl systems have to be employed showing large dispersion contributions (favored by the concave face that places more carbon atoms closer to the cation) or with induction effects also favoring the concave face. In a study by our group it has been shown that the interaction with these large aromatic systems is partly controlled by electrostatics, as expected. However, several striking effects have been also observed. In the case of lithium cation complexes with a series of buckybowls of increasing size it has been observed that for some of them the electrostatic contribution is repulsive, so the fragments are held together by large induction contributions that stabilize the complex.[64] Also, as the size of the cation grows the difference in stability between concave and convex faces decrease, so it can be expected that for complex cations, coordination could be favored by the concave face, thus effectively forming an inclusion complex.

In the case of anion interactions with curved aromatic surfaces the field has been even less explored than interactions with cations. The possibility of employing buckybowls as anion receptor opens new possibilities, with neutral receptors with properties that could be modulated through subtle changes in their structures. The studies in this field are mostly confined to those shown in the present thesis. In similar systems, but based on molecular tweezers as proposed by Klärner,[107, 117] Hermida-Ramón and collaborators have show that properly changing the structure of the tweezers can make them amenable for interacting with anions.[118-122] Among the different structural changes proposed by these authors, simple substitution in the aromatic ring by electron-withdrawing groups emerges as a simple way of changing the electrostatic properties of the tweezers, thus making possible interaction with anions. Substitution with electron-withdrawing groups can invert the MEP of the molecule, thus creating regions of positive MEP that can interact favorably with anions. Therefore, the catching capabilities of ions by buckybowls could be modulated by substitution or changes on the carbon structure of the buckybowl, as it will be shown in this work.

1.5. References

[1] J.-M. Lehn, Supramolecular Chemistry: concepts and perspectives, VCH, Weinheim, **1995**.

[2] H.-J. Schneider, A. Yatsimirski, Principles and Methods in Supramolecular Chemistry, Wiley, New York, **2000**.

[3] J.-M. Lehn. *PROC. NATL. ACAD. SCI. USA* **2002**, *99*, 4763-4768.

[4] D. J. Cram. *Angew. Chem. Int. Ed.* **1988**, *27*, 1009-1020.

[5] D. J. Cram, J. M. Cram. *Science* **1974**, *183*, 803-809.

[6] A. J. Stone, The theory of intermolecular forces, Oxford University Press, Oxford, **2013**.

[7] I. Kaplan, Intermolecular Interactions: Physical Picture , Computational Methods, John Wiley & Sons, Chichester, **2006**.

[8] P. Hobza, R. Zaradnik, Intermolecular complexes : the role of van der Waals systems in physical chemistry and the biodisciplines, Elsevier, Amsterdam, **1988**.

[9] F. London. *Zeitschrift für Physik* **1930**, *63*, 245-279.

[10] R. S. Mulliken. *J. Am. Chem. Soc.* **1950**, *72*, 600-608.

[11] E. A. Meyer, R. K. Castellano, F. Diederich. *Angew. Chem. Int. Ed.* **2003**, *42*, 1210-1250.

[12] L. M. Salonen, M. Ellermann, F. Diederich. *Angew. Chem. Int. Ed.* **2011**, *50*, 4808-4842.

[13] S. Tsuzuki, T. Uchimaru. *Curr. Org. Chem.* **2006**, *10*, 745-762.

[14] Several Authors. *Acc. Chem. Res.* **2012**, *46*. Complete Volume.

[15] M. L. Waters. *Biopolymers (Peptide Sci.)* **2004**, *76*, 435-445.

[16] S. Burley, G. Petsko. *Science* **1985**, *229*, 23-28.

[17] M. Nishio. *Phys. Chem. Chem. Phys.* **2011**, *13*, 13873-13900.

[18] O. Takahashi, Y. Kohno, M. Nishio. *Chem. Rev.* **2010**, *110*, 6049-6076.

[19] S. Tsuzuki, K. Honda, T. Uchimaru, M. Mikami, K. Tanabe. *J. Am. Chem. Soc.* **2000**, *122*, 11450-11458.

[20] S. Tsuzuki, K. Honda, T. Uchimaru, M. Mikami, K. Tanabe. *J. Am. Chem. Soc.* **2000**, *122*, 3746-3753.

[21] S. Tsuzuki, A. Fujii. *Phys. Chem. Chem. Phys.* **2008**, *10*, 2584-2594.

[22] M. Tamres. *J. Am. Chem. Soc.* **1952**, *74*, 3375-3378.

[23] M. Nishio in The CH/π hydrogen bond. http://www.tim.hi-ho.ne.jp/dionisio/, **2014**. Last accessed 16/09/14.

[24] M. O. Sinnokrot, E. F. Valeev, C. D. Sherrill. *J. Am. Chem. Soc.* **2002**, *124*, 10887-10893.

[25] S. Tsuzuki, K. Honda, T. Uchimaru, M. Mikami, K. Tanabe. *J. Am. Chem. Soc.* **2001**, *124*, 104-112.

[26] A. Sygula, F. R. Fronczek, R. Sygula, P. W. Rabideau, M. M. Olmstead. *J. Am. Chem. Soc.* **2007**, *129*, 3842-3843.

[27] C. A. Hunter, J. K. M. Sanders. *J. Am. Chem. Soc.* **1990**, *112*, 5525-5534.

[28] A. N. Sokolov, T. Friščić, S. Blais, J. A. Ripmeester, L. R. MacGillivray. *Cryst. Growth Des.* **2006**, *6*, 2427-2428.

[29] A. N. Sokolov, T. Friščić, L. R. MacGillivray. *J. Am. Chem. Soc.* **2006**, *128*, 2806-2807.

[30] M. O. Sinnokrot, C. D. Sherrill. *J. Am. Chem. Soc.* **2004**, *126*, 7690-7697.

[31] A. L. Ringer, C. D. Sherrill. *J. Am. Chem. Soc.* **2009**, *131*, 4574-4575.
[32] E. G. Hohenstein, C. D. Sherrill. *J. Phys. Chem. A* **2009**, *113*, 878-886.
[33] S. E. Wheeler. *Acc. Chem. Res.* **2012**, *46*, 1029-1038.
[34] S. E. Wheeler, J. W. G. Bloom. *J. Phys. Chem. A* **2014**, *118*, 6133-6147.
[35] J. Sunner, K. Nishizawa, P. Kebarle. *J. Phys. Chem.* **1981**, *85*, 1814-1820.
[36] G. R. Dennis, G. L. D. Ritchie. *J. Phys. Chem.* **1991**, *95*, 656-660.
[37] J. H. Williams. *Acc. Chem. Res.* **1993**, *26*, 593-598.
[38] M. Luhmer, K. Bartik, A. Dejaegere, J. Reisse, P. Bovy. *Bull. Soc. Chim France* **1997**, *131*, 603-606.
[39] J. P. Gallivan, D. A. Dougherty. *PROC. NATL. ACAD. SCI. USA* **1999**, *96*, 9459-9464.
[40] D. A. Dougherty. *J. Nutr.* **2007**, *137*, 1504S-1508S.
[41] A. S. Mahadevi, G. N. Sastry. *Chem. Rev.* **2013**, *113*, 2100-2138.
[42] F. G. Gatti, D. A. Leigh, S. A. Nepogodiev, A. M. Z. Slawin, S. J. Teat, J. K. Y. Wong. *J. Am. Chem. Soc.* **2001**, *123*, 5983-5989.
[43] P. L. Anelli, P. R. Ashton, N. Spencer, A. M. Z. Slawin, J. F. Stoddart, D. J. Williams. *Angew. Chem. Int. Ed.* **1991**, *30*, 1036-1039.
[44] F. M. Raymo, K. N. Houk, J. F. Stoddart. *J. Org. Chem.* **1998**, *63*, 6523-6528.
[45] X. Bao, I. Isaacsohn, A. F. Drew, D. B. Smithrud. *J. Org. Chem.* **2007**, *72*, 3988-4000.
[46] J. M. Heemstra, J. S. Moore. *Chem. Commun.* **2004**, 1480-1481.
[47] C. Biot, E. Buisine, M. Rooman. *J. Am. Chem. Soc.* **2003**, *125*, 13988-13994.
[48] R. Wintjens, J. Liévin, M. Rooman, E. Buisine. *J. Mol. Biol.* **2000**, *302*, 393-408.
[49] J. S. Lamoureux, J. T. Maynes, J. N. Mark Glover. *J. Mol. Biol.* **2004**, *335*, 399-408.
[50] J. C. Ma, D. A. Dougherty. *Chem. Rev.* **1997**, *97*, 1303-1324.
[51] N. Zacharias, D. A. Dougherty. *Trends Pharmacol. Sci.* **2002**, *23*, 281-7.
[52] N. S. Scrutton, A. R. Raine. *Biochem. J* **1996**, *319*, 1-8.
[53] J. P. Gallivan, D. A. Dougherty. *J. Am. Chem. Soc.* **2000**, *122*, 870-874.
[54] D. L. Beene, G. S. Brandt, W. Zhong, N. M. Zacharias, H. A. Lester, D. A. Dougherty. *Biochemistry* **2002**, *41*, 10262-10269.
[55] G. W. Gokel, L. J. Barbour, R. Ferdani, J. Hu. *Acc. Chem. Res.* **2002**, *35*, 878-886.
[56] S. Yamada, C. Morita. *J. Am. Chem. Soc.* **2002**, *124*, 8184-8185.
[57] N. J. Singh, S. K. Min, D. Y. Kim, K. S. Kim. *J. Chem. Theory Comput.* **2009**, *5*, 515-529.
[58] E. M. Cabaleiro-Lago, J. Rodríguez-Otero, Á. Peña-Gallego. *J. Chem. Phys.* **2011**, *135*, 214301/1-214301/9.
[59] S. E. Wheeler, K. N. Houk. *J. Am. Chem. Soc.* **2009**, *131*, 3126-3127.
[60] C. H. Suresh, S. R. Gadre. *J. Phys. Chem. A* **2007**, *111*, 710-714.
[61] A. S. Reddy, H. Zipse, G. N. Sastry. *J. Phys. Chem. B* **2007**, *111*, 11546-11553.
[62] I. Soteras, M. Orozco, F. J. Luque. *Phys. Chem. Chem. Phys.* **2008**, *10*, 2616-2624.
[63] H.-J. Schneider. *Angew. Chem. Int. Ed.* **1991**, *30*, 1417-1436.
[64] J. A. Carrazana-García, J. s. Rodríguez-Otero, E. M. Cabaleiro-Lago. *J. Phys. Chem. B* **2011**, *115*, 2774-2782.
[65] C. D. Sherrill. *Acc. Chem. Res.* **2012**, *46*, 1020-1028.
[66] A. Bauza, P. M. Deya, A. Frontera, D. Quiñonero. *Phys. Chem. Chem. Phys.* **2014**, *16*, 1322-1326.
[67] B. W. Berry, M. M. Elvekrog, C. Tommos. *J. Am. Chem. Soc.* **2007**, *129*, 5308-5309.
[68] C. J. Pedersen. *J. Am. Chem. Soc.* **1967**, *89*, 7017-7036.
[69] C. H. Park, H. E. Simmons. *J. Am. Chem. Soc.* **1968**, *90*, 2431-2432.

[70] B. L. Schottel, H. T. Chifotides, K. R. Dunbar. *Chem. Soc. Rev.* **2008**, *37*, 68-83.
[71] O. B. Berryman, V. S. Bryantsev, D. P. Stay, D. W. Johnson, B. P. Hay. *J. Am. Chem. Soc.* **2006**, *129*, 48-58.
[72] A. Frontera, D. Quiñonero, P. M. Deyà. *WIREs Comput. Mol. Sci.* **2011**, *1*, 440-459.
[73] D. Quiñonero, C. Garau, C. Rotger, A. Frontera, P. Ballester, A. Costa, P. M. Deyà. *Angew. Chem. Int. Ed.* **2002**, *41*, 3389-3392.
[74] C. Garau, D. Quiñonero, A. Frontera, P. Ballester, A. Costa, P. M. Deya. *New J. Chem.* **2003**, *27*, 211-214.
[75] C. Garau, A. Frontera, D. Quiñonero, P. Ballester, A. Costa, P. M. Deyà. *ChemPhysChem* **2003**, *4*, 1344-1348.
[76] C. Garau, D. Quiñonero, A. Frontera, P. Ballester, A. Costa, P. M. Deyà. *J. Phys. Chem. A* **2005**, *109*, 9341-9345.
[77] J. Rodríguez-Otero, E. M. Cabaleiro-Lago, A. Peña-Gallego. *Chem. Phys. Lett.* **2008**, *452*, 49-53.
[78] D. Kim, P. Tarakeshwar, K. S. Kim. *J. Phys. Chem. A* **2004**, *108*, 1250-1258.
[79] H. T. Chifotides, K. I. M. R. Dunbar. *Acc. Chem. Res.* **2013**, *46*, 894-906.
[80] P. Ballester. *Acc. Chem. Res.* **2012**, *46*, 874-884.
[81] S. E. Wheeler, K. N. Houk. *J. Phys. Chem. A* **2010**, *114*, 8658-8664.
[82] A. García-Raso, F. M. Albertí, J. J. Fiol, A. Tasada, M. Barceló-Oliver, E. Molins, C. Estarellas, A. Frontera, D. Quiñonero, P. M. Deyà. *Cryst. Growth Des.* **2009**, *9*, 2363-2376.
[83] D. Escudero, A. Frontera, D. Quiñonero, P. M. Deya. *Chem. Phys. Lett.* **2008**, *456*, 257-261.
[84] D. Escudero, X. Lucas, C. Estarellas, A. Frontera, D. Quiñonero, P. M. Deya. *Trends Pharmacol. Sci.* **2008**, *13*, 31-52.
[85] C. Estarellas, A. Frontera, D. Quiñonero, P. M. Deya. *Chem. Phys. Lett.* **2009**, *479*, 316-320.
[86] C. Estarellas, A. Frontera, D. Quiñonero, P. M. Deya. *Cent. Eur. J. Chem.* **2011**, *9*, 25-34.
[87] A. Frontera, D. Quiñonero, C. Garau, A. Costa, P. Ballester, P. M. Deya. *J. Phys. Chem. A* **2006**, *110*, 9307-9309.
[88] M. D. Blanchard, R. P. Hughes, T. E. Concolino, A. L. Rheingold. *Chem. Mater.* **2000**, *12*, 1604-1610.
[89] R. G. Harvey, Polycyclic aromatic hydrocarbons, Wiley-VCH, New York, **1997**.
[90] W. E. Barth, R. G. Lawton. *J. Am. Chem. Soc.* **1966**, *88*, 380-381.
[91] M. A. Petrukhina, L. A. Scott, Fragments of fullerenes and carbon nanotubes, John Wiley & Sons, Hoboken, **2012**.
[92] S. Reich, C. Thomsen, J. Maultzsch, Carbon Nanotubes: Basic Concepts and Physical Properties, Wiley-VCH, Weiheim, **2004**.
[93] A. Hirsch, M. Brettreich, Fullerenes: chemistry and reactions, Wiley-VCH, Weiheim, **2005**.
[94] H. Sakurai, T. Daiko, T. Hirao. *Science* **2003**, *301*, 1878-1878.
[95] T. Amaya, H. Sakane, T. Hirao. *Angew. Chem. Int. Ed. Engl.* **2007**, *46*, 8376-8379.
[96] M. A. Petrukhina. *Angew. Chem., Int. Ed.* **2008**, *47*, 1550-1552.
[97] T. Amaya, H. Sakane, T. Muneishi, T. Hirao. *Chem. Commun.* **2008**, 765-767.
[98] T. Amaya, H. Sakane, T. Muneishi, T. Hirao. *Chem. Commun.* **2009**, 7593-7594.

[99] T. Amaya, S. Seki, T. Moriuchi, K. Nakamoto, T. Nakata, H. Sakane, A. Saeki, S. Tagawa, T. Hirao. *J. Am. Chem. Soc.* **2009**, *131*, 408-409.
[100] D. Josa, J. R. Otero, E. M. Cabaleiro Lago. *Phys. Chem. Chem. Phys.* **2011**, *13*, 21139-21145.
[101] D. Josa, L. Azevedo dos Santos, I. Gonzalez-Veloso, J. Rodriguez-Otero, E. M. Cabaleiro-Lago, T. de Castro Ramalho. *RSC Advances* **2014**, *4*, 29826-29833.
[102] P. A. Denis. *Chem. Phys. Lett.* **2014**, *591*, 323-327.
[103] P. A. Denis. *RSC Adv.* **2013**, *3*, 25296-25305.
[104] P. A. Denis. *Chem. Phys. Lett.* **2011**, *516*, 82-87.
[105] U. D. Priyakumar, G. N. Sastry. *J. Org. Chem.* **2001**, *66*, 6523-6530.
[106] M. R. Kennedy, L. A. Burns, C. D. Sherrill. *J. Phys. Chem. A* **2012**, *116*, 11920-11926.
[107] F.-G. Klarner, J. Panitzky, D. Preda, L. T. Scott. *J. Mol. Model.* **2000**, *6*, 318-327.
[108] A. S. Filatov, M. A. Petrukhina. *Coord. Chem. Rev.* **2010**, *254*, 2234-2246.
[109] U. D. Priyakumar, G. N. Sastry. *Tetrahedron Lett.* **2003**, *44*, 6043-6046.
[110] S. N. Spisak, A. V. Zabula, A. S. Filatov, A. Y. Rogachev, M. A. Petrukhina. *Angew. Chem., Int. Ed.* **2011**, *50*, 8090-8094.
[111] D. Vijay, H. Sakurai, V. Subramanian, G. N. Sastry. *Phys. Chem. Chem. Phys.* **2012**, *14*, 3057-3065.
[112] M. A. Petrukhina, L. T. Scott. *Dalton Trans.* **2005**, 2969-2975.
[113] R. C. Dunbar. *J. Phys. Chem. A* **2002**, *106*, 9809-9819.
[114] M. W. Stoddart, J. H. Brownie, M. C. Baird, H. L. Schmider. *J. Organomet. Chem.* **2005**, *690*, 3440-3450.
[115] J. R. Green, R. C. Dunbar. *J. Phys. Chem. A* **2011**, *115*, 4968-4975.
[116] M. Rellán-Piñeiro, J. Rodríguez-Otero, E. Cabaleiro-Lago, D. Josa. *J. Mol. Model.* **2013**, *19*, 2049-2055.
[117] F.-G. Klärner, T. Schrader. *Acc. Chem. Res.* **2013**, *46*, 967-978.
[118] J. M. Hermida-Ramon, C. M. Estevez. *Chem. Eur. J.* **2007**, *13*, 4743-4749.
[119] J. M. Hermida-Ramon, M. Mandado, M. Sanchez-Lozano, C. M. Estevez. *Phys. Chem. Chem. Phys.* **2010**, *12*, 164-169.
[120] M. Mandado, J. M. Hermida-Ramon, C. M. Estevez. *J. Mol. Struct. (THEOCHEM)* **2008**, *854*, 1-9.
[121] M. Sanchez-Lozano, N. Otero, J. M. Hermida-Ramon, C. M. Estevez, M. Mandado. *J. Phys. Chem. A* **2011**, *115*, 2016-2025.
[122] J. M. Hermida-Ramon, M. Sanchez-Lozano, C. M. Estevez. *Phys. Chem. Chem. Phys.* **2013**, *15*, 18204-18216.

2. Objectives

USC
UNIVERSIDADE
DE SANTIAGO
DE COMPOSTELA

The main objective of this thesis is to gain more insight into the characteristics of systems that establish interactions between aromatic and charged species by applying computational chemistry methods. The interest on ion···π interactions has grown in the last decades with new evidences of their importance in many fields covering from biochemistry to materials science. More specifically, the upcoming of anion····π interactions has produced a renewed interest about the characteristics and nature of the interactions with aromatic systems, as well as their relationship with other types of interactions.

Computational chemistry has also recently evolved with new methods and functionals specifically designed for studying intermolecular interactions, especially regarding the treatment of dispersion interactions. These new approaches, together with techniques allowing significant reductions of the computational cost, have made possible the application of appropriate methods to systems of increasing size, thus avoiding being restricted to the simplest cases as benzene complexes with alkaline or halogen ions.

The study of ion···π interactions constitutes a wide field for research, including very different systems and phenomena, so in this thesis the goal will be focused on a series of specific aspects of the cation···π (chapters 4 and 5) and anion···π (chapters 6 to 9) interactions. More precisely, the goals of the different chapters are summarized in the following.

Chapter 4 is devoted to phenol···cation (K^+, Na^+, Li^+ and Mg^{2+}) complexes. Though the interaction of simple aromatic molecules, mostly benzene, with simple cations as alkaline ones has already been studied in detail, there are several aspects of the interaction that deserve more attention. Cation···π interactions are strong in the gas phase, but the presence of solvent molecules or other donating groups nearby can modulate the strength and characteristics of the interaction. Microhydration of complexes opens a route for isolating the effects due to specific interactions with the solvent. Clusters formed by phenol and simple cations will be subjected to stepwise microhydration in order to determine the most stable arrangements of the hydrated complexes. That way, the balance among the different attractive contacts in the clusters can be analyzed and their impact on cluster properties determined. Moreover, systems containing a small number of molecules can be monitored by infrared spectroscopy, so the vibrational spectra will be predicted for the complexes studied. The results will be compared to the experimental ones obtained by Vaden and Lisy (*J. Chem. Phys.* **2004**, 120, 721-730) for phenol complexes with K^+ and Na^+ and four water molecules.

Chapter 5 deals with the analysis of another possible modulating effect in cation···π complexes. Besides solvent molecules, other electron donating groups can also interact with the cation in a cation···π contact. In this chapter, the effect of a second aromatic

unit interacting with a cation···π contact will be analyzed. Ternary systems formed by two aromatic molecules and one cation will be studied in order to quantify the balance between the different cation···π, X-H···π and π···π interactions and their mutual influence. The systems are formed by a cation and aromatic rings selected as to represent possible contacts between amino acid side chains. Benzene, phenol and indole are employed as aromatic units, whereas guanidinium cation is selected as a model of the cationic side chain of arginine. The most stable structures of these ternary complexes will be determined and their characteristics analyzed. Consequently, possible specific interactions, as hydrogen bonds in phenol and indole complexes, or the role played by dispersion interactions would be revealed. Also, a pair energy decomposition will allow determining the magnitude of possible cooperative effects in this kind of complexes.

Chapter 6 is the first one devoted to anion···π interactions. Recently, Matile et al. (*J. Am. Chem. Soc*. **2006**, 128, 14788-14789) synthesized the first anionic channel which is supposed to be based on anion···π interactions. This anion channel is constructed by a series of oligomers of naphthalendiimides (NDIs), which arrange themselves as to create a pore through which anion transportation has been verified. However, several questions remain unanswered about how this channel works. Specifically, it has been suggested that solvent molecules can play an active role in anion transport, maybe going into the channel and facilitating the process. Two simple models will be employed for studying the interaction of anions with NDI, and the effect of water molecules will be estimated by explicitly incorporating a small number of water molecules into the model and also by using a continuous representation of the solvent. The results will help understanding the role of the solvent molecules closest to the anion in order to favor the interaction with the channel units.

Chapters 7 to 9 are dedicated to an emergent field in chemistry related to the properties and interactions of curved aromatic systems (buckybowls). In these chapters, the possible use of these buckybowls as ion receptors will be analyzed by introducing different modifications in the structures of the bowls. Substituted derivatives of corannulene and sumanene will be employed in these studies.

Chapter 7 is our first approach to this subject. Corannulene shows negative molecular electrostatic potential (MEP) by both faces of the bowl, but proper substitution with electron-withdrawing groups can invert its molecular electrostatic potential and provide a favorable interaction with anions. Substitution of corannulene with five and ten F, Cl and CN groups will be considered, and its effect upon the properties of the bowls will be analyzed, specially regarding their MEPs, seeking a stronger interaction with anions. The effect of these substitutions upon the interaction with anions will be studied in

complexes formed with Cl^-, Br^- and BF_4^- anions, obtaining their optimal geometries and interaction strengths. It is intended to form remarkably stable complexes, looking for inclusion structures with the anion by the concave side of the bowl, as opposed to the convex complexation already observed in cations.

Chapter 8 is more oriented to the performance of different computational methods. It has been observed that in this kind of systems a reliable method is difficult to find, the errors being quite large in many cases. Since there are no reference values, the method employed is somewhat blindly chosen. In order to alleviate this problem, a thorough study will be carried out in complexes of Na^+ and Cl^- with buckybowls. Two typical buckybowls, corannulene and sumanene, will be considered and substituted by CH_3, F and CN groups to promote changes in the molecular electrostatic potentials. Consequently, the interaction will be modulated favoring cations or anions. Reference values for the interaction will be obtained by employing high-level calculations, being used afterwards for checking the performance of a variety of more affordable methods. A reliable account on how substitution affects the interaction in both anion and cation complexes will be obtained, allowing the direct comparison of cation···π and anion···π interactions in the same set of systems. The detailed analysis of the characteristics of the interaction will hopefully reveal the intrinsic different nature of the interaction with cations and anions in these extended π systems.

Chapter 9 completes the studies on the interaction between anions and buckybowls. After selecting an appropriate method in chapter 8, now this method will be applied in order to gain insight about how the shape, size and disposition of the anions affect the properties of the complexes. CN-substituted corannulene and sumanene will be employed to study the interaction with six different anions, going from monoatomic Cl^- and Br^-, to planar trigonal NO_3^- and CO_2H^-, and to tetrahedral BF_4^- and ClO_4^-. Several orientations of the polyatomic anions as well as different approaching lines to the bowl will be considered. The characteristics of these complexes will be analyzed in detail in order to find the key factors controlling the interaction in each case and the possible differences associated to the different anion's nature. Also, solvent effects as modeled by a continuum model will be evaluated to check whether the proposed complexes would be formed in solution. A series of solvents with different dielectric constant will be used to quantify how the gas-phase interaction is altered and to which extent anion's nature favors or hinders the formation of complexes in solution.

USC
UNIVERSIDADE
DE SANTIAGO
DE COMPOSTELA

3. Methodology

USC
UNIVERSIDADE
DE SANTIAGO
DE COMPOSTELA

3.1. Interaction Energy

Though interaction energies are several orders of magnitude smaller than electronic energies, and usually significantly smaller than bond energies, the usual approximate methods employed for solving the Schrödinger equation in chemical systems can be employed for studying noncovalent interactions.[1-3]

The concept of interaction energy appears naturally within the Born-Oppenheimer approximation when a system formed by say, two molecules, atoms or ions is considered.[3] Quantum chemistry treats the system as a whole so after calculating with a given method, the energy of the complete system (supermolecule) is obtained. As indicated in Figure 3.1, a system defined by a set of nuclei at given positions together with the corresponding electrons has to be divided (arbitrarily or not) in a set of separable atoms, molecules or ions.

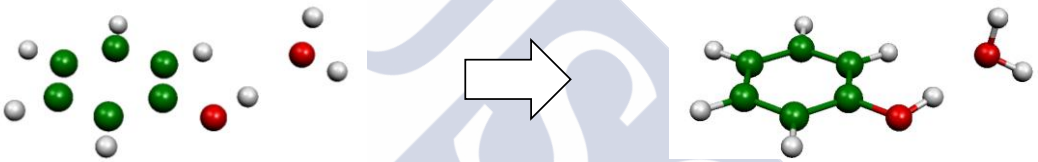


Figure 3.1. A phenol···water dimer. Left: the set of atoms forming the system. Right: the division employed for studying the interaction between phenol and water.

Once this separation is done, the energy of the system can be expressed as:[3-5]

$$E_{AB} = E_A + E_B + \Delta E_{AB}^{\text{int}}. \qquad \text{(eq. 3.1)}$$

The energy of the system is then expressed as a sum of the energies of the isolated fragments plus a contribution coming from their interaction. Following this line, the interaction energy could then be obtained within the supermolecule approach as:

$$\Delta E_{AB}^{\text{int}}(\mathfrak{R}) = E_{AB}(\mathfrak{R}) - E_A(\mathfrak{R}) - E_B(\mathfrak{R}), \qquad \text{(eq. 3.2)}$$

where it has been highlighted that the same set of nuclear positions has been employed in the calculation of the three quantities.[3, 6-8]

However, if we are interested in studying the process of complex formation, a new term has to be included, since the geometries of the species forming the complex can change as a consequence of the interaction and formation of the complex.[6-8] Therefore, a new term has to be included describing this effect,

$$E_{def}(\Re) = E_A(\Re) + E_B(\Re) - E_A(\Re_0) - E_B(\Re_0) \cdot \quad \text{(eq. 3.3)}$$

Along this work this term will be called the deformation energy,[9, 10] though in literature other names can be found for this quantity, such as relaxation energy (in the sense that if we think of dissociation, the geometry has to relax to that of the isolated fragments)[6-8] or preparation energy (in the sense that this is the energy needed to prepare the fragments in order to form the complex at the final geometry).[4]

The sum of these two quantities defines the complexation energy, the energy change observed when a complex is formed from the isolated, relaxed molecules that form it. The negative of this quantity is often called the binding energy, related to the energy needed for separating the complex into isolated fragments. Other effects such as zero point energy corrections or thermal effect are added as usual to each of the energies needed for obtaining the magnitudes described above. In summary, the complexation process can be formally divided into two steps: deformation plus interaction, so the complexation energy is obtained as:

$$\Delta E_{AB}^{complex}(\Re) = \Delta E_{Ab}^{\text{int}}(\Re) + E_{def}(\Re) \quad \text{(eq. 3.4)}$$

or

$$\Delta E_{AB}^{complex}(\Re) = E_{AB}(\Re) - E_A(\Re) - E_B(\Re) + \\ + E_A(\Re) + E_B(\Re) - E_A(\Re_0) - E_B(\Re_0) \quad \text{(eq. 3.5)}$$

and:

$$\Delta E_{AB}^{complex}(\Re) = E_{AB}(\Re) - E_A(\Re_0) - E_B(\Re_0) \quad \text{(eq. 3.6)}$$

So, the complexation energy could be obtained without making any reference to the interaction and deformation energies. However, it could be interesting to separate the complexation process into these two contributions in order to obtain a better interpretation of the system, especially when large deformation effects are present as consequence of important geometry changes. In such situations, a very large interaction could be hidden by opposing large deformation effects.[7, 8, 11, 12] Also, the practical calculation of complexation energies faces some problems, which make advisable to separate them into these two contributions as it will be commented below.

3.1.1. Basis Set Superposition Error

Any researcher dealing with the quantum chemistry calculation of interaction energies has faced the problem of Basis Set Superposition Error (BSSE).[3, 5, 6, 13] The problems appear when using (eq. 3.2) for obtaining the interaction energy. With this expression, the interaction energy of a dimer is obtained as a difference between three quantities.

As commented above, interaction energies are several orders of magnitude smaller than electronic energies, so the interaction energy, a small quantity, is obtained from the difference among large quantities. Therefore, it has to be ensured that all electronic energies are obtained coherently, and that any errors coming from the method employed will be properly cancelled out. However, a practical quantum chemistry calculation is performed with a finite basis set employed for constructing the wavefunction, and this is the origin of the problem.

Consider a dimer AB. When monomer A approaches monomer B in order to form the dimer AB, the energy of the dimer is artificially lowered because monomer A can employ the basis set centered onto the atoms of B in order to improve the description of its electron distribution, and the same applies for monomer B using basis functions centered in A. This energy lowering is not possible in the calculations in isolated monomers where only the basis set of each monomer is present. As indicated by van Duijneveldt,[14] this energy lowering as extra basis functions are employed is not an error in itself. The error comes from an inconsistent treatment of the monomers, which cannot take benefit from the basis set of the other as the distance becomes larger. This inconsistent treatment of the monomers as the distances change is the origin of the BSSE. Therefore, BSSE depends on the geometry of the systems, and a different value is obtained for each different arrangement of nuclei. It has to be taken into account that even if BSSE is removed completely, there still remain other errors associated to the method employed and the finite basis set used.

The usual procedure for correcting BSSE is the counterpoise method proposed by Boys and Bernardi, explained below.[15, 16] The uncorrected interaction energy or a dimer AB would be obtained as in eq 3.2, or:

$$\Delta E_{AB}^{\text{int}}(AB) = E_{AB}^{\text{dimer}}(AB) - E_{A}^{\text{dimer}}(A) - E_{B}^{\text{dimer}}(B)\,, \qquad \text{(eq. 3.7)}$$

where now the terms in parentheses indicate the basis set employed in the calculations and superscripts the geometry employed. These quantities are obtained in three separate calculations for the dimer, monomer A with its basis functions and monomer B with its basis functions. As commented above, the different basis sets employed in the calculations introduce BSSE, so the counterpoise correction consists on obtaining the three energies using the same basis set and energy in all calculations.

$$\Delta E_{AB}^{\text{int}}(AB) = E_{AB}^{\text{dimer}}(AB) - E_{A}^{\text{dimer}}(AB) - E_{B}^{\text{dimer}}(AB)\,. \qquad \text{(eq. 3.8)}$$

Now the energy of monomer A is obtained in a calculation with the basis set of B in the same positions as in the dimer, and the same applies to monomer B. In that way, the same basis set is employed in all calculations and BSSE is corrected. Therefore, BSSE can be defined as:

$$BSSE = E_{A}^{\text{dimer}}(A) + E_{B}^{\text{dimer}}(B) - E_{A}^{\text{dimer}}(AB) - E_{B}^{\text{dimer}}(AB) \qquad \text{(eq. 3.9)}$$

and is a positive quantity that destabilizes the complex. A lot of literature has been devoted to arguing whether counterpoise procedure overcorrects BSSE, since the whole basis set of B (occupied and virtual) is allowed to be used by B. The debate about the convenience of counterpoise correction is not closed, and very recently studies have suggested its inconvenience.[17-19] In any case, using counterpoise correction is common practice and the results seem to converge more smoothly to basis limit, so it will be employed throughout this work. It has to be mentioned, however, that using counterpoise correction increases significantly computation time, since it is geometry-dependent and it has to be calculated for each configuration of the nuclei of the system.

Therefore, the counterpoise-corrected complexation energy will be obtained as:

$$\Delta E_{AB}^{comp}(AB) = E_{AB}^{\text{dimer}}(AB) - E_{A}^{\text{dimer}}(AB) - E_{B}^{\text{dimer}}(AB) + \\ + E_{A}^{\text{dimer}}(A) + E_{B}^{\text{dimer}}(B) - E_{A}^{isolated}(A) - E_{B}^{isolated}(B) \quad \text{(eq. 3.10)}$$

Just for finishing this section it is important to indicate that, even though BSSE is most often associated to intermolecular interactions, the error is present in any electronic structure calculation, since the basis sets employed are finite.[20, 21] Therefore the energy obtained for an isolated molecule is also affected by BSSE taking as reference isolated atoms. Fortunately, test calculations indicate that intramolecular BSSE saturates quickly with basis set in molecular systems and the errors are negligible. Another different question is intramolecular BSSE in large molecules, where a part of the molecule can interact with another section of it. To date there is no recipe for treating these situations, the only option being using the largest basis set possible in order to reduce BSSE.[22-25]

3.1.2. Many-body effects

An interesting aspect of intermolecular interactions is the possibility of many-body effects.[26] In order to understand what is meant by many-body effects, the following expression for the total energy of a given system should be considered:[2-4, 27]

$$E_{ijk\ldots} = \sum_i E_i + \sum_i \sum_{j>i} E_{ij} + \sum_i \sum_{j>i} \sum_{k>i,j} E_{ijk} + \ldots \quad \text{(eq. 3.11)}$$

In this expression the energy of the system is expressed as sum over all fragments, plus a correction coming from all pairs of fragments, plus a correction for all trios, and so on. Taking into account the definition of interaction energy, the monomer term affects only to deformation, so the interaction energy in a cluster of several units is represented in a first approach as a pairwise sum of interaction between pairs of molecules, plus a correction involving trios, quartets, etc. For example, in a trimer and applying counterpoise correction, the interaction energy is given by:

$$\Delta E_{AB}^{\text{int}} = E_{AB}^{\text{trimer}}(ABC) - E_{A}^{\text{trimer}}(ABC) - E_{B}^{\text{trimer}}(ABC) - E_{C}^{\text{trimer}}(ABC) \,. \quad \text{(eq. 3.12)}$$

This interaction energy could be split in contributions for pair interactions, so:

$$\Delta E_{AB}^{\text{int}} = E_{AB}^{\text{trimer}}(ABC) - E_{A}^{\text{trimer}}(ABC) - E_{B}^{\text{trimer}}(ABC) \quad \text{(eq. 3.13)}$$

$$\Delta E_{AC}^{\text{int}} = E_{AC}^{\text{trimer}}(ABC) - E_{A}^{\text{trimer}}(ABC) - E_{C}^{\text{trimer}}(ABC) \quad \text{(eq. 3.14)}$$

$$\Delta E_{BC}^{\text{int}} = E_{BC}^{\text{trimer}}(ABC) - E_{B}^{\text{trimer}}(ABC) - E_{C}^{\text{trimer}}(ABC) \quad \text{(eq. 3.15)}$$

with the superscript stressing that the same geometry of the whole complex is employed. The total interaction energy of the trimer would be given by:

$$\Delta E_{ABC}^{\text{int}} = \Delta E_{AB}^{\text{int}} + \Delta E_{AC}^{\text{int}} + \Delta E_{BC}^{\text{int}} + E_{3-body} \,. \quad \text{(eq. 3.16)}$$

Thus, the three-body contribution to the interaction energy of the trimer would be:

$$E_{3-body} = \Delta E_{ABC}^{\text{int}} - \Delta E_{AB}^{\text{int}} - \Delta E_{AC}^{\text{int}} - \Delta E_{BC}^{\text{int}} \quad \text{(eq. 3.17)}$$

and a similar procedure could be employed for higher order terms.[10, 13, 28, 29] Though three-body effects are usually small in trimers, there are systems in which they become relevant, especially in hydrogen-bonded ones or where polarizing effects are important. In any case, as the number of molecules forming the cluster grows, the contribution of many-body effects becomes larger, being able to conditioning the behavior of the system. Another important aspect of many-body systems is that in our experience, even in cases where the BSSE for a given dimer is small, the error grows as molecules are included, so a proper treatment of BSSE is almost mandatory in clusters formed by a large number of molecules.

3.2. Wavefunction-based Methods

In the previous sections an introduction to the problems posed by the calculation of intermolecular interactions has been given. In the following ones a brief exposition of the most popular methods employed for obtaining electronic energies will be done, also stressing on the sources of error present in the typical electronic structure calculations.[20, 30-32]

3.2.1. The Hartree-Fock method

The Hartree-Fock method (HF) is the *ab initio* method which occupies the central position in electronic structure calculations. It is the easiest method to implement and the one with smallest computational cost. In the typical electronic structure calculations, the Born-Oppenheimer approach is assumed, as well as the non-relativistic Hamiltonian. In common approaches, a *N*-electron wavefunction is constructed as a combination of molecular orbitals which in turn are formed by combination of one-electron functions

(atomic orbitals). In order to account for the proper antisymmetry of the wavefunction, molecular orbitals are arranged into Slater determinants.[30]

The HF wavefunction is constructed from a single Slater determinant $\Phi_{HF} = |\chi_1 \chi_2 \cdots \chi_N|$, so products of *N* orthogonal molecular spin-orbitals, $\chi_1(\mathbf{x_1})$ $\chi_1(\mathbf{x_2})$... $\chi_1(\mathbf{x_N})$, are combined in an antisymmetric way. The HF electronic energy for a closed shell system is given by the following expression

$$E_{HF} = \left\langle \Phi_{HF} \middle| \hat{H} \middle| \Phi_{HF} \right\rangle = 2\sum_{a}^{N/2} \left\langle a \middle| \hat{h} \middle| a \right\rangle + 2\sum_{a<b}^{N/2} \left\langle ab \middle| ab \right\rangle - 2\sum_{a<b}^{N/2} \left\langle ab \middle| ba \right\rangle. \qquad \text{(eq. 3.18)}$$

As it can be seen in eq. 3.18, the HF energy comes from three terms: the sum of the one-electron energies of the MO, the Coulomb electron-electron interaction energy (*J*) and the exchange energy (*K*) due to the antisymmetry of the wavefunction,

$$E_{HF} = E^{(1)} + J - K\,. \qquad \text{(eq. 3.19)}$$

In order to obtain the HF energy of the ground state the variational principle is applied on a trying function, leading to the minimization of the energy with respect to the shape of the molecular orbitals. This procedure leads to the Hartree-Fock equations

$$\left(\hat{h} + \sum_{b}^{N/2} \left(2\hat{J}_b - \hat{K}_b \right) \right) \chi_a = \varepsilon_a \chi_a\,, \qquad \text{(eq. 3.20)}$$

$$\hat{f}\chi_a = \varepsilon_a \chi_a\,, \qquad \text{(eq. 3.21)}$$

where $\hat{h}$ is the one-electron operator, while the two-electron operators, Coulomb and exchange, contain the average electron repulsion on an electron described by the χ_a orbital. $\hat{f}$ may be considered as an effective Hamiltonian for a single electron suffering the influence of the nuclear field and the averaged Coulomb and exchange repulsion of the other electrons.

Solving the HF equations produces a set of molecular orbitals with energies ε_a, which are filled up with the electrons of the system. The wavefunction is represented as a single determinant constructed from these occupied orbitals. The HF method is able to recover more than 99% of the electronic energy in many systems, but in most cases is unsuitable as a consequence of some of the approximations included in the model. The use of a single determinant wavefunction together with the averaged description of electron-electron interaction restricts the applicability of the HF method.

As it is commonly known, the main problem of HF is that it treats electrons in a mean field approach, thus failing to describe the correlated motion of electrons. Thus, it is

widespread practice to denote as correlation energy the difference between the exact result and the HF energy for a given basis set,[32, 33]

$$E_{corr} = E_{exact} - E_{HF} \,. \qquad \text{(eq. 3.22)}$$

Though correlation energy is normally a small fraction of the electronic energy, experiences remarkable changes in chemical processes and is also a key ingredient to understand the intermolecular interactions. Therefore, the electron correlation is generally no negligible and should be considered for all molecular systems regardless of their size. It is worth noting that HF already describes the correlation of the electrons with the same spin as a consequence of the antisymmetry of the wavefunction, so correlation energy deals with the correlated motion of electrons with different spin.[20, 33] The usual way of introducing electron correlation in the model is by using more than one Slater determinant in constructing the wavefunction.[30, 32] Therefore, the wavefunction is now expressed as a sum of Slater determinants (usually a very large number) whose contribution depends on the coefficients of the expansion,

$$\Psi = \sum_k C_k \psi_k \,. \qquad \text{(eq. 3.23)}$$

Each of the terms of the sum is a *N*-electron Slater determinant constructed by replacing one or more occupied spinorbitals in the HF determinant by virtual ones. This is the idea behind Configuration Interaction methods, which leads to the exact solution (FCI) within a given basis set if all the possible excited configurations are included. However, using FCI is unaffordable in practical calculations and truncated expansions as to include only double or triple excitations face the problem of size inconsistency, which make this kind of methods unpractical.

Therefore, other methods approaching to the FCI solution are needed behaving properly with system size. The two most common among these methods are exposed in the following sections.

3.2.2. Many Body Perturbation Theory (MPn)

The simplest of the wavefunction methods employed for obtaining electron correlation is based on perturbation theory.[31, 32] The Hamiltonian is divided into a reference Hamiltonian plus a perturbation, which in the case of the Möller-Plesset method becomes:

$$\hat{H} = \hat{H}_0 + \hat{V} \,, \qquad \text{(eq. 3.24)}$$

being $\hat{H}_0 = \sum_i \hat{f}_i$ the zeroth-order Hamiltonian representing a model of independent electrons and the perturbation being given by the difference between the real electron-electron repulsion and the HF averaged one $\hat{V} = \hat{H} - \sum_i \hat{f}_i = \hat{H} - \hat{H}_0$.

The MP method expands the total energy *E* and the exact wavefunction for *I*-th electronic state as:

$$\Phi_I = \Phi_I^{(0)} + \Phi_I^{(1)} + \Phi_I^{(2)} + \ldots \quad \text{(eq. 3.25)}$$

$$E_I = E_I^{(0)} + E_I^{(1)} + E_I^{(2)} + \ldots \quad \text{(eq. 3.26)}$$

Therefore, the MP method allows estimating the exact solution by including a series of terms of increasingly higher order that, ideally, would approach the FCI solution. After different transformations, expressions can be derived for the different corrections to the wavefunction and electronic energy (the energy to *n+1* order is obtained after the wavefunction to order *n* is derived).

To first order the MP method matches the HF method. Therefore, the first contribution to the correlation energy of a system is the second order energy term, to be obtained from the correction to the first order wavefunction. The final expression for the MP2 contribution to the electronic energy is given by:

$$E_0^{(2)} = E_{MP2} = \sum_{a<b}^{N} \sum_{r<s}^{V} \frac{\left| \langle ab \| rs \rangle \right|^2}{\varepsilon_a + \varepsilon_b - \varepsilon_r - \varepsilon_s}. \quad \text{(eq. 3.27)}$$

That is, the correlation contribution at the MP2 level is obtained from a sum of contributions coming from integrals involving doubly-excited determinants. Within this approach, around 80 % of the total correlation energy can be recovered. Going further in the perturbation to order 3 (MP3) also involves only double excitations, whereas to fourth order contributions from single, double, triple and quadruple excitations are involved. Of course, as the perturbation order is increased the accuracy and the computational cost also increase. Therefore, only MP2 is employed in routine calculations, whereas MP3 hardly offers any advantage. More accurate results can be obtained at the MP4 level, but with an important increase in computational cost. Also, MP4 calculations have becoming scarcer with the coming of coupled cluster methods. MP2, the cheapest approach to correlation, has also seen its presence diminished with the growing of Density Functional Theory methods (see below).

In any case, the MP2 method still constitutes an interesting choice in the field of intermolecular interactions since, at a moderate cost, includes correlation and more specifically dispersion. This latter fact is a clear advantage of the MP2 approach over

common density functional theory methods which are not able to include dispersion properly.

Despite the advantages of MP2 in treating intermolecular interactions, it has been observed that the results tend to be overestimated, especially in complexes dominated by dispersion effects, such as stacked aromatic clusters.[34-37] Trying to correct the inaccuracies in the behavior of the MP2 method, Grimme proposed an empirical modification which could improve the results obtained.[38, 39] In this approach, called the Spin Component Scaled MP2 method (SCS-MP2), an empirical scaling of the contributions to correlation coming from same-spin electrons and different-spin electrons is performed. Thus, the contributions coming from equal spin electron pairs are scaled by a factor or 0.33, whereas those coming from different spin pairs are scaled by 1.20. Therefore, the SCS-MP2 energy is given by:

$$E_{SCS-MP2} = E_{HF} + 1.20E_{E2}^{\alpha\beta} + 0.33E_{E2}^{\alpha\alpha} . \qquad \text{(eq. 3.28)}$$

Applying this scaling the results show an improvement over the native MP2 method.[39-45] However, the scaling is performed for a given basis set and it has been proposed that the parameters could be employed in order to also take into account basis set incompleteness. Therefore, the MP2 results are scaled in order to obtain the best fit to a set of benchmark complexes. This has been the approach followed by several authors like Hill and Platts[46] or Distasio and Head-Gordon[47]. In the case of the parameterization proposed by Hill and Platts (SCSN-MP2), the coefficients are 0.00 for different spin pairs and 1.76 for same spin pairs:

$$E_{SCSN-MP2} = E_{HF} + 0.00E_{E2}^{\alpha\beta} + 1.76E_{E2}^{\alpha\alpha} . \qquad \text{(eq. 3.29)}$$

Also, extensions of this approach to other methods have been proposed.[48-53] In any case, these approaches can be employed in order to estimate interaction energies at a moderate cost with quite good results, but careful checking should be done because the quality could change quite erratically depending on the system studied.

3.2.3. Coupled Cluster

Coupled cluster constitutes the nowadays reference method in order to obtain accurate results. In fact, results obtained at the CCSD(T) level are considered as the actual “gold standard” of electronic structure methods. Coupled cluster methodology offers an alternative way of approaching the FCI solution for a given system. The main difference between CI and CC methods is that the latter leaves the linear combination approach to the wavefunction and instead uses an exponential antsazt.[20, 31, 32]

The starting point of both CI and CC can be expressed in a similar way, with a wave operator that is able to transform the reference HF wavefunction into the exact wavefunction for the system

$$|\Phi_0\rangle = \hat{\Omega}_0 |\psi_0\rangle \cdot \quad \text{(eq. 3.30)}$$

$\hat{\Omega}_0$ is the wave operator, that in CI is a linear operator, but in CC is an exponential one:

$$\hat{\Omega}_0^{CI} = 1 + \hat{C}_1 + \hat{C}_2 + \hat{C}_3 + \ldots \quad \text{(eq. 3.31)}$$

$$\hat{\Omega}_0^{CC} = \exp(\hat{T}) = 1 + \hat{T} + \frac{1}{2}\hat{T}^2 + \frac{1}{6}\hat{T}^3 + \ldots \quad \text{(eq. 3.32)}$$

$$\hat{T} = \hat{T}_1 + \hat{T}_2 + \hat{T}_3 + \ldots \cdot \quad \text{(eq. 3.33)}$$

More explicitly, the expansion of the exponential will be (only singles and doubles included):

$$\hat{\Omega}_0 = 1 + \hat{T}_1 + \hat{T}_2 + \frac{1}{2!}\hat{T}_1^2 + \frac{1}{3!}\hat{T}_1^3 + \frac{1}{4!}\hat{T}_1^4 + \frac{1}{2!}\hat{T}_2^2 + \hat{T}_1\hat{T}_2 + \frac{1}{2!}\hat{T}_2\hat{T}_1^2 + \ldots . \quad \text{(eq. 3.34)}$$

The *C* and *T* operators are excitation operators that change one, two, …. occupied spinorbitals by virtual ones. For example:

$$\hat{T}_2 \psi_0 = \sum_{\substack{a<b \\ r<s}} t_{ab}^{rs} \psi_{ab}^{rs} , \quad \text{(eq 2. 35)}$$

where t_{ab}^{rs} are the coefficients (or amplitudes) to be determined in CC calculations.

The great advantage of CC methods over CI ones is that the exponential antsazt employed in CC methods ensures that the method will be size consistent, thus avoiding the major problem faced by CI calculations. Usually, CC methods are employed truncated up to a given excitation order, typically including single and double excitations, CCSD. Though amplitudes are only calculated for singles and doubles, the exponential expansion introduces estimations of higher-order excitations expressed as products of singles and doubles. For example, quadruple excitations are not included, but their effect is estimated by products of doubles. Therefore, to a given truncation level CC behaves better than CI since these so-called disconnected clusters include the effect of higher excitations. CI methods, on the other hand, only include excitations up to the truncation level.

The most common choice in present calculations is to employ CCSD method combined with a suitably flexible basis set. Including triple excitations implies a huge computational effort so CCSDT is only applicable to small systems. Most often, after the CCSD solution has been reached, a perturbative estimation of the triples is added in the so-called CCSD(T) method. That way the effect of triple excitations (often very important) is included without needing to solve the full CCSDT equations. In any case,

inclusion of triples is also a demanding task, so CCSD(T) can only be used for systems with moderate size.

Nowadays, results obtained at the CCSD(T) level with a large basis set are considered as the golden standard of quantum chemistry calculations, especially in the case of intermolecular interactions dominated by dispersion effects. Very recently, results obtained with CCSD(T) have been compared with those obtained with higher order CC calculations such as CCSDT[Q] for a set of complexes, confirming the very good behavior of CCSD(T).[54-56]

3.2.4. Errors in Wavefunction-based Methods

From previous sections it is clear that a typical calculation with a wavefunction-based method is affected by two sources of error as depicted in Figure 3.2. When comparing the result of an actual calculation employing a post-HF method with the exact solution (within Born-Oppenheimer approximation and non-relativistic Hamiltonian) an apparent error is observed coming from two different sources.[21]

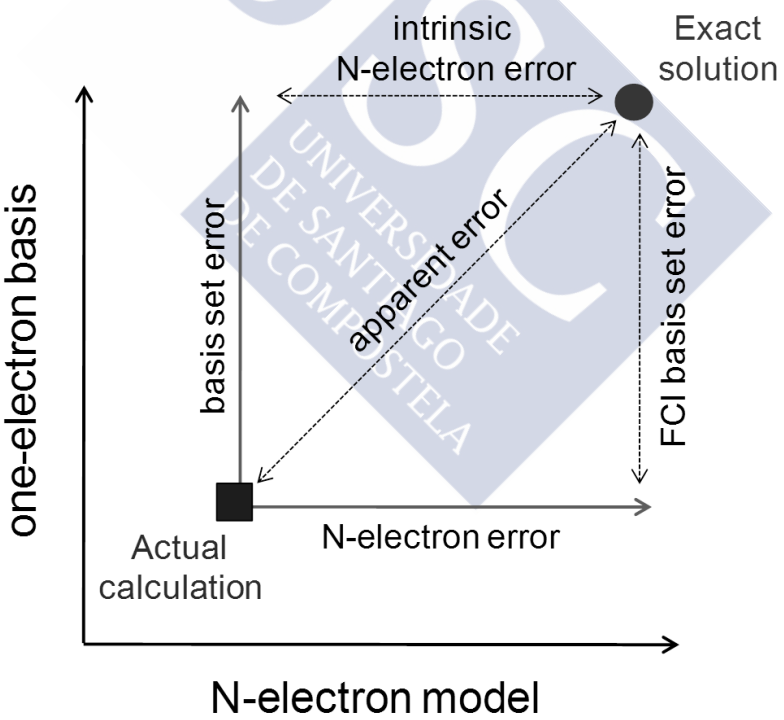


Figure 3.2. Representation of the errors associated to electronic structure calculations.

Considering that FCI solution is the exact solution for a given basis set, an error is introduced due to the deficiencies of our method for describing correlation. MPn and CC methods are different approaches for approximating to the FCI solution, but in actual calculations both MPn and CC have to be truncated somehow, thus introducing an error as compared with the FCI result (the *N*-electron error in Figure 3.2). In any case, the methods currently employed for including electron correlation already show a very good performance, so the N-electron error can be reduced including higher orders of MPn or CC, of course at the cost of much more expensive calculations.

The other source of error is related with the set of one-electron basis functions employed for constructing the *N*-electron wavefunction. That is, for a given *N*-electron model (MP2, MP4, CCSD, …) there is an error associated with the basis of one electron functions employed, the basis set. When the result of an actual calculation is compared with the same calculation employing a complete basis set, a difference is observed corresponding to the basis set error. In order to reduce this error, larger basis sets have to be employed, ideally reaching the limit of complete basis set. When this limit is reached, there still remains an error related with the deficiencies of our *N*-electron model as commented above.

Therefore, in order to obtain accurate results from a wavefunction based method, one has to take care in order to reduce both sources of errors, thus trying to employ an adequate representation of correlation by means of a good N-electron model, combined with a one-electron basis set large enough in order to reduce the errors associated to incompleteness of the basis set. That is, one has to use the obvious choice of a good correlation method combined with a large basis set.

The choice of *N*-electron model and basis set is of course conditioned by the computing resources since an increment in the quality of any of them has a deep impact on the computation time. The currently used *N*-electron models perform quite a good job approaching the FCI results, including correlation energy to a great extent. In practical calculations, however, one is normally reduced to the use of MP2 if the size of the system is moderate, or to CCSD(T) if the size of the system and resources allow it. As commented above, the use of CCSD(T) combined with a flexible basis set is nowadays considered as the gold standard in quantum chemistry calculations. As indicated in a recent paper, CCSD(T) to the basis limit is able of reproducing the interaction energies of a set of complexes within 1.5% error.[54] In summary, as for the *N*-electron model, we are limited in the practice to choose between the practical and cheapest MP2 and the more accurate and demanding CCSD(T). Other intermediate options could be of interest in particular problems.

The error associated to the one-electron basis set deserves a little more attention, so it will be analyzed in the following section.

3.2.4.1. Extrapolating to basis limit

The problem of the error associated to the one-electron basis set is that it converges very slowly as the size of the basis set is increased, so very large basis sets are needed to approach the limiting value of complete basis set (CBS). Figure 3.3 represents the convergence of the correlation energy of a water molecule as the size of the basis set is increased. It can be observed that the convergence is very slow, and even with the enormous cc-pV6Z basis set the result is still far from the limit. This bad convergence with respect to the one-electron basis set is related with the inability of the usual one-electron basis function to reproduce the electron-electron cusp.[21, 57, 58]

In any case, in practical calculations the largest basis sets to be employed as routine are cc-pVQZ or aug-cc-pVTZ or similar, so it can be observed from Figure 3.3 that the results will be far from the CBS limit. It has to be taken into account that when computing energy differences as for example in obtaining interaction energies part of these errors can be cancelled and the results could be nearer the limiting value.

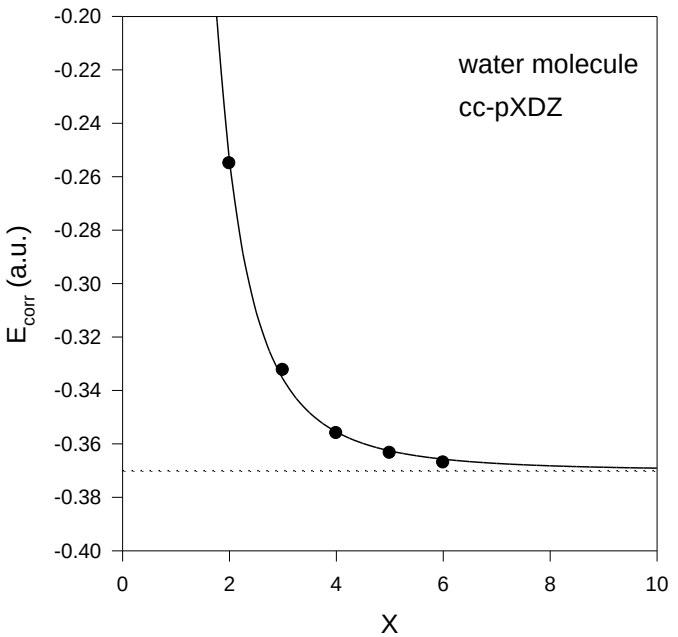


Figure 3.3. Variation of the correlation energy in water molecule as the size of the basis set is increased.

The solutions to this problem depend on using very large basis sets, which is impractical or, more recently, by using explicitly correlated methods, which tend more quickly to the limit than the standard ones.[57, 58] However, there is an intermediate solution used quite often which passes by extrapolating the results obtained with moderate-sized basis set in order to obtain an estimation of the limiting value.[59-65]

These extrapolation schemes are only applicable if the behavior of the energy as the basis set grows is smooth so it can be fitted to a function and then obtain the limiting value. Thus, this kind of extrapolation schemes are mostly limited to well-balanced basis set as the correlation consistent cc-pVXZ family proposed by Dunning.[66] In this respect, one should distinguish between the behavior of HF energies and the contributions coming from correlation.

In the case of HF energies, it has been found that in atoms the energies approximately follow an exponential behavior.[20, 57, 67] Assuming that this exponential decay can be also employed in molecules, an often-employed extrapolation scheme assumes that the HF energy behaves as:

$$E_X^{HF} \approx E_{CBS}^{HF} + A\exp(-BX)\,. \qquad \text{(eq. 3.36)}$$

So, if three calculations are performed with correlation consistent basis set of increasing X, the limiting value could be estimated as:

$$E_{CBS}^{HF} \approx \frac{E_X^{HF} - bE_{X-1}^{HF}}{1-b}\,;\; b = \exp(-B) = \frac{E_X^{HF} - E_{X-1}^{HF}}{E_{X-1}^{HF} - E_{X-2}^{HF}}\,. \qquad \text{(eq. 3.37)}$$

However, the need for three calculation of increasing size is uncomfortable, so other two-point extrapolation schemes have been devised. For example, Karton and Martin proposed the following two-point procedure:[68, 69]

$$E_X^{HF} = E_{CBS}^{HF} + A(X+1)\exp(-9\sqrt{X})\,. \qquad \text{(eq. 3.38)}$$

In any case, HF energies converge quite quickly with the basis set, and especially when energy differences are considered, as interaction energies. Thus, it is usually found that obtaining the HF interaction energies with a basis set of cc-pVTZ quality is often enough since the errors associated to correlation are normally larger.

When dealing with correlation energies, the dependency on the basis set size is still more important, so a good estimation of correlation energies often demands very large basis sets. Furthermore, the convergence of correlation energy with the basis set size is even slower than in the HF case, so larger basis sets would be needed, as represented in Figure 3.3. Fortunately, there are extrapolation schemes that seem to perform reasonably well allowing a good estimation of the correlation energy at a moderate cost. In He atom it has been observed that the error in correlation energy varies as

$\Delta E_N \approx cN^{-3}$, being *N* the principal quantum number.[57] That is, there is a cubic decay of the correlation energy as larger basis sets are included. Assuming a similar behavior in molecules and identifying *N* with the *X* ordinal in Dunning basis sets,[59, 60, 63] it can be assumed that the correlation energy changes as:

$$E_{CBS} \approx E_X + AX^{-3}. \quad \text{(eq. 3.39)}$$

This expression contains only two unknowns and therefore can be solved if two calculations are performed for obtaining the correlation energy,

$$E_{CBS} = E_X + AX^{-3}, \quad \text{(eq. 3.40)}$$

$$E_{CBS} = E_Y + AY^{-3}. \quad \text{(eq. 3.41)}$$

So:

$$E_{exact} = \frac{X^3 E_X - Y^3 E_Y}{X^3 - Y^3}. \quad \text{(eq. 3.42)}$$

Of course the result will depend on the values used for X and Y, but it has been found that a T-Q extrapolation employing cc-pVXZ basis sets already gives results better than the direct calculation employing a cc-pV6Z basis set. In practical calculations in systems of moderate size, one is usually limited to perform T-Q extrapolations with the cc-pVXZ basis set or D-T ones with the aug-cc-pVXZ basis sets.

3.2.4.2. Obtaining benchmarking values

In the previous section it has been exposed how applying an extrapolation scheme to correlation energies there is an affordable route for obtaining correlation values at the CBS limit. However, this kind of extrapolation is still quite demanding so it is usually performed with MP2 estimations of the correlation energy. Therefore, even when the MP2 values are obtained at the basis limit, there still remains an error associated to the low quality of the *N*-electron model employed.

The straightforward solution would be employing a better model, say CCSD(T), in order to obtain better estimations of the correlation energy, and then apply an extrapolation scheme. This option, though formally appropriate, is very demanding, and for systems of moderate size cannot be applied in routine calculations due to the high cost of the CCSD(T) calculations with the larger basis set. Therefore, other approaches have been devised in order to estimate the CCSD(T)/CBS values but with a reduced computational cost, many of them proposed by Hobza. Hobza and collaborators observed that even though the correlation energy contributions to the interaction energy of a dimer are very different with MP2 and CCSD(T), the differences between both methods were pretty independent of the basis set size.[52, 70, 71] Therefore, the

CCSD(T)/CBS limiting value for the correlation contribution to the interaction energy could be obtained as:

$$\Delta E_{CCSD(T)}^{corr,CBS} = \Delta E_{MP2}^{corr,CBS} + \left(\Delta E_{CCSD(YT)}^{corr,smallbasis} - \Delta E_{MP2}^{corr,smallbasis} \right). \quad \text{(eq. 3.43)}$$

In this expression, the MP2 contribution to the correlation energy is estimated to basis limit with the extrapolation procedures explained above, and the result is corrected from the inefficiencies of the *N*-electron model, by using a CCSD(T) calculation with a small basis set, and assuming that the difference between CCSD(T) and MP2 is fairly constant. An alternative way of understanding eq. 3.43 is by considering that the correlation contribution is obtained at the CCSD(T) level with a small basis set, and the basis set incompleteness error is estimated at the MP2 level, eq. 3.44.

$$\Delta E_{CCSD(T)}^{corr,CBS} = \Delta E_{CCSD(YT)}^{corr,smallbasis} + \left(\Delta E_{MP2}^{corr,CBS} - \Delta E_{MP2}^{corr,smallbasis} \right) \quad \text{(eq. 3.44)}$$

In any case, this procedure is commonly used in order to obtain benchmark values for the interaction energies of complexes. It should not be forgotten however that errors are still present, depending on the size of the small basis set employed for the CCSD(T) calculation. Applying this approach, several dataset have been constructed which are widely used as reference for developing approximate methods.[72-75]

Still within this approach, for moderate-sized systems the bottleneck of the calculations is the CCSD(T) calculation that, even with a basis set of aug-cc-pVDZ quality can be very demanding. Thus, Hobza and Rezak proposed an alternative way of estimating the correction to the MP2/CBS value avoiding the expensive CCSD(T) calculation. The first of these proposals (MP2.5)[76] and the subsequent refinement (MP2.X)[77] substitute the CCSD(T) calculation by cheaper MP3 ones. Thus in the MP2.X approach, the correlation contribution to the interaction energy is obtained as:

$$\Delta E_{CCSD(T)}^{corr,CBS} = \Delta E_{MP2}^{corr,CBS} + C\left(\Delta E_{MP3}^{corr,smallbasis} - \Delta E_{MP2}^{corr,smallbasis} \right). \quad \text{(eq. 3.45)}$$

Hobza and Rezak introduced an empirical scaling coefficient obtained by fitting to the CCSD(T)/CBS estimates of a set of complexes of different nature. With this approach it has been observed that the accuracy of the MP2.X results is almost independent of the basis set employed for the MP3 calculation given a proper *C* coefficient. Thus, modest basis sets as 6-31G* can be employed giving results pretty similar to those obtained by performing an actual CCSD(T) calculation.[78, 79] As a consequence, the MP2.X procedure allows saving computational resources by using the cheaper MP3 method, but also allowing the use of smaller basis set in order to estimate the *N*-electron correction to the MP2 limit.

3.3. Density Functional Theory Methods

Density Functional Theory (DFT) is an alternative to methods based on the calculation of the wavefunction as the goal for the description of the system and its properties. In the last decades DFT has been developed intensely because it becomes very useful for a lot of different kind of systems due to its advantageous relation between the quality of the results and computational cost. Like post-HF methods, DFT includes the electronic correlation term but with a cost similar to HF calculations.[32, 80]

The foundation of DFT is based on the idea that the information that can be extracted from the wavefunction can also be obtained from the electronic density. Whereas the energy in wavefunction-based method is a functional of the wavefunction (*N* spatial coordinates + *N* spin coordinates in a *N*-electron system), which is dependent on the number of atoms, in DFT the energy is a functional of the electron density, so it only depends on the three spatial coordinates

$$\mathrm{E} = \mathrm{f}\left[\rho(\mathrm{r})\right], \qquad \text{(eq. 3.46)}$$

In order to work with the density functional theory it is necessary to apply the first theorem of Hohenberg and Kohn (1964).[32, 81]

> *"Any observable of a stationary non-degenerate ground state can be calculated, exactly in theory, from the electron density of the ground state. In other words, any observable can be written as a functional of the electron density of the ground state".*

In a system with *M* nuclei of charge Z_a located in R_a, the interaction of *N* electrons of the system with the *M* nuclei can be described through V operator.

$$\hat{V} = \sum_i \sum_a \frac{-Z_a}{|\vec{r}_i - \vec{R}_a|} = \int \sum \frac{-Z_a}{|\vec{r}_i - \vec{R}_a|} \sum_i \delta(\vec{r} - \vec{r}_i) d\vec{r} = \int \rho(\vec{r}) \vartheta(\vec{r}) d\vec{r}\ , \qquad \text{(eq. 3.47)}$$

where $\vartheta(\vec{r})$ is the effective potential of an electron and $\rho(\vec{r}) = \sum_i \delta(\vec{r} - \vec{r}_i)$ is the operator for the electronic density. The rest of the operators in the Hamiltonian depend exclusively on the coordinates of the electrons, so their expressions are equal in all systems and only the number of electrons changes. Therefore, the total electronic energy depends only on the total number of electrons (*N*) and external potential $\vartheta(\vec{r})$. In addition to this, other essential characteristic of the first Hohenberg-Kohn theorem is that the relationship between energy and density is univocal. Therefore, if there exist two different external potentials that generate the same electronic density, then both potentials must be the same.

On the other hand, the second Hohenberg-Kohn theorem provides a variational principle:[32, 81]

"The electron density of a non-degenerate ground state can be calculated, exactly in theory, determining the density that minimizes the energy of the ground state".

The second Hohenberg-Kohn theorem establishes the existence of a variational principle for the energy, verifying that for a test electronic density $\rho(\vec{r})$, the energy for such system is larger than or equal to the energy for the real ground state of the system. So, the energy reaches a minimum value for the exact ground state.

$$E[\rho(\vec{r})] \geq E_0[\rho_0(\vec{r})]. \qquad \text{(eq. 3.48)}$$

Therefore, the differential equation

$$\frac{\delta E[\rho(\vec{r})]}{\delta \rho(\vec{r})} - \mu = 0 \qquad \text{(eq. 3.49)}$$

Is fulfilled, in which the Lagrange multiplier μ ensures that the electronic density is normalized for *N* electrons. Therefore, the density can be variationally optimized in order to approach the real ground state density.

Starting from these two fundamental theorems, the main goal of the DFT methods consists on designing functionals that connect energy and electronic density but, unfortunately, Hohenberg-Kohn theorems do not establish how the exact connection between both magnitudes is. In order to solve this problem, Kohn and Sham developed a practical application of this theory through a method with a formulation similar in structure to the Hartree-Fock method.

3.3.1. Kohn-Sham procedure

A general expression for the energy taking into account the Born Oppenheimer approximation could be the next one: [32, 80]

$$E[\rho] = T[\rho] + E_{ne}[\rho] + E_{ee}[\rho]. \qquad \text{(eq. 3.50)}$$

The energy is divided into three parts: kinetic energy $T[\rho]$, attraction between the nuclei and electrons $E_{ne}[\rho]$ and electron-electron repulsion $E_{ee}[\rho]$ (the nuclear-nuclear repulsion is a constant within the Born-Oppenheimer approximation). Furthermore, similarly as in Hartree-Fock theory, the $E_{ee}[\rho]$ term may be divided into a Coulomb and Exchange part $J[\rho]$ and $K[\rho]$, though implicitly including correlation energy in all terms. The $E_{ne}[\rho]$ and $J[\rho]$ functionals are given by their classical expressions, where the ½ factor in $J[\rho]$ allows the integration to run over all space for both variables.

$$E_{ne}[\rho] = -\sum_a \int \frac{Z_a \rho(\vec{r})}{|\vec{R}_a - \vec{r}\,|} d\vec{r}\,, \qquad \text{(eq. 3.51)}$$

$$J[\rho] = \frac{1}{2}\frac{\int\int \rho(\vec{r})\rho(r')}{|\vec{r} - r'|} d\vec{r} d\vec{r}' . \qquad \text{(eq. 3.52)}$$

The basic idea in the Kohn-Sham formalism is splitting the kinetic energy functional into two parts, one which can be calculated exactly and a small correction term. In the real molecular system, the electronic density and the kinetic energy will be written as:

$$T[\rho] = \sum_i \left\langle \varphi_i \left| -\frac{1}{2}\nabla_i^2 \right| \varphi_i \right\rangle , \qquad \text{(eq. 3.53)}$$

$$\rho = \sum_i \left\langle \varphi_i \right\rangle^2 . \qquad \text{(eq. 3.54)}$$

Kohn-Sham formalism establishes then the calculation of the kinetic energy under the assumption of a reference system of non-interacting electrons *S* (in the same sense as HF orbitals in wave mechanics describe non-interacting electrons) but under an external potential such that the density is the same as in the real system. The solution, within the Born-Oppenheimer approximation, is provided by Schrödinger equation, and the system could be described by a Slater determinant of molecular orbitals ϕ_i which have the following exact kinetic energy:

$$T_S[\rho] = \sum_i \left\langle \phi_i \left| -\frac{1}{2}\nabla_i^2 \right| \phi_i \right\rangle , \qquad \text{(eq. 3.55)}$$

$$\rho_S = \sum_i \left\langle \varphi_i \right\rangle^2 . \qquad \text{(eq. 3.56)}$$

Of course, the electrons interact among themselves and the previous equations do not provide the correct total kinetic energy. However, just as HF theory provides ~99% of the correct answer, the difference between the exact kinetic energy and that calculated by assuming non-interacting electrons is small. The remaining kinetic energy not included in $T_S[\rho]$ is absorbed into an exchange-correlation term, and a general DFT expression for the energy can be written as:

$$E_{DFT}[\rho] = T_S[\rho] + E_{ne}[\rho] + J[\rho] + E_{xc}[\rho]. \qquad \text{(eq. 3.57)}$$

If $E_{xc}[\rho]$ is expanded up, it becomes easier to understand which are the contributions to this exchange-correlation energy.

$$E_{xc}[\rho] = (T[\rho] - T_S[\rho]) + (E_{ee}[\rho] - J[\rho]). \qquad \text{(eq. 3.58)}$$

The problem is similar to that encountered in wave mechanics HF theory: determining a set of orthogonal orbitals that minimize the energy. The electron density is expressed

as a linear combination of basis functions similar in mathematical form to the HF orbitals. A Slater determinant is then formed from these functions, called Kohn-Sham orbitals. It is the electron density from this determinant the one employed to compute the energy. Since the J and E_{xc} functionals depend on the total density, a determination of the orbitals involves an iterative sequence.

The major problem in DFT is deriving suitable formulas for the exchange-correlation term. If the exact E_{xc} were known, DFT would provide the exact total energy, including electron correlation. Therefore, the difference between DFT methods is the choice of the functional form of the exchange-correlation energy. There is little guidance from theory about how such functional should be chosen, and consequently many different alternatives have been proposed. The great developing in the last years of DFT methods has been focused in finding suitable functionals because, as mentioned, the exact density functional is not known. Therefore, there is a whole list of different functional depending on the approximations assumed in each case that may provide advantages or disadvantages.

Designing the different functionals it is customary to separate E_{xc} into two parts, a pure exchange and a correlation

$$E_{xc}[\rho] = E_x[\rho] + E_c[\rho]. \qquad \text{(eq. 3.59)}$$

Density functionals can be broken down into several classes. The simplest is called the Xα method. This type of method includes electron exchange but not correlation. It was introduced by J. C. Slater who, while attempting to make an approximation to Hartree-Fock unwittingly discovered the simplest form of DFT.

3.3.2. Functional types

The simplest approximation to the complete exchange plus correlation problem is the one called the local density approximation (LDA). In the Local Density Approximation it is assumed that the density can be treated locally as a uniform electron gas or, equivalently, that the density is a slowly varying function with position. The correlation energy of a uniform electron gas has been determined by Monte Carlo methods for a number of different densities, and analytical interpolation formulae have been constructed by Vosko, Wilk and Nusair $E_c^{VWN}[\rho]$. The combination with the functional $E_x^{LDA}[\rho]$ results in the SVWN approximation. The LDA approximation in general underestimates the exchange energy by 10%, thereby creating errors which are larger than the whole correlation energy. Electron correlation is furthermore overestimated, often by a factor close to 2, and bond strengths are as a consequence overestimated. Despite the simplicity of the fundamental assumptions, LDA methods are often found to provide results with an accuracy similar to that obtained by wave mechanics HF methods.[32, 80]

A more complex set of functionals depends on the electron density and its gradient, constituting the so-called gradient-corrected methods. Generalized gradient approach (GGA) methods do not consider the electronic density as a uniform electron gas, so electron density and the suitable density gradient are taken into account. Thus, the change on the electron density with respect to the position is integrated in the calculation. GGA methods are also sometimes referred to as non-local methods. It is usual that these methods take LDA functional as starting point and gradient corrections are added. For instance, Becke proposed a widely used correction for the exchange part of the functional, $E_x^{B88}[\rho]$ including a *β* parameter determined by fitting to known atomic data. On the other hand, there have been various gradient corrected functional forms proposed for the correlation energy. One popular functional is due to Lee, Yang and Parr, $E_c^{LYP}[\rho]$, where parameters are determined by fitting to data for helium. The combination of these exchange and correlation functionals constitutes the B-LYP functional.[82-84]

Hybrid methods correct the functionals above by including part of the exact exchange energy as in HF, E_x^{HF}, in the exchange part of the functional. This method is based in the fact that when a uniform gas of non-interacting electrons is considered there is no correlation energy, only exchange energy. Furthermore, since the exact wavefunction in this case is a single Slater determinant the exchange energy is exactly that given by HF theory. If the KS orbitals are identical to the HF orbitals, the exact exchange is precisely the exchange energy calculated by the HF method. Exchange energy could be written as a suitable combination of LDA, exact exchange and a gradient correction term. The correlation energy may similarly be taken as the LDA formula plus a gradient correction term.

$$E_{xc}^{B3} = (1-a)E_x^{LDA} + aE_x^{HF} + bE_x^{B88} + E_c^{LDA} + c\Delta E_c^{GGA} \quad \text{(eq. 3.60)}$$

The *a*, *b* and *c* parameters are determined by fitting to experimental data and depend on the form chosen for E_c^{GGA}. This B3 procedure has been generalized to include more fitting parameters, though the improvement is rather small. The combination of the B3 exchange functional with the Lee-Yang-Parr correlation functional constitutes B3LYP, one of the most famous functionals of DFT and therefore one of the most employed. [83-85]

To go beyond the generalized gradient approximation and the non-separable gradient approximation, it is necessary to add more ingredients to the functional form, and the most popular way to do so has been to add either the second derivatives (Laplacian) of the spin densities or the spin-labeled non-interacting kinetic energy densities. Functionals incorporating either of these ingredients receive the label “meta”. This kind of semilocal functionals are computationally efficient and they are of special interest because they can achieve high simultaneous accuracy for atoms, molecules, solids and

surfaces at equilibrium. Among these meta-GGA functionals a relevant place is occupied by the set of functionals developed by Truhlar and coworkers and known as the Minessota functionals, which have demonstrated that can be competitive with popular approaches as B3LYP for a wide range of chemical systems.[86-94]

Focusing on the M06 family, this set is composed by four functionals that have similar functional forms for the DFT part, but each has parameters optimized to be used with a different percentage of HF exchange.[86-88] The functionals go from M06-L without HF exchange (a non-hybrid functional) to M06-HF with 100% of HF exchange. In between are M06 with 27% of HF exchange, leading to a well-balanced functional for overall good performance for chemistry, and M06-2X with 54% HF exchange, with good performances in all areas of chemistry including thermochemistry and reaction kinetics, but excluding multireference systems such as many systems containing transition metals. In fact M06-2X was reported as the first functional with overall better accuracy than B3LYP.

In DFT, a double hybrid functional includes a certain amount of HF exchange and PT2 correlation (thus "*double*" hybrid). This idea was first proposed by Donald Truhlar in 2004 and the more well-known by Stefan Grimme in 2006.[95, 96] In a certain way it is the fifth step in Jacob's ladder for DFT, where unoccupied KS orbitals are included in the calculation in a similar way as in MP2. The perturbational correction corrects for HF deficiencies while improving the self-interaction error. In this way kinetic barriers and diffuse orbitals can be improved. At the same time dispersion forces (van der Waals) can be more accurately computed because of the perturbational term (HF and DFT traditionally fail with this), although it still predicts too weak dispersion forces.

The fact is that most of the DFT functionals only provide local correlation effects that correspond with short-range effects. The development of new DFT methods designed to overcome this problem is a current research topic. One of the solutions proposed to overcome the problem of dispersion description by DFT will be explained in detail in the next section

3.3.3. Dispersion-corrected DFT methods

In reviewing the performance of density functional theory applied to hydrogen bonded complexes of moderate strength, researches repeatedly noted a systematic underestimation of the interaction energies for many types of functionals. This has been related to the inability of functionals to describe those contributions to intermolecular binding energies that stem from dispersion forces.

In order to describe dispersion interactions, a fully nonlocal functional must be applied since a local density functional is in principle not capable of describing this long-range, nonlocal correlation effect. Accordingly, some standard functionals, while correctly describing the short-range repulsion, were found to completely fail in the description of

the attractive branches in the potential curves of van der Waals complexes like He_2, Ne_2 or Ar_2.

There are different approximations to dispersion in DFT, which can be divided into four areas becoming steadily more accurate and expensive:

- Semi-empirical, pairwise approaches to the $C_6 \cdot R^{-6}$ terms, such as DFT-D2.[97, 98]
- Semi-empirical with environment-dependent C_6 coefficients and *ab initio* information, such as DFT-D3.[99-104]
- Density functional approaches based on the vdW-DF-04 of Langreth and Lundqvist.[105,106]
- Approaches which go beyond pairwise additivity, such as many-body dispersion and the random-phase approximation (RPA).[107]

Two of the methods mentioned above were employed in this study, DFT-D2 and DFT-D3 as developed in the group of Grimme.[101] The calculation is based in a term for the usual self-consistent Kohn-Sham energy as obtained from the chosen Density Functional and an empirical dispersion correction term

$$E_{DFT-D} = E_{KS-DFT} + E_{disp}\,. \qquad \text{(eq. 3.61)}$$

The role of the empirical dispersion term is to recover the part of the dispersion contribution that cannot be described by the functional employed. The inclusion of this term, when properly parameterized, greatly enhances the performance of the functional in describing noncovalent interactions.[108] Besides, the inclusion of dispersion comes to a negligible computational cost.

3.3.3.1. DFT-D2

DFT-D2 has the following expression for the dispersion term:

$$E_{disp} = -s_6 \sum_{i=1}^{N_{at}-1} \sum_{j=i+1}^{N_{at}} \frac{C_6^{ij}}{R_{ij}^6} f_{dmp}(R_{ij})\,, \qquad \text{(eq. 3.62)}$$

where N_{at} is the number of atoms in the system, C_6^{ij} denotes the dispersion coefficient for atom pair ij, s_6 is a global scaling factor that only depends on the functional used, and R_{ij} is an interatomic distance. In order to avoid near-singularities for small *R*, a damping function f_{dmp} must be used. This damping function does not depend on the atomic environment of the atoms in the molecules, but only on the values for free atoms.

$$f_{dmp}(R_{ij}) = \frac{1}{1+e^{-d(R_{ij}/R_r - 1)}}\,. \qquad \text{(eq. 3.63)}$$

R_r is the sum of atomic vdW radii and *d* is a value which provides larger corrections at intermediate distances (*d*=20).

Grimme et al. proposed a simple computational scheme for atomic C_6 coefficients that is derived from the London formula for dispersion.[97, 98] It is based on DFT/PBE0 calculations of atomic ionization potentials I_p and static dipole polarizabilities α. The C_6 coefficient for atom *a* is then given as:

$$C_6^a = 0.05 N I_p^a \alpha^a , \qquad \text{(eq. 3.64)}$$

where N has values 2, 10, 18, 36 and 54 for atoms from rows 1-5 of periodic table. The pair coefficient for a given pair of atoms is obtained as an average:

$$C_6^{ij} = \sqrt{C_6^i C_6^j} . \qquad \text{(eq. 3.65)}$$

As commented above, inclusion of the D2 term greatly improves the performance of the functional in treating noncovalent interactions, especially those with significant dispersion contributions, as it happens in stacking interactions between aromatic molecules. However, this simple model could be still improved in the so-called DFT-D3 model.

3.3.3.2. DFT-D3

DFT-D3 improves some aspects of DFT-D2: it is less empirical, the approach is asymptotically correct with all functionals for finite systems or nonmetallic infinite systems, atom pair-specific dispersion coefficients and cutoff radii are explicitly computed, and coordination number dependent dispersion coefficients are used that do not rely on atom connectivity information. Among these improvements, the most relevant one is the definition of environment-dependent coefficients, which allow a better description of dispersion in chemically different systems.

In an initial version of DFT-D3 a Chai-Gordon damping function was selected to add to the dispersion term.[99] This damping function has as main characteristic that tends to zero when *R*=0. In a following paper Grimme has proposed another damping function developed by Becke,[109] which is now the default treatment in DFT-D3. So the dispersion energy is obtained as:

$$E = -\sum_{k=6,8} \sum_{i>j} \frac{C_k^{ij}}{(kC_k^{ij} / E_c^{ij}) + R_{ij}^k} . \qquad \text{(eq. 3.66)}$$

This expression retains the C_k/R^k form at large *R*, but at small *R* approaches a constant value given by the sum of the absolute values of the correlation energies of the free atoms. The method for obtaining dispersion coefficients also changes in DFT-D3 with respect to DFT-D2. Instead of using an empirically derived formula as in DFT-D2, the

dispersion coefficients are now computed *ab initio* by time-dependent DFT (TDDFT) employing known recursion relations for the higher-multipole terms. The starting point is the well-known Casimir-Polder formula,

$$C_6^{AB} = \frac{\pi}{3}\int_0^{\infty} \alpha^A(i\omega)\alpha^B(i\omega)d\omega . \qquad \text{(eq. 3.67)}$$

where $a(iw)$ is the averaged dipole polarizability at imaginary frequency ω.

Although the C_6^{AB} values can be computed easily for any pair of free atoms, this would lead to a rather inconsistent treatment of dispersion in and between molecules. The polarizabilities can change significantly from the free atom to atoms in a molecular environment. Therefore, coefficients are computed for simple hydrides, so coefficients for AB pair in molecular environment are obtained from computations for A_mH_n and B_kH_l reference molecules removing the contribution of the hydrogens.

$$C_6^{AB} = \frac{3}{\pi}\int_0^{\infty} d\omega \frac{1}{m}\left[\alpha^{A_mH_n}(i\omega) - \frac{\pi}{2}\alpha H_2(i\omega)\right] x \frac{1}{k}\left[\alpha^{B_kH_l}(i\omega) - \frac{1}{2}\alpha^{H^2}(i\omega)\right] \qquad \text{(eq. 3.68)}$$

This new approach opens a route to system (Coordination Number) dependent "atomic" C_6 coefficients. The contribution of an atom to the total dispersion coefficient of a molecule depends on its "chemical" environment. A coordination number is computed for a pair of atoms in their specific environments which will be employed in an interpolation procedure employing the coordination number using the hydride and free atom values as references. Including this new development on dispersion-corrected methods, standard functionals improve their behavior to a great extent when dealing with systems with important dispersion contributions.[101,108]

3.4. Reducing computational cost

The bottleneck in DFT and HF calculations is due to integral transformation related to the four-index two-electron integrals employed for describing the interaction between electron pairs. The calculation of these integrals can be greatly speeded up by means of approximations that allow treating the charge densities into the integral in a simplified way. The Density Fitting procedure, also known as the Resolution of the Identity (RI) approach, allows reducing the computational cost needed for evaluating the four-index integrals by reducing their evaluation to simpler two- and three-index integrals.[110-112]

Consider a four-index two-electron integral as:

$$(pq|rs) = \int d\mathbf{r}_1 \int d\mathbf{r}_2 \phi_p(\mathbf{r}_1)\phi_q(\mathbf{r}_1)\frac{1}{r_{12}}\phi_r(\mathbf{r}_2)\phi_s(\mathbf{r}_2) = \int d\mathbf{r}_1 \int d\mathbf{r}_2 \frac{\rho_{pq}(\mathbf{r}_1)\rho_{rs}(\mathbf{r}_2)}{r_{12}} . \qquad \text{(eq. 3.69)}$$

As it can be observed the integral can be expressed as a product of two generalized densities. Then, these densities can be approximated by using a linear expansion employing an adequate auxiliary basis set:

$$\bar{\rho}_{pq}(\mathbf{r}) = \sum_{P}^{Nbas} d_P^{pq} \chi_P(\mathbf{r}) \,. \qquad \text{(eq. 3.70)}$$

There are different methods for obtaining the expansion coefficients, but one of the most common options leads to the following fitting coefficients:

$$d_P^{pq} = \sum_P (pq|P)[\mathbf{J}^{-1}]_{PQ} \qquad \text{(eq. 3.71)}$$

with

$$(pq|P) = \int d\mathbf{r}_1 \int d\mathbf{r}_2 \phi_p(\mathbf{r}_1)\phi_q(\mathbf{r}_1)\frac{1}{r_{12}}\chi_P(\mathbf{r}_2) \qquad \text{(eq. 3.72)}$$

and

$$J_{PQ} = \int d\mathbf{r}_1 \int d\mathbf{r}_2 \chi_P(\mathbf{r}_1)\frac{1}{r_{12}}\chi_Q(\mathbf{r}_2) \,. \qquad \text{(eq. 3.73)}$$

Thus, making the proper substitutions, the four-index integral can be expressed as:

$$(pq|rs) = \sum_Q d_Q^{pq}(Q|rs) = \sum_{PQ}(pq|P)[\mathbf{J}^{-1}](Q|rs) \,. \qquad \text{(eq. 3.74)}$$

The important aspect in this expression is that the four-index integral has been factorized into an expression running through three indexes. One advantage of this procedure is that the storage requirements are greatly reduced when only three-index integrals are needed at most. Also, three- and two-index integrals are more easily evaluated that the corresponding four-index ones, thus saving computational time.

This kind of approximation expressing four-index integrals in two or three-index ones, can be applied to different methods, the computational saving being different depending on each case. This technique has been applied very successfully in order to speed up DFT calculations employing pure functionals, where the time for Coulomb contribution can be greatly reduced. Also, MP2 calculations benefit from this approach since the correlation contribution comes from two-electron integrals involving two occupied and two virtual orbitals. Resolution of the Identity can also be applied to the exchange contribution (RI-JK), though in this case the speedup is not as advantageous as for the Coulomb part.

The central point in the resolution of the identity approach is the design of proper auxiliary basis sets which are capable of reproducing the density introducing negligible errors. Different sets of auxiliary basis functions are available in literature specifically designed for applying the RI approach for the Coulomb,[112] exchange[113] or correlation[114] energy calculations.

3.5. Interaction Energy Partitioning

Applying the above-described supermolecule method with any of the wavefunction-based or DFT methods provides a magnitude for the interaction energy for a given geometry. However, it would be desirable to obtain more information about the nature, origins and characteristics of the interaction itself, but this kind of information is not provided by the supermolecule approach.

Considering the classical and historical description of intermolecular forces, the interaction is usually rationalized in terms of contributions from electrostatics, repulsion, polarization and dispersion. Thus, a method providing such a kind of physical partitioning would be desirable, and it will be the subject of this section.[2, 3]

3.5.1. Energy Decomposition Analysis (EDA) Methods

With the common denomination of Energy Decomposition Analysis (EDA) there is a variety of methods devised for partitioning the interaction energy obtained from variational supermolecule HF and DFT methods.[4, 115] Most EDA methods are variants of the original partitioning scheme proposed by Kitaura and Morokuma.[116] In the original formulation the interaction energy of a dimer was decomposed in electrostatic, repulsion, polarization and charge transfer contributions as obtained at the HF level. Therefore, no dispersion contribution was obtained. EDA methods have been later extended to many-body systems by Chen and Gordon, thus allowing the partitioning in trimers, tetramers or larger clusters.[117] In any case, the original EDA partitioning posed some problems, and the attempts of solving them give way to a variety of EDA methods, such as the natural energy decomposition analysis (NEDA),[118-120] the reduced variational space analysis (RVS),[117, 121] and the generalized Kohn-Sham EDA (GKS-EDA)[122]

Following there is a general description of how most EDA methods work.[4] The formation of the complex is divided in a series of steps, each one associated with a given physical contribution. Consider a dimer AB formed by two separate units A and B already in the final geometry they have in the complex.

1. In the first step of dimer formation according to EDA, fragments A and B with frozen charge distribution are taken from infinite separation and brought together to the position in the dimer. The interaction between the frozen charge densities of A and B gives the electrostatic interaction:

$$\Delta E_{elec} = \sum_{\alpha \in A}\sum_{\beta \in B} \frac{Z_\alpha Z_\beta}{R_{\alpha\beta}} + \int dr V_B(r)\rho_A(r) + \int dr V_A(r)\rho_B(r) + \int dr_1 dr_2 \frac{\rho_A(r)\rho_B(r)}{r_{12}}$$. (eq. 3.75)

2. In the second step of EDA the product wavefunction employed before, normalized but not antisymmetrical, is antisymmetrized. As a consequence of the antisymmetrization the energy changes, leading to a term called Exchange or Pauli repulsion.

3. The wavefunction is allowed to relax to give the final state of the dimer AB with energy E_{AB}. The energy lowering associated with this orbital relaxation is the orbital relaxation contribution.

Therefore, the interaction energy is split into three contributions as indicated in eq. 3.76,

$$\Delta E_{AB}^{\text{int}} = \Delta E_{electrostatic} + \Delta E_{Pauli} + \Delta E_{orbital} .$$ (eq. 3.76)

This is the global framework, but different EDA approaches further split the interaction energy by dividing Pauli and orbital relaxation terms. Depending on the method employed, Pauli repulsion can be split as Exchange + Repulsion, and orbital relaxation is further divided in A polarization, B polarization and charge transfer terms.

EDA partitioning has been employed in one chapter of this thesis. The LMO-EDA method[123] used can be considered an extension and modification of the methods developed by Kitaura and Morokuma[116], Ziegler and Rauk,[124] and Hayes and Stone.[125] The main features of this partitioning are listed as follows:

1. The electrostatic, exchange and repulsion terms are obtained from the Heitler-London interaction energy as proposed by Hayes and Stone from an antisymmetric product of the monomer HF spinorbitals.

2. Polarization energy is defined as orbital relaxation energy going from monomer orbitals to dimer orbitals. Thus, no charge transfer term is defined.

3. A dispersion contribution can be computed via a supermolecule calculation with a post-HF or DFT method. Dispersion is defined as the difference between the sum of all contributions and the interaction energy obtained with the post-HF method. Though this has been common practice, it has to be taken into account that using HF partitioning, the dispersion contribution really corresponds to correlation energy contribution, containing other effects over electrostatic, induction and repulsion terms.

4. The partitioning can be applied similarly to DFT methods.

In summary, LMO-EDA allows partitioning the global interaction energy into contributions that can give hints on the effects controlling the interaction. Within the Hartree-Fock framework the interaction energy is expressed as:

$$\Delta E_{AB}^{\text{int},HF} = \Delta E_{elec} + \Delta E_{exch} + \Delta E_{rep} + \Delta E_{pol} \,. \qquad \text{(eq. 3.77)}$$

Applying a post-HF method as, say, CCSD(T), a dispersion contribution is defined:

$$\Delta E_{AB}^{\text{int},CCSD(T)} = +\Delta E_{elec} + \Delta E_{exch} + \Delta E_{rep} + \Delta E_{pol} + \Delta E_{disp} \,, \qquad \text{(eq. 3.78)}$$

with dispersion (correlation contribution) defined as:

$$\Delta E_{disp} = \Delta E_{AB}^{CCSD(T)} - \Delta E_{AB}^{HF} \,. \qquad \text{(eq. 3.79)}$$

In the case of employing a DFT method a similar partition is employed, so

$$\Delta E_{AB}^{\text{int},DFT} = \Delta E_{elec} + \Delta E_{exch} + \Delta E_{rep} + \Delta E_{pol} + \Delta E_{disp} \,. \qquad \text{(eq. 3.80)}$$

Dispersion is obtained as:

$$\Delta E_{disp} = \Delta E_{AB}^{\text{int},DFT} - (\Delta E_{elec} + \Delta E_{exch} + \Delta E_{rep} + \Delta E_{pol}) \,. \qquad \text{(eq. 3.81)}$$

3.5.2. Symmetry-Adapted Perturbation Theory Methods (SAPT)

Symmetry Adapted Perturbation theory methods employ a totally different approach in order to directly obtain the interaction energy.[126, 127] SAPT is based on perturbation theory, where the interaction itself is treated as the perturbation and its magnitude is directly computed. Applying a perturbational scheme (Rayleigh-Schrodinger) to a complex naturally provides expressions which can be identified with contributions from electrostatic, induction and dispersion. The most obvious partitioning of the Hamiltonian operator of an interacting pair of molecules A and B is the following:

$$\hat{H} = \hat{H}_A + \hat{H}_B + \hat{V} = \hat{H}_0 + \hat{V} \,, \qquad \text{(eq. 3.82)}$$

where $\hat{H}_0$ is the solution for the unperturbed system and $\hat{V}$ is the operator for the intermolecular interaction. The reference system consists on the isolated non-interacting molecules and the perturbation is the interaction. $H_A\psi_A = E_A\psi_A$ and equivalently for the monomer B $H_B\psi_B = E_B\psi_B$. As a consequence, the reference wavefunction is the product of the isolated molecules' wavefunctions $\psi_0 = \psi_0^A\psi_0^B$.

Applying Rayleigh-Schrödinger perturbation theory under these assumptions, the typical expression can be obtained for the different corrections to first, second, … order.[3] That way, the first order correction will be:

$$E_{el}^{(1)} = \left\langle \psi_0^A \psi_0^B \middle| V \middle| \psi_0^A \psi_0^B \right\rangle. \qquad \text{(eq. 3.83)}$$

This expression corresponds to the coulombic interaction between the electron density of both monomers, and is therefore associated to the electrostatic energy. To second order, terms appear depending on single and double excitations which can be associated with induction and dispersion contributions. Thus:

$$E_{ind}^{A} = -\sum_{m\neq 0} \frac{\left\langle \psi_0^A \psi_0^B \middle| V \middle| \psi_m^A \psi_0^B \right\rangle^2}{E_m^A - E_0^A} \qquad \text{(eq. 3.84)}$$

corresponds to single excitations within monomer A due to the presence of the nearby monomer B, and therefore is associated to the induction contribution of monomer A. An equivalent expression is also found for single excitations involving B

$$E_{ind}^{B} = -\sum_{n\neq 0} \frac{\left\langle \psi_0^A \psi_0^B \middle| V \middle| \psi_0^A \psi_n^B \right\rangle^2}{E_n^B - E_0^B}. \qquad \text{(eq. 3.85)}$$

Finally, to second order another term remains involving double excitations which is assigned as dispersion contribution.

$$E_{disp} = -\sum_{m\neq 0; n\neq 0} \frac{\left\langle \psi_0^A \psi_0^B \middle| V \middle| \psi_m^A \psi_n^B \right\rangle^2}{E_m^A + E_n^B - E_0^A - E_0^B}. \qquad \text{(eq. 3.86)}$$

It is worth noting that these expressions, together with the multipole expansion, provide much of our qualitative and quantitative discussion on the role of noncovalent bonding forces, allowing to describe intermolecular interactions as functions of molecular properties such as multipoles or polarizabilities.[2, 3]

The perturbation theory for well-separated molecules described above (the long-range approximation or polarization approximation) is very successful if the molecules are a long distance apart, but at short range fails completely.[3] Part of the reason for the failure of the theory as usually formulated is that the multipole expansion breaks down. A more fundamental failure is that the repulsion between molecules that occurs at short-range is completely missed from the long-range theory. This failure arises from the fact that if the molecules are close enough for their wavefunctions to overlap, exchange cannot be ignored.

The source of the difficulties of Rayleigh-Schrödinger perturbation theory for describing intermolecular interactions at short range is the wrong symmetry of the reference wavefunction.[2, 3] The reference wavefuntion $\psi_0 = \psi_0^A \psi_0^B$ is antisymmetric upon electron exchange within A or within B, but it is not upon exchange of electrons

between A and B. Therefore, the reference wavefunction is physically unsound, thus leading to the lack of proper repulsion forces as the molecules come together. Therefore, the reference wavefunctions should be properly antisymmetrized in order to satisfy the Pauli principle.

There have been different approaches to overcome the antisymmetry problem, but the prevailing one is the symmetrized Rayleigh-Schrödinger theory, a nowadays synonym of Symmetry Adapted Perturbation Theory (SAPT). Within SAPT, antisymmetry is forced in the energy expressions, modifying the electron density in such a way as to cause a repulsive force on the nuclei. This is the force corresponding to the exchange-repulsion energy.[126, 127]

The outcome of SAPT procedure is a series of contributions that to low order can be associated to physical effects as in polarization theory. The main difference, however, is that each of the polarization terms is now accompanied by an exchange-repulsion term arising from proper antisymmetry. Therefore, the interaction energy is expressed in SAPT as:

$$E_{\text{int}} = E_{el}^{(1)} + E_{exch}^{(1)} + E_{ind}^{(2)} + E_{exch\text{-}ind}^{(2)} + E_{disp}^{(2)} + E_{exch\text{-}disp}^{(2)} + \ldots. \qquad \text{(eq. 3.87)}$$

Thus, it can be seen that antisymmetrization produces new terms that are completely missed when a simple product wavefunction is used. The most important fact is that there is a strong repulsion between closed-shell molecules when their wavefunctions overlap significantly.

The description of SAPT presented above assumed that one knows the exact wavefunctions for monomers. In practice, the wavefunctions are computed separating the HF and the correlation contributions. Since electron correlation significantly affects molecular properties required as input to SAPT it is mandatory to account for intramolecular electron correlation. [52, 126, 127]

If the MP decomposition of the Hamiltonians is used for monomers, SAPT becomes a double-perturbation theory according to the following splitting of the Hamiltonian,

$$H = F + V + W \qquad \text{(eq. 3.88)}$$

so the sum of monomer's Fock operators $F = F_A + F_B$ is now the unperturbed Hamiltonian, whereas V and the sum of MP potentials of monomers $W = W_A + W_B$ are the two perturbation operators. Accordingly, the interaction energy can now be expressed as

$$E_{\text{int}} = \sum_{i=1;\, j=0} \left(E_{pol}^{ij} + E_{exch}^{ij} \right), \qquad \text{(eq. 3.89)}$$

where *ij* is the order in *V*-*W*. A large number of terms in this expansion have been developed up to *i*=3 and *j* from 0 to 4, depending on *i* and the physical component. Thus, SAPT allows describing the interaction with increasing accuracy by including terms to higher orders in both expansions. Depending on the contributions included, different models can be defined, though the series expansion is typically truncated at second-order in *V*, resulting in a complete neglect of third- and higher order terms. It has been observed that in polar systems higher order effects can be important, often associated with induction effects. A correction is recommended in order to at least introduce an estimation of such effects. The correction is defined as

$$\delta_{HF} = E_{\text{int}}^{HF} - E_{el}^{(10)} - E_{exch}^{(10)} - E_{ind}^{(20)} - E_{exch\text{-}ind}^{(20)}, \qquad \text{(eq. 3.90)}$$

where E_{int}^{HF} is the Hartree-Fock interaction energy calculated using the supermolecular method.

Therefore, SAPT can partition the interaction energy at the HF level as:

$$E_{\text{int}}^{HF} = E_{el}^{(10)} + E_{exch}^{(10)} + E_{ind}^{(20)} + E_{exch\text{-}ind}^{(20)} + \delta_{HF}. \qquad \text{(eq. 3.91)}$$

Of course, at the HF level, the interaction energy does not include dispersion, but applying perturbation theory based on HF wavefunctions the dispersion term can be obtained in SAPT. Thus, the Hartree-Fock calculation can be corrected with the dispersion contribution obtaining the HF+D method (in a similar way as the already commented DFT-D methods).

$$E_{\text{int}}^{HF+D} = E_{el}^{(10)} + E_{exch}^{(10)} + E_{ind}^{(20)} + E_{exch\text{-}ind}^{(20)} + \delta_{HF} + E_{disp}^{(20)} + E_{exch\text{-}disp}^{(20)}. \qquad \text{(eq. 3.92)}$$

The last expression contains all SAPT contributions to order 2 obtained employing HF wavefunctions. As commented above, higher-order terms in induction are taken care of by the δ_{HF} contribution.

The next step would be including intramonomer correlation effects, leading to a more accurate description of the interactions. For example, the so-called SAPT2 level corresponds to:

$$E_{\text{int}}^{SAPT} = E_{\text{int}}^{HF+D} + E_{el}^{(12)} + E_{exch}^{(11)} + E_{exch}^{(12)} + E_{ind}^{(22)} + E_{exch\text{-}ind}^{(22)}, \qquad \text{(eq. 3.93)}$$

including corrections similar to MP2. More accurate models would include contributions to third order both in the intermolecular perturbation and the intramonomer correlation perturbation. The problem of using such expression is its high computational demand, which has led to other approaches to be commented in the following section. In any case, it is worth noting that, recently, Hohenstein and Sherrill have developed a SAPT scheme exploiting the resolution of the identity approach in order to reduce the

computational cost, which could make SAPT calculations more feasible.[52, 128, 129] This approach has been coded into the PSI4 program.[130]

3.5.2.1. SAPT(DFT)

Despite the successes of SAPT, the calculation of the intramonomer correlation terms makes it computationally prohibitive for larger molecular systems. Williams and Chabalowski suggested that if a correlated description of the monomers was used, the costly correlation terms can be avoided.[131] Due to computational considerations, Williams and Chabalowski suggested that a DFT description of the monomers would be best suited. This fact allows SAPT to be performed on much larger systems than previously allowed although the initial results were rather poor. Thus, the idea was simply changing the HF orbitals and energies by their Kohn-Sham counterparts. This way, a SAPT calculation including only the perturbation on the intermolecular interaction will suffice, because intramonomer correlation effects were already taken care of in the DFT calculations. [131]

The results obtained following this procedure were disappointing. It was observed that one of the reasons for this inaccuracy was the incorrect asymptotic behavior of the exchange-correlation functions for obtaining the Kohn-Sham energies. While the exchange-correlation potential should decay as *1/r* for a neutral system, the standard local or/and gradient-corrected DFT exchange-correlation potentials decay too quickly.

The method was soon improved by Hesselmann and Jansen[132-136] and Szalewicz[137-140] independently, leading to essentially identical methods. In both proposals, a correction for the asymptotic behavior is assumed. In Jansen's proposal the functional employed is combined with the LB94 functional, which has a correct asymptotic behavior at long-range (but fails at short-range).[136] This fact creates a new problem that it is the breaking at intermediate distances between the behavior of the two functionals.[141, 142] In order to arrange this, a gradient-regulated connection method as developed by Grüning et al. was employed.[141] This scheme (Adiabatic Correction AC) requires the sum $IP + \varepsilon_{HOMO}$ as the input parameter (which vanishes in the case of exact KS DFT). The value of ε_{HOMO} is obtained from a calculation with the uncorrected *xc* functional, whereas the ionization potentials can either be taken from experiment or calculated from the difference of KS DFT calculations of the neutral and the ionized systems, respectively.

Once these problems affecting accuracy are solved, the equation obtained for SAPT(DFT) is the following:

$$E_{\text{int}}^{SAPT-DFT} = E_{el}^{(10)} + E_{exch}^{(10)} + E_{ind,resp}^{(20)} + E_{exch-ind,resp}^{(20)} + E_{disp}^{(20)} + E_{exch-disp}^{(20)} + \delta_{HF} \,. \qquad \text{(eq. 3.94)}$$

The same correction term δ_{HF} is included in the calculation in order to take into account higher-order contributions. Despite of the difficulties in the implementation of

DFT in a complicated theory like SAPT, SAPT(DFT) presents many advantages in comparison to SAPT. The main reason, and the origin of this method, is the decreased computational cost for the description of intramonomer correlation, which allows the application of SAPT partitioning to larger systems that could not be afforded with SAPT based in MBPT or CC. In addition to this, it is worth noting that density fitting approach can be employed, greatly reducing the computational cost. Also, simplified extrapolation schemes have been proposed in order to reach the complete basis set limit in the framework of SAPT(DFT) calculations.[143]

3.6. Electron density analysis

Atoms in Molecules quantum theory (QTAIM), that was developed by Bader, is a theory based on the topological analysis of the electron density, which brought quantum mechanics into applicability to an atom within a molecule.[144] When a molecular property can be expressed in terms of a property density, the contribution of a given atom to that molecular property can be obtained by integrating this density over the volume of the atom in the molecule. Thus, the theory relates concepts as bonding, functional groups or chemical reactivity to the topology of the underlying electron density, though the aspect of the molecular density is always the same: large cups at the nucleus and an exponential decreasing behavior in all directions.

The characterization of critical points is based on the behavior of the gradient vector in the zone nearby. So, a critical point in the electron density can be defined as a point in space at which the first derivates of the density vanish,

$$\nabla\rho = i\frac{d\rho}{dx} + j\frac{d\rho}{dy} + k\frac{d\rho}{dz} = \rho_x i + \rho_y j + \rho_z k\,, \qquad \text{(eq. 3.95)}$$

meaning that each individual derivative in the gradient operator, ∇, is zero and not just their sum. The gradient of a scalar function such as $\rho(r)$ at a point in space is a vector pointing in the direction in which $\rho(r)$ undergoes the greatest rate of increase and having a magnitude equal to the rate of increase in that direction.

Considering the second derivatives, the elements of the tensor $\nabla\nabla\rho$, one can discriminate between a local minimum, a local maximum, or a saddle point. There are nine second derivatives of $\rho(r)$ that can be arranged in the so-called Hessian matrix, which when diagonalized at a critical point *rc* gives:

$$\Lambda = \begin{pmatrix} \frac{\partial^2 \rho}{\partial x^2} & 0 & 0 \\ 0 & \frac{\partial^2 \rho}{\partial y^2} & 0 \\ 0 & 0 & \frac{\partial^2 \rho}{\partial z^2} \end{pmatrix}_{r'=r_c} = \begin{pmatrix} \lambda_1 & 0 & 0 \\ 0 & \lambda_2 & 0 \\ 0 & 0 & \lambda_3 \end{pmatrix}. \qquad \text{(eq. 3.96)}$$

λ_1, λ_2 and λ_3 are the eigenvalues of the Hessian matrix (ordered as $\lambda_1 \leq \lambda_2 \leq \lambda_3$) and represent the curvatures of the density with respect to the three principal axes *x'*, *y'* and *z'*.

There are four types of stable critical points having three non-zero eingenvalues:

- $\lambda_1, \lambda_2, \lambda_3 < 0$; (3,-3): all curvatures are negative. ρ is a local maximum. This is called a Nuclear Critical Point.
- $\lambda_1, \lambda_2 < 0$, $\lambda_3 > 0$; (3,-1): two negative curvatures. ρ is a maximum in the plane defined by the corresponding eigenvectors and a minimum along the third axis which is perpendicular to this plane. This is called a Bond Critical Point.
- $\lambda_1 < 0$, $\lambda_2, \lambda_3 > 0$; (3,+1): two positive curvatures. ρ is a minimum in the plane defined by the corresponding eigenvectors and a maximum along the third axis which is perpendicular to this plane. This is called a Ring Critical Point.
- $\lambda_1, \lambda_2, \lambda_3 > 0$; (3,+3): Three curvatures are positive. ρ is a local minimum and corresponds to a Cage Critical Point.

The collection of paths linking the nuclei of bonded atoms in an equilibrium geometry with the associated critical points is known as the molecular graph, which provides an unambiguous definition of the "molecular structure" and can thus be used to locate changes in structure along a reaction path. Also, the strength of a chemical bond is reflected on the electron density at the bond critical point (ρ_b). ρ_b is greater than 0.20 a.u. in shared (covalent) bonding and less than 0.10 a.u. in a closed-shell interaction (ionic, vdW, hydrogen bond, etc.). ρ_b has been shown to be strongly correlated with the binding energy for several types of bonding interaction.

In conclusion, the analysis of the electron density and its derivatives through its main topological features provides much information about the characteristics of the system and can be employed to analyze the most relevant noncovalent interactions present in the systems under study.

3.6.1. NCI index

As commented in the preceding section, Atoms in Molecules Theory can be employed to analyze in detail the characteristics of the interaction in intermolecular systems. However, in large systems, QTAIM provides an overwhelming amount of information: a large number of critical points, their characteristics, a large set of bond paths, etc.

Therefore, it would be desirable a method allowing visualizing in a quick and simple way the most relevant features of the interaction. The Non Covalent Interaction index (NCI) has been devised with this purpose.[145, 146]

The NCI index identifies interactions in a chemical system solely on the basis of the electron density and its derivatives, and it is based on an analysis of the reduced density gradient, s , and the electron density, ρ, where

$$s = \frac{1}{2\left(3\pi^2\right)^{1/3}} \frac{|\nabla\rho|}{\rho^{4/3}}. \qquad \text{(eq. 3.97)}$$

On the other hand, the sign of the laplacian $\nabla^2\rho$ determines if the density is concentrated or depleted at one point relative to the surroundings. Thus, $\nabla^2\rho < 0$ is characteristic of covalent interactions while $\nabla^2\rho > 0$ is characteristic of weak interactions, both bonding and nonbonding.

To distinguish among different types of weak interactions, the sign of the Laplacian itself cannot be used, because the sign is dominated by negative contributions from nuclei. Instead, contributions to the Laplacian along the axis of its maximal variation must be analyzed. These contributions are the eigenvalues λ_i of the electron density Hessian matrix,

$$\nabla^2\rho = \lambda_1 + \lambda_2 + \lambda_3 \;\; ; \;\; (\lambda_1 < \lambda_2 < \lambda_3). \qquad \text{(eq. 3.98)}$$

At the nuclei all eigenvalues are negative, while away from them $\lambda_3 > 0$. In molecules, λ_3 values vary along the internuclear direction, while λ_1 and λ_2 report the variation of density in the plane normal to the λ_3 eigenvector. On one hand, bonding interactions, such as hydrogen bonds, are characterized by an accumulation of density perpendicular to the bond, and $\lambda_2 < 0$. Non-bonded interactions, such as steric repulsion, produce density depletion, such that $\lambda_2 > 0$. Finally, vdW interactions are characterized by a negligible density overlap that gives $\lambda_2 \leq 0$. Thus, the sign of λ_2 enables to distinguish different types of weak interactions, while the density itself enables to assess the interaction strength.[146]

Therefore, since noncovalent interactions are characterized by low density and low reduced gradient values, they can be located by generating gradient isosurfaces enclosing the corresponding regions of space.[145] These isosurfaces are the basis of the noncovalent interaction method (NCI). The gradient isosurfaces are colored according to the corresponding values of *sign*(λ_2)·ρ, which is found to be a good indicator of interaction strength. Large, negative values of *sign*(λ_2)·ρ are indicative of attractive interactions (such as dipole-dipole or hydrogen bonding); while if *sign*(λ_2)·ρ is large and

positive, the interaction is nonbonding. Values near zero indicate very weak, van der Waals interactions.

Consider for example the results shown in Figure 3.4 obtained for benzene and benzene dimer in two different orientations. Considering first the results for benzene molecule it can be observed that among the cloud of points shown in the graph, there is a peak going to reduced density close to zero, at density values around 0.2 (0.0197) a.u. This corresponds to the ring critical point in benzene molecule.

Now, having a look to the results obtained for benzene dimers, it can be observed that the main change in the representation is located in regions of very low density, with the appearance of new peaks going to almost-zero reduced density gradient at very low density values. This kind of behavior is the one associated with intermolecular interactions, and the goal of NCI. In the bottom section of Figure 3.4 the NCI plots are shown for benzene dimer for a reduced density gradient isosurface with value 0.5 a.u. It can be observed that surfaces appear on the intermolecular regions and in the center of the rings. The latter ones correspond to regions around the ring critical points of benzene molecules, whereas the former one is that revealing intermolecular contacts. It can be observed how in both benzene dimers a green surface is indicative of a weak interaction between benzene molecules. This surface is indicative of the stacking interaction in parallel benzene dimer (left), but also reveals the somewhat stronger (bluer) C-H···π contact characteristic of the T-shaped structure.

To summarize, plotting low reduced density gradient isosurfaces, subject to a further low density constraint, allows visualization of noncovalent interactions. Surfaces with very low density values (i.e., $\rho < 0.005$ au) map to weaker dispersion interactions. Surfaces with slightly higher density values ($0.005 < \rho < 0.05$ au) generally map to stronger noncovalent interactions, including both attractive H-bonding (negative λ_2) and steric clashes (positive λ_2).

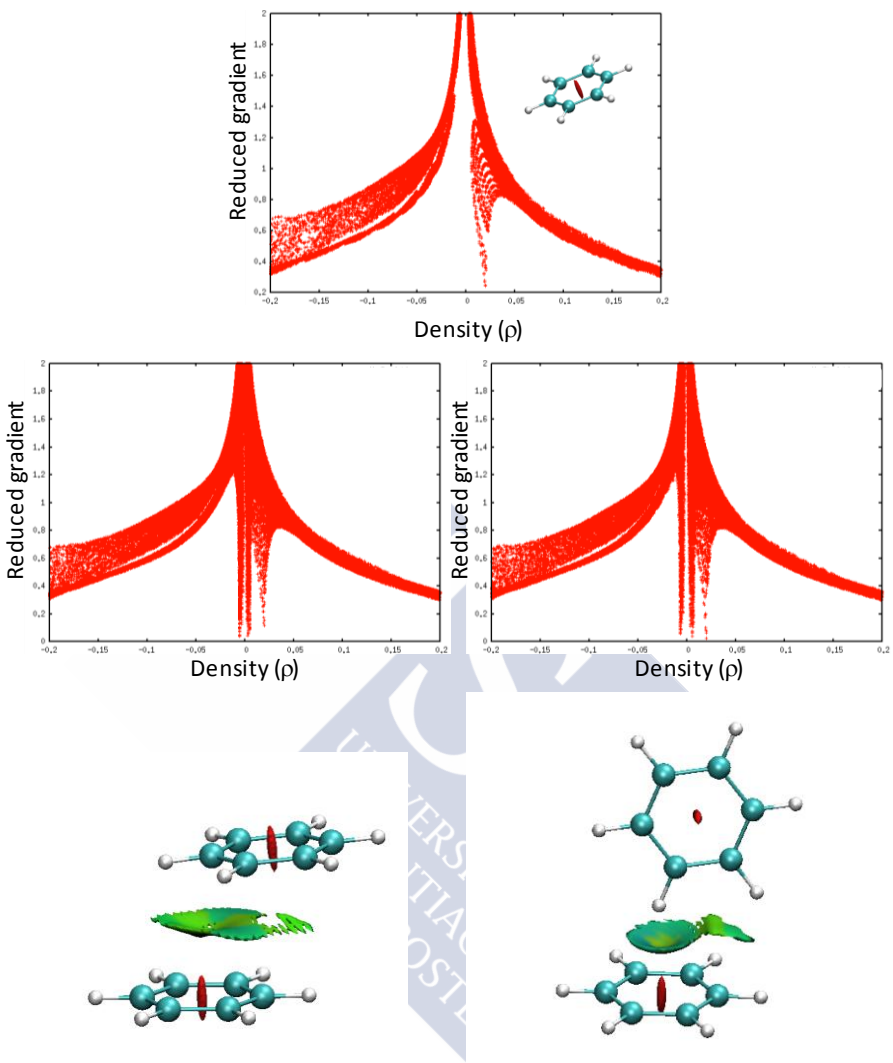


Figure 3.4. Top: Changes in the reduced density gradient vs. density. Bottom: Noncovalent Interaction index plot for benzene dimer in parallel and T-shaped structures, using an isosurface of 0.5 a.u. for the reduced density gradient and a color scale going from -0.015 a.u. (blue) to 0.015 (red) a.u. Results at the B97-D/6-31G* level of calculation.

3.7. Solvation effects

Most electronic structure calculations are performed assuming gas-phase conditions, but the presence of solvent can significantly alter the properties of a molecule. Thus, the values obtained for vibrational frequencies, geometry, charge distribution and so on will differ from those obtained in the gas phase.

If the specific effect of solvent molecules wants to be modelled (normally due to solvent in the first solvation shell), the appropriate choice is to explicitly include an appropriate number of molecules, usually ranging from one to a couple of dozens, as indicated in Figure 3.5. That way the most important solvent effects due to specific interactions between molecules can be represented and information about their effect upon different properties can be assessed, but also direct comparison can be done with experiments in microsolvated clusters in the gas phase. This is especially significant when hydrogen bonds are present, the effects being easily followed both by experiment and calculation, mainly regarding to vibration frequencies.

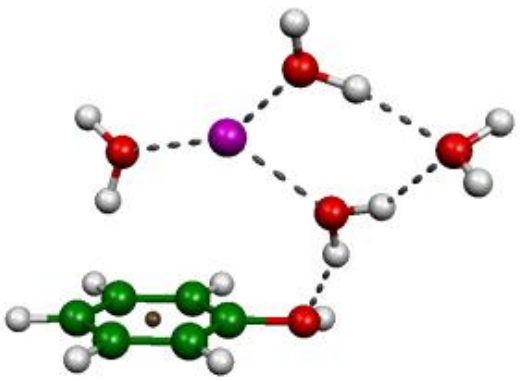


Figure 3.5. Phenol-sodium complex microhydrated with four water molecules.

Of course, this approach is not feasible if bulk effects are of interest. In that case, the obvious choice would be the extension of the microsolvation model to incorporate more and more solvent molecules as to properly represent the bulk solution. However, this approach is unaffordable for most electronic structure methods, due to the large number of atoms and electrons, as well as degrees of freedom, which would need an enormous amount of computational effort. Therefore, a model is needed capable of treating the different physical influences of solvent upon the solute, being simple enough as to be computationally feasible.

3.7.1. Continuum models

The basic approach in continuum models is that all solvent molecules are replaced by a medium characterized by its dielectric constant. Thus, the huge number of degrees of freedom associated to solvent is drastically reduced, making the problem easily tractable. Usually, the solvation energy is divided into contributions coming from different physical influences of solvent molecules upon the solute.[147] These effects are quite often classified as cavitation (the effort needed for creating the cavity in the dielectric medium), repulsion plus dispersion (introducing non-electrostatic interaction between solute and solvent) and electrostatic (reflecting the mutual interaction between the charge distribution of the solute molecule and the medium). For a polar solute in a polar solvent the electrostatic interactions are dominant, so the procedure for treating them is exposed below in some detail.

The model consists on a molecule inside a cavity immersed in a continuous polarizable medium of dielectric constant ε. With these conditions, the charge distribution of the solute polarizes the solvent creating a nonzero electrostatic potential (reaction potential and corresponding reaction field), which in turn modifies the solute's charge distribution. This corresponds to a self-consistent process, solved by following an iterative procedure, and leading to a favorable interaction between solute and solvent. This is the reason why these methods are often called self-consistent reaction field methods (SCRF). The main advantage of such approach is that with this model the most important electrostatic effects due to the solvent can be modelled, but with a very simple approach avoiding the explicit treatment of the huge number of solvent molecules. Different methods mainly change in how the electrostatic problem is solved and in peculiarities about how the cavity for placing the solute is constructed.

In order to solve the electrostatic problem, Poisson equation is the one to take into consideration, its solution giving the exact answer of the electrostatic problem defined by the dielectric continuum model. Thus, Poisson equation is:

$$\nabla^2 V(\vec{r}) = -4\pi\rho(\vec{r}) \qquad \text{(eq. 3.99)}$$

inside the cavity (ρ is the solute charge density), and

$$\nabla^2 V(\vec{r}) = 0 \qquad \text{(eq. 3.100)}$$

outside the cavity, assuming all charge of the solute is inside the cavity. *V* is the sum of the electrostatic potential generated by the molecule and the reaction potential generated by the medium:

$$V(\vec{r}) = V_M(\vec{r}) + V_R(\vec{r})\,. \qquad \text{(eq. 3.101)}$$

Applying the proper boundary conditions, the equation could be solved. One of these conditions is that the potential has to be continuous when crossing the surface of the cavity. The other condition imposes that the electric field must exhibit a discontinuity when crossing the surface as we pass from a medium with vacuum dielectric constant inside the cavity to the solvent's dielectric constant value. Once the electrostatic potential is obtained, the free energy of solvation is obtained from

$$G^{elec} = -\frac{1}{2}\int \rho(\vec{r})V_R(\vec{r})dr_3 . \qquad \text{(eq. 3.102)}$$

However, no analytic solution of Poisson equation is possible except for simple model problems, so it has to be solved approximately.

One method for solving Poisson equation often employed in electronic structure calculations is to use a Boundary Element Method (BEM) as introduced by Tomasi and widely employed in subsequently developed methods.[147] The cavity is discretized in a series of elements (Figure 3.6) and, instead of directly solving for $V_R(\vec{r})$ itself, the model is solved for a set of apparent surface charges (ASC) that produces the same reaction potential

$$V_\sigma(\vec{r}) = V_R(\vec{r}) = \int_\Gamma \frac{\sigma(s)}{|\vec{r}-\vec{s}|}d^2s \qquad \text{(eq. 3.103)}$$

Finally, the reaction potential is coupled to the quantum calculation by including it into the Hamiltonian.

This is the basic setup of the so-called PCM (or D-PCM) methods, pioneered by Tomasi. The reduction of the source of the solvent reaction potential to a charge distribution limited to the cavity surface greatly simplifies the electrostatic problem with respect to formulations which have to deal with a reaction potential generated by the whole dielectric medium. Along the years the basic PCM setup has seen different evolutions and changes giving way to different models.

A different approach to the electrostatic problem, though sharing much of the D-PCM setup is the Conductor-Like Screening Model (COSMO) proposed by Klamt and Schüürman.[148] The main difference between COSMO and D-PCM models is that the dielectric constant of the solvent is changed from its specific value ε to infinite as corresponds to a conductor. Considering the solvent as a conductor, the total potential vanishes on the cavity surface, greatly simplifying the electrostatic equations. In order to recover the effects of the finite value of the dielectric constant of the medium, the apparent charge distribution for the ideal conductor is scaled by a proper function of the dielectric constant:

$$f(\varepsilon) = \frac{\varepsilon - 1}{\varepsilon + x}, \qquad \text{(eq. 3.104)}$$

where x is a fitted parameter, originally set to 0.5, though other values have been proposed. The choice of this parameter has little impact in solvents with large dielectric constant whereas the results are more affected if the solvent shows low dielectric constant.

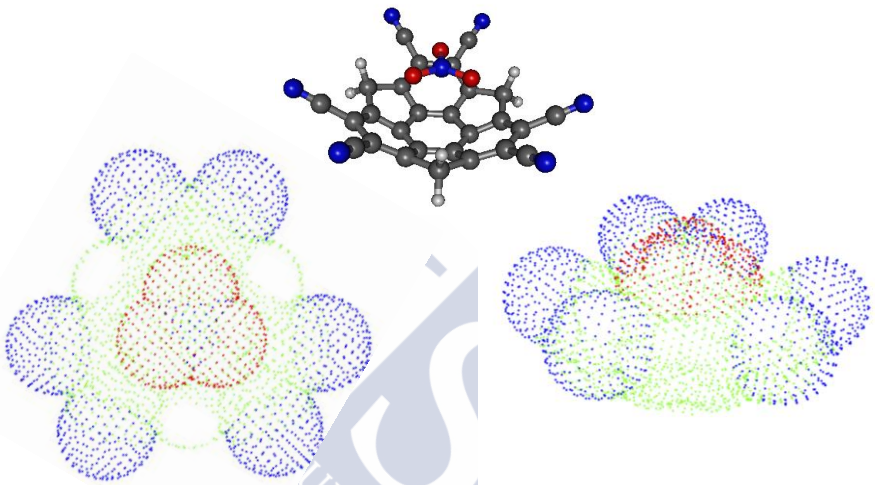


Figure 3.6. Cavity construction for the PCM calculations as performed with Gaussian.

Therefore, the solvent is treated as a dielectric, with apparent charges defining the reaction field obtained applying conductor boundary conditions, and properly scaled as to represent a specific value of the dielectric constant. COSMO is especially robust with respect to artifacts that result from the small percentage of the solute's charge reaching the outer side of the cavity, the so-called outlying charge.

In any unconstrained electronic structure calculation of the solute there is a tail that extends beyond the cavity surface. Therefore, there is a small percentage of the electron density in the dielectric.[149] A proper formulation for this problem should include not only the surface polarization but also a volume polarization outside the cavity, introducing apparent volume charges at points outside the cavity. COSMO includes an approximation to volume polarization making a final calculation extending somewhat the limits of the cavity and comparing the values obtained with the original and the extended surfaces. It should be taken into account that outlying charge errors can easily

reach 20% for neutral species, and be even larger for anions, so a proper correction for these effects should be considered. This has been a problem in D-PCM methods which led to incorporate COSMO into the PCM suite (C-PCM), though the latest developments in PCM models such as the integral equation formalism variant PCM (IEFPCM) include an approximate correction to this problem.[147]

3.8. References

[1] P. Hobza, R. Zaradnik, Intermolecular complexes : the role of van der Waals systems in physical chemistry and the biodisciplines, Elsevier, Amsterdam, **1988**.

[2] I. Kaplan, Intermolecular Interactions : Physical Picture , Computational Methods, John Wiley & Sons, Chichester, **2006**.

[3] A. J. Stone, The theory of intermolecular forces, Oxford University Press, Oxford, **2013**.

[4] M. v. Hopffgarten, G. Frenking. *WIREs Comput. Mol. Sci.* **2012**, *2*, 43-62.

[5] G. Chalasinski, M. M. Szczesniak. *Chem. Rev.* **1994**, *94*, 1723-1765.

[6] G. Chałasiński, M. M. Szczęśniak. *Chem. Rev.* **2000**, *100*, 4227-4252.

[7] K. Szalewicz, B. Jeziorski. *J. Chem. Phys.* **1998**, *109*, 1198-1200.

[8] S. S. Xantheas. *J. Chem. Phys.* **1996**, *104*, 8821-8824.

[9] E. Cabaleiro-Lago, J. Rodríguez-Otero, Á. Peña-Gallego. *Theor. Chem. Acc.* **2011**, *128*, 531-539.

[10] E. M. Cabaleiro-Lago, M. A. Ríos. *J. Chem. Phys.* **2000**, *112*, 2155-2163.

[11] A. Campo-Cacharrón, E. M. Cabaleiro-Lago, J. Rodríguez-Otero. *ChemPhysChem* **2012**, *13*, 570-577.

[12] E. M. Cabaleiro-Lago, Á. Peña-Gallego, J. Rodríguez-Otero. *J. Chem. Phys.* **2008**, *128*, 194311/1-194311/8.

[13] C. D. Sherrill *Computations of Noncovalent π Interactions,* in Reviews in Computational Chemistry *Vol. 26*, John Wiley & Sons, New York, **2009**.

[14] F. B. van Duijneveldt, J. G. C. M. van Duijneveldt-van de Rijdt, J. H. van Lenthe. *Chem. Rev.* **1994**, *94*, 1873-1885.

[15] H. B. Jansen, P. Ros. *Chem. Phys. Lett.* **1969**, *3*, 140-143.

[16] S. F. Boys, F. Bernardi. *Mol. Phys.* **1970**, *19*, 553-566.

[17] J. Alvarez-Idaboy, A. Galano. *Theor. Chem. Acc.* **2010**, *126*, 75-85.

[18] A. J. C. Varandas. *J. Phys. Chem. A* **2009**, *114*, 8505-8516.

[19] Ł. M. Mentel, E. J. Baerends. *J. Chem. Theory Comput.* **2013**, *10*, 252-267.

[20] T. Helgaker, P. Jørgensen, J. Olsen, Molecular electronic-structure theory John Wiley & Sons, Chichester, **2000**.

[21] T. Helgaker, W. Klopper, D. P. Tew. *Mol. Phys.* **2008**, *106*, 2107-2143.

[22] R. M. Balabin. *J. Chem. Phys.* **2010**, *132*, 211103/1-211103/4.

[23] D. Asturiol, M. Duran, P. Salvador. *J. Chem. Phys.* **2008**, *128*, 144108/2-144108/5.

[24] H. Valdés, V. Klusák, M. Pitoňák, O. Exner, I. Starý, P. Hobza, L. Rulíšek. *J. Comput. Chem.* **2008**, *29*, 861-870.

[25] D. Asturiol, M. Duran, P. Salvador. *J. Chem. Theory Comput.* **2009**, *5*, 2574-2581.

[26] M. J. Elrod, R. J. Saykally. *Chem. Rev.* **1994**, *94*, 1975-1997.

[27] E. E. Dahlke, D. G. Truhlar. *J. Phys. Chem. B* **2006**, *110*, 10595-10601.

[28] K. Walczak, J. Friedrich, M. Dolg. *J. Chem. Phys.* **2011**, *135*, 134118/1-134118/11.
[29] J. F. Ouyang, M. W. Cvitkovic, R. P. A. Bettens. *J. Chem. Theory Comput.* **2014**, *10*, 3699-3707.
[30] A. Szabo, N. S. Ostlund. Modern Quantum Chemistry: Introduction to Advanced Electronic Structure Theory, Dover Publications, **2012**.
[31] C. J. Cramer, Essentials of Computational Chemistry: Theories and Models, 2nd Edition, John Wiley & Sons, Chichester, **2004**.
[32] F. Jensen, Introduction to computational chemistry, John Wiley and Sons, Chichester, **2001**.
[33] D. P. Tew, W. Klopper, T. Helgaker. *J. Comput. Chem.* **2007**, *28*, 1307-1320.
[34] C. D. Sherrill, T. Takatani, E. G. Hohenstein. *J. Phys. Chem. A* **2009**, *113*, 10146-10159.
[35] S. Tsuzuki, K. Honda, T. Uchimaru, M. Mikami. *J. Chem. Phys.* **2004**, *120*, 647-659.
[36] S. Tsuzuki, K. Honda, T. Uchimaru, M. Mikami, K. Tanabe. *J. Am. Chem. Soc.* **2001**, *124*, 104-112.
[37] M. O. Sinnokrot, E. F. Valeev, C. D. Sherrill. *J. Am. Chem. Soc.* **2002**, *124*, 10887-10893.
[38] S. Grimme. *J. Chem. Phys.* **2003**, *118*, 9095-9102.
[39] S. Grimme, L. Goerigk, R. F. Fink.*WIRES Comput. Mol. Sci.* **2012**, *2*, 886-906.
[40] M. Gerenkamp, S. Grimme. *Chem. Phys. Lett.* **2004**, *392*, 229-235.
[41] T. P. M. Goumans, A. W. Ehlers, K. Lammertsma, E.-U. Wuerthwein, S. Grimme. *Chem. Eur. J.* **2004**, *10*, 6468-6475.
[42] S. Grimme. *J. Phys. Chem. A* **2005**, *109*, 3067-3077.
[43] J. Antony, S. Grimme. *J. Phys. Chem. A* **2007**, *111*, 4862-4868.
[44] F. Neese, T. Schwabe, S. Kossmann, B. Schirmer, S. Grimme. *J. Chem. Theory Comput.* **2009**, *5*, 3060-3073.
[45] K. E. Riley, J. A. Platts, J Řezáč, P. Hobza, J. G. Hill. *J. Phys. Chem. A* **2012**, *116*, 4159-4169.
[46] J. G. Hill, J. A. Platts. *J. Chem. Theory Comput.* **2006**, *3*, 80-85.
[47] R. A. Distasio Jr, M. Head-Gordon. *Mol. Phys.* **2007**, *105*, 1073-1083.
[48] S. Grimme. *J. Comput. Chem.* **2003**, *24*, 1529-1537.
[49] I. Hyla-Kryspin, S. Grimme. *Organometallics* **2004**, *23*, 5581-5592.
[50] M. Pitonak, J. Řezáč, P. Hobza. *Phys. Chem. Chem. Phys.* **2010**, *12*, 9611-9614.
[51] T. Takatani, E. G. Hohenstein, C. D. Sherrill. *J. Chem. Phys.* **2008**, *128*, 124111/1-124111/8.
[52] E. G. Hohenstein, C. D. Sherrill. *WIREs Comput. Mol. Sci.* **2012**, *2*, 304-326.
[53] A. Hellweg, S. A. Grün, C. Hättig. *Phys. Chem. Chem. Phys.* **2008**, *10*, 4119–4127.
[54] J. Řezáč, P. Hobza. *J. Chem. Theory Comput.* **2013**, *9*, 2151-2155.
[55] J. Řezáč, L. Šimová, P. Hobza. *J. Chem. Theory Comput.* **2012**, *9*, 364-369.
[56] D. G. A. Smith, P. Jankowski, M. Slawik, H. A. Witek, K. Patkowski. *J. Chem. Theory Comput.* **2014**, 10, 3140-3150.
[57] C. Hättig, W. Klopper, A. Köhn, D. P. Tew. *Chem. Rev.* **2011**, *112*, 4-74.
[58] L. Kong, F. A. Bischoff, E. F. Valeev. *Chem. Rev.* **2011**, *112*, 75-107.
[59] T. Helgaker, W. Klopper, H. Koch, J. Noga. *J. Chem. Phys.* **1997**, *106*, 9639-9646.
[60] A. Halkier, T. Helgaker, P. Jørgensen, W. Klopper, H. Koch, J. Olsen, A. K. Wilson. *Chem. Phys. Lett.* **1998**, *286*, 243-252.
[61] D. G. Truhlar. *Chem. Phys. Lett.* **1998**, *294*, 45-48.

[62] A. J. C. Varandas. *J. Chem. Phys.* **2007**, *126*, 244105-244120.
[63] A. Halkier, T. Helgaker, P. Jørgensen, W. Klopper, J. Olsen. *Chem. Phys. Lett.* **1999**, *302*, 437-446.
[64] D. G. Liakos, F. Neese. *J. Phys. Chem. A* **2012**, *116*, 4801-4816.
[65] F. Neese, E. F. Valeev. *J. Chem. Theory Comput.* **2010**, *7*, 33-43.
[66] R. A. Kendall, T. H. Dunning, R. J. Harrison. *J. Chem. Phys.* **1992**, *96*, 6796-6806.
[67] W. Klopper, W. Kutzelnigg. *J. Mol. Struct. (THEOCHEM)* **1986**, *135*, 339-356.
[68] A. Karton, J. L. Martin. *Theor. Chem. Acc.* **2006**, *115*, 330-333.
[69] F. Jensen. *Theor. Chem. Acc.* **2005**, *113*, 267-273.
[70] K. E. Riley, P. Hobza. *WIREs Comput. Mol. Sci.* **2011**, *1*, 3-17.
[71] P. Jurecka, J. Sponer, J. Cerny, P. Hobza. *Phys. Chem. Chem. Phys.* **2006**, *8*, 1985-1993.
[72] J. Řezáč, K. E. Riley, P. Hobza. *J. Chem. Theory Comput.* **2014**, *10*, 1359-1360.
[73] J. Řezáč, K. E. Riley, P. Hobza. *J. Chem. Theory Comput.* **2011**, *7*, 2427-2438.
[74] P. Hobza, J. Šponer. *J. Am. Chem. Soc.* **2002**, *124*, 11802-11808.
[75] P. Hobza in http://www.begdb.com. Last accesed: 15/09/14.
[76] M. Pitoňák, P. Neogrády, J. Černý, S. Grimme, P. Hobza. *ChemPhysChem* **2009**, *10*, 282-289.
[77] K. E. Riley, J. Rezac, P. Hobza. *Phys. Chem. Chem. Phys.* **2011**, *13*, 21121-21125.
[78] R. Sedlak, K. E. Riley, J. Řezáč, M. Pitoňák, P. Hobza. *ChemPhysChem* **2013**, *14*, 698-707.
[79] K. E. Riley, J. Rezac, P. Hobza. *Phys. Chem. Chem. Phys.* **2012**, *14*, 13187-13193.
[80] W. Koch, M. C. Holthausen, A Chemist's guide to density functional theory, Wiley-VCH, Weinhem, **2000**.
[81] P. Hohenberg, W. Kohn. *Phys. Rev.* **1964**, *136*, B864-B871.
[82] A. D. Becke. *Phys. Rev. A* **1988**, *38*, 3098-3100.
[83] C. Lee, W. Yang, R. G. Parr. *Phys. Rev. B* **1988**, *37*, 785-789.
[84] B. Miehlich, A. Savin, H. Stoll, H. Preuss. *Chem. Phys. Lett.* **1989**, *157*, 200-206.
[85] A. D. Becke. *J. Chem. Phys.* **1993**, *98*, 1372-1377.
[86] Y. Zhao, D. G. Truhlar. *J. Chem. Phys.* **2006**, *125*, 194101-194119.
[87] Y. Zhao, D. G. Truhlar. *Theor. Chem. Acc.* **2007**, *120*, 215-241.
[88] Y. Zhao, D. Truhlar. *Theor. Chem. Acc.* **2008**, *120*, 215-241.
[89] Y. Zhao, D. G. Truhlar. *J. Chem. Theory Comput.* **2008**, *4*, 1849-1868.
[90] R. Peverati, D. G. Truhlar. *J. Phys Chem. Lett.* **2011**, *3*, 117-124.
[91] R. Peverati, D. G. Truhlar. *J. Phys Chem. Lett.* **2011**, *2*, 2810-2817.
[92] R. Peverati, D. G. Truhlar. *J. Chem. Theory Comput.* **2012**, *8*, 2310-2319.
[93] R. Peverati, D. G. Truhlar. *Phys. Chem. Chem. Phys.* **2012**, *14*, 16187-16191.
[94] R. Peverati, D. G. Truhlar. *Phys. Chem. Chem. Phys.* **2012**, *14*, 13171-13174.
[95] S. Grimme. *J. Chem. Phys.* **2006**, *124*, 0341081-0341097.
[96] Y. Zhao, B. J. Lynch, D. G. Truhlar. *J. Phys. Chem. A* **2004**, *108*, 4786-4791.
[97] S. Grimme. *J. Comput. Chem.* **2004**, *25*, 1463–1473.
[98] S. Grimme. *J. Comput. Chem.* **2006**, *27*, 1787–1799.
[99] S. Grimme, J. Antony, S. Ehrlich, H. Krieg. *J. Chem. Phys.* **2010**, *132*, 214301/1-214320.
[100] S. Grimme, S. Ehrlich, L. Goerigk. *J. Comput. Chem.* **2011**, *32*, 1456-1465.
[101] S. Grimme. *WIREs Comput. Mol. Sci.* **2011**, *1*, 211-228.

[102] A. Krishtal, C. Van Alsenoy, P. Geerlings. *J. Chem. Phys.* **2014**, *140*, 184105/1-184105/14.
[103] S. N. Steinmann, C. Corminboeuf. *J. Chem. Theory Comput.* **2010**, *6*, 1990-2001.
[104] S. N. Steinmann, C. Corminboeuf. *J. Chem. Phys.* **2011**, *134*, 044117/1-044117/5.
[105] O. A. Vydrov, T. Van Voorhis. *J. Chem. Phys.* **2010**, *133*, 244103/1-244103/9.
[106] M. Dion, H. Rydberg, E. Schröder, D. C. Langreth, B. I. Lundqvist. *Phys. Rev. Lett.* **2004**, *92*, 246401.
[107] F. D. John, G. Tim. *J. Phys.: Condens. Matter* **2012**, *24*, 073201.
[108] L. A. Burns, Á. V. Mayagoitia, B. G. Sumpter, C. D. Sherrill. *J. Chem. Phys.* **2011**, *134*, 084107/2-084107/25.
[109] E. R. Johnson, A. D. Becke. *J. Chem. Phys.* **2005**, *123*, 024101/1-024101/7.
[110] C. Van Alsenoy. *J. Comput. Chem.* **1988**, *9*, 620-626.
[111] H.-J. Werner, F. R. Manby, P. J. Knowles. *J. Chem. Phys.* **2003**, *118*, 8149-8160.
[112] K. Eichkorn, O. Treutler, H. Öhm, M. Häser, R. Ahlrichs. *Chem. Phys. Lett.* **1995**, *240*, 283-290.
[113] F. Weigend. *J. Comput. Chem.* **2008**, *29*, 167-175.
[114] C. Hattig. *Phys. Chem. Chem. Phys.* **2005**, *7*, 59-66.
[115] M. S. Gordon, D. G. Fedorov, S. R. Pruitt, L. V. Slipchenko. *Chem. Rev.* **2011**, *112*, 632-672.
[116] K. Morokuma. *J. Chem. Phys.* **1971**, *55*, 1236-1244.
[117] W. Chen, M. S. Gordon. *J. Phys. Chem.* **1996**, *100*, 14316-14328.
[118] E. D. Glendening, A. Streitwieser. *J. Chem. Phys.* **1994**, *100*, 2900-2909.
[119] G. K. Schenter, E. D. Glendening. *J. Phys. Chem.* **1996**, *100*, 17152-17156.
[120] E. D. Glendening. *J. Phys. Chem. A* **2005**, *109*, 11936-11940.
[121] W. J. Stevens, W. H. Fink. *Chem. Phys. Lett.* **1987**, *139*, 15-22.
[122] P. Su, Z. Jiang, Z. Chen, W. Wu. *J. Phys. Chem. A* **2014**, *118*, 2531-2542.
[123] P. Su, H. Li. *J. Chem. Phys.* **2009**, *131*, 014102/1-014102/15.
[124] T. Ziegler, A. Rauk. *Theor. Chim. Acta* **1977**, *46*, 1-10.
[125] I. C. Hayes, A. J. Stone. *Mol. Phys.* **1984**, *53*, 83-105.
[126] B. Jeziorski, R. Moszynski, K. Szalewicz. *Chem. Rev.* **1994**, *94*, 1887-1930.
[127] R. Moszynski. *Mol. Phys.* **1996**, *88*, 741-758.
[128] E. G. Hohenstein, C. D. Sherrill. *J. Chem. Phys.* **2010**, *133*, 014101/1-014101/12.
[129] E. G. Hohenstein, C. D. Sherrill. *J. Chem. Phys.* **2010**, *132*, 184111/1-184111/10.
[130] J. M. Turney, A. C. Simmonett, R. M. Parrish, E. G. Hohenstein, F. A. Evangelista, J. T. Fermann, B. J. Mintz, L. A. Burns, J. J. Wilke, M. L. Abrams, N. J. Russ, M. L. Leininger, C. L. Janssen, E. T. Seidl, W. D. Allen, H. F. Schaefer, R. A. King, E. F. Valeev, C. D. Sherrill, T. D. Crawford. *WIREs Comput. Mol. Sci.* **2012**, *2*, 556-565.
[131] H. L. Williams, C. F. Chabalowski. *J. Phys. Chem. A* **2000**, *105*, 646-659.
[132] A. Heßelmann, G. Jansen. *Chem. Phys. Lett.* **2002**, *357*, 464-470.
[133] A. Heßelmann, G. Jansen. *Chem. Phys. Lett.* **2002**, *362*, 319-325.
[134] A. Heßelmann, G. Jansen. *Chem. Phys. Lett.* **2003**, *367*, 778-784.
[135] A. Heßelmann, G. Jansen, M. Schütz. *J. Chem. Phys.* **2005**, *122*, 014103/1-014103/17.
[136] G. Jansen. *WIREs Comput. Mol. Sci.* **2014**, *4*, 127-144.
[137] A. J. Misquitta, R. Podeszwa, B. Jeziorski, K. Szalewicz. *J. Chem. Phys.* **2005**, *123*, 214103/1-214103/14.
[138] R. Bukowski, R. Podeszwa, K. Szalewicz. *Chem. Phys. Lett.* **2005**, *414*, 111-116.

[139] R. Podeszwa, R. Bukowski, K. Szalewicz. *J. Chem. Theory Comput.* **2006**, *2*, 400-412.
[140] K. Szalewicz. *WIREs Comput. Mol. Sci.* **2012**, *2*, 254-272.
[141] M. Grüning, O. V. Gritsenko, S. J. A. van Gisbergen, E. J. Baerends. *J. Chem. Phys.* **2001**, *114*, 652-660.
[142] D. J. Tozer, N. C. Handy. *Mol. Phys.* **2003**, *101*, 2669-2675.
[143] J. Řezáč, P. Hobza. *J. Chem. Theory Comput.* **2011**, *7*, 685-689.
[144] R. F. W. Bader, Atoms in Molecules: A Quantum Theory, Clarendon Press, Oxford **1990**.
[145] J. Contreras-García, E. R. Johnson, S. Keinan, R. Chaudret, J.-P. Piquemal, D. N. Beratan, W. Yang. *J. Chem. Theory Comput.* **2011**, *7*, 625-632.
[146] E. R. Johnson, S. Keinan, P. Mori-Sánchez, J. Contreras-García, A. J. Cohen, W. Yang. *J. Am. Chem. Soc.* **2010**, *132*, 6498-6506.
[147] J. Tomasi, B. Mennucci, R. Cammi. *Chem. Rev.* **2005**, *105*, 2999-3094.
[148] A. Klamt, G. Schuurmann. *J. Chem. Soc. Perkin Trans. 2* **1993**, 799-805.
[149] M. J. Vilkas, C.-G. Zhan. *J. Chem. Phys.* **2008**, *129*, 194109/1-194109/7.

USC UNIVERSIDADE DE SANTIAGO DE COMPOSTELA

USC
UNIVERSIDADE
DE SANTIAGO
DE COMPOSTELA

4. Effects of microhydration on the characteristics of cation-phenol complexes

USC
UNIVERSIDADE
DE SANTIAGO
DE COMPOSTELA

4.1. Introduction

Intermolecular interactions are known to play a key role in many aspects of chemistry and biology, being crucial to phenomena as protein···ligand interaction and molecular recognition.[1, 2] Among the different intermolecular forces, those involving aromatic moieties present especial character due to the presence of conjugated electrons and a planar geometry.[3-5] Also, as regards biochemistry, interactions involving aromatic units are crucial in protein structure. It is believed that aromatic groups interact in a different manner than aliphatic units in the side chains of amino acids, and can provide specificity in protein folding.[4-8]

Cation···π interactions are strong interactions in the gas phase and have been recognized as one of the structural motifs conditioning the structure in proteins.[5, 9] Since the initial works from Dougherty et al. the cation···π interaction is now regarded as one key factor in determining the characteristics of proteins, together with hydrogen bonds, stacking interactions and salt bridges.[5-7, 9, 10] The importance of these cation···π interactions in proteins is easily understood taking into account that some amino acids as phenylalanine, tyrosine, tryptophan and histidine bear an aromatic unit in their side chains, whereas other amino acids as arginine, lysine and histidine possess cationic groups depending on the pH. Thus, interactions between side chains of these amino acids are often observed in protein structure suggesting their relevance as a stabilizing motif.[5, 9, 11]

Though cation···π interactions are known to be strong interactions in the gas phase, this has not to be true in solution. Different studies give contradictory results ranging from an important contribution to protein stabilization to an almost negligible effect.[11-22] These discrepancies are generally addressed to solvent effects, depending on the degree of exposure of the cation···π contact to the solvent. Several studies exist in literature dealing with the interaction of alkali cations with benzene, showing the usual trend of stronger interaction as the size of the cation decreases.[23-26] Also, several authors have studied the effect of water coordinated to the cation on the strength of the cation···benzene interaction.[27-32] However, most studies have been carried out with benzene as a model for aromatic interaction, with few works devoted to other aromatic units.[33-36] In this work, a study of the interaction between a K^+, Na^+, Li^+ or Mg^{2+} cation with phenol in the presence of a small number of water molecules has been performed by employing ab initio and density functional theory methods. Phenol is not only a common chemical but also the chromophore of the aromatic amino acid tyrosine. Contrary to benzene, phenol possesses two different regions where a cation can establish a stabilizing interaction: the aromatic cloud and the lone pairs of the hydroxyl oxygen.[37, 38] Also, the hydroxyl group can act both as donor or acceptor in hydrogen bonds with the water molecules included in the cluster. Therefore, even when phenol is

very similar to benzene, the presence of the hydroxyl group introduces a greater complexity on the potential energy surface of the clusters, allowing for a greater variety of stable structures.[39-49]

Vaden and Lisy experimentally determined the vibrational spectra of clusters formed by phenol with K^+ and Na^+ cations, calculations being employed for explaining the characteristics of the spectra for clusters with four water molecules.[37] However, no calculations were performed for the smaller clusters so no information was provided about the stepwise microhydration process. Therefore, the present work is intended to shed light on the characteristics of the interaction between cations and phenol, and how this interaction is affected by the progressive incorporation of a small number of water molecules. The results thus obtained would help rationalize the behavior observed in protein cation···π interactions in different environments with distinct degree of exposure to the solvent.

4.2. Computational Details

The geometries of complexes formed by K^+, Na^+, Li^+ or Mg^{2+}, one phenol molecule, and up to four water molecules have been optimized both at the B3LYP/6-31+G(2d,p) and MP2/6-31+G(d) levels of calculation. A common problem in this kind of study is how to employ a procedure that is able to ensure a good exploration of the potential energy surface of the clusters in order to characterize the most stable structures. Taking into account the characteristics of the clusters is more than probable that the most stable structures will correspond to direct contacts of water and phenol with the cation, and to hydrogen bond arrangements. Therefore, the following procedure has been employed: a set of different structures for the complexes without water molecules has been considered as starting points for optimizations. Once the minima of cation···phenol complexes have been located, a new water molecule is included so it contacts directly with the cation, establishes hydrogen bonds to phenol as donor or acceptor, or intercalates between the cation and phenol. All these possibilities are considered as starting structures and optimized in order to localize the minima for monohydrated cation···phenol complexes. The same procedure is repeated as more water molecules are included. In this way, we have selected plenty of starting structures (more than one hundred for complexes with 3 water molecules) which, after optimization, gave rise to a great variety of minima. Only the most stable ones have been included for discussion. We expect that in this way a quite thorough exploration of the potential energy surface is ensured, so the most relevant structures are already included in our analysis and probably even more rigorous procedures would finish in a similar set of minima, without affecting the results and general conclusions of this work. This kind of hierarchical procedure is quite frequently used, though restricted to a small number of molecules since the number of different starting structures grows very quickly when all possible

hydrogen bonds or favorable contacts are considered for including the new water molecule.[50-54]

After reaching a stationary point, frequency calculations were carried out at both levels of calculation to ensure that the geometry corresponds to a minimum and does not exhibit imaginary frequencies. Once the stationary points have been located the complexation energies have been obtained by means of the supermolecule method as the difference between the energy of the complex and the energies of its constituent fragments. The counterpoise method as proposed by Boys and Bernardi has been employed for avoiding basis set superposition error (BSSE).[55-57] Therefore, the interaction energy for a given complex is obtained as:

$$\Delta E_{\text{int}} = E^{complex}(ijk\ldots) - \sum_i E_i^{complex}(ijk\ldots) \quad \text{(eq. 4.1)}$$

.

Where the terms in parentheses indicate that the whole basis set of the complex is employed in all calculations and the superscripts indicate the geometry employed in the calculations (in this case the geometry of the fragments in the complex). Besides this interaction energy, the formation of the complex implies some geometric deformation to accommodate the fragments to the geometry of the complex.[56, 57] Therefore, the total complexation energy is obtained by adding to the interaction energy the deformation energy caused by this geometric distortion:

$$E_{def} = \sum \left(E_i^{complex}(i) - E_i^{isolated}(i) \right), \quad \text{(eq. 4.2)}$$

$$\Delta E_{complex} = \Delta E_{\text{int}} + E_{def} \quad \text{(eq. 4.3)}$$

.

Complexation energies for the different complexes studied in the present work have been obtained at the B3LYP/6-31+G(2d,p) level and at the MP2/6-31+G(2d,p) level employing geometries optimized with different levels of calculation. All calculations have been done by using the Gaussian09 program.[58]

4.3. Results

In the following section the results obtained for the complexes studied will be presented. For the sake of simplicity, results will be grouped attending to the number of water molecules present in the complex, and will be presented in order of increasing polarizing power of the cation; that is from K^+ to Mg^{2+}.

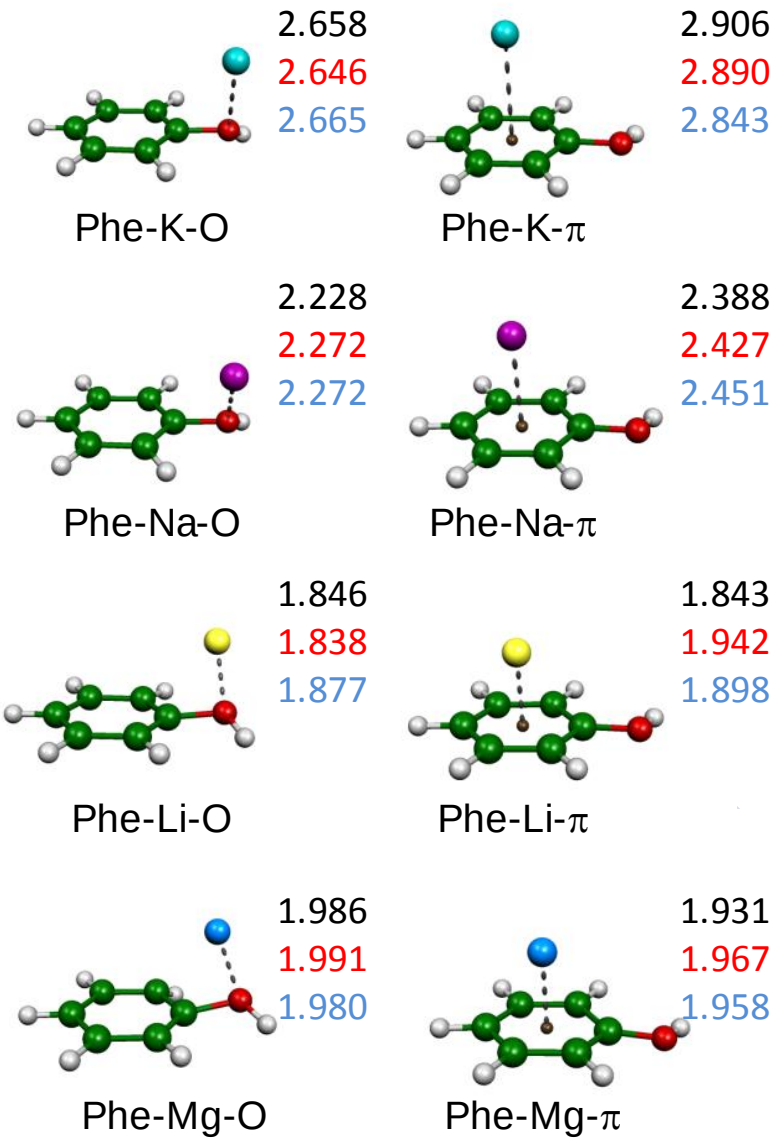


Figure 4.1. Structures of the cation···phenol complexes in absence of water molecules. The numbers correspond to distances in Å as obtained with different levels of calculation. From top to bottom: B3LYP/6-31+G(2d,p); MP2/6-31+G(d); MP2/6-31+G(2d,p).

4.3.1. Cation···phenol complexes

Figure 4.1 shows the structures of the most stable minima located for the complexes formed by phenol and each of the cations considered in this work, whereas Table 4.1 lists the values obtained for the complexation energies of these complexes as obtained with different levels of calculation. In concordance with previous results for sodium and potassium complexes with phenol, two different minima have been found for the complexes formed by any of the cations and a phenol moiety. Phenol presents two electron-rich regions corresponding to the aromatic ring and to the hydroxyl oxygen, so the cations are located interacting with these regions.[37, 38] Figure 4.1 also lists the intermolecular distances obtained with different methods, though it can be observed that the results are similar in all cases. As expected, K^+ cation is placed over the aromatic ring a bit tilted away from the hydroxyl group, at about 2.9 Å from the ring center. As the polarizing power of the cation increases the intermolecular distance to the center of the ring decreases to about 2.5 Å for Na^+ and 1.9 Å for Li^+. For Mg^{2+} cation a somewhat larger distance of 2.0 Å is obtained. In the case of the minima where the cation interacts with the oxygen atom, the behavior is pretty similar. In any case, it can be observed that whereas the larger cations are tilted away from the aromatic ring, in the case of Li^+ and especially in the Mg^{2+} complex the cation also tries to interact with the electron-rich region over the aromatic ring. Also, with the two smallest cations phenol molecule is significantly distorted, with the hydroxyl group going out of the plane of the ring (more than 30º in the case of Mg^{2+} complex). As indicated by Marshall et al. the interaction energy in cation···benzene complexes is also sensitive to the angle of the cation with respect to the symmetry axis of benzene.[59] Though in the minima shown in Figure 4.1 cations are not exactly over the center of the ring, the deviations are smaller than 10 degrees. Therefore, it cannot be expected deviations from the ring center to have a significant impact on energies.

As regards complexation energies listed in Table 4.1, all methods provide pretty similar values, with B3LYP providing more negative complexation energies except in the case of potassium complexes. Though it is known that B3LYP does not provide a proper description of dispersion interactions, it can be expected to perform fairly well in systems controlled by electrostatics as those considered in this work. Also, the values obtained with the MP2/6-31+G(2d,p) are independent of the method employed for the geometry optimization. The values obtained at the MP2/6-31+G(2d,p) level are quite similar to those obtained with larger basis sets, especially for Li^+, Na^+ and Mg^{2+} complexes. However, the largest difference is observed for K^+ complexes, with energy differences between MP2/6-31+G(2d,p) and the largest basis set amounting to more than 1 kcal/mol. Similar relatively small energy differences are observed for some of the complexes containing one water molecule, though in general the order of stability is well reproduced (see Appendix A).

Table 4.1. Complexation energies (kcal/mol) for cation···phenol clusters as obtained with different levels of calculation.

	K^+	Na^+	Li^+	Mg^{+2}
	Phe-X-O			
B3LYP/6-31+G(2d,p)	-16.27	-24.31	-36.25	-124.10
MP2-A[(a)]	-17.27	-22.18	-33.64	-112.69
MP2-B[(b)]	-17.14	-22.61	-33.67	-112.49
MP2/6-31+G(2d,p)	-17.11	-22.49	-33.90	-112.78
MP2-C[(c)]	-17.49	-21.96	-33.58	-111.80
MP2-D[(d)]	-17.76	-22.09	-33.71	-112.52
	Phe-X-π			
B3LYP/6-31+G(2d,p)	-15.97	-24.76	-39.39	-126.35
MP2-A[(a)]	-17.34	-22.28	-36.10	-116.57
MP2-B[(b)]	-17.19	-22.61	-35.99	-116.40
MP2/6-31+G(2d,p)	-17.25	-22.49	-36.10	-116.60
MP2-C[(c)]	-18.10	-21.79	-35.90	-115.00
MP2-D[(d)]	-18.78	-22.16	-36.08	-115.91

a) MP2/6-31+G(2d,p)// B3LYP/6-31+G(2d,p); b) MP2/6-31+G(2d,p)//MP2/6-31+G(d); c) MP2/6-311++G(2d,2p)//MP2/6-31+G(d); d) MP2/6-311++G(3d,2p) //MP2/6-31+G(d).

Therefore, taking into account these results, it can be expected that the error in complexation energies at the level of calculation employed in this work is probably around 1 kcal/mol. Thus, small energy differences found between different minima should be considered with care, especially in the case of K^+ complexes, even though we expect the overall behavior observed with the level of calculation employed in this work will be similar to that with the larger basis sets.

The values in Table 4.1 are in agreement with those obtained for benzene···cation complexes, which amount to -35.41, -21.31, -16.99 and -108.76 kcal/mol for Li^+, Na^+, K^+ and Mg^{2+}, respectively.[30, 59] The only significant differences are observed for the complexes with Mg^{2+} interacting with the ring, which are more stable by around 8 kcal/mol as compared with benzene complexes. As the size of the cation decreases the complexation energies become more negative, changing from about -17 kcal/mol for K^+ to -22 kcal/mol for Na^+, in agreement with values from literature. In the case of Li^+ complexes, the complexation energy reaches around -36 kcal/mol for the Phe-X-π, whereas amounts to -34 kcal/mol for the Phe-X-O minimum. In Mg^{2+} complexes, Phe-X-π structure shows a complexation energy of -116 kcal/mol, with Phe-X-O reaching -113 kcal/mol. Therefore, as expected, the complexation energies become steeply more negative as the size of the cation decreases. Also, Li^+ and Mg^{2+} prefer to bind to the π

cloud, probably due to an increased polarization effect. In any case, the results shown here, in agreement with published data,[37, 38] correspond to bare cations. In the next sections, the effect of including discrete water molecules to the complexes will be analyzed.

4.3.2. Monohydrated cation···phenol complexes

After optimization with the B3LYP/6-31+G(2d,p) or the MP2/6-31+G(d) level of calculation six different structures have been found for complexes of phenol with K^+ and Na^+, as shown in Figure 4.2. It can be appreciated that these minima correspond to the minima shown in the preceding section by adding a new water molecule on the cation or on the hydroxyl group of phenol. Structures Phe-X1-1H_2O and Phe-X4-1H_2O, present both phenol and the water molecule located in opposite sides of the cation in an almost linear fashion. The difference between these two structures comes from the cation being coordinated with the phenol via the aromatic ring or the hydroxyl oxygen. Phe-X2-1H_2O and Phe-X5-1H_2O minima present the water molecule hydrogen bonded to the hydroxyl group whereas the cation coordinates to the phenol molecule. Finally, Phe-X3-1H_2O and Phe-X6-1H_2O are similar to Phe-X1-1H_2O and Phe-X4-1H_2O, but in this case the water molecule is oriented establishing a hydrogen bond with the aromatic cloud or the hydroxyl oxygen of phenol. For doing so, the geometry has to be distorted from the ideal quasi-linear array around the cation.

As observed in Table 4.2, when the water molecule is hydrogen bonded to the phenol unit and simultaneously interacts with the cation (Phe-X3-H_2O and Phe-X6-H_2O), there is preference for K^+ to be located over the aromatic cloud. Coordination with the oxygen atom of phenol is more than 2 kcal/mol less stable. This is partly a consequence of the strongest hydrogen bond that water forms with the hydroxyl oxygen as compared with the OH···π interaction (typical values are around 5 kcal/mol for O-H···O and 3 kcal/mol for OH···π). The contribution of this O-H···O hydrogen bond is also reflected in the stability difference between structures Phe-X4-1H_2O and Phe-X6-H_2O.

The behavior is similar for Na^+ complexes, though the differences between linear and bent structures are smaller than in the K^+ complexes. This is due to the larger cation···water interaction, which is optimal in a linear arrangement. Therefore, it takes more effort to bend the water interacting with Na^+ than it takes for K^+. Considering the structures in Figure 4.2, it is also worth noting the short OH···O distances observed in the Phe-X2-1H_2O and Phe-X5-1H_2O minima, as a consequence of the cation polarizing the phenol molecule. Therefore the hydroxyl group interacts more strongly with water than it should be the case with isolated phenol. In the case of Li^+ and Mg^{2+} cations only four structures were obtained as shown in Figure 4.2, since minima such as Phe-X3-1H_2O and Phe-X6-1H_2O are not located. Optimizations starting from these structures lead to the minima with water and phenol occupying opposite sides of the cation. As indicated above, the larger interaction between water and Li^+ and Mg^{2+} favors structures with

optimum cation···water interaction, even at the cost of loosing part of the stabilization gained by the formation of OH···O or O-H···π contacts. With the smaller cations, there are larger differences between structures with water coordinated to the cation with respect to other structures with water hydrogen bonded to phenol. In fact, it can be observed from Table 4.2 that the energy difference between structures Phe-X1-1H_2O and Phe-X2-1H_2O decreases as the size of the cation increases. That is, for K^+ complexes the hydroxyl group of phenol can compete with the cation for interacting with water, whereas for smaller cations the direct coordination to the cation is clearly favored.

Table 4.2. Complexation energies (kcal/mol) of the most stable monohydrated cation···phenol complexes as obtained at the MP2/6-31+G(2d,p)//MP2/6-31+G(d) level.

	Phe-X1-1H_2O	**Phe-X2-1H_2O**	**Phe-X3-1H_2O**	**Phe-X4-1H_2O**	**Phe-X5-1H_2O**	**Phe-X6-1H_2O**
K^+	-31.87	-30.24	-33.30	-33.07	-29.94	-35.72
Na^+	-41.80	-36.13	-42.41	-42.35	-35.56	-43.70
Li^+	-61.01	-48.99	-	-62.23	-50.02	-
Mg^{+2}	-171.40	-140.45	-	-174.91	-140.61	-

4.3.3. Dihydrated cation···phenol complexes

With the inclusion of the second water molecule, a greater variety of structures has been located, so only the most stable among the minima located will be discussed for each cation. Generally speaking, the larger the cation, the larger the number of different minima within a given energy interval, so the behavior is simpler for Li^+ and Mg^{2+} clusters, whereas for K^+ the most complex behavior arises.

Figure 4.3 shows the most stable minima located for complexes formed by phenol with K^+ and Na^+ cations including two water molecules. It can be observed that the first four structures have similar characteristics for both cations, whereas differences appear for the other two presented in Figure 4.3. Considering K^+ complexes and the values for complexation energies listed in Table 4.3, it can be observed that structures with the K^+ cation over the aromatic ring of phenol are more stable than the analogous structure with K^+ interacting with the oxygen atom.

The three structures named as Phe-X2-2H_2O, Phe-X4-2H_2O and Phe-X6-2H_2O present similar complexation energies, showing that in the case of K^+ complexes there is no significant energy difference when water molecule coordinates to K^+ directly of interacts with the OH group of phenol, and the same can be observed in the rest of structures with K^+ interacting with the hydroxyl group.

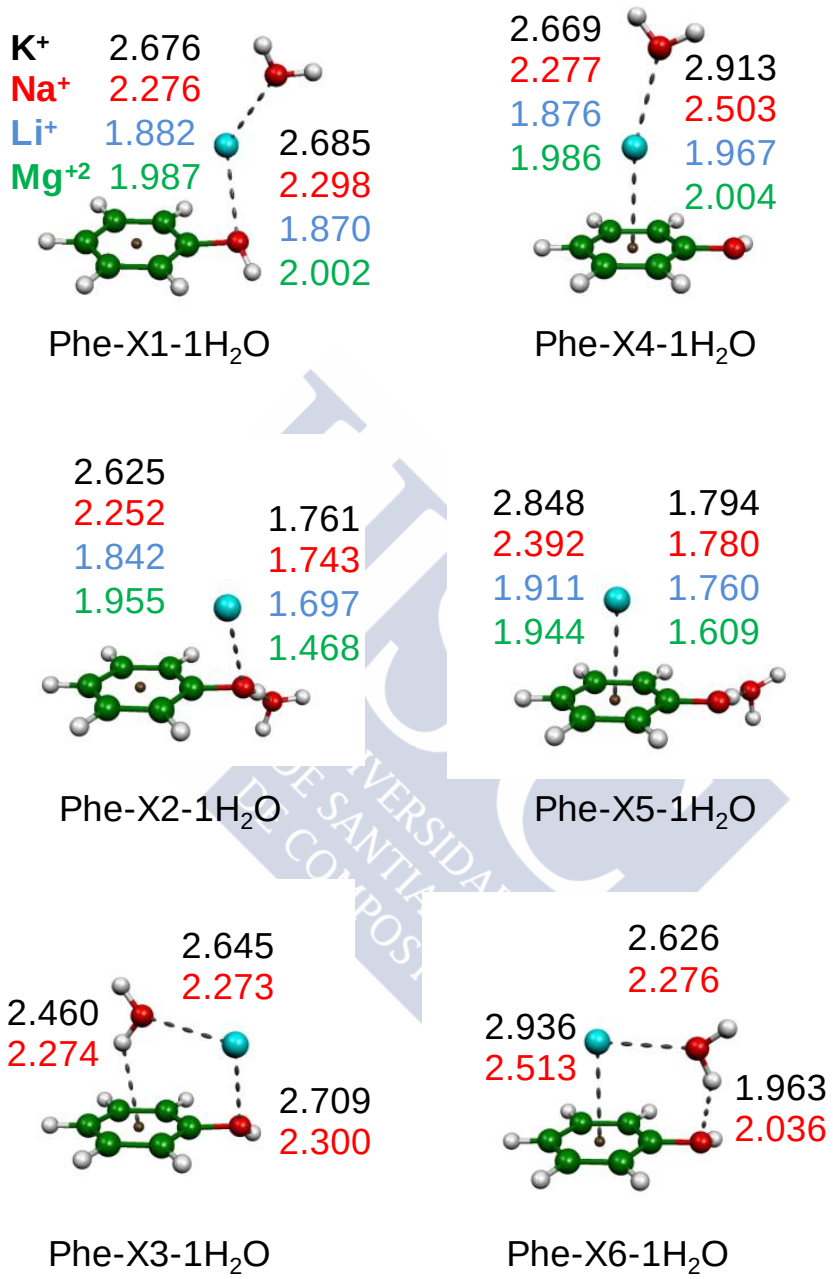


Figure 4.2. Most stable minima of the monohydrated cation···phenol complexes. The numbers correspond to distances in Å as obtained at the MP2/6-31+G(d) level of calculation.

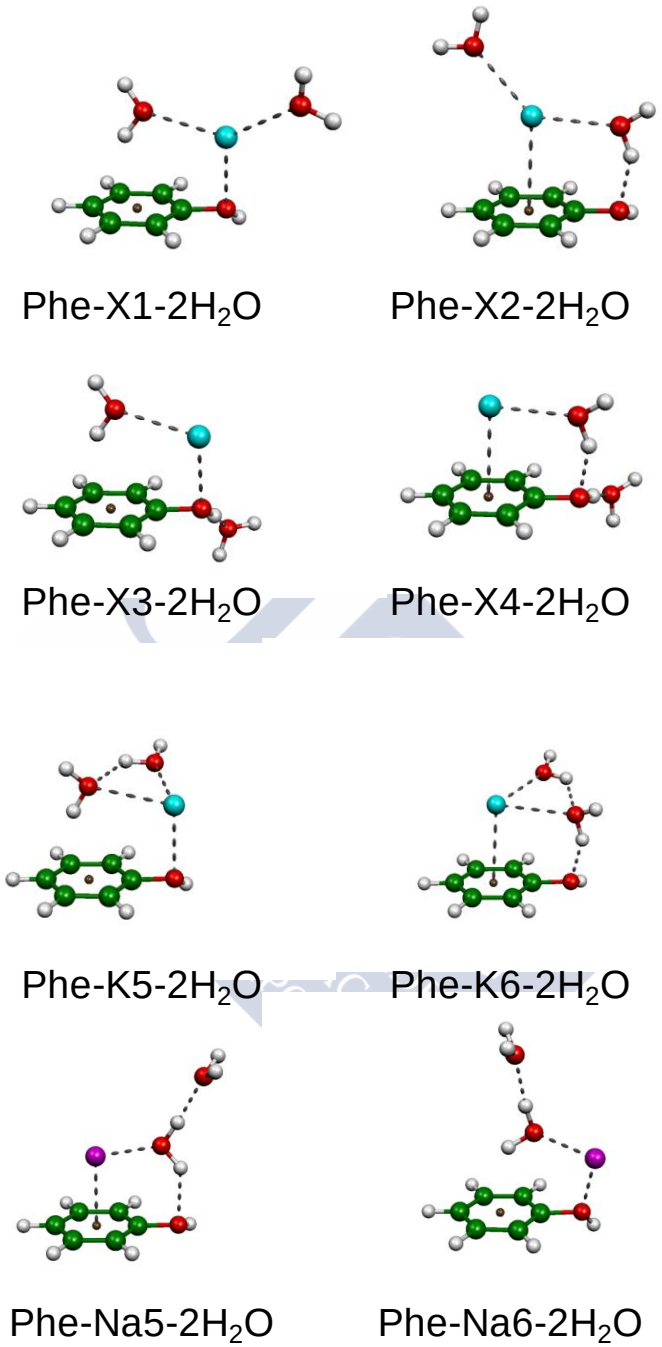


Figure 4.3. Most stable minima located at the MP2/6-31+G(d) level for the dihydrated complexes of K^+ and Na^+ with phenol.

The most stable minima corresponds to a trigonal arrangement of the two water molecules and the phenyl ring around the K^+ cation, though Phe-X6-2H_2O shows similar stability, with both water molecules interacting directly with K^+, simultaneously establishing a hydrogen bond between them, keeping an O···K···O angle of only 65 degrees. However, as indicated above, several of these minima show stability differences within the error of the methods employed, so the behavior could slightly change if more sophisticated (and costly) methods are employed.

Table 4.3. Complexation energies (kcal/mol) of the most stable dihydrated complexes as obtained at the MP2/6-31+G(2d,p)//MP2/6-31+G(d) level of calculation.

	Phe-X1-2H_2O	Phe-X2-2H_2O	Phe-X3-2H_2O	Phe-X4-2H_2O	Phe-X5-2H_2O	Phe-X6-2H_2O
K^+	-46.77	-48.30	-45.30	-47.07	-46.42	-47.92
Na^+	-59.46	-59.89	-55.15	-55.76	-54.36	-54.00
Li^+	-83.52	-81.95	-74.81	-75.14	-75.15	-75.84
Mg^{+2}	-218.63	-218.96	-196.73	-196.97	-198.46	-201.75

In the case of Na^+ complexes, though the minima are similar, the energy ordering depends more on the arrangement of water molecules around the cation, so the two most stable structures correspond to a similar trigonal arrangement, the difference being the location of the cation over the ring or close to the hydroxyl group. The rest of the structures are less stable with relative energies more than 4 kcal/mol above the most stable minimum. It is worth noting that no stable minimum was found similar to those observed for K^+ cation, with water molecules bound to the cation and interacting between themselves. In the case of Na^+, the interaction with water is stronger, so the distorted hydrogen bond between water molecules cannot overcome the energy loss when departing from the trigonal arrangement. For K^+ complexes, minima similar to those obtained for Na^+ can be found, with complexation energies amounting to -44.9 and -43.5 kcal/mol. Li^+ and Mg^{2+} complexes shown in Figure 4.4 present similar characteristics to those found for Na^+. For both cations the same minima are obtained, with energies listed in Table 4.3. The most stable structures correspond to a trigonal arrangement around the cation, with no large differences regarding whether the cation is on the ring or over the hydroxyl group. There is a significant energy gap with the rest of structures, reaching 6 kcal/mol and 17 kcal/mol for Li^+ and Mg^{2+}, respectively. It is also worth noting that in Mg^{2+} complexes, coordination with a water molecule in the second shell is energetically favored over coordination to the hydroxyl group of phenol, contrary to the behavior observed with the other cations, where the hydroxyl group can be competitive for coordinating water molecules compared with other water units already present in the complex.

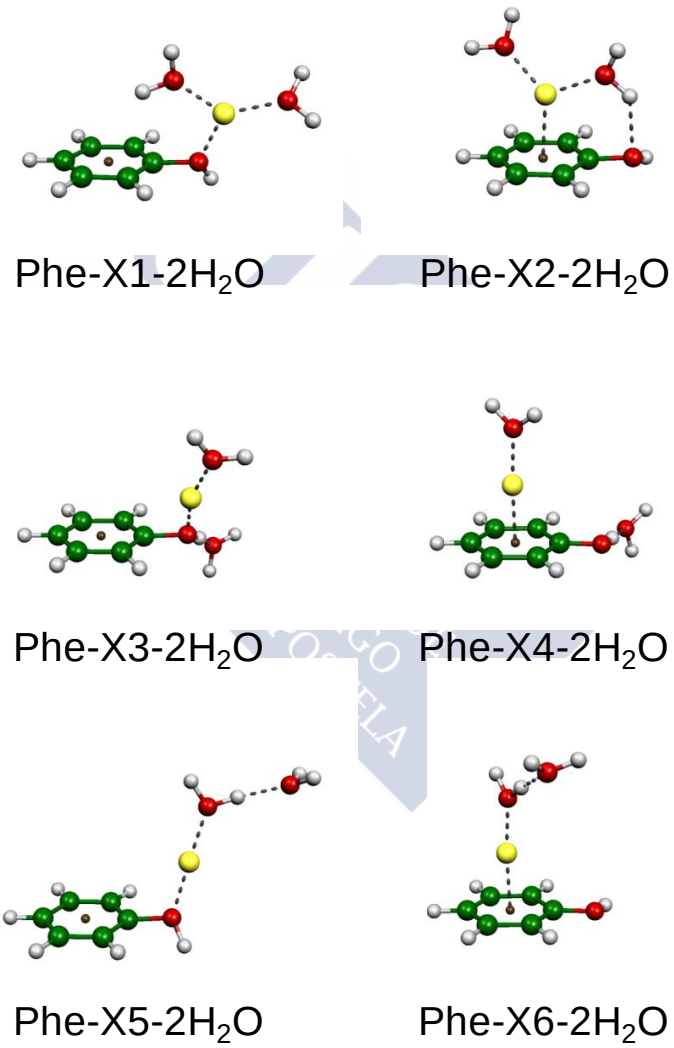


Figure 4.4. Most stable minima located at the MP2/6-31+G(d) level for the dihydrated complexes of Li^+ and Mg^{2+} with phenol.

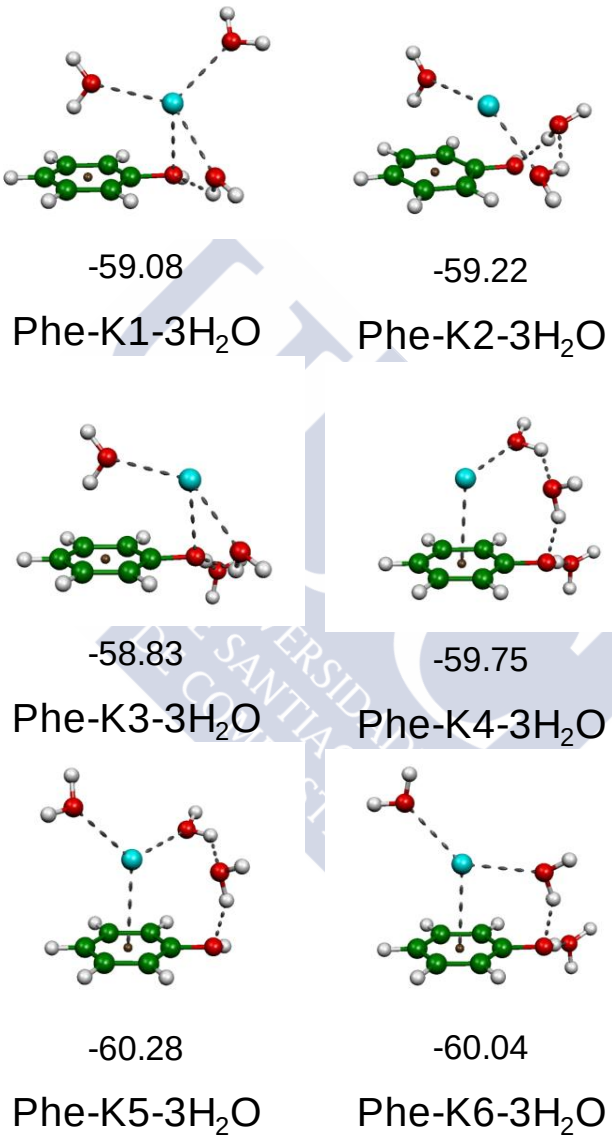


Figure 4.5. Most stable minima located for the trihydrated complexes of K^+ with phenol. Numbers correspond to complexation energies in kcal/mol at the MP2/6-31+G(2d,p)//MP2/6-31+G(d) level.

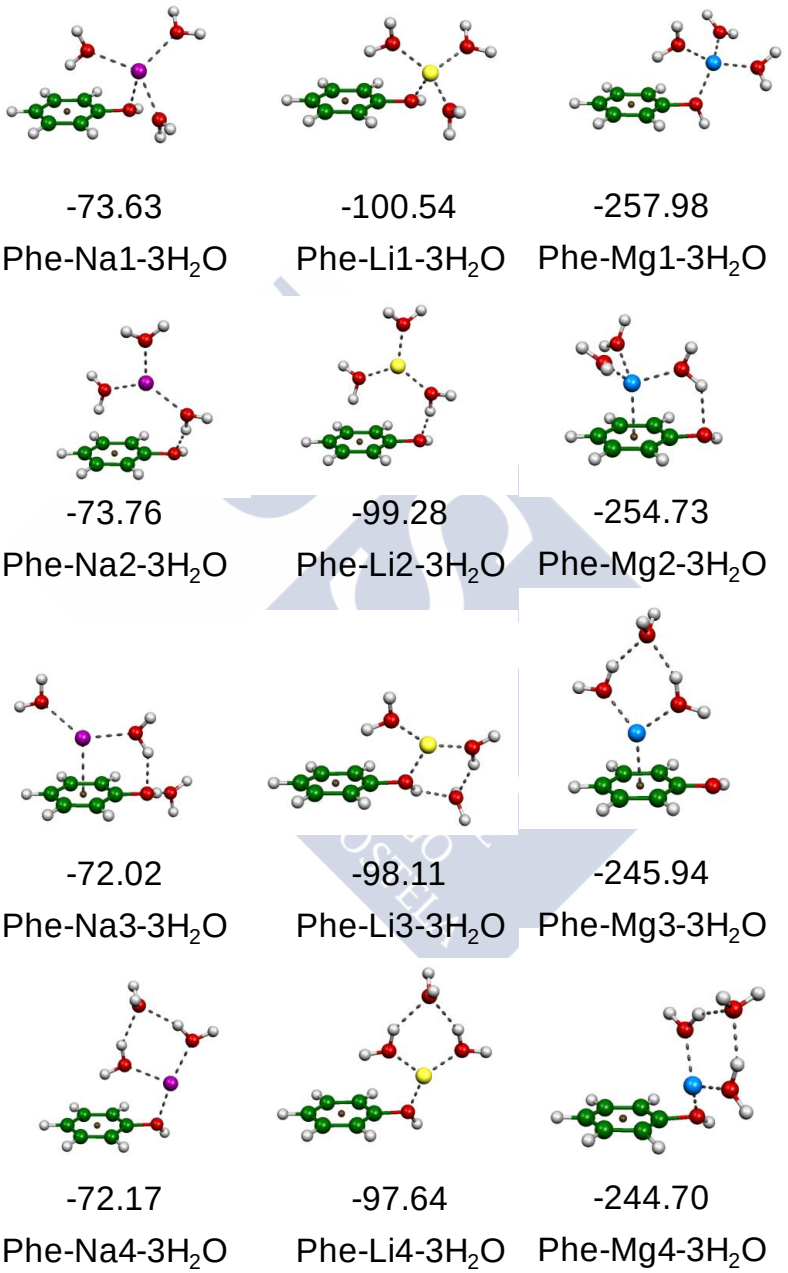


Figure 4.6. Most stable minima located for the trihydrated complexes of Na^+, Li^+ and Mg^{2+} with phenol. Numbers correspond to complexation energies in kcal/mol at the MP2/6-31+G(2d,p)//MP2/6-31+G(d) level.

4.3.4. Trihydrated complexes

The incorporation of a third water molecule increases the complexity of the potential energy surface of the complexes giving rise to a great variety of minima, usually with similar stabilities, especially for the larger cations. Therefore, K^+ complexes present the most complex behavior with the largest number of minima within a small energy interval. The most stable minima found are shown in Figure 4.5, differing in stability by less than 1 kcal/mol. Therefore, as water molecules are included in the complex, there are smaller differences between direct coordination to the K^+ cation, to another water molecule or to the hydroxyl group, thus allowing for a greater variety of structures.

The most stable complexes formed with Na^+, Li^+ and Mg^{2+} are shown in Figure 4.6. In Na^+ and Li^+ clusters, the two most stable structures show very different structural arrangements. Whereas Phe-X1-3H_2O corresponds to the tetrahedral arrangement of water and phenol around the cation, in Phe-X2-3H_2O the cation is surrounded by the three water molecules and does not interact directly with phenol, so the interaction takes place between a hydrated cation and the phenol moiety. Finally, in Mg^{2+} complexes the tetrahedral arrangements are the most stable, the rest of the minima found being less stable by more than 10 kcal/mol.

4.3.5. Tetrahydrated clusters

The inclusion of a fourth water molecule complicates even more the exploration of the potential energy surface of the clusters. Therefore, a partial exploration starting from the most stable complexes found for trihydrated clusters was performed. The fourth most stable minima for each of the cations found in this work are shown in Figure 4.7 together with their complexation energies. These minima are similar to those already found by Vaden and Lisy [37] though since the levels of calculation are different, differences arise. For example, the minima in Figure 4.7 for K^+ are within 1.5 kcal/mol, whereas those reported by Vaden and Lisy span over 5 kcal/mol.

Though complexation energies become more negative as the polarizing power of the cation increases as before, the energy differences among structures for a given cation are almost negligible. No stable structure with the five oxygen atoms surrounding the cation was located, so most complexes present a tetrahedral arrangement of oxygen atoms around the cation, whereas the fifth oxygen atom interacts in a second hydration shell.

Therefore, all tetrahydrated complexes exhibit interactions among water molecules or between water and phenol. In summary, it can be observed that as more water molecules are included, there are fewer differences between the different kinds of union: water···water, water···phenol or water···cation. For the smallest cations this implies that only a couple of structures present similar stability whereas the rest are significantly less stable. However, for Na^+ complexes and, especially for K^+ complexes,

there can be more stable structures within a small energy interval so there can be contributions for several conformers to the properties of the system, as already suggested by the infrared spectra to be discussed in the following section.

If the variations on complexation energy upon incorporation of a water molecule are considered (Table 4.4), the following behaviors can be observed. For K^+ complexes, the addition of the first water molecule stabilizes the complex in a larger quantity than the complexation of K^+ to phenol. This is due to the strong $K^+\cdots H_2O$ interaction, but also to the formation of the O-H···O hydrogen bond. In Na^+ complexes the stability gain associated to this first water molecule is slightly smaller than the cation···π interaction. For Li^+ and Mg^{2+}, even though the interaction with water is stronger, the complex is stabilized by a considerably smaller quantity than the original cation···π interaction. As more water molecules are included in the complex the stability gain decreases steadily, though for K^+ complexes the energy changes upon inclusion of the second and third water molecules are equivalent, suggesting the greater capacity of potassium for accommodating water molecules and also the extra stabilization due to the formation of hydrogen bonds. For all cations, the inclusion of the fourth water molecule is accompanied by a stability gain roughly half of that obtained with the first water unit.

Table 4.4. Complexation energy changes (kcal/mol) for the incorporation of one water molecule to a complex as obtained at the MP2/6-31+G(2d,p)//MP2/6-31+G(d) level of calculation.

Water molecules n	K^+	Na^+	Li^+	Mg^{2+}
0	-17.19	-22.61	-35.99	-116.4
1	-18.56	-21.09	-26.21	-58.51
2	-12.55	-16.19	-21.32	-43.72
3	-11.98	-13.87	-17.02	-39.35
4	-10.29	-12.24	-13.36	-23.97

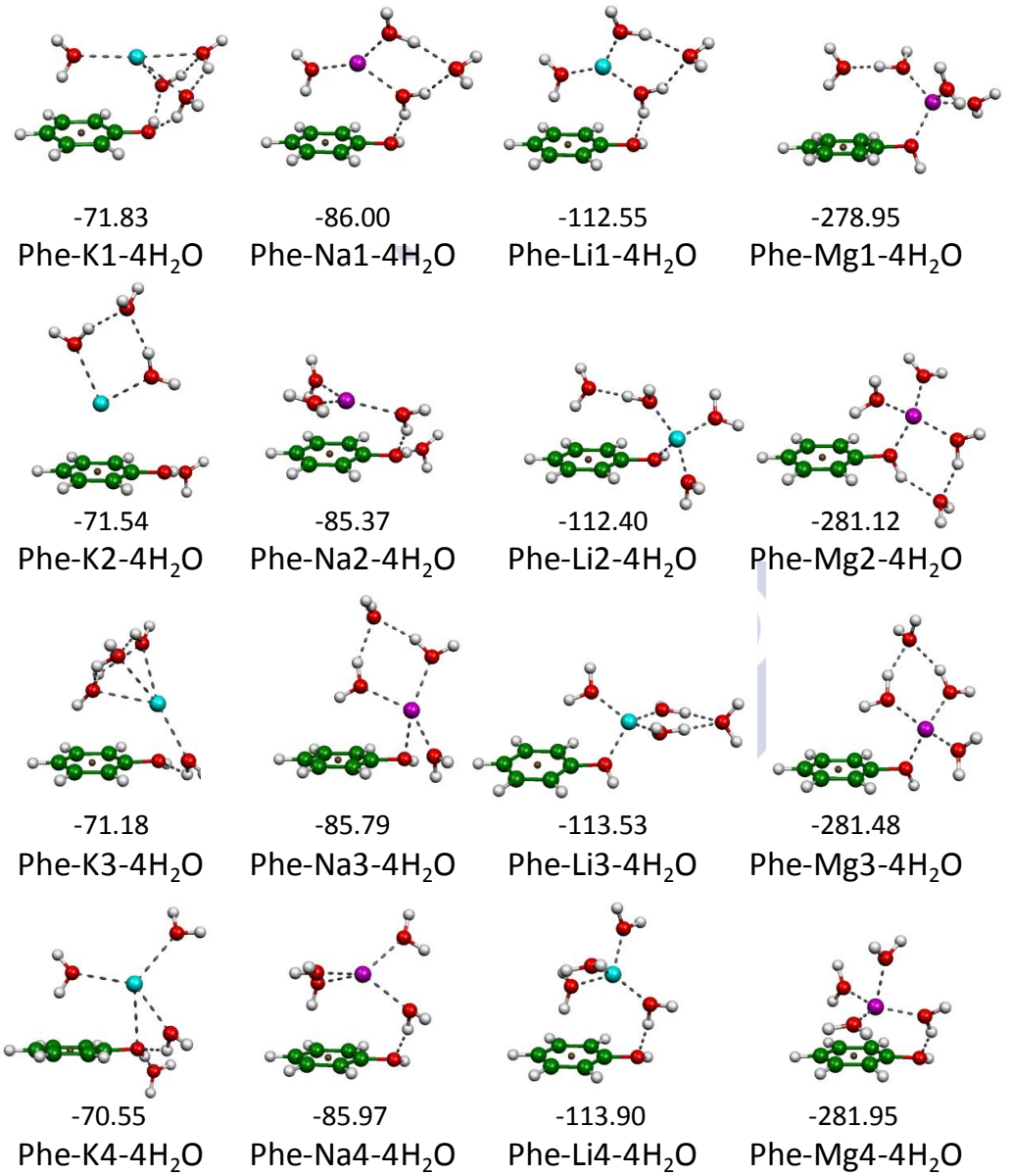


Figure 4.7. Most stable minima located for tetrahydrated complexes. Numbers correspond to complexation energies in kcal/mol at the MP2/6-31+G(2d,p)//MP2/6-31+G(d) level.

4.3.6. Vibrational spectra

The complexes formed by Na^+ and K^+ have been experimentally studied by Vaden and Lisy, with supporting calculations for explaining the results obtained for clusters with 4 water molecules.[37] Briefly, the results obtained for these complexes suggest that up to three water molecules, there is no participation, or a small one, of the hydroxyl group on the hydrogen bond network, as indicated by the absence of red-shifted signals corresponding to the O-H stretching of phenol (see Fig, 8). However, when 4 water molecules are included, there are contributions from structures with the hydroxyl group being part of the hydrogen bond network, as well as others coming from water···water hydrogen bonds. Vaden and Lisy performed MP2 calculations for explaining the behavior of complexes with 4 water molecules, but no results were shown for the smaller clusters and the trends that could be observed.

In this section these results will be analyzed with the calculations carried out in this work. Harmonic frequencies have been obtained both at the MP2/6-31+G(d) and the B3LYP/6-31+G(2d,p) levels of calculation, but the results obtained are pretty similar so the discussion will be focused on the MP2 results. Spectra for the complexes studied in this work have been constructed as follows. Firstly, a scaling factor (0.98) has been applied to the calculated frequencies to reproduce the experimental value of the O-H stretching of phenol.[37] Each spectrum is the result of contributions from the most stable conformers. For each minimum the spectrum is generated by fitting to Lorentzian functions with a halfwidth of 10 cm^{-1}. Afterwards, the spectra of the most stable structures are combined by using a Boltzmann average employing the differences in complexation Gibbs energy as obtained at 298.15 K (testing other temperatures does not introduce great differences). The resulting intensities are:

$$I = \frac{\sum_i I_i \exp(-\Delta G_i / RT)}{\sum_i \exp(-\Delta G_i / RT)} \quad \text{(eq. 4.4)}$$

Some concern can be raised about the quality of the harmonic approximation in getting good frequencies. Therefore, anharmonic corrections to the O-H stretching modes have been obtained for selected clusters by numerical differentiation along normal modes. As expected, the values are somewhat different, but after scaling to reproduce the experimental value of the O-H stretching of phenol, the general pattern is similar to that obtained with the harmonic approximation, so only harmonic frequencies will be employed in the discussion of the predicted spectra (see Appendix A).

The final spectra thus obtained are shown in Figure 4.8 for the region between 3200 to 4000 cm^{-1} together with the experimental results as adapted from ref. 37. Firstly, it can be observed that in absence of water molecules there is a single signal corresponding to the O-H stretching mode of phenol. The position of this band around

3640 cm^{-1} reproduces fairly well the experimental value for this normal mode, since a scaling factor has been applied precisely to reproduce this value. The signal appears unshifted for all cation complexes except in the case of Mg^{2+} complex, which shows an important red shift, so the band appears at about 3540 cm^{-1}. This is a consequence of the great intensity of the interaction between phenol and a bare Mg^{2+} cation, which significantly distorts the phenol moiety, thus producing this shift in the frequency of the hydroxyl group.

The inclusion of the first water molecule does not affect the position of the phenol O-H band since no structure presenting hydrogen bonds between hydroxyl OH group and water contributes to the final spectrum (these structures are much less stable than the global minima). Therefore, the spectra for all cations show two distinct peaks, corresponding to the O-H stretching mode of phenol at around 3640 cm^{-1}, the other due to the asymmetric O-H stretching mode of the water molecule located at around 3750 cm^{-1}. The symmetric motion of water O-H appears in the same region as the phenol O-H so only one band is observed in agreement with experiment. In fact, this is not true for Mg^{2+} complexes, and in this case three bands appear corresponding to phenol stretching and water symmetric and asymmetric O-H motions.

The inclusion of the second water molecule hardly changes this picture, since no hydrogen bond between water molecules has been observed for most complexes. However, in the case of K^+ complexes, the spectrum is more complex, due to the presence of new bands corresponding to hydrogen bonds between water acting as donor to the phenol molecule (not clearly observed in the experimental spectrum though clearly developed when the third water molecule is included), appearing at around 3600 cm^{-1}. This is not observed in Na^+ complexes in agreement with the experiment. The inclusion of the third water molecule does not introduce any remarkable change in Li^+ and Mg^{2+} complexes, whereas for Na^+ clusters, weak signals appear corresponding to hydrogen bonds between water molecules, red-shifted up to around 3500 cm^{-1}. In the case of K^+ complexes the situation is similar, the most remarkable feature of the spectrum being a very intense band corresponding to the hydrogen bond of phenol to a water molecule, appearing red-shifted below 3400 cm^{-1}, and indicating the contribution of structures where the hydroxyl group participates as donor in the hydrogen bond network. This does not properly match the experimental spectrum, where only a broad less intense band is registered. In any case, this band should correspond to this kind of hydrogen bond, and the problem is a bad prediction of the intensities. This effect has already been observed by Vaden and Lisy,[37] indicating that the relative energy predictions of the calculations do not totally agree with the relative intensity of the signals observed experimentally. As the fourth water molecule is included, the spectrum for K^+ complexes remains mainly the same, with an intense band at around 3400 cm^{-1} corresponding to a ϕ-OH···O hydrogen bond and a series of bands around 3500-3600 cm^{-1} corresponding to hydrogen bonds between water molecules.

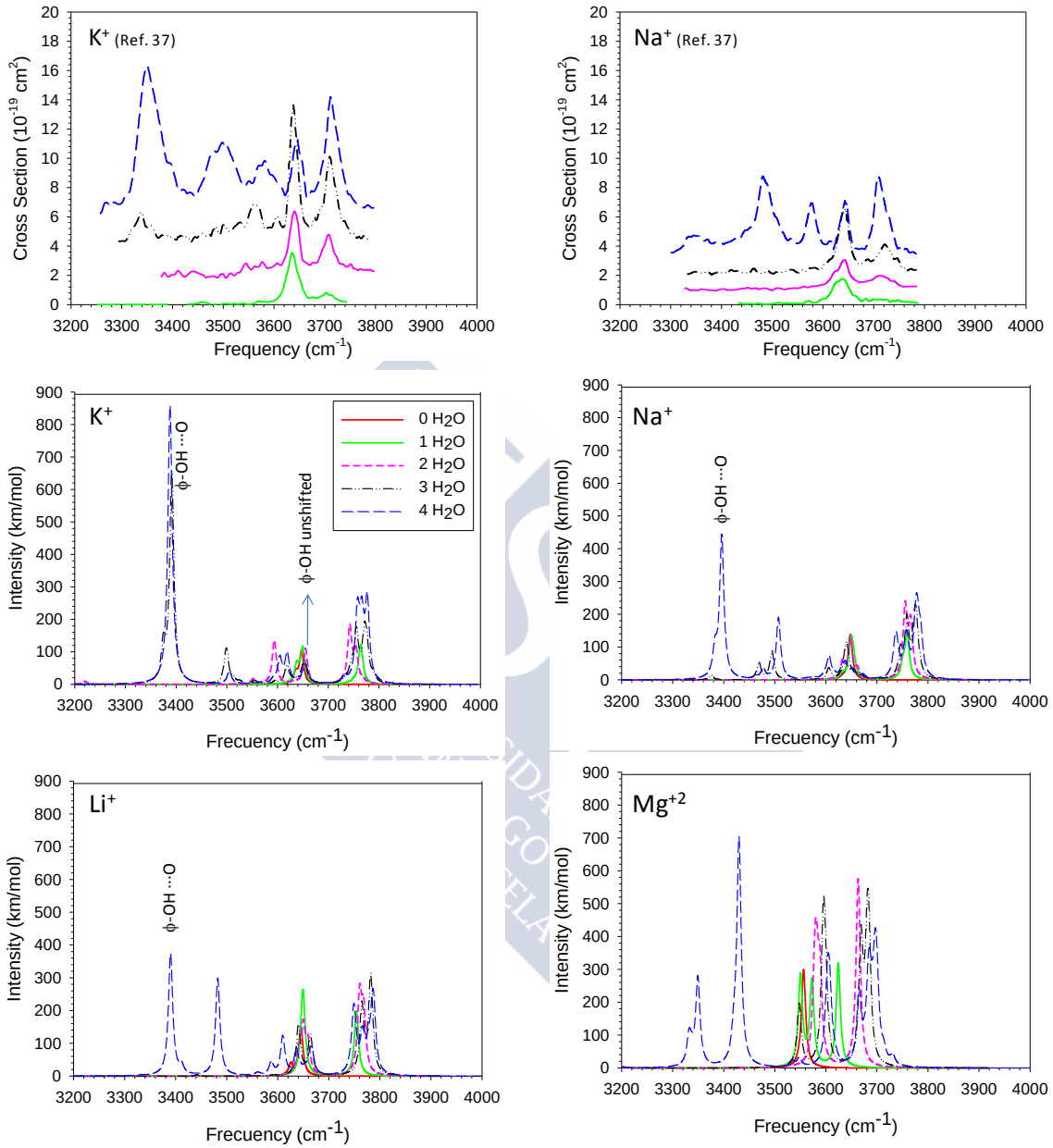


Figure 4.8. Predicted spectra of the cation···phenol complexes studied in this work with different microhydration levels. On top, experimental spectra of M^+ (Phenol)$(H_2O)_n$ for *M= K, Na* and *n=1-4* by Vaden and Lisy (Ref. 37).

The behavior is similar for Na^+ complexes, though a new intense band at 3400 cm^{-1} appears, corresponding to a ϕ-OH···O hydrogen bond. The main features of the experimental spectra are reproduced, indicating participation of different conformers with different kinds of hydrogen bonds, though differences in intensities are significant. Finally, in Li^+ and Mg^{2+} complexes a new series of red-shifted bands appears. This happens because in the most stable minima with four water molecules, at least one water molecule or phenol is located in a second solvation shell, thus interacting with the other water molecules in the complex. Therefore, Li^+ complexes behave as Na^+, with bands around 3500-3600 cm^{-1} describing hydrogen bonds between water molecules, and a more intense band at 3400 cm^{-1} corresponding to a ϕ-OH···O hydrogen bond. The behavior is similar for Mg^{2+}, though in this case the signals are more red-shifted, with hydrogen bonds between water molecules appearing around 3400-3550 cm^{-1}. A less intense band corresponding to a ϕ-OH···O hydrogen bond is also observed at 2900 cm^{-1}.

4.4. Conclusions

Complexes formed by one phenol molecule, a K^+, Na^+, Li^+ or Mg^{2+} cation and up to four water molecules have been computationally studied employing DFT and ab initio methods. Minima for the different clusters have been obtained at the B3LYP/6-31+G(2d,p) and MP2/6-31+G(d) levels of calculation, whereas complexation energies have been obtained at the MP2/6-31+G(2d,p) level.

The results show that several minima are possible for any of the clusters studied. As a general trend, the potential energy surface of the clusters increases in complexity as the size of the cation grows. Therefore, whereas for the smallest cations Li^+ and Mg^{2+}, only one or two structures contribute at room temperature to the properties of the system, in the case of K^+ clusters a wider range of different structures are possible within a narrow margin of complexation energies.

The characteristics of the complexes are determined by the balance of the different interactions that can be established. Therefore, a balance between cation···water, water···water, cation···phenol and phenol···water interactions determines the stability of the complexes. Thus, in the case of Li^+ and Mg^{2+} the interaction of water and phenol with the cation is much stronger than the interaction between neutral molecules (water and phenol) so the most stable structures present phenol and water surrounding the cation. However, in K^+ complexes and to a smaller extent in Na^+ complexes, as water molecules are included the stability gain obtained by coordinating a water molecule to the cation or adding it to the hydrogen bond network becomes more similar. Therefore, structures with all molecules coordinated to the cation or with hydrogen bonds among molecules become equally stable.

The calculations are capable of reproducing the main features of the experimentally obtained vibrational spectra for Na^+ and K^+ complexes. For complexes with Li^+ and Mg^{2+} quite simple spectra are predicted, and only when the fourth water molecule is included bands associated to hydrogen bonds among water molecules or phenol are present.

The results obtained can help understanding how a phenol unit (for example in tyrosine) interacts with cations, and how the presence of nearby water molecules can affect the characteristics of the complexes.

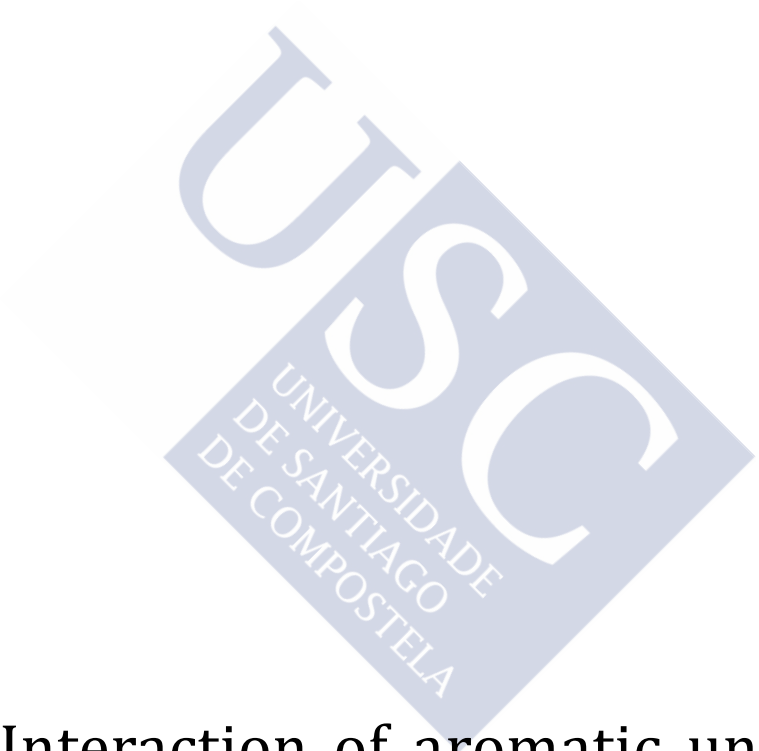
4.5. References

[1] P. Hobza, R. Zaradnik, Intermolecular complexes: the role of van der Waals systems in physical chemistry and the biodisciplines, Elsevier, Amsterdam, **1988**.
[2] J.-M. Lehn, Supramolecular Chemistry: concepts and perspectives, Wiley-VCH, Weinheim, **1995**.
[3] S. Tsuzuki, T. Uchimaru. *Curr. Org. Chem.* **2006**, *10*, 745-762.
[4] E. A. Meyer, R. K. Castellano, F. Diederich. *Angew. Chem. Int. Ed.* **2003**, *42*, 1210-1250.
[5] L. M. Salonen, M. Ellermann, F. Diederich. *Angew. Chem. Int. Ed.* **2011**, *50*, 4808-4842.
[6] N. S. Scrutton, A. R. Raine. *Biochem. J.* **1996**, *319*, 1-8.
[7] D. A. Dougherty. *J. Nutr.* **2007**, *137*, 1504S-1508S.
[8] M. L. Waters. *Biopolymers (Peptide Sci.)* **2004**, *76*, 435-445.
[9] J. C. Ma, D. A. Dougherty. *Chem. Rev.* **1997**, *97*, 1303-1324.
[10] J. P. Gallivan, D. A. Dougherty. *Proc. Natl. Acad. Sci. USA* **1999**, *96*, 9459-9464.
[11] J. P. Gallivan, D. A. Dougherty. *J. Am. Chem. Soc.* **2000**, *122*, 870-874.
[12] M. A. Anderson, B. Ogbay, R. Arimoto, W. Sha, O. G. Kisselev, D. P. Cistola, G. R. Marshall. *J. Am. Chem. Soc.* **2006**, *128*, 7531-7541.
[13] B. W. Berry, M. M. Elvekrog, C. Tommos. *J. Am. Chem. Soc.* **2007**, *129*, 5308-5309.
[14] R. M. Hughes, M. L. Benshoff, M. L. Waters. *Chem. Eur. J.* **2007**, *13*, 5753-5764.
[15] R. M. Hughes, M. L. Waters. *J. Am. Chem. Soc.* **2005**, *127*, 6518-6519.
[16] R. M. Hughes, M. L. Waters. *J. Am. Chem. Soc.* **2006**, *128*, 13586-13591.
[17] R. M. Hughes, M. L. Waters. *J. Am. Chem. Soc.* **2006**, *128*, 12735-12742.
[18] H. Khandelia, Y. N. Kaznessis. *J. Phys. Chem. B* **2006**, *111*, 242-250.
[19] P. E. Mason, C. E. Dempsey, G. W. Neilson, S. R. Kline, J. W. Brady. *J. Am. Chem. Soc.* **2009**, *131*, 16689-16696.
[20] A. J. Riemen, M. L. Waters. *Biochemistry* **2009**, *48*, 1525-1531.
[21] Z. Shi, C. A. Olson, N. R. Kallenbach. *J. Am. Chem. Soc.* **2002**, *124*, 3284-3291.
[22] C. D. Tatko, M. L. Waters. *Prot. Sci.* **2003**, *12*, 2443-2452.
[23] D. Kim, S. Hu, P. Tarakeshwar, K. S. Kim, J. M. Lisy. *J. Phys. Chem. A* **2003**, *107*, 1228-1238.
[24] O. M. Cabarcos, C. J. Weinheimer, J. M. Lisy. *J. Chem. Phys.* **1999**, *110*, 8429-8435.
[25] O. M. Cabarcos, C. J. Weinheimer, J. M. Lisy. *J. Chem. Phys.* **1998**, *108*, 5151-5154.

[26] X. Jian Tan, W. Liang Zhu, M. Cui, X. Min Luo, J. De Gu, I. Silman, J. L. Sussman, H. Liang Jiang, R. Yun Ji, K. Xian Chen. *Chem. Phys. Lett.* **2001**, *349*, 113-122.
[27] C. Adamo, G. Berthier, R. Savinelli. *Theor. Chem. Acc.* **2004**, *111*, 176-181.
[28] Y. Xu, J. Shen, W. Zhu, X. Luo, K. Chen, H. Jiang. *J. Phys. Chem. B* **2005**, *109*, 5945-5949.
[29] E. M. Cabaleiro-Lago, J. Rodríguez-Otero, Á. Peña-Gallego. *J. Chem. Phys.* **2011**, *135*, 214301-214310.
[30] A. S. Reddy, H. Zipse, G. N. Sastry. *J. Phys. Chem. B* **2007**, *111*, 11546-11553.
[31] D. Vijay, H. Zipse, G. N. Sastry. *J. Phys. Chem. B* **2008**, *112*, 8863-8867.
[32] J. S. Rao, H. Zipse, G. N. Sastry. *J. Phys. Chem. B* **2009**, *113*, 7225-7236.
[33] J. Šponer, J. E. Šponer, J. Leszczynski. *J. Biomol. Struct. Dyn.* **2000**, *17*, 1087-1096.
[34] F. M. V. Leavens, C. D. M. Churchill, S. Wang, S. D. Wetmore. *J. Phys. Chem. B* **2011**, *115*, 10990-11003.
[35] J. Larrucea, E. Rezabal, T. Marino, N. Russo, J. M. Ugalde. *J. Phys. Chem. B* **2010**, *114*, 9017-9022.
[36] D. J. Miller, J. M. Lisy. *J. Chem. Phys.* **2006**, *124*, 184301-184308.
[37] T. D. Vaden, J. M. Lisy. *J. Chem. Phys.* **2004**, *120*, 721-730.
[38] R. Amunugama, M. T. Rodgers. *J. Phys. Chem. A* **2002**, *106*, 9718-9728.
[39] H. Watanabe, S. Iwata. *J. Chem. Phys.* **1996**, *105*, 420-431.
[40] M. Gerhards, K. Kleinermanns. *J. Chem. Phys.* **1995**, *103*, 7392-7400.
[41] R. Wu, B. Brutschy. *Chem. Phys. Lett.* **2004**, *390*, 272-278.
[42] D. M. Benoit, D. C. Clary. *J. Phys. Chem. A* **2000**, *104*, 5590-5599.
[43] T. Ebata, A. Fujii, N. Mikami. *Int. J. Mass Spectrom. Ion Processes* **1996**, *159*, 111-124.
[44] C. Janzen, D. Spangenberg, W. Roth, K. Kleinermanns. *J. Chem. Phys.* **1999**, *110*, 9898-9907.
[45] W. Roth, M. Schmitt, C. Jacoby, D. Spangenberg, C. Janzen, K. Kleinermanns. *Chem. Phys.* **1998**, *239*, 1-9.
[46] M. Sodupe, A. Oliva, J. Bertrán. *J. Phys. Chem. A* **1997**, *101*, 9142-9151.
[47] J. Küpper, A. Westphal, M. Schmitt. *Chem. Phys.* **2001**, *263*, 41-53.
[48] E. S. Kryachko, M. T. Nguyen. *J. Phys. Chem. A* **2002**, *106*, 4267-4271.
[49] E. M. Cabaleiro-Lago, Á. Peña-Gallego, J. Rodríguez-Otero. *J. Chem. Phys.* **2008**, *128*, 194311-194319.
[50] C. Michaux, J. Wouters, E. A. Perpète, D. Jacquemin. *J. Phys. Chem. B* **2008**, *112*, 2430-2438.
[51] C. Michaux, J. Wouters, E. A. Perpète, D. Jacquemin. *J. Phys. Chem. B* **2008**, *112*, 7702-7705.
[52] Y. Yao, D. Chen, S. Zhang, Y. Li, P. Tu, B. Liu, M. Dong. *J. Phys. Chem. B* **2011**, *115*, 6213-6221.
[53] M. Prakash, V. Subramanian, S. R. Gadre. *J. Phys. Chem. A* **2009**, *113*, 12260-12275.
[54] B. Sharma, J. S. Rao, G. N. Sastry. *J. Phys. Chem. A* **2011**, *115*, 1971-1984.
[55] S. F. Boys, F. Bernardi. *Mol. Phys.* **1970**, *19*, 553-566.
[56] G. Chałasiński, M. M. Szczęśniak. *Chem. Rev.* **2000**, *100*, 4227-4252.
[57] E. Cabaleiro-Lago, J. Rodríguez-Otero, Á. Peña-Gallego. *Theor. Chem. Acc.* **2011**, *128*, 531-539.

[58] M. J. Frisch, G. W. Trucks, H. B. Schlegel, G. E. Scuseria, M. A. Robb, J. R. Cheeseman, G. Scalmani, V. Barone, B. Mennucci, G. A. Petersson, H. Nakatsuji, M. Caricato, X. Li, H. P. Hratchian, A. F. Izmaylov, J. Bloino, G. Zheng, J. L. Sonnenberg, M. Hada, M. Ehara, K. Toyota, R. Fukuda, J. Hasegawa, M. Ishida, T. Nakajima, Y. Honda, O. Kitao, H. Nakai, T. Vreven, J. J. A. Montgomery, J. E. Peralta, F. Ogliaro, M. Bearpark, J. J. Heyd, E. Brothers, K. N. Kudin, V. N. Staroverov, R. Kobayashi, J. Normand, K. Raghavachari, A. Rendell, J. C. Burant, S. S. Iyengar, J. Tomasi, M. Cossi, N. Rega, J. M. Millam, M. Klene, J. E. Knox, J. B. Cross, V. Bakken, C. Adamo, J. Jaramillo, R. Gomperts, R. E. Stratmann, O. Yazyev, A. J. Austin, R. Cammi, C. Pomelli, J. W. Ochterski, R. L. Martin, K. Morokuma, V. G. Zakrzewski, G. A. Voth, P. Salvador, J. J. Dannenberg, S. Dapprich, A. D. Daniels, Ö. Farkas, J. B. Foresman, J. V. Ortiz, J. Cioslowski, D. J. Fox, Gaussian 09, revision A.02, **2009**.

[59] M. S. Marshall, R. P. Steele, K. S. Thanthiriwatte, C. D. Sherrill. *J. Phys. Chem. A* **2009**, *113*, 13628-13632.



5. Interaction of aromatic units of amino acids with guanidinium cation. The interplay of π···π, X-H···π and M^+···π contacts

USC
UNIVERSIDADE
DE SANTIAGO
DE COMPOSTELA

5.1. Introduction

Non-covalent interactions play a key role in many areas of modern chemistry, especially in the field of supramolecular chemistry and molecular recognition, as well as in biochemistry.[1, 2] Among the different kinds of non-covalent contacts relevant in biological systems, a special place is occupied by interactions with participation of aromatic units.[3-6]

It is believed that aromatic groups interact in a different manner than aliphatic units in the side chains of amino acids, and can provide specificity in protein folding. More specifically, three kinds of non-covalent interactions involving π systems are usually considered: ion···π, XH···π and π···π contacts, which are attractive interactions that can affect significantly to the behavior of a given system.[3-5]

π···π interactions, like in benzene dimer, are usually governed by dispersion effects and play an essential role in the folding of proteins and in the structure of DNA as well as in its interactions with small molecules.[3, 5] Hydrogen bonding interactions to the aromatic cloud (XH···π) are also important as to determine the characteristics of many systems.[4, 7, 8] These hydrogen bonds are usually weaker than the typical OH···O ones, and usually exhibit a larger dispersive nature. These two kinds of π interactions are normally weak, though the combined effect of many of them can have a deep impact on the characteristics of the system. On the other hand, ion···π interactions are strong interactions in the gas phase,[4, 9-11] usually dominated by electrostatic and polarization terms as a consequence of the presence of the ion and a polarizable π cloud.[12, 13] Cation···π interactions are recognized to be an important factor in ion selectivity in potassium channels, and their importance has been demonstrated in neurotransmitter receptors.[4, 11, 14, 15]

The importance of the cation···π interaction in proteins is easily understood taking into account that some amino acids such as phenylalanine, tyrosine, tryptophan, and histidine bear an aromatic unit in their side chains, whereas other amino acids as arginine, lysine, and histidine possess cationic groups depending on the pH.[6, 16] Thus, interactions between side chains of these amino acids are often observed in protein structure suggesting their relevance as a stabilizing motif. Though the cation···π interaction is usually stronger than π···π or XH···π contacts in the gas phase, as corresponds to the interaction of a bare cation with a polarizable and electron-rich aromatic cloud, the environment can significantly alter its characteristics.[11, 17] Several studies have shown how the coordination of electron-rich solvent molecules to the cation decreases the intensity of the interaction with the cation, as it would be expected taking into account the decrease of the effective charge carried by the cation due to the solvent molecules.[18-22] In any case, the behavior and stability of a system, even a simple one, will be usually the result of the interplay of different non-covalent interactions. If aromatic molecules are present it is probable for all π···π, XH···π and ion···π to play a role.

In the present work, the interplay among these intermolecular contacts is analysed in ternary systems containing one cationic unit and two equal or different aromatic units. Trying to represent possible contacts among amino acid side chains the aromatic molecules considered have been benzene, phenol and indole, as models for phenylalanine, tyrosine and tryptophan, respectively. Guanidinium $C(NH_2)_3^+$ has been chosen as cation since it is part of the side chain or arginine. Guanidinium is widely used as a denaturant since it is believed to interact with the side chains of proteins, as well as a basic unit for constructing anion selective receptors or ionic liquids.[23, 24] Besides, due to its special planar structure guanidinium cation is more prone than simpler cations to present parallel-stacked structures which can be of importance in these systems.[20, 25] In fact, stacking has been observed between solvated guanidinium cations in water solution.[26, 27]

An interesting phenomenon when dealing with intermolecular interactions is the possibility of cooperative or anticooperative effects in systems with more than two species.[28, 29] These phenomena are usually weak though they can be of importance as to characterize the behavior of the system, as indicated by several studies recently devoted to the task of evaluating these effects.[12, 30-34] Usually, cooperative effects are associated to polarization, so the combination of a cation and a polarizable aromatic cloud, like in the trimers object of this study, is indicative that cooperativity, a priori, could be significant in determining the characteristics of these systems.[12]

In summary, the present work intends to shed light on the characteristics on the interaction between guanidinium and aromatic moieties of amino acids. The results obtained would help to rationalize the results observed in multiple cation···π interactions in proteins and their mutual influence.

5.2. Methods

As commented above, systems consisting on a guanidinium cation and two aromatic molecules among benzene, phenol and indole have been considered in this study. These complexes have been fully optimized at the M06-2X/6-31+G* level of calculation[35] starting from a variety of different structures. Starting structures were constructed from prototypes observed in the guanidinium-aromatic and aromatic-aromatic dimers. Therefore, the parallel, displaced-parallel and T-shaped structures for benzene dimer have been employed, and analogous structures have also been used for phenol and indole.[5, 36] T-shaped and parallel orientation of the guanidinium cation with respect to the aromatic clouds have been considered,[20, 37] with the cation located between the aromatic molecules or bounded to only one of them. Other possible structures corresponding to hydrogen-bonded clusters have also been tested following chemical knowledge (i.e. O-H···O in phenol dimer, N-H···π in indole-containing clusters, etc.). After

one stationary point is located a frequency calculation has been carried out in order to ensure that the structure corresponds to a minimum.

For the minima the complexation energy has been obtained by applying the counterpoise procedure with a variety of methods.[38, 39] Therefore, the complexation energy of the complexes has been obtained as:

$$\Delta E_{complex} = E^{complex}(ijk...) - \sum_i E_i^{isolated}(i) - \sum_i \left(E_i^{complex}(ijk...) - E_i^{complex}(i)\right) \quad \text{(eq. 5.1)}$$

where superscripts refer to the geometry employed, subscripts to the fragment considered and terms in parentheses to the basis set employed in the calculation. Applying this procedure, M06-2X/6-31+G* complexation energies have been obtained. Also, complexation energies have been obtained with the MP2 method. Single point calculations have been carried out at the M06-2X/6-31+G* optimized geometries employing MP2 with the aug-cc-pVDZ and aug-cc-pVTZ basis sets. With these results, a two-point extrapolation of the correlation energy to the basis set limit has been performed applying[40]

$$\Delta E_{corr,MP2}^{CBS} = \frac{X^3}{X^3-(X-1)^3}\Delta E_{corr,MP2}^{pVXZ} - \frac{(X-1)^3}{X^3-(X-1)^3}\Delta E_{corr,MP2}^{pV(X-1)Z} \;;\; X=3 \quad \text{(eq. 5.2)}$$

.

The MP2 complexation energy to basis limit is the estimated as

$$\Delta E_{MP2}^{CBS} = \Delta E_{HF}^{pVTZ} + \Delta E_{corr,MP2}^{CBS} \quad \text{(eq. 5.3)}$$

.

However, it is well know that MP2 tends to overestimate the magnitude of the interaction when aromatic molecules are involved, especially when oriented in parallel.[5, 41] A variety of empirical procedures have been proposed to correct for this deficiency, mostly based in a different scaling of the contributions of parallel and antiparallel electrons to correlation. The first proposal of this kind is the Spin Component Scaled MP2 (SCS-MP2) proposed by Grimme, where opposite-spin and same-spin contributions are scaled by 1.20 and 0.33, respectively.[42] Therefore SCS-MP2 complexation energies have been obtained with the aug-cc-pVDZ and aug-cc-pVTZ basis sets, and were also extrapolated to basis set limit (SCS-MP2/CBS).

In order to analyze the balance of the interactions between fragments in the trimer, pair energy contributions have also been calculated. Therefore, the interaction energy is expressed as

$$\Delta E = \sum_{ij} \Delta E_{ij} + E_{3-body} \quad \text{(eq. 5.4)}$$

where the ΔE_{ij} are the interaction energies for each pair formed in the trimer as computed employing the whole basis set and the optimized geometry of the trimer.[28,

[29] The difference between the summation of pair energies and the interaction energy of the trimer is the contribution from 3-body effects. This partitioning has been performed with the methods commented above.

Finally, in order to have more insight into the nature of the interaction and the balance of different contributions, an energy partitioning scheme has been applied. Therefore, the interaction energies have been decomposed in electrostatic, repulsion (exchange + repulsion), polarization and dispersion components by applying the Local Molecular Orbital-Energy Decomposition Analysis (LMO-EDA).[43] The partitioning has been performed with both the M06-2X and MP2 methods.

Optimizations and frequency calculations have been performed with Gaussian09;[44] LMO-EDA calculations were performed with GAMESS,[45, 46] and Turbomole has been employed in the MP2 calculations.[47] In order to save computation time, the resolution of the identity has been applied in MP2 calculations, both to the correlation calculation (RI-MP2) and to the HF one (RI-JK), employing suitable auxiliary basis sets as provided in Turbomole. Therefore the corresponding aug-cc-pVXZ fitting basis sets have been employed in the correlation part whereas def2-TZVPP has been used for RI-JK calculations.[47-49]

5.3. Results

Minimum energy structures and complexation energies will be presented first for complexes formed by guanidinium and two equal aromatic units, followed by results obtained for complexes formed by guanidinium cation and two different aromatic molecules (mixed complexes).

5.3.1. Complexes with the same aromatic molecules

Figure 5.1 shows the structures of the most stable minima located for the complexes formed by guanidinium cation and two benzene molecules, whereas Table 5.1 lists the values obtained for their complexation energies with different levels of calculation.

Four different minima have been found for these complexes. Bz-Bz-1 corresponds to a structure with stacked aromatic rings and the guanidinium cation interacting with one of them, adopting a perpendicular arrangement which has been shown to be the most stable minimum in guanidinium···Bz complexes.[20, 37] Two N-H···π contacts are observed: one at 2.3 Å and a longer one at 2.9 Å. Bz-Bz-2 and Bz-Bz-3 correspond to structures where benzene rings display a perpendicular arrangement (T-shaped) with C-H···π contacts at around 2.5-2.6 Å to the center of the other aromatic ring. These arrangements roughly correspond to the typical structures found for benzene dimer (parallel displaced and C-H···π).[5] Finally, Bz-Bz-4 corresponds to a doubly T-shaped structure, where the aromatic rings are far apart, both of them coordinating the

guanidinium cation in perpendicular arrangements, forming hydrogen bonds at 2.3 Å of the center of the ring.

Table 5.1 shows the complexation energies of Bz-Bz complexes as obtained with a variety of methods. Taking into account the values in Table 5.1 the results obtained at the M06-2X/6-31+G* and at the SCS-MP2/CBS levels of calculation are pretty similar, whereas MP2 gives in all cases overestimated complexation energies, especially with the larger basis set. Therefore, in the following we will mainly discuss values obtained with these two levels of calculation.

Table 5.1. Complexation energies (kcal/mol) obtained for complexes formed by guanidinium and two equal aromatic molecules as obtained with different methods, all employing the optimized M06-2X/6-31+G* geometry.

	631+G*	aug-cc-pVDZ		CBS	
	M062X	MP2	SCS-MP2	MP2	SCS-MP2
Bz-Bz-1	-18.55	-21.03	-16.97	-22.79	-18.54
Bz-Bz-2	-21.03	-22.44	-18.58	-24.30	-20.27
Bz-Bz-3	-20.58	-21.41	-17.20	-23.25	-18.85
Bz-Bz-4	-25.62	-27.12	-23.52	-29.25	-25.48
Ph-Ph-1	-33.19	-31.93	-27.83	-34.05	-29.71
Ph-Ph-2	-31.21	-30.47	-25.76	-32.80	-27.85
Ph-Ph-3	-29.47	-29.93	-26.34	-31.88	-28.10
Ph-Ph-4	-28.73	-27.31	-22.36	-29.58	-24.36
Ph-Ph-5	-32.20	-31.05	-26.76	-33.20	-28.67
Ph-Ph-6	-32.21	-32.71	-29.05	-34.67	-30.81
Ph-Ph-7	-32.81	-30.63	-27.90	-32.17	-29.35
In-In-1	-29.61	-34.47	-27.43	-36.87	-29.53
In-In-2	-32.72	-36.01	-30.25	-38.37	-32.36
In-In-3	-31.54	-34.70	-28.94	-37.04	-31.04
In-In-4	-33.14	-36.39	-30.55	-38.79	-32.70
In-In-5	-38.16	-40.04	-34.70	-42.69	-37.09

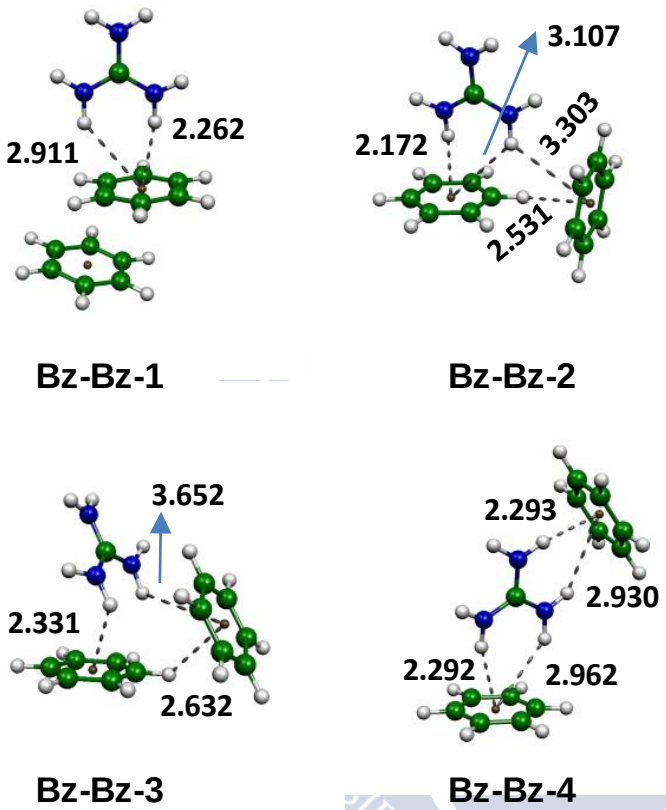


Figure 5.1. Most stable minima found for complexes of guanidinium with two benzene molecules as obtained at the M06-2X/6-31+G* level. Selected distances in Å.

As expected, Bz-Bz-4, with a doubly T-shaped structure is the most stable complex with a complexation energy of -25.5 kcal/mol because guanidinium can coordinate at the same time the two benzene rings, establishing two simultaneous cation···π interactions. Bz-Bz-2, with one T-shaped contact, is about 5 kcal/mol less stable (-20.3 kcal/mol). Here, one of the benzene rings coordinates to the guanidinium cation through a cation···π interaction and by means of a CH···π contact to the other benzene ring. Bz-Bz-1 corresponds to a parallel-displaced benzene dimer coordinated to guanidinium by one of the phenyl rings. The lack of direct contact between guanidinium and one of the benzene moieties makes this structure less stable, reaching only -18.5 kcal/mol. Finally, in Bz-Bz-3 the benzene ring that does not interact directly with the guanidinium cation moves away from the perpendicular arrangement. This structure could be considered as a combination of two of the minima of guanidinium···benzene complexes; one T-shaped and one parallel displaced with guanidinium parallel to the ring.[20, 37] This is the only structure which shows significant differences between M06-2X (-20.6 kcal/mol) and SCS-MP2/CBS (-18.9 kcal/mol) results.

Contrary to benzene, phenol possesses two different regions where a cation can establish a stabilizing interaction: the aromatic cloud and the lone pairs of the hydroxyl oxygen. Therefore, even when phenol is very similar to benzene, the presence of the hydroxyl group introduces a greater complexity on the potential energy surface of the clusters, allowing for a greater variety of stable structures. Figure 5.2 shows the structures of the most stable minima located for the complexes formed by guanidinium cation and two phenol molecules. It can be observed that phenol complexes cannot be classified into prototypical structures as easily as benzene ones, since due to the presence of the hydroxyl group there is a tendency to form O-H···O hydrogen bond contacts. Ph-Ph-6 and Ph-Ph-7 correspond to doubly T-shaped structures. In Ph-Ph-6 guanidinium cation coordinates the phenyl ring and the hydroxyl group whereas in Ph-Ph-7 it is coordinated only to the hydroxyl groups. It is worth noting that similar structures but with different disposition of the rings have been located, though only the most stable ones are included in Figure 5.2. In most cases the structures show O-H···O short hydrogen bonds at 1.7-1.9 Å, whereas guanidinium is also hydrogen-bonded to the hydroxyl group by means of N-H···O hydrogen bonds at around 1.8-1.9 Å. The contacts between guanidinium and the phenyl ring show similar behavior as that observed in benzene complexes.

No typical stacked structure has been found in complexes with phenol because the hydroxyl group tends to interact establishing OH···π or OH···O hydrogen bonds as it can be observed in all minima in Figure 5.2 except the doubly T-shaped ones. As regards T-shaped structures, only Ph-Ph-3 could be considered within this arrangement because it is the only one that presents both aromatic rings interacting in a perpendicular disposition, even though the interaction takes place by means of a O-H···O contact.

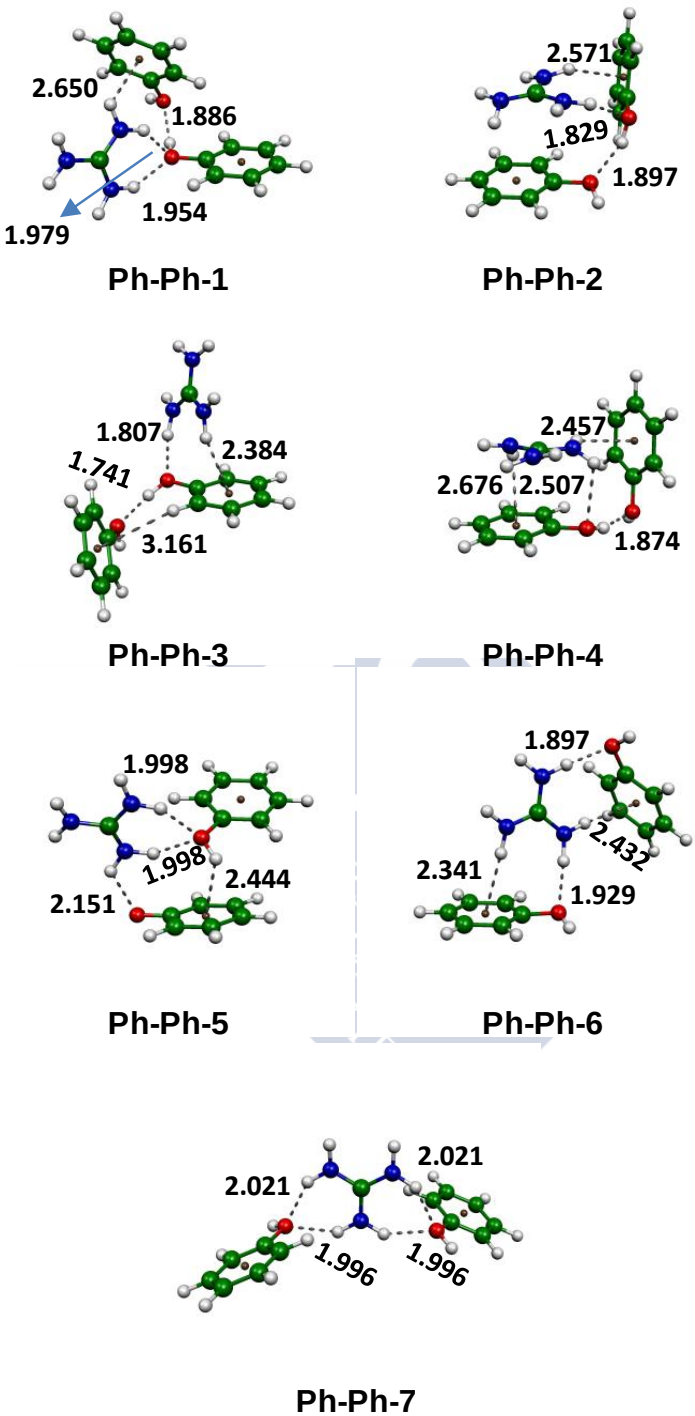


Figure 5.2. Most stable minima found for complexes of guanidinium with two phenol molecules as obtained at the M06-2X/6-31+G* level. Selected Distances in Å.

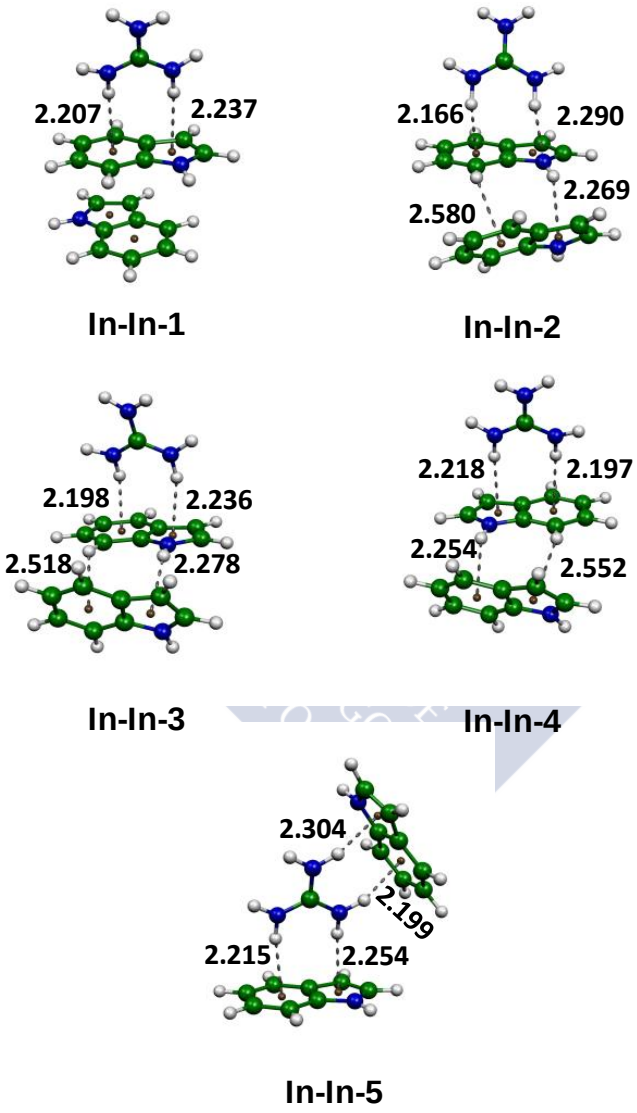


Figure 5.3. Most stable minima found for complexes of guanidinium with two indole molecules as obtained at the M06-2X/6-31+G* level. Selected Distances in Å.

Complexation energies are listed in Table 5.1. In these complexes more discrepancies are found between M06-2X/6-31+G* and the SCS-MP2/CBS values though, overall, M06-2X tends to overestimate the interaction whereas the order of stability of the complexes is almost unaffected. As expected, the doubly T-shaped minima Ph-Ph-6 and Ph-Ph-7 are among the most stable ones with both methods, though it can be observed that M06-2X favors the contact with the hydroxyl oxygens, a trend that can be observed in the rest of the complexes with phenol. The interaction energy is larger than those observed in benzene complexes, reaching -30 kcal/mol or more. Therefore, an increment in stability of around -5 kcal/mol is obtained with respect to benzene complexes. This happens when comparing doubly T-shaped structures, but differences are even larger for other arrangements, as a consequence of the interaction of guanidinium with the hydroxyl group and the formation of O-H···O or O-H···π contacts.

The relevance of the hydrogen bonds can be observed in Ph-Ph-1, which is as stable as the doubly T-shaped structures. This minimum consists of a guanidinium cation coordinated to the hydroxyl group of one phenol unit which establishes a hydrogen bond to the hydroxyl group of the other phenol unit, reaching complexation energies around -30 kcal/mol (-33 kcal/mol with M06-2X, the most stable minimum). The rest of minima are less stable, differing mainly in the orientation of the guanidinium cation with respect to the rings, whereas both hydroxyl groups form a hydrogen bond.

Complexes of guanidinium cation with two indole molecules are shown in Figure 5.3. As in Bz-Bz complexes, the complexes with indole can be classified in the established arrangements: doubly T-shaped, T-shaped and parallel displaced. Guanidinium cation interacts with the two rings of indole by means of N-H···π hydrogen bonds, the one formed with the phenyl ring being always shorter than that formed with the pyrrol ring. Again, like in Bz-Bz complexes, the stability order of the structures does not change with the level of calculation employed as it can be observed in Table 5.1. As expected, the doubly T-shaped In-In-5 minimum where guanidinium cation coordinates both aromatic rings is the most stable complex with -37.1 kcal/mol. Comparing with complexes formed with benzene and phenol, it can be observed an increment in the stability of the complexes of around -5 kcal/mol when going from benzene to phenol, and a further -6 kcal/mol when passing from phenol to indole. In any case, the energy gain in phenol is mainly related to the presence of the hydroxyl group, whereas in indole complexes has its origin in the larger size of the aromatic systems leading lo larger dispersion and induction contributions to the stability. The increase in stability as the size of the aromatic unit grows is in line with previous work where the size of the interacting units was identified as one of the most important factors controlling the interaction.[50, 51]

As in phenol complexes, the structures of indole complexes are conditioned by the tendency of the N-H group of indole to establish hydrogen bonds with the aromatic rings of the other indole moiety at around 2.3 Å of the center of the other ring. C-H···π contacts at around 2.6 Å are also observed in T-shaped minima. The only true stacked structure found is In-In-1, where both indole molecules are rotated by about 90^{o}, thus avoiding the formation of N-H···π contacts. The complexation energy for his structure reaches -29.5 kcal/mol, about -10 kcal/mol more stable than the corresponding stacked structure in benzene complexes Bz-Bz-1. The rest of minima show in some way or another a N-H···π contact which contributes to the stability of the complexes, so all of them are more stable than the stacked one. Thus, in In-In-4 indole rings have a quasi-perpendicular disposition, forming an angle of 67º, being the structure among those found which closest resembles a T-shaped contact. However, the indole ring that interacts directly with guanidinium also establishes a N-H···π hydrogen bond with the phenyl ring of the second indole unit. The combination of stacking and hydrogen bond makes this structure the second most stable one, reaching -32.7 kcal/mol. As in benzene complexes, there is a large energy gap between the doubly T-shaped structure and the rest of minima.

However, when the aromatic units are part of the side chain of amino acids they could rarely be so free as to adopt this doubly T-shaped structure, so T-shaped or stacked ones can be of importance to the stability of the system. In-In-2 and In-In-3 are structures closely related to In-In-4, the main difference being that the N-H···π contact takes place with the pyrrol ring of the second indole unit. In any case, the stability of the structures is pretty similar. Therefore, in all cases the most stable arrangement corresponds to the doubly T-shaped structures, with the stability increasing from benzene to phenol and to indole. The next stable structures are T-shaped ones, especially in phenol and indole complexes, where O-H···X or N-H···π hydrogen bonds can be formed. Finally, the least favorable arrangement is the parallel displaced stacked structure, with differences of about 1.5-2.5 kcal/mol with respect to T-shaped ones. Trends are not so clear in phenol complexes due to the great tendency of phenol to form O-H···X hydrogen bonds. As a consequence, no true stacked structure has been located and the T-shaped one has a O-H···O hydrogen bond. Also, the possibility of forming hydrogen bonds gives rise to other structures as Ph-Ph-1, where a chain of N-H···O-H···O hydrogen bonds is formed leading to a structure with the same stability as the doubly T-shaped ones.

5.3.2. Complexes with different aromatic molecules

When different aromatic molecules are combined with guanidinium cation to create the complexes, the number of possible structures grows quickly. In order to make the discussion simpler, several prototypical structures have been selected among the minima located. It is worth noting that, as commented before, especially in the case of

phenol-containing complexes, these prototypical structures are not always found, so only the closest among the minima found were considered. In most cases, T-shaped structures containing phenol coordinated to guanidinium cation show a O-H···π hydrogen bond, whereas purely stacked structures are not found. All these preventions in mind, in the following sections the results for these mixed complexes will be discussed. Five different structures have been considered for mixed complexes of guanidinium, benzene and phenol, as shown in Figure 5.4: two parallel ones and two T-shaped ones, whereas for the doubly T-shaped structure there is only one since Bz-Ph and Ph-Bz are equivalent.

Table 5.2 lists the values obtained for the complexation energies at the M06-2X/6-31+G* and SCS-MP2/CBS levels of calculation. Considering the values in Table 5.2 for Bz-Ph complexes, it can be appreciated that the doubly T-shaped minimum Bz-Ph-DT reaches a complexation energy of around -28.2 kcal/mol, which is an intermediate value between the results obtained for complexes containing only phenol or benzene. This is as expected since in doubly T-shaped minima the two aromatic molecules do not interact significantly between them, so the interaction depends entirely on the guanidinium···π interaction. As for stacked minima, both show a similar stability around -19 kcal/mol, which is slightly larger than that observed in benzene complexes (no stacked minima were found for phenol complexes). Finally, T-shaped minima show results which are more difficult to rationalize. Bz-Ph-T is more stable than Ph-Bz-T by 2.5 kcal/mol, but this is a consequence of the contact of guanidinium cation with the hydroxyl oxygen in the former structure. On the other hand Ph-Bz-T shows a O-H···π hydrogen bond which makes it more stable than the corresponding Bz-Bz structure, but less stable than complexes with only phenol, where O-H···O hydrogen bonds are formed.

In the case of complexes formed by guanidinium, benzene and indole (Figure 5.5) the behavior is simpler since the minima correspond closely with the prototypical arrangements considered. It is clearly observed that for stacked structures it is more favorable for the indole molecule (In-Bz-P) to be coordinated to guanidinium, with a stability gain of around -4 kcal/mol with respect to coordination to benzene (Bz-In-P). Since the interaction between indole and benzene must be similar in both cases, this difference is related to the stronger interaction of guanidinium with indole. Again, an intermediate behavior between Bz-Bz and In-In complexes is observed. In T-shaped minima coordination to indole is also preferred by about -4 kcal/mol, but this could be also related to the formation of a N-H···π hydrogen bond in the In-Bz-T minimum. Doubly T-shaped structures show a similar behavior with stability midway between indole and benzene complexes.

Table 5.2. Complexation energies (kcal/mol) obtained for mixed complexes formed by guanidinium and two aromatic molecules as obtained with different methods, all employing the optimized M06-2X/6-31+G* geometry.

		Bz-Ph	Ph-Bz	Bz-In	In-Bz	Ph-In	In-Ph
M06-2X/ 6-31+G*	Parallel (P)	-19.78	-20.78	-21.86	-26.78	-35.06	-28.14
	T-Shaped (T)	-29.78	-26.15	-26.06	-28.88	-30.95	-28.65
	Doubly T-Shaped (DT)	-29.10		-30.13		-34.97	
SCS-MP2/ CBS	Parallel (P)	-19.66	-19.27	-21.94	-26.38	-31.69	-26.93
	T-Shaped (T)	-27.42	-24.98	-24.69	-28.52	-29.82	-27.82
	Doubly T-Shaped (DT)	-28.22		-30.10		-33.44	

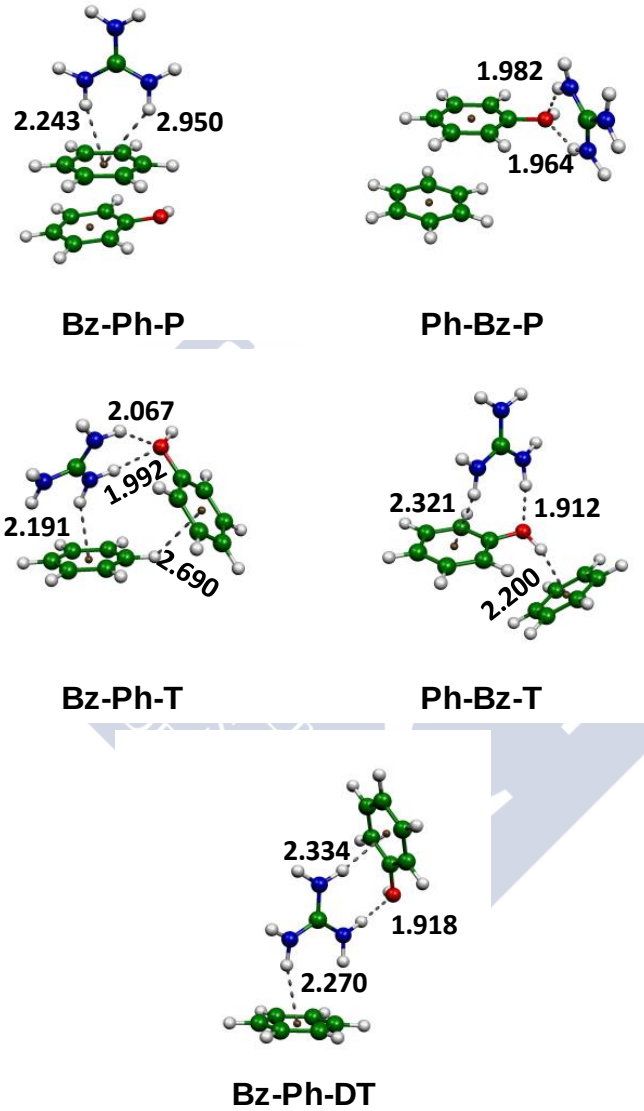


Figure 5.4. Selected minima for complexes formed by guanidinium, benzene and phenol as obtained at the M06-2X/6-31+G* level. Selected Distances in Å.

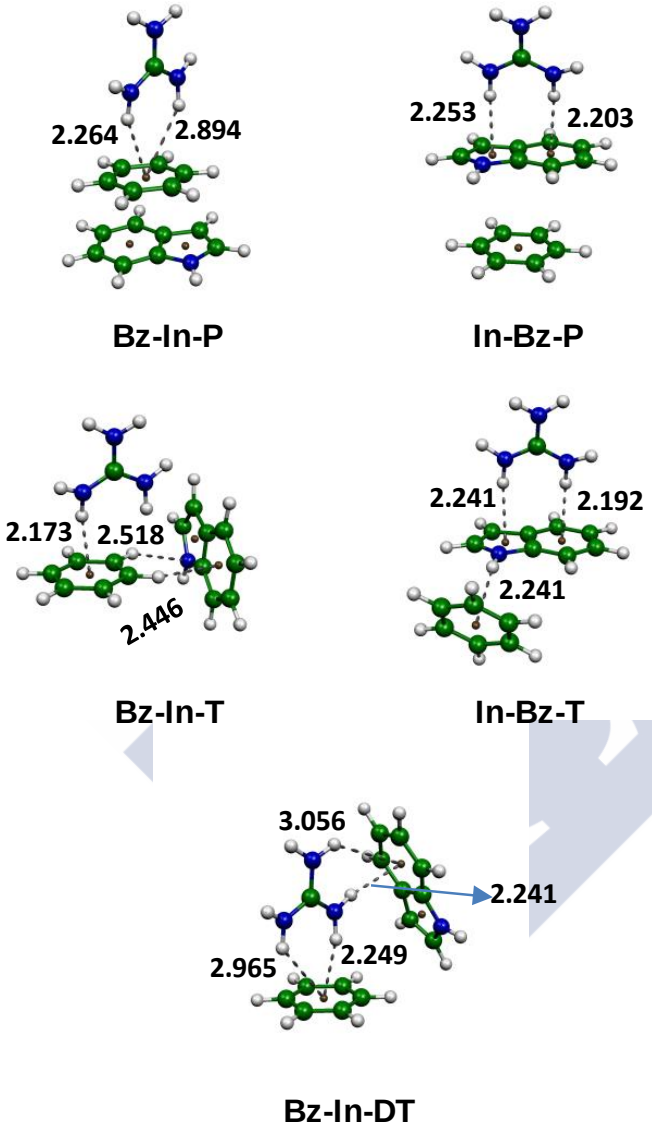


Figure 5.5. Selected minima for complexes formed by guanidinium, benzene and indole as obtained at the M06-2X/6-31+G* level. Selected Distances in Å.

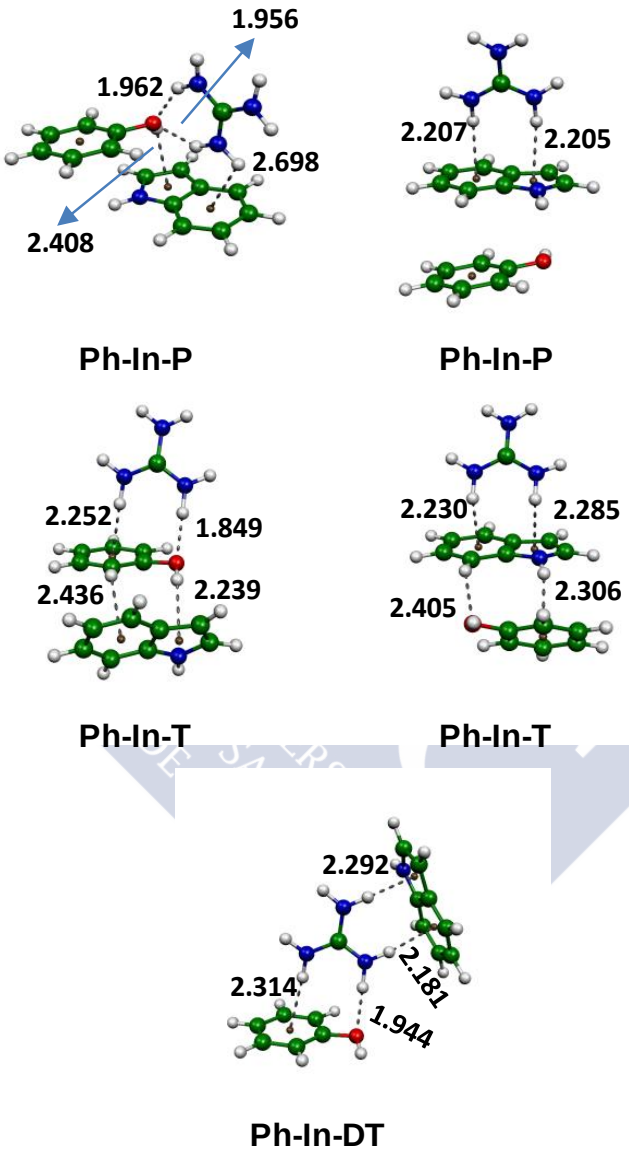


Figure 5.6. Selected minima for complexes formed by guanidinium, phenol and indole as obtained at the M06-2X/6-31+G* level. Selected Distances in Å.

Finally, for complexes containing the cation plus indole and phenol (Figure 5.6) the behavior is similar overall. For the doubly T-shaped minimum the complexation energy is halfway between those of complexes with only one kind of aromatic molecule. However, it can be observed that phenol coordination is preferred over indole for stacked and T-shaped structures. This is because in the presence of phenol, In-Ph structures correspond to our prototypes, but for Ph-In complexes there are clear deviations. Therefore whereas In-Ph-P is a typical stacked structure with a complexation energy of -27 kcal/mol, Ph-In-P minimum is not stacked, and guanidinium interacts with both aromatic units leading to a complexation energy of -31.7 kcal/mol. In fact this minimum corresponds more closely to a guanidinium coordinated to the hydroxyl group which establishes a O-H···π hydrogen bond to the pyrrol ring of indole. T-shaped minima both present hydrogen bonds. Ph-In-T forms a O-H···π hydrogen bond to the pyrrol ring of indole, whereas a N-H···π hydrogen bond is observed in In-Ph-T, this latter structure being disfavored by about 2 kcal/mol.

So, these mixed complexes behave halfway the complexes formed with only one kind of aromatic molecule. This is especially evident in the case of doubly T-shaped structures, which always show complexation energies almost midway the complexes with only one kind of aromatic molecule. These doubly T-shaped structures are always the most stable found among the clusters studied. A similar behavior is observed in stacked clusters of benzene and indole, but the presence of phenol and the tendency of its hydroxyl group to form hydrogen bonds introduce other possibilities for the interaction. In the absence of extra interactions with the guanidinium cation or hydrogen bonds, stacked structures are the least stable. T-shaped minima are usually the second most stable, but again in phenol complexes the formation of hydrogen bonds can alter the order of stability, favoring coordination of phenol by the guanidinium cation. In the absence of these effects guanidinium coordinates preferentially to indole over phenol and over benzene.

A question arises about whether the kind of structures already discussed is present in proteins. It is known that stacking interactions between aromatic side chains are frequent, as it is the case with the cation···aromatic interactions.[4, 11] It is expected, however that the motifs considered in this work, simultaneously involving three different side chains will be less frequent. However, searching into the Protein Data Bank Europe it is possible to find the kind of structures considered in this work.[52] As example, searching for a pattern formed by a nitrogen atom of guanidinium in arginine contacting with indole ring in tryptophan, which in turn is stacked to phenyl group of phenylalanine (like in In-Bz-P) results in more than forty coincidences. Among these structures there are several of them that resemble the patterns shown in the manuscript. Of course there are geometrical differences that are mainly associated to the more complex environment in the protein, and to the rest of the side chains hindering the free orientation of the aromatic rings and the cationic fragment to interact

in an optimal way. In any case, many of the structures found resemble the minima considered in this work, so it can be expected that their characteristics would be helpful in order to understand these kind of contact in proteins. Also, gas phase results would help to isolate other factors like solvent effects of other groups nearby which can alter the mutual arrangement of aromatic and cationic side chains.

5.3.3. Pair energies

In order to understand more closely the behavior of these ternary systems, a decomposition on pair contributions has been performed for the clusters discussed above. Table 5.3 shows the results obtained for the pair energies of complexes as obtained at the M06-2X/6-31+G* level of calculation, together with the contributions from three-body effects. It can be observed that in all complexes the interaction of guanidinium with benzene, phenol and indole amounts to -14 kcal/mol, -18 kcal/mol and -21 kcal/mol, respectively. The strength of these interactions is almost the same in all minima considered, thus indicating that the presence of a second aromatic unit hardly affects the guanidinium···π interaction. For example guanidinium···benzene interaction varies between -12.8 and -13.9 kcal/mol, and similar variations are observed for the other aromatic species. Part of these changes can be attributed to changes in the geometry of the cation···π interaction depending on the complex considered. In any case, the effect of the second aromatic unit on the guanidinium···π interaction is described by the 3-body contribution to the interaction energy, which in most cases is not large.

In doubly T-shaped structures there is a similar pattern for the pair interactions in all cases. As expected, there are two strong interactions due to guanidinium···π interactions, plus one weak repulsive interaction due to the interaction of the two aromatic molecules located far apart. For the doubly T-shaped minima the contribution of the 3-body term is destabilizing, amounting to between 1.3 kcal/mol for Bz-Bz complex to 2.7 kcal/mol in In-In complex. This is a consequence of the charge of the cation being shared by the two aromatic molecules. Mixed complexes show a similar behavior, but the two cation···π contacts are not equivalent showing a pair of values typical for the two aromatic units considered.

T-shaped minima typically show one strong interaction due to the cation interacting with the closer aromatic molecule, plus two similar weak attractive interactions between the cation and the other aromatic molecule, and between both aromatic molecules. Therefore, in Bz-Bz-2 there is a guanidinium···benzene contact amounting to around -13 kcal/mol, plus an interaction of -6 kcal/mol between guanidinium and the other benzene molecule far apart. Finally, both benzene molecules contribute with -2 kcal/mol to the interaction due to a C-H···π contact. As in the case of doubly T-shaped minima, 3-body effects are repulsive and small.

Table 5.3. Pair energy decomposition (kcal/mol) for selected complexes formed by guanidinium and two aromatic molecules as obtained at the M06-2X/6-31+G* level.[a]

	ΔE_{AB}	ΔE_{AC}	ΔE_{BC}	$E_{3\text{-body}}$		ΔE_{AB}	ΔE_{AC}	ΔE_{BC}	$E_{3\text{-body}}$
	Parallel					**T-Shaped**			
Bz-Bz-1	-2.38	-13.92	-2.17	-0.36	**Bz-Bz-2**	-2.09	-13.45	-5.90	0.22
Ph-Ph-1	-5.96	-17.15	-12.09	0.36	**Ph-Ph-3**	-6.28	-18.25	-4.03	-2.68
In-In-1	-5.19	-21.09	-3.44	-0.51	**In-In-4**	-7.68	-21.05	-3.13	-1.95
Bz-Ph-P	-2.43	-13.90	-2.70	-0.33	**Bz-Ph-T**	-2.01	-12.83	-18.27	1.55
Ph-Bz-P	-2.42	-18.50	-0.73	-0.33	**Ph-Bz-T**	-4.69	-18.52	-2.90	-1.42
Bz-In-P	-4.09	-13.93	-3.36	-0.88	**Bz-In-T**	-3.71	-13.30	-9.64	0.33
In-Bz-P	-4.61	-21.03	-1.87	0.21	**In-Bz-T**	-5.08	-21.01	-1.72	-1.53
Ph-In-P	-6.80	-17.88	-14.54	1.65	**Ph-In-T**	-7.29	-18.45	-4.39	-2.24
In-Ph-P	-5.84	-21.05	-1.73	-0.13	**In-Ph-T**	-5.70	-20.02	-3.08	-1.47
	Doubly T-Shaped					**Doubly T-Shaped**			
Bz-Bz-4	0.10	-13.76	-13.76	1.33	**Bz-Ph-DT**	0.12	-13.74	-18.02	1.66
Ph-Ph-6	0.32	-17.89	-17.89	2.04	**Bz-In-DT**	-0.69	-13.68	-18.56	2.22
In-In-5	0.14	-20.79	-20.63	2.65	**Ph-In-DT**	0.33	-17.85	-20.59	2.33

[a] C is always guanidinium cation. In the X-Y pair, A corresponds to X and B to Y.

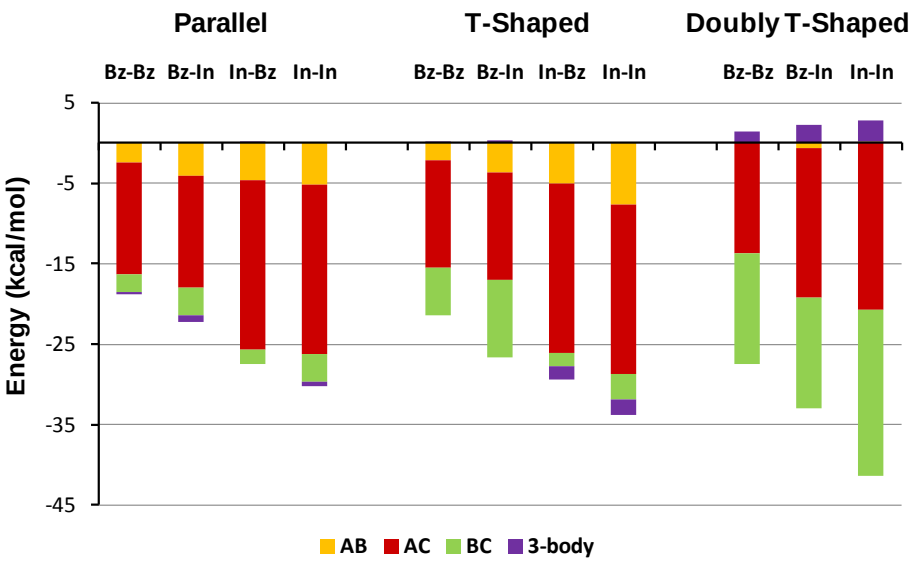


Figure 5.7. Pair energy contributions in complexes with benzene and indole as obtained at the M06-2X/6-31+G* level. C is always guanidinium cation. In the X-Y pair, A corresponds to X and B to Y.

A similar behavior is observed in mixed complexes where benzene is coordinated to the cation. In the case of indole and phenol complexes there is also a strong cation···π interaction together with two weaker contributions from the other molecule pairs. However, in these complexes the interaction between the two aromatic molecules occurs by means of a hydrogen bond, so the stabilization increases with respect to benzene complexes. Thus, in the T-shaped minima containing two indole molecules, the N-H···π hydrogen bond contributes with around -8 kcal/mol to the stability of the complex. Most complexes with phenol or indole coordinated to guanidinium show similar values (though somewhat weaker, around -4 to -5 kcal/mol). Comparing the values obtained for the mixed Ph-In complexes, it can be appreciated how the O-H···π contact (-7.3 kcal/mol) is stronger than the N-H···π one (-5.7 kcal/mol). Also, in these structures, contrary to benzene ones, 3-body effects are attractive, amounting between -1.5 to -2.7 kcal/mol, these values being a consequence of the presence of the hydrogen bonds. Parallel minima show similar energy decomposition as T-shaped structures, with a strong cation···π contact plus two weak contacts from the other pairs. When phenol and indole are involved, the interaction between aromatic molecules can reach around -5 kcal/mol, being only slightly weaker than the interaction in hydrogen-bonded structures present in T-shaped minima. Three body effects are mostly attractive but weaker than those observed in the other structural arrangements. The different pair contributions can be easily seen in Figure 5.7, where results are shown for benzene and indole-containing complexes, showing the patterns discussed above.

5.3.4. LMO-EDA analysis

LMO-EDA decomposition has been performed with both M06-2X and MP2 methods. It has to be taken into account that in the case of post-HF methods, the so-called dispersion contribution corresponds to the contribution of the correlation to the interaction energy. With DFT methods, on the other hand, dispersion (obtained as a difference between a sum of terms and the interaction energy from a supermolecule calculation) also recovers deviations from other contributions. Along this section only results obtained with the MP2/aug-cc-pVDZ partitioning will be considered, the M06-2X ones presented in Appendix B. The largest differences between both methods have been observed in the repulsion term, which is larger with M06-2X, thus leading as compensation to too large dispersion contributions. Figures 5.8 and 5.9 show the results obtained for this decomposition for the structures presented in Figures 5.1 to 5.6.

It can be observed that in Bz-Bz complexes the repulsion is almost constant and provides a kind of background against which the attractive contributions of electrostatics, polarization and dispersion bring close together the fragments in the complex. In the doubly T-shaped minimum Bz-Bz-4 the main contribution to the stability of the complex is electrostatic, amounting to -21 kcal/mol, as a consequence of the interaction of the cation with both aromatic clouds of the benzene molecules. On the other hand, dispersion contributes with almost -13 kcal/mol to the stability of the complex. The polarization due to the cation also contributes significantly to the stability, reaching -15 kcal/mol. In the parallel structure Bz-Bz-1 the electrostatic contribution drops to -17 kcal/mol, and consequently, the contribution of polarization also decreases to -11 kcal/mol. These joined contributions introduce a difference of about 8-9 kcal/mol with respect to the doubly T-shaped one. This is partly recovered by an increase of dispersion contribution due to the stacking of the rings. As regards T-shaped structures the distribution of contributions is pretty similar to the parallel ones. Therefore, the preference of doubly T-shaped minima is a consequence of larger electrostatic and polarization contributions, whereas other structures are more favored by dispersion.

In Ph-Ph clusters, the electrostatic contribution is large in all minima, even in parallel or T-shaped ones. This is related to the formation of hydrogen bonds in most of the minima. In Ph-Ph-1 and Ph-Ph-5 the electrostatic contribution is the largest, because in these minima guanidinium is coordinated to the hydroxyl group, which simultaneously forms a O-H···O (Ph-Ph-1) or O-H···π (Ph-Ph-5) hydrogen bond. The chain-like arrangement of the contacts produces large electrostatic and polarization contributions. In-In complexes resemble the behavior of benzene aggregates. The doubly T-shaped minimum presents large electrostatic, polarization and dispersion contributions, combined with the smallest repulsion term. On the other hand the parallel structure In-In-1 shows much smaller electrostatic and polarization terms, while dispersion is larger, partly cancelled out with the increase in repulsion.

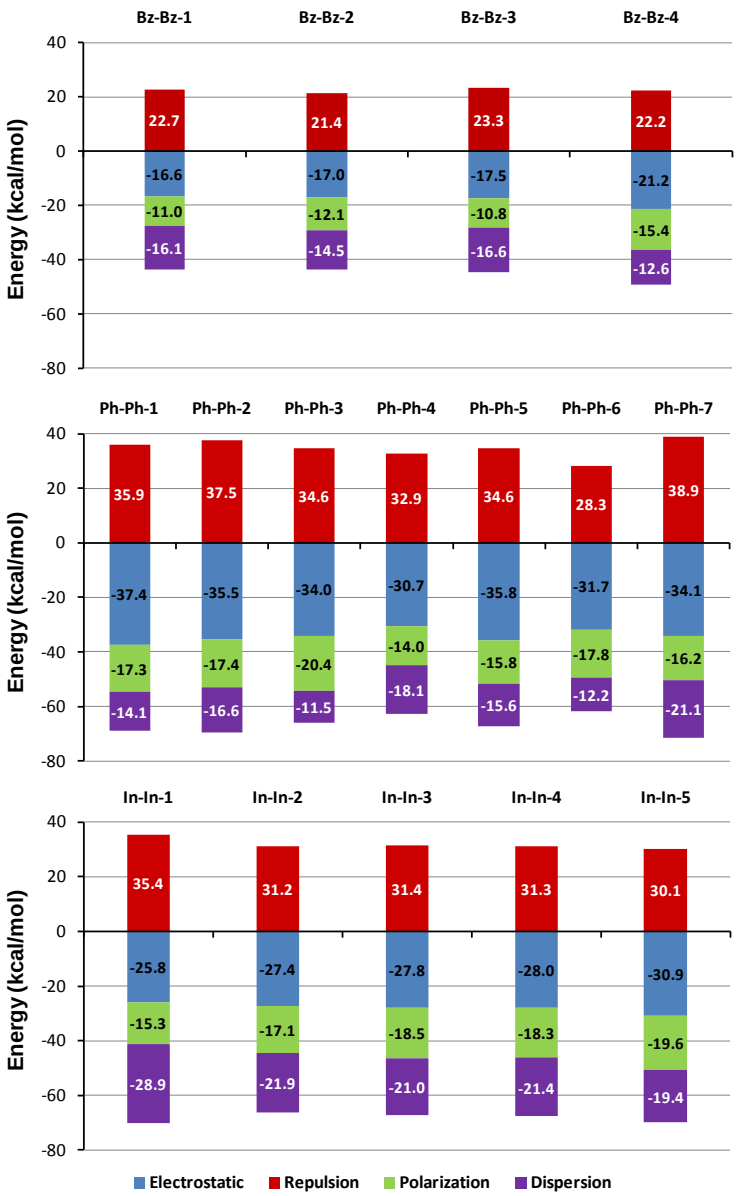


Figure 5.8. LMO-EDA decomposition of complexes with the same aromatic molecules at the MP2/aug-cc-pVDZ level.

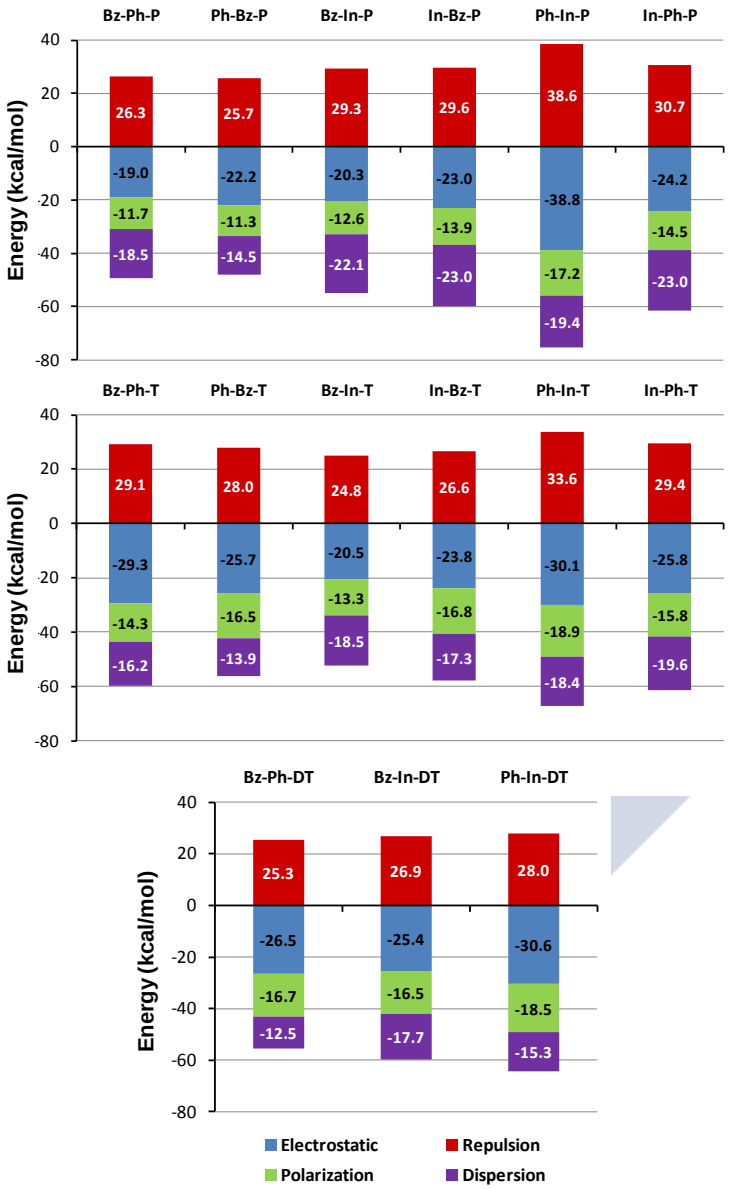


Figure 5.9. LMO-EDA decomposition of complexes with different aromatic molecules at the MP2/aug-cc-pVDZ level.

Finally, for the T-shaped structures an intermediate behavior is observed, with dispersion slightly larger than that observed in the doubly T-shaped minimum, and large electrostatic and polarization terms (larger than stacked but smaller than doubly T-shaped).

The results for mixed complexes are shown in Figure 5.9. The behavior is midway between that found for complexes with only one kind or aromatic unit. Therefore, in doubly T-shaped minima there is a large electrostatic component of the interaction, together with significant polarization and dispersion terms. T-shaped minima exhibit a greater variety. In Bz-In T-shaped minima the coordination of guanidinium to indole in In-Bz-T is favored due to larger contributions of electrostatics and polarization, even though dispersion is larger for Bz-In-T despite the larger size of indole. This is a consequence of the formation of a N-H···π hydrogen bond in In-Bz-T which locates the benzene molecule farther apart leading to a smaller dispersion contribution than in Bz-In-T where the molecules are packed closer together. In In-Ph-T complex the largest contribution clearly comes from electrostatics, whereas the formation of the O-H···π hydrogen bond in Ph-In-T causes an increment in the electrostatic and polarization contributions, whereas dispersion slightly decreases. Parallel minima present a similar pattern, with the largest contribution coming from electrostatics, though in this case dispersion reaches similar values except in complexes with guanidinium directly bounded to phenol.

Overall, it becomes clear that the interaction with indole introduces larger dispersion contributions reflecting the larger size of the molecule. On the other hand, phenol interacts more strongly on an electrostatic basis due to the formation of hydrogen bonds and to the interactions of guanidinium with the hydroxyl group. Polarization contributions are similar in indole and phenol complexes, and both larger than in benzene systems. Therefore the preference for interaction with phenol is mainly due to electrostatics, whereas indole is preferred on the basis of a combination of all stabilizing contributions.

5.3.5. Non Covalent Interaction Index (NCI)

As another tool for further analyzing the nature of the interaction in these systems, Figure 5.10 shows the Non Covalent Interaction (NCI) index plots for complexes containing benzene and indole (NCI plots for the rest of minima are attached in Appendix B). NCI is an index based on the analysis of the reduced density gradient which can be employed to visualize both favorable and unfavorable interactions.[53, 54] These interactions can be graphically displayed as a plot of the product of the sign of the second eigenvalue of the hessian of the density times the density ($\text{sign}(\lambda_2)\cdot\rho$), mapped onto an isosurface of reduced density gradient.

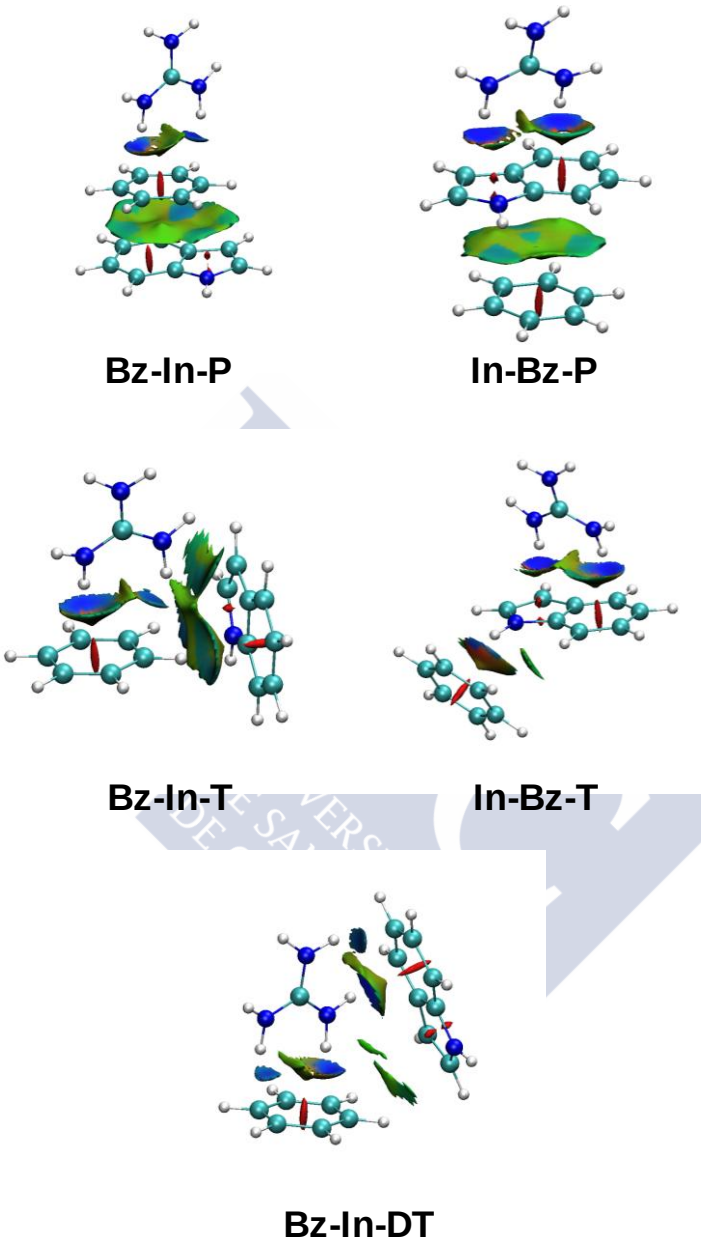


Figure 5.10. NCI surfaces corresponding to the mixed complexes containing benzene and indole. A reduced density gradient isosurface of 0.5 a.u. and a colour scale of −0.015 (blue) to 0.015 (red) a.u. are employed.

It can be observed in Figure 5.10 how the NCI index reveals the different nature of the interactions established in each of the complexes. In parallel minima, two strong hydrogen bonds are observed between the guanidinium cation and the aromatic unit close by. In the case of In-Bz-P it is clear that guanidinium forms hydrogen bonds with both rings of indole. Besides, a wide weakly attractive region is observed between the two aromatic molecules, clearly showing the stacking interaction.

On the other hand, Bz-In-T shows the contact between guanidinium and benzene, plus a weaker contact between guanidinium and indole. The C-H···π contact from benzene to the phenyl ring of indole is also observed. As regards In-Bz-T, the most relevant feature is the N-H···π hydrogen bond from indole to benzene. In Bz-In-DT, the four strong contacts between the guanidinium NH groups and the aromatic molecules are also revealed. Therefore, the NCI plots allow easily checking the most relevant contacts for a given complex, which in the present case correspond to N-H···π, C-H···π and π···π contacts.

5.4. Conclusions

Ternary complexes formed by guanidinium cation and two aromatic units selected from those present in amino acid side chains have been computationally studied in order to model the interaction of arginine side chain with contiguous aromatic amino acids. A variety of different structures have been found, but most can be classified as parallel stacked (two parallel rings), T-shaped (perpendicular rings) and doubly T-shaped (guanidinium between both rings). In almost all minima guanidinium is located perpendicularly to the aromatic rings interacting with them by means of two of its NH_2 groups, as previously observed in guanidinium···benzene complexes. The most stable minima correspond in all cases to the doubly T-shaped structures where the cation can interact with both aromatic rings. The largest stabilizing contribution to the interaction is electrostatic for most complexes. In benzene and indole parallel and T-shaped minima the contribution from dispersion is also important, with significant though smaller induction terms. Complexes containing phenol exhibit even larger electrostatic and induction contributions as a consequence of the formation of hydrogen bonds.

The interaction strength grows when passing from benzene to phenol and to indole. This behavior is also observed in mixed complexes, so guanidinium tends to coordinate to indole in order to form the most stable trimers. In the so-called T-shaped structures the behavior is partially conditioned by the possibility of forming hydrogen bonds in indole- and phenol-containing clusters. Overall, three body effects are repulsive in doubly T-shaped structures and attractive in the case of parallel stacked and T-shaped ones. Stabilizing three body effects only become significant in structures where phenol or indole form hydrogen bonds.

The characteristics of the complexes are roughly determined by the strength of the cation···π interactions, but secondary interactions between the aromatic species can modulate their behavior, especially when hydrogen bonds are formed in phenol and indole complexes. Besides, the stability of these trimers comes from a delicate balance among different contributions that change depending on the nature and the relative orientation of the fragments. All these factors should be considered in order to understand the behavior of multiple cation···π interactions involving aromatic amino acids.

5.5. References

[1] P. Hobza, R. Zaradnik, Intermolecular complexes : the role of van der Waals systems in physical chemistry and the biodisciplines, Elsevier, Amsterdam, **1988**.

[2] H.-J. Schneider, A. K. Yatsimirski, Principles and methods in supramolecular chemistry, Wiley, Chichester, **2000**.

[3] E. A. Meyer, R. K. Castellano, F. Diederich. *Angew. Chem. Int. Ed.* **2003**, *42*, 1210-1250.

[4] L. M. Salonen, M. Ellermann, F. Diederich. *Angew. Chem. Int. Ed.* **2011**, *50*, 4808-4842.

[5] S. Tsuzuki, T. Uchimaru. *Curr. Org. Chem.* **2006**, *10*, 745-762.

[6] M. L. Waters. *Biopolymers (Peptide Sci.)* **2004**, *76*, 435-445.

[7] M. Nishio. *Phys. Chem. Chem. Phys.* **2011**, *13*, 13873-13900.

[8] N. J. Zondlo. *Acc. Chem. Res.* **2013**, *46*, 1039-1049.

[9] D. A. Dougherty. *Acc. Chem. Res.* **2013**, *46*, 885-893.

[10] A. Frontera, D. Quiñonero, P. M. Deyà. *WIREs Comput. Mol. Sci.* **2011**, *1*, 440-459.

[11] A. S. Mahadevi, G. N. Sastry. *Chem. Rev.* **2013**, *113*, 2100-2138.

[12] D. Kim, E. C. Lee, K. S. Kim, P. Tarakeshwar. *J. Phys. Chem. A* **2007**, *111*, 7980-7986.

[13] I. Soteras, M. Orozco, F. J. Luque. *Phys. Chem. Chem. Phys.* **2008**, *10*, 2616-2624.

[14] J. P. Gallivan, D. A. Dougherty. *Proc. Natl. Acad. Sci. USA* **1999**, *96*, 9459-9464.

[15] N. Zacharias, D. A. Dougherty. *Trends Pharmacol. Sci.* **2002**, *23*, 281-287.

[16] D. A. Dougherty. *J. Nutr.* **2007**, *137*, 1504S-1508S.

[17] J. P. Gallivan, D. A. Dougherty. *J. Am. Chem. Soc.* **2000**, 870-874.

[18] Y. Xu, J. Shen, W. Zhu, X. Luo, K. Chen, H. Jiang. *J. Phys. Chem. B* **2005**, *109*, 5945-5949.

[19] C. Adamo, G. Berthier, R. Savinelli. *Theor. Chem. Acc.* **2004**, *111*, 176-181.

[20] E. M. Cabaleiro-Lago, J. Rodríguez-Otero, Á. Peña-Gallego. *J. Chem. Phys.* **2011**, *135*, 214301-214309.

[21] A. Campo-Cacharron, E. M. Cabaleiro-Lago, J. Rodriguez-Otero. *Theor. Chem. Acc.* **2012**, *131*, 1-13.

[22] A. A. Rodriguez-Sanz, J. Carrazana-Garcia, E. M. Cabaleiro-Lago, J. Rodriguez-Otero. *J. Mol. Model.* **2013**, *19*, 1985-1994.

[23] E. M. Duffy, P. J. Kowalczyk, W. L. Jorgensen. *J. Am. Chem. Soc.* **1993**, *115*, 9271-9275.

[24] T. L. Greaves, C. J. Drummond. *Chem. Rev.* **2007**, *108*, 206-237.

[25] P. E. Mason, C. E. Dempsey, G. W. Neilson, S. R. Kline, J. W. Brady. *J. Am. Chem. Soc.* **2009**, *131*, 16689-16696.
[26] P. E. Mason, G. W. Neilson, J. E. Enderby, M.-L. Saboungi, C. E. Dempsey, A. D. MacKerell Jr., J. W. Brady. *J. Am. Chem. Soc.* **2004**, *126*, 11462-11470.
[27] J. Vondrasek, P. E. Mason, J. Heyda, K. D. Collins, P. Jungwirth. *J. Phys. Chem. B* **2009**, *113*, 9041-9045.
[28] I. Kaplan, Intermolecular Interactions : Intermolecular Interactions : Physical Picture , Computational Methods, John Wiley & Sons, Chichester, **2006**.
[29] A. J. Stone, The theory of intermolecular forces, Oxford University Press, Oxford, **2013**.
[30] D. Escudero, X. Lucas, C. Estarellas, A. Frontera, D. Quiñonero, P. M. Deya. *Trends Pharmacol. Sci.* **2008**, *13*, 31-52.
[31] C. Estarellas, A. Frontera, D. Quiñonero, P. M. Deya. *Chem. Phys. Lett.* **2009**, *479*, 316-320.
[32] C. Estarellas, A. Frontera, D. Quiñonero, P. M. Deya. *Cent. Eur. J. Chem.* **2011**, *9*, 25-34.
[33] D. Vijay, G. N. Sastry. *Chem. Phys. Lett.* **2010**, *485*, 235-242.
[34] D. Vijay, H. Zipse, G. N. Sastry. *J. Phys. Chem. B* **2008**, *112*, 8863-8867.
[35] Y. Zhao, D. G. Truhlar. *Theor. Chem. Acc.* **2007**, *120*, 215-241.
[36] Y. Geng, T. Takatani, E. G. Hohenstein, C. D. Sherrill. *J. Phys. Chem. A* **2010**, *114*, 3576-3582.
[37] N. J. Singh, S. K. Min, D. Y. Kim, K. S. Kim. *J. Chem. Theory Comput.* **2009**, *5*, 515-529.
[38] S. F. Boys, F. Bernardi. *Mol. Phys.* **1970**, *19*, 553-566.
[39] G. Chałasiński, M. M. Szczęśniak. *Chem. Rev.* **2000**, *100*, 4227-4252.
[40] T. Helgaker, W. Klopper, H. Koch, J. Noga. *J. Chem. Phys.* **1997**, *106*, 9639-9646.
[41] E. G. Hohenstein, C. D. Sherrill. *WIREs Comput. Mol. Sci.* **2012**, *2*, 304-326.
[42] S. Grimme. *J. Chem. Phys.* **2003**, *118*, 9095-9102.
[43] P. Su, H. Li. *J. Chem. Phys.* **2009**, *131*, 014102/1-014102/15.
[44] M. J. Frisch, G. W. Trucks, H. B. Schlegel, G. E. Scuseria, M. A. Robb, J. R. Cheeseman, J. J. A. Montgomery, T. Vreven, K. N. Kudin, J. C. Burant, J. M. Millam, S. S. Iyengar, J. Tomasi, V. Barone, B. Mennucci, M. Cossi, G. Scalmani, N. Rega, G. A. Petersson, H. Nakatsuji, M. Hada, M. Ehara, K. Toyota, R. Fukuda, J. Hasegawa, M. Ishida, T. Nakajima, Y. Honda, O. Kitao, H. Nakai, M. Klene, X. Li, J. E. Knox, H. P. Hratchian, J. B. Cross, V. Bakken, C. Adamo, J. Jaramillo, R. Gomperts, R. E. Stratmann, O. Yazyev, A. J. Austin, R. Cammi, C. Pomelli, J. W. Ochterski, P. Y. Ayala, K. Morokuma, G. A. Voth, P. Salvador, J. J. Dannenberg, V. G. Zakrzewski, S. Dapprich, A. D. Daniels, M. C. Strain, O. Farkas, D. K. Malick, A. D. Rabuck, K. Raghavachari, J. B. Foresman, J. V. Ortiz, Q. Cui, A. G. Baboul, S. Clifford, J. Cioslowski, B. B. Stefanov, G. Liu, A. Liashenko, P. Piskorz, I. Komaromi, R. L. Martin, D. J. Fox, T. Keith, M. A. Al-Laham, C. Y. Peng, A. Nanayakkara, P. M. W. Gill, B. Johnson, W. Chen, M. W. Wong, C. Gonzalez, J. A. Pople, Gaussian 09, revision B.01, Gaussian, Inc., Wallingford CT, **2009**..
[45] M. S. Gordon, M. W. Schmidt in *Advances in electronic structure theory: GAMESS a decade later, Vol.* (Eds.: C. E. Dykstra, G. Frenking, K. S. Kim, G. E. Scuseria), ELSEVIER, AMSTERDAM, **2005**, pp.1167-1189.

[46] M. W. Schmidt, K. K. Baldridge, J. A. Boatz, S. T. Elbert, M. S. Gordon, J. H. Jensen, S. Koseki, N. Matsunaga, K. A. Nguyen, S. Su, T. L. Windus, M. Dupuis, J. A. Montgomery. *J. Comput. Chem.* **1993**, *14*, 1347-1363.
[47] TURBOMOLE V6.3 , a development of University of Karlsruhe and Forschungszentrum Karlsruhe GmbH, 1989-2007, TURBOMOLE GmbH, since 2007; available from http://www.turbomole.com., **2011**.
[48] F. Weigend. *Phys. Chem. Chem. Phys.* **2002**, *4*, 4285-4291.
[49] F. Weigend, A. Köhn, C. Hättig. *J. Chem. Phys.* **2002**, *116*, 3175-3183.
[50] D. Vijay, G. N. Sastry. *Phys. Chem. Chem. Phys.* **2008**, *10*, 582-590.
[51] J. R. Premkumar, D. Vijay, G. N. Sastry. *Dalton Trans.* **2012**, *41*, 4965-4975.
[52] S. Velankar, Y. Alhroub, C. Best, S. Caboche, M. J. Conroy, J. M. Dana, M. A. Fernandez Montecelo, G. van Ginkel, A. Golovin, S. P. Gore, A. Gutmanas, P. Haslam, P. M. S. Hendrickx, E. Heuson, M. Hirshberg, M. John, I. Lagerstedt, S. Mir, L. E. Newman, T. J. Oldfield, A. Patwardhan, L. Rinaldi, G. Sahni, E. Sanz-García, S. Sen, R. Slowley, A. Suarez-Uruena, G. J. Swaminathan, M. F. Symmons, W. F. Vranken, M. Wainwright, G. J. Kleywegt. *Nuc. Acids Res.* **2012**, *40*, D445-D452.
[53] E. R. Johnson, S. Keinan, P. Mori-Sánchez, J. Contreras-García, A. J. Cohen, W. Yang. *J. Am. Chem. Soc.* **2010**, *132*, 6498-6506.
[54] J. Contreras-García, E. R. Johnson, S. Keinan, R. Chaudret, J.-P. Piquemal, D. N. Beratan, W. Yang. *J. Chem. Theory Comput.* **2011**, *7*, 625-632.

USC UNIVERSIDADE DE SANTIAGO DE COMPOSTELA

USC
UNIVERSIDADE
DE SANTIAGO
DE COMPOSTELA

6. A DFT study of the interaction between microhydrated anions and naphthalendiimides

USC
UNIVERSIDADE
DE SANTIAGO
DE COMPOSTELA

6.1. Introduction

Cation···π interactions have proven of importance on different aspects of molecular recognition and stability in biological systems.[1-3] Cation···π contacts can be found in almost any protein due to the presence of amino acids containing aromatic residues in their side chain, together with other amino acids which present cationic groups, usually depending on the pH of the medium.[4-6] These cation···π interactions are usually very strong in the gas phase, but much weaker in the presence of solvent, though there is some controversy about the contribution of the cation···π interactions in real systems.[7-12]

On the other hand, anion receptors are of great interest in different chemical and biological applications.[13, 14] The possibility of stabilizing interactions between anions and electron-deficient aromatic systems in the so-called anion···π interaction has also aroused interest.[15, 16] The extensive work of Deyá et al. has already shown that the interaction is mainly electrostatic in nature, so one must have an electron-deficient aromatic system with positive quadrupole moment.[15-20] The attractive interaction between this quadrupole and the negative charge of the anion is mainly responsible of the stabilizing interaction, with strengths similar to those observed for cation···π interactions. Most studies in this field have been carried out employing benzene as a model for the aromatic system, so these works have mostly considered hexafluorobenzene, trifluorobenzene or triazine complexes with halogen anions.[16, 21, 22] Several authors have performed studies of the interaction of anions with aromatic systems showing a significant interaction, thus suggesting the possibility of anion receptors based on anion···π interactions.[15, 17, 21-28]

Recently, Matile at al. have explored the possibility of using anion···π interactions as the driving force in synthetic anion channels allowing anion transport through lipid bilayers.[29-33] These channels are based on oligomers of naphthalendiimides, and exhibit a quite unusual selectivity for anion transport, which was attributed to the presence of important anion···π interactions compensating the cost of anion dehydration. The system used by these authors is shown in Figure 6.1 together with an schematic representation of the mechanism for ion transport proposed, where multi anion hopping due to anion···π interactions occurs through the channel formed by naphthalendiimide molecules.[30, 32] In these systems the questions concerning the extent and cost of anion dehydration required for anion···π interactions are still open.[30] However, solvent effects on anion···π interactions have been scarcely studied.[21, 25, 27, 28, 34] The channels have diameters which could allow the anion to go into the channel keeping part of its hydration shell, thus decreasing the cost of dehydration. Also, it is possible for water molecules accompanying the anion to establish stabilizing interactions with the naphthalendiimide units thus contributing to the interaction.[30]

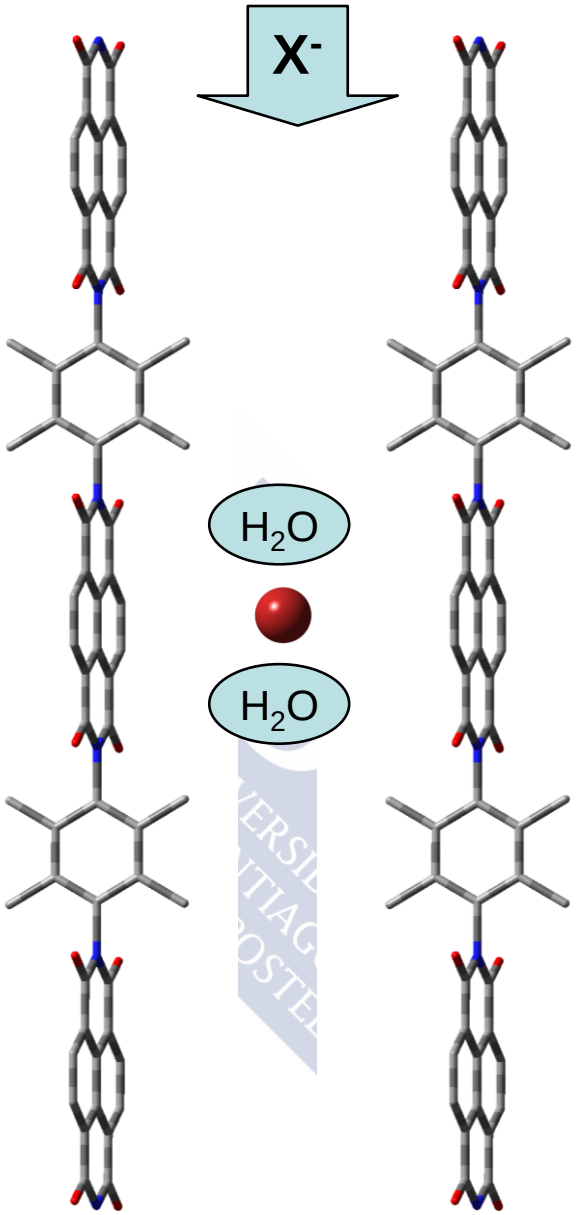
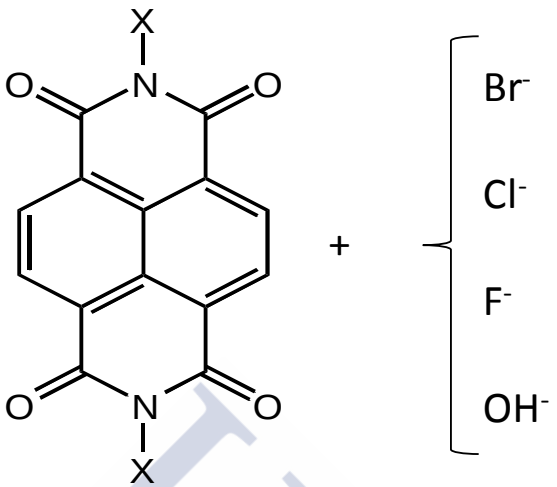


Figure 6.1. Synthetic anion channel proposed by Matile et al.[33]



NDI: X=H

2Φ-NDI: X=C_6H_5

Figure 6.2. Naphthalendiimide molecules and anions employed in the present study.

In the present work a density functional theory (DFT) study is carried out for establishing the characteristics of the interaction between anions and naphthalendiimides similar to those proposed by Matile et al.[33] The calculations are expected to give information about the characteristics of anion···π interactions in these systems, and how they are affected by the presence of a small number of water molecules. Taking into account the large size and complexity of these channels, the system was simplified to make it affordable for a computational approach. Therefore, considering that the ion channel is formed by repeating naphthalenediimide units,[33] only one unit was considered when studying anion···π interactions. Two models, para-diphenyl-naphthalendiimide (2Φ-NDI) and the simpler naphthalendiimide (NDI) molecule, have been employed to represent the units forming the ion channel as indicated in Figure 6.2.

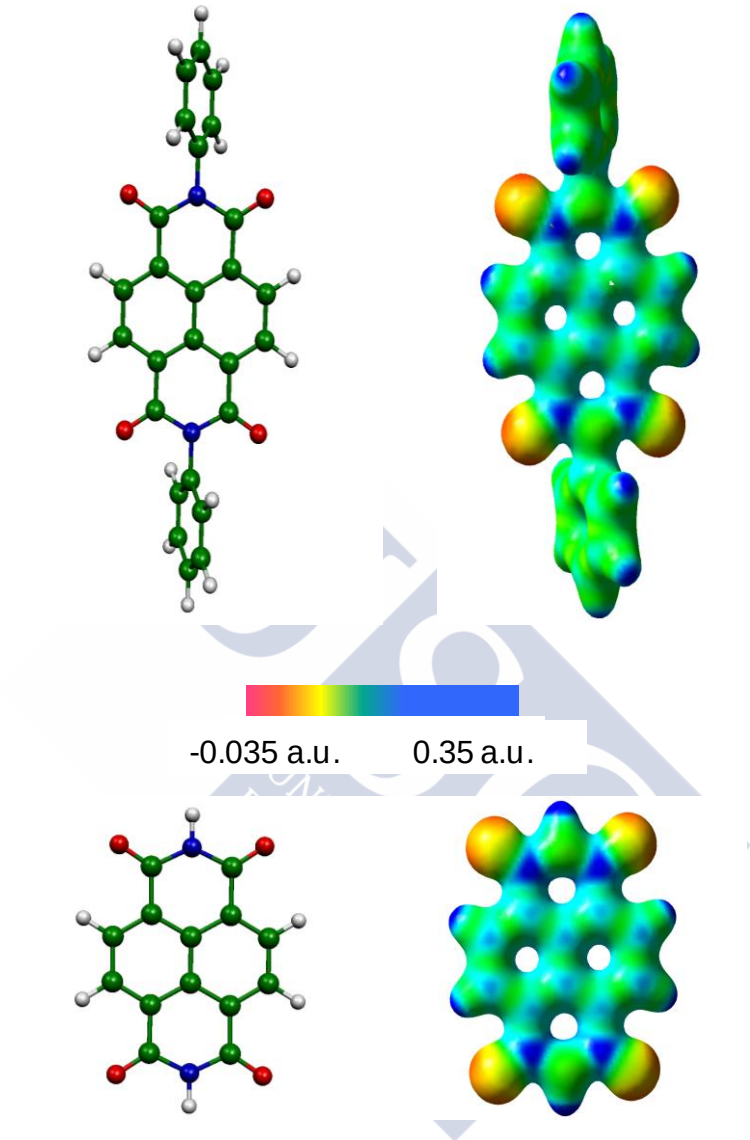


Figure 6.3. Molecular electrostatic potential of 2Φ-naphthalendiimide and naphthalendiimide as obtained at the BLYP-D/cc-pVTZ level of calculation, mapped onto an isosurface of electron density of 0.05 a.u.

6.2. Computational Details

The systems indicated in Figure 6.2 have been studied in the gas phase. The effect of solvent molecules accompanying the anion has been considered by studying anion···NDI clusters containing up to three water molecules. As a way of estimating the magnitude of the interaction in bulk solvent, calculations were performed with the COSMO model, representing water as a dielectric continuum. All calculations were performed with the Orca program.[35]

Common DFT functionals are known to have problems describing the interaction when aromatic units are involved, usually as a consequence of an improper description of dispersion contributions. On the other hand, cation···π interactions are easily described since dispersion plays a minor role in most studied systems. However, it could be expected dispersion contributions to be larger in anion···π interactions,[36] the effect being larger in microhydrated clusters. To minimize this problem, all calculations in this work were performed by employing the empirically dispersion-corrected BLYP-D functional.[37, 38] This method has been shown to provide improved results with respect to common functionals. [39, 40]

The cc-pVTZ basis set was employed for all calculations. Taking into account that the description of anions needs more diffuse basis functions, the aug-cc-pVTZ basis set was employed for F, Cl, Br and O atom in hydroxide. This mixed basis set has been denoted as pVTZ. Computational effort has been saved by applying the resolution of the identity (RI) approach using the def2-TZVPP fitting basis set.[41]

After locating the stationary points of the potential energy surface of each cluster, the interaction energies were calculated by means of the counterpoise method to avoid basis set superposition error.[42, 43] The interaction energy results from subtracting the energies of the fragments that constitute the clusters employing the geometry and the whole basis set of the cluster. Thus,

$$\Delta E_{\text{int}} = E_{ij}(ij\ldots) - \sum_i E_i^{clus.}(ij\ldots) \qquad \text{(eq. 6.1)}$$

where terms in parentheses indicate the basis set employed and superscripts the geometry used in the calculation.

As the geometry of the molecules changes when the cluster is formed, an additional contribution describing this effect must be included, obtained as the energy difference between the molecules in the cluster geometry and in isolation.

$$E_{def} = \sum_i \left(E_i^{clus.}(i) - E_i^{isol.}(i) \right) \qquad \text{(eq. 6.2)}$$

The total complexation energy results from adding these two contributions, though deformation effects are usually small and negligible for many clusters.[43, 44]

$$\Delta E_{compl.} = \Delta E_{\text{int}} + E_{def} \quad \text{(eq. 6.3)}$$

Finally, taking into account that BLYP-D method is just BLYP plus an empirical dispersion term, the complexation energy will be further divided as:

$$\Delta E_{compl.} = \Delta E_{BLYP} + \Delta E_{disp} + E_{def}, \quad \text{(eq. 6.4)}$$

giving more information about the complex characteristics.

6.3. Results and Discussion

Figure 6.3 shows the molecular electrostatic potential (MEP) of para-diphenylnaphthalendiimide (2ϕ-NDI) and naphthalendiimide (NDI). It can be observed that the electrostatic potential is mostly positive in the whole molecule with the exception of the carbonyl groups, resembling other similar cases reported in literature.[30, 32] Therefore, the 2ϕ-NDI molecule is suitable for establishing favorable electrostatic interactions with anions. The most favorable regions for these interactions are located over the carbon atom of the carbonyl groups, over the C-C external bonds of phenyl rings and also in the regions near the C-H groups. In consequence, starting structures for the complexes studied were constructed trying to locate anions near the electrostatically favorable regions. The MEP of the smaller NDI is almost identical to that of 2ϕ-NDI, exhibiting the same regions bearing the most positive electrostatic potential. The absence of the phenyl rings hardly affects the electrostatic potential of the 2ϕ-NDI unit. In NDI the N-H groups constitute the most favorable location for anion interaction, though they are not significant since they are not present in the extended system.

6.3.1. Complexes with para-diphenylnaphthalendiimide

Figure 6.4 shows the optimized structures for the complexes formed by 2ϕ-NDI and bromide anion as obtained with the BLYP-D method together with the cc-pVTZ basis set in all atoms and aug-cc-pVTZ basis set for bromine (hereafter pVTZ). As indicated above, different starting points were employed for the optimizations, leading to four different structures, in accordance with the favorable regions observed in the MEP of 2ϕ-NDI shown in Figure 6.3.

Table 6.1. Selected distances (Å) of the complexes formed with 2Φ-NDI. *next* indicates the nearest heavy atom; *ringcent* the nearest ring center and *molcent* the middle C-C bond in the center of the molecule.

	2Φ-NDI-Br1	**2Φ-NDI-Br2**	**2Φ-NDI-Br3**	**2Φ-NDI-Br4**
$R_{X\cdots next}$	3.190	3.070	3.591	3.717
$R_{X\cdots ringcent}$	3.209	3.652	4.738	4.871
$R_{X\cdots molcent}$	3.878	4.531	5.968	8.047
	2Φ-NDI-Cl1	**2Φ-NDI-Cl2**	**2Φ-NDI-Cl3**	**2Φ-NDI-Cl4**
$R_{X\cdots next}$	3.061	2.945	3.428	3.574
$R_{X\cdots ringcent}$	3.090	3.544	4.571	4.733
$R_{X\cdots molcent}$	3.818	4.442	5.801	7.972
	2Φ-NDI-F1	**2Φ-NDI-F2**	**2Φ-NDI-F3**	**2Φ-NDI-F4**
$R_{X\cdots next}$	2.137	1.596	2.817	3.025
$R_{X\cdots ringcent}$	2.424	2.518	3.969	4.162
$R_{X\cdots molcent}$	3.443	3.457	5.200	7.592
	2Φ-NDI-OH1	**2Φ-NDI-OH2**	**2Φ-NDI-OH3**	**2Φ-NDI-OH4**
$R_{X\cdots next}$	2.149	1.476	2.919	3.115
$R_{X\cdots ringcent}$	2.439	2.678	4.051	4.273
$R_{X\cdots molcent}$	3.461	3.751	5.283	7.740

Thus, two structures of minimum energy are located corresponding to anion···π interactions (**2ϕ-NDI-Br1** and **2ϕ-NDI-Br2**) whereas in the other two (**2ϕ-NDI-Br3** and **2ϕ-NDI-Br4**) hydrogen bonds are established between the anion and the C-H groups of the benzene units in the molecule. Complexes formed with chloride are similar to those presented in Figure 6.4. The minimum energy structures found for 2ϕ-NDI complexes with fluoride are also shown in Figure 6.4, being also similar to those found for hydroxide complexes. The structures found in complexes with fluoride and hydroxide anions are quite similar to those obtained for the larger anions. However, due to the larger polarizing power of fluoride and hydroxide anions, several differences arise. First, in structure **2ϕ-NDI-F2** a bond is formed between fluoride and a carbon atom of 2ϕ-NDI, leading to an important deformation of 2ϕ-NDI structure due to the pyramidalization of the carbon atom participating in the bond. This behavior is similar to that reported in complexes formed by anions and substituted benzenes.[23] The behavior in complexes with hydroxide is similar with an O-C bond formed in **2ϕ-NDI-OH2**.

This can be observed in the geometric parameters listed in Table 6.1, where it comes clear that intermolecular distances correlate with anion size and, as commented above, in structures **2ϕ-NDI-F2** and **2ϕ-NDI-OH2** the anion is located very close to one carbon atom of the phenyl ring (around 1.5-1.6 Å), establishing a bond instead of an intermolecular interaction.

Table 6.2. Complexation energies (kcal/mol) of the complexes formed with 2Φ-NDI.

	$\Delta E_{complex}$		$\Delta E_{complex}$
2ϕ-NDI-Br1	-20.73	**2ϕ-NDI-F1**	-37.56
2ϕ-NDI-Br2	-19.23	**2ϕ-NDI-F2**	-35.89
2ϕ-NDI-Br3	-15.67	**2ϕ-NDI-F3**	-26.32
2ϕ-NDI-Br4	-14.66	**2ϕ-NDI-F4**	-23.38
2ϕ-NDI-Cl1	-22.14	**2ϕ-NDI-OH1**	-52.83
2ϕ-NDI-Cl2	-20.18	**2ϕ-NDI-OH2**	-50.11
2ϕ-NDI-Cl3	-16.77	**2ϕ-NDI-OH3**	-32.56
2ϕ-NDI-Cl4	-15.42	**2ϕ-NDI-OH4**	-30.86

Table 6.2 lists the complexation energies obtained for the complexes formed by 2ϕ-NDI and the anions considered in this work. In Figure 6.5 the contributions to the total complexation energy are represented for the complexes studied as indicated in Computational Details. The most stable structure for bromide complexes, with complexation energy of -20.7 kcal/mol, corresponds to **2ϕ-NDI-Br1**, with the anion located above the carbon atoms of the ring with the carbonyl group. **2ϕ-NDI-Br2**, the other complex showing an anion···π interaction is slightly less stable by about 1.5 kcal/mol. On the other hand, structures with the anion interacting with the C-H groups of benzene are less stable (around -15 kcal/mol). **2ϕ-NDI-Br3** and **2ϕ-NDI-Br4** are therefore the least stable structures, reflecting the less favorable interaction of the anion with the C-H groups of the phenyl rings. In the case of chloride complexes, also shown in Table 6.2, the behavior is pretty similar. These complexes are slightly more stable than bromide ones due to the larger polarizing power of chloride anion, reaching -22.1 kcal/mol. The values obtained for the anion···π complexes are similar to others reported in literature,[30, 32] though differences arise from the different method and larger basis set employed in the present study.

Considering the contributions in which the complexation energy was decomposed as shown in Figure 6.5 (see Computational Details) it can be observed that, as expected, the dispersion contribution is small in all cases, though slightly larger for bromide complexes in anion···π structures (Grimme et al. have recently presented a new parameterization for the dispersion contribution (DFT-D3).[45] Test calculations carried out for the complexes studied in the present work show minor differences with the results in Table 6.2). In summary, in complexes formed by 2ϕ-NDI and chloride or bromide anion, the complexation energies amount to about -20 kcal/mol, with small contributions from dispersion. Also, deformation contributions to the complexation energy are small in all complexes.

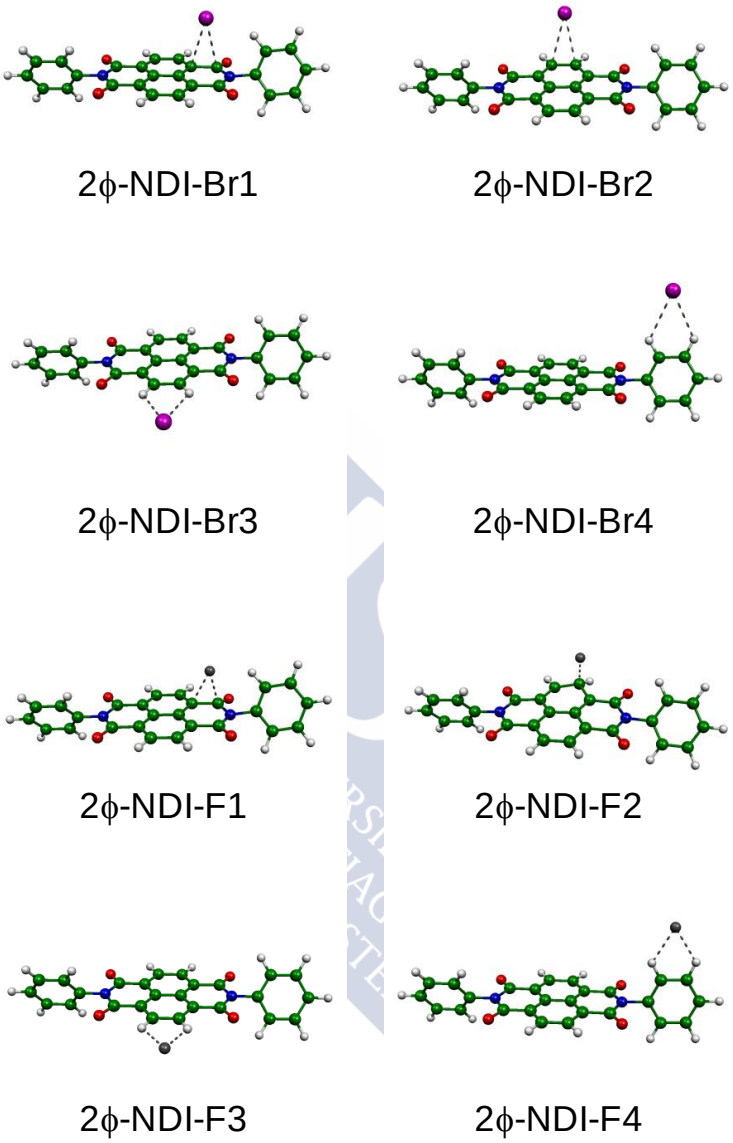


Figure 6.4. Optimized structures of the complexes formed by 2ϕ-NDI with bromide (top) and fluoride (bottom) anions. The structures of complexes formed with chloride and hydroxide anions are similar to those of bromide and fluoride, respectively.

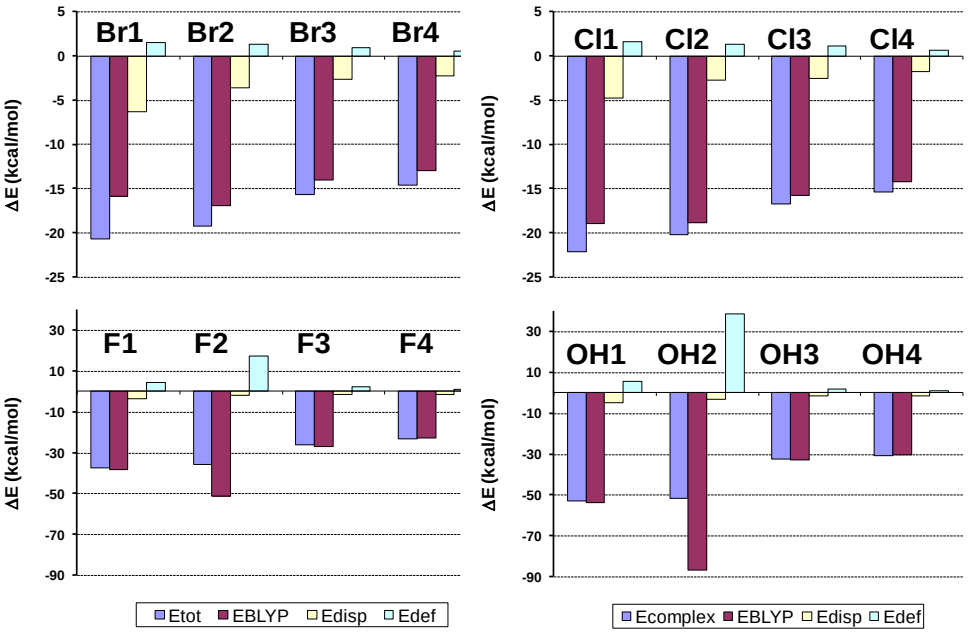


Figure 6.5. Contributions to the complexation energy for the complexes formed by 2ϕ-NDI and the anions.

The behavior is different when complexes of 2ϕ-NDI with fluoride or hydroxide are considered. In fluoride complexes exhibiting anion···π contacts, complexation energies amount to -37.6 kcal/mol for **2ϕ-NDI -F1** and -35.9 kcal/mol for **2ϕ-NDI-F2**. Therefore, as for bromide or chloride complexes, **2ϕ-NDI–F1** is slightly more stable than **2ϕ-NDI-F2**, though complexation energies are much larger due to the greater polarizing power of fluoride. The decomposition of the complexation energies in Figure 6.5 shows larger differences. **2ϕ-NDI-F1** exhibits a similar pattern to that observed for the larger anions, with small contributions from dispersion and deformation (this is larger due to the more intense interaction). On the other hand, **2ϕ-NDI-F2** shows an interaction energy amounting to -51.2 kcal/mol, which is partially compensated with a huge deformation energy contribution. This happens because in **2ϕ-NDI-F2**, the fluoride anion is located at almost bond distance, producing an important deformation of the 2ϕ-NDI molecule, which loses the planarity of one carbon atom in the phenyl ring as shown in Figure 6.4. Thus, the formation of the complex is favorable, but overcoming a large deformation of the 2ϕ-NDI molecule. In consequence, the interaction energy is huge but partially balanced by a large deformation term, leading to a stable complex.

In hydroxide complexes, the behavior is similar to that of fluoride complexes, but the complexation energies are even larger, reaching -52.8 kcal/mol for **2ϕ-NDI-OH1**. Again **2ϕ-NDI-OH2** is a very stable complex as a consequence of a balance of huge interaction energy and large deformation contribution. It can be appreciated that in **2ϕ-NDI-F1** and **2ϕ-NDI-OH1** the situation is similar though less evolved leading to moderate deformation energies. Complexes formed with hydroxide anion are the most stable among the ones studied in this work.

Therefore, the results indicate that the complexes are stable for all anions, but with the most polarizing ones a situation where a real bond is established was found. Of course these results correspond to complexes in the gas phase, and it can be expected that the presence of solvent molecules will modify the behavior, so calculations were performed by including a small number of water molecules. However, in order to save computational time, a simplification of the model was carried out, substituting the 2ϕ-NDI molecule by NDI. In order to assess the suitability of this approach calculations were performed for the complexes formed by NDI and the anions in the gas phase.

6.3.2. Complexes with naphthalendiimide

Figure 6.6 shows the optimized structures of the complexes formed by NDI and the anions studied in the present work, whereas several geometrical parameters are listed in Table 6.3. The structures are similar to those found for 2ϕ-NDI though, of course, the complex with the anions interacting with the phenyl groups is no longer possible, and a new possibility arises, with the anions interacting with the N-H groups of NDI. For the other structures there are no remarkable differences between complexes formed with 2ϕ-NDI or NDI. The only significant changes are observed for the **X1** structures which present shorter distances in the complexes with NDI.

This is because in the complexes with 2ϕ-NDI, the anion can interact with the π systems while simultaneously interacts with one C-H group of the adjacent phenyl group. The lack of this interaction in NDI complexes produces a shortening on the intermolecular distances, the most striking one for hydroxide complex, which forms a bond.

Figure 6.7 shows the energetic differences between complexes formed with NDI and 2ϕ-NDI. It can be observed that complexation energies are similar in both cases, the only differences appearing in **X1** structures, which are more stable in 2ϕ-NDI due to the secondary interaction of the anion with the CH group. Therefore, the interaction is similar to that found in complexes with 2ϕ-NDI and also agrees with values found in literature for similar systems.[30, 32] Taking into account these results, we believe appropriate employing the NDI unit as a model of the interaction in the whole systems.

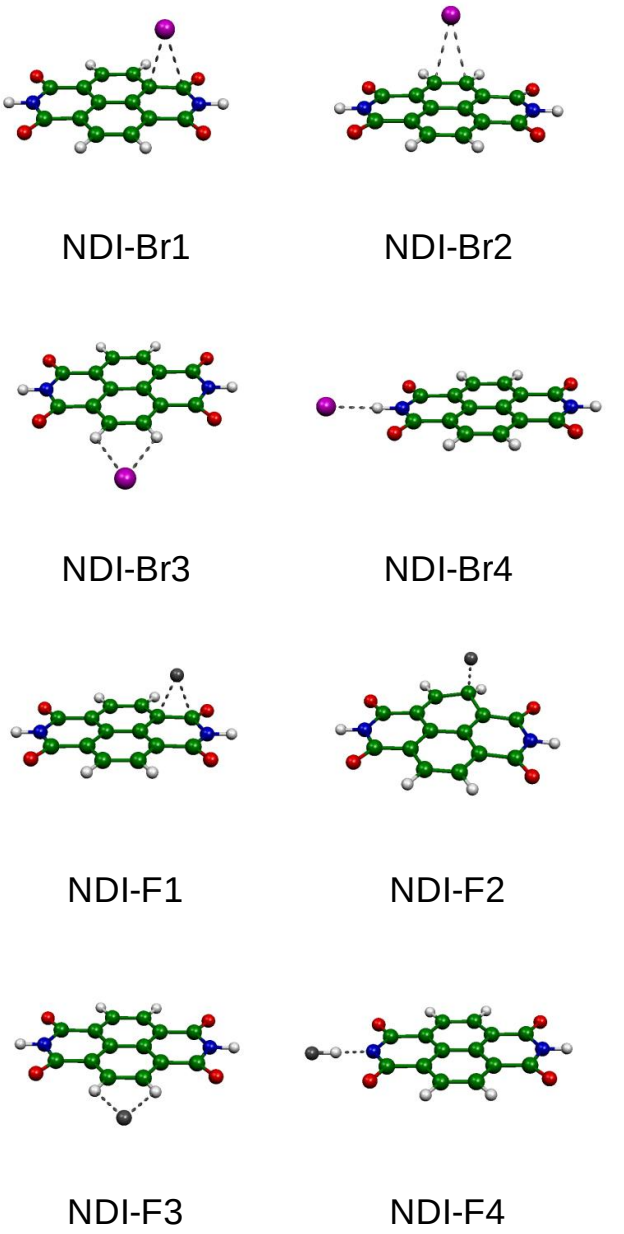


Figure 6.6. Optimized structures of the complexes formed by NDI with bromide (top) and fluoride (bottom) anions. The structures of complexes formed with chloride and hydroxide anions are similar to those of bromide and fluoride, respectively.

Table 6.3. Selected distances (Å) of the complexes formed with NDI. *next* indicates the nearest heavy atom; *ringcent* the nearest ring center and *molcent* the middle C-C bond in the center of the molecule.

	NDI-Br1	NDI-Br2	NDI-Br3	NDI-Br4
$R_{X\cdots next}$	3.067	3.041	3.590	3.267
$R_{X\text{-}ringcent}$	3.140	3.603	4.739	4.657
$R_{X\text{-}molcent}$	3.738	4.487	5.974	6.818
	NDI-Cl1	**NDI-Cl2**	**NDI-Cl3**	**NDI-Cl4**
$R_{X\cdots next}$	3.006	2.967	3.427	3.093
$R_{X\cdots ringcent}$	3.043	3.570	4.572	4.487
$R_{X\cdots molcent}$	3.703	4.486	5.807	6.650
	NDI-F1	**NDI-F2**	**NDI-F3**	**NDI-F4**
$R_{X\cdots next}$	2.195	1.602	2.841	2.595
$R_{X\cdots ringcent}$	2.361	2.521	3.969	4.018
$R_{X\cdots molcent}$	3.252	3.463	5.205	6.201
	NDI-OH1	**NDI-OH2**	**NDI-OH3**	**NDI-OH4**
$R_{X\cdots next}$	1.560	1.487	2.918	2.849
$R_{X\cdots ringcent}$	2.503	2.685	4.054	4.249
$R_{X\cdots molcent}$	2.812	3.759	5.291	6.417

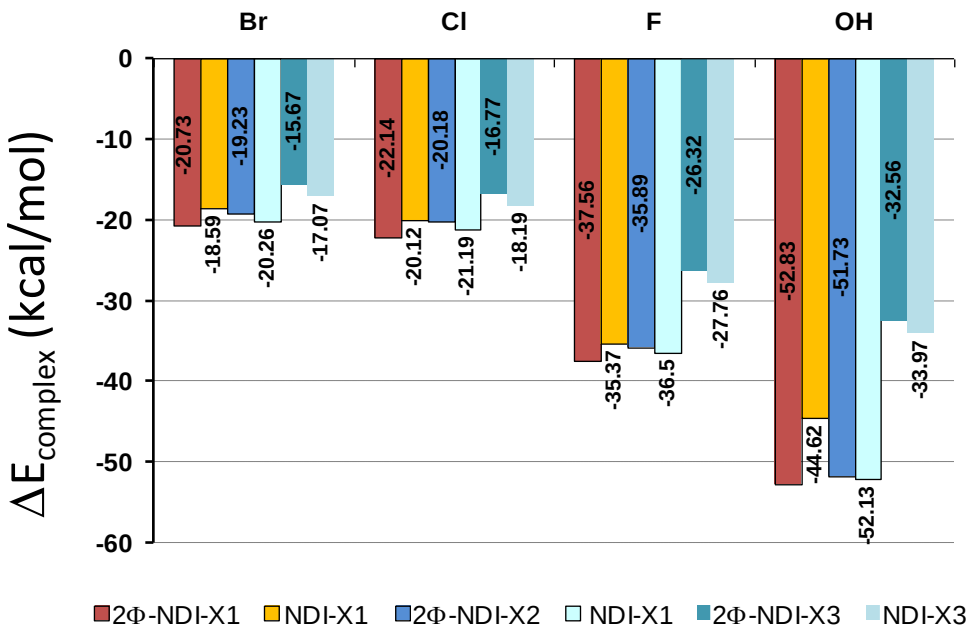


Figure 6.7. Comparison of the complexation energies for the complexes formed with NDI and 2Φ-NDI.

6.3.3. Microhydrated complexes with naphthalendiimide

As commented above the results in gas phase indicate that all anions will form stable complexes with the NDI units following the polarizing power of the anions, so hydroxide anion would form the strongest complex. It can be expected some water molecules to move attached to the anions as they pass through the channel. Therefore, calculations were performed for complexes including up to three water molecules to assess their effect over the anion···NDI interaction. No thorough exploration of the potential energy surface of these clusters has been performed, though several different starting geometries have been employed in the optimizations. It can be expected that the most stable structures found give a fairly good representation of the minima of the hydrated anion···NDI clusters. Only the most stable complexes showing anion···π interactions were considered (**X1** and **X2**), since these are the only geometries which could be possible inside the channel.

The optimized structures of the complexes containing up to three water molecules are shown in Figure 6.8 for bromide and fluoride complexes, though, as before, chloride and hydroxide complexes behave in a similar manner. When the first water molecule is included, it establishes a O-H···X hydrogen bond, simultaneously locating the oxygen atom over regions of positive electrostatic potential of NDI. The second water molecule establishes a second hydrogen bond to X, but also binds to the other water molecule giving a cyclic hydrogen bonded pattern with three hydrogen bonds, while the oxygen atoms and the anion interact with the positive regions of NDI. Finally, the third water molecule also interacts with the anion and previous water molecules giving a three-dimensional network of up to six hydrogen bonds. It is worth noting that with one water molecule only the **NDI-OH1** complex still presents a proper O-C bond, which disappears as the second water molecule is included. Therefore, the inclusion of water molecules weakens the interaction, the anions being at larger distances than in gas phase, and therefore all systems presenting typical intermolecular interactions.

Table 6.4. Complexation energies (kcal/mol) for complexes containing up to three water molecules

		X1	X2		X1	X2
Br^-	1-H_2O	-29.69	-30.66	**F^-**	-51.54	-48.83
	2-H_2O	-42.60	-43.89		-66.17	-66.46
	3-H_2O	-57.24	-58.02		-82.47	-82.30
Cl^-	1-H_2O	-31.99	-33.53	**OH^-**	-55.41	-60.94
	2-H_2O	-45.60	-46.67		-68.44	-68.90
	3-H_2O	-60.43	-60.93		-83.45	-84.33

Table 6.4 lists the values obtained for complexation energies at the BLYP-D/pVTZ level. As expected, complexation energies become more negative as more favorable contacts are established in the complexes. It can be appreciated that the energy gain as water is included is similar for bromide and chloride, but significantly larger for fluoride. Surprisingly, in the case of hydroxide complexes the stabilization is smaller than with other anions, even when the interaction with water molecules must be stronger. It must be taken into account that with fluoride and hydroxide the interactions with water are stronger but simultaneously diminish the intensity of the anion···π contact, the compensation of these two factors leading to the final value. This is clearly observed in the **NDI-OH2** complexes, where the energy gain obtained including water molecules is the smallest due to the need to overcome the strong O-C interaction in the gas phase.

The relative stabilities of the complexes do not suffer major changes. The energy difference between bromide and chloride complexes with respect to hydroxide ones does not change significantly, being kept around the 20-30 kcal/mol shown in the gas phase. The most noticeable changes correspond to the differences between fluoride and hydroxide complexes which as water molecules are included become equally stable. This already happens as the second water molecule is incorporated to the complex.

A better way of studying the effects of water molecules on the anion···π interactions is by obtaining the complexation energies between NDI and the hydrated anion:

$$NDI + X^-(H_2O)_n \rightarrow (NDI)\cdots X^-(H_2O)_n \qquad \text{(eq. 6.5)}$$

The results for this process are shown in Figure 6.9, where it can be observed that the inclusion of water molecules hardly affects the interaction of bromide and chloride anions with the NDI molecule. Therefore, these anions are able to accommodate up to three water molecules without significantly losing intensity in the interaction with NDI. Of course, some interaction is lost due to charge transfer from the anion to the interacting water molecules, which compete with NDI for the anion, but these looses are small with one and two water molecules. Only in the complex with three water molecules the interaction diminishes by about 4-5 kcal/mol with respect to the gas phase value.

The behavior is totally different in fluoride and hydroxide complexes, where the interaction with NDI weakens significantly already with one water molecule, continuing decreasing as more water molecules are included. Thus, differences of up to 18 and 25 kcal/mol are observed with respect to the gas phase. Therefore, it becomes clear that fluoride and especially hydroxide interactions with NDI are very sensible to the presence of water. In fact, with three water molecules the differences among the intensities of the different anion···π interactions become around 3-4 kcal/mol, a significant decrease with respect to the values obtained in the gas phase.

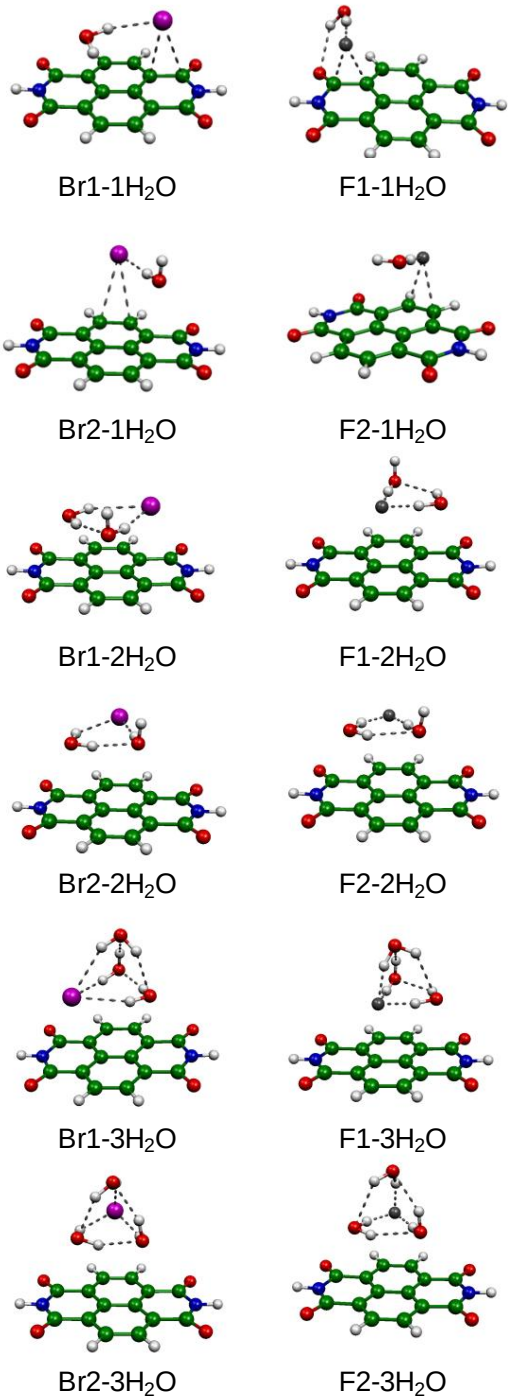


Figure 6.8. Optimized structures of the complexes formed by NDI and the anions in the presence of up to three water molecules.

Therefore, the presence of a small number of water molecules is able to significantly modulate the interaction of the anion with the NDI unit. The effect is especially significant in fluoride and hydroxide complexes, as a consequence of the larger polarizing power of these anions. As water molecules are incorporated to the complex, fluoride and hydroxide strongly interact with them, sharing their charge and therefore weakening the interaction with NDI. The effect is smaller in bromide and chloride, which are able to microhydrate without significantly loosing strength in the interaction with NDI.

Though microhydration can produce large effects as commented in the preceding paragraph, one of the key aspects of these anion channels is the role played by anion dehydration and whether anion···π interactions are able to overcome it. In spite of the decrease in the strength of the anion···π interaction caused by microhydration, the interaction energies are still quite significant, rounding 15-20 kcal/mol (Figure 6.9). Table 6.5 shows the values obtained for these complexation energies by applying the COSMO model to represent bulk solvent. The optimized geometries for the microhydrated complexes in gas phase were employed and up to three explicit water molecules were considered to check for specific hydration effects. As listed in Table 6.5, without explicit water molecules no stable anion···π complex is formed, so none of the anion···π interactions studied in this work is able to overcome the dehydration cost. However, with one explicit water molecule changes are significant, and even larger with two water molecules. With three explicit water molecules the formation of the complex is already favorable for all anions except hydroxide. These results can be a consequence of favorable water···NDI specific interactions via the lone pairs of oxygen with positive regions of the NDI unit.

Table 6.5. Complexation energies (kcal/mol) in bulk solvent (COSMO) for complexes containing up to three explicit water molecules.

	0	**1**	**2**	**3**
NDI-Br1	7.07	3.37	0.92	-3.73
NDI-Br2	7.72	3.69	1.28	-3.44
NDI-Cl1	7.14	4.41	1.92	-0.61
NDI-Cl2	7.75	4.77	2.07	-0.39
NDI-F1	12.44	6.55	3.69	-5.09
NDI-F2	19.68	8.76	3.86	-4.74
NDI-OH1	15.31	8.41	6.98	3.04
NDI-OH2	8.04	6.57	7.14	3.33

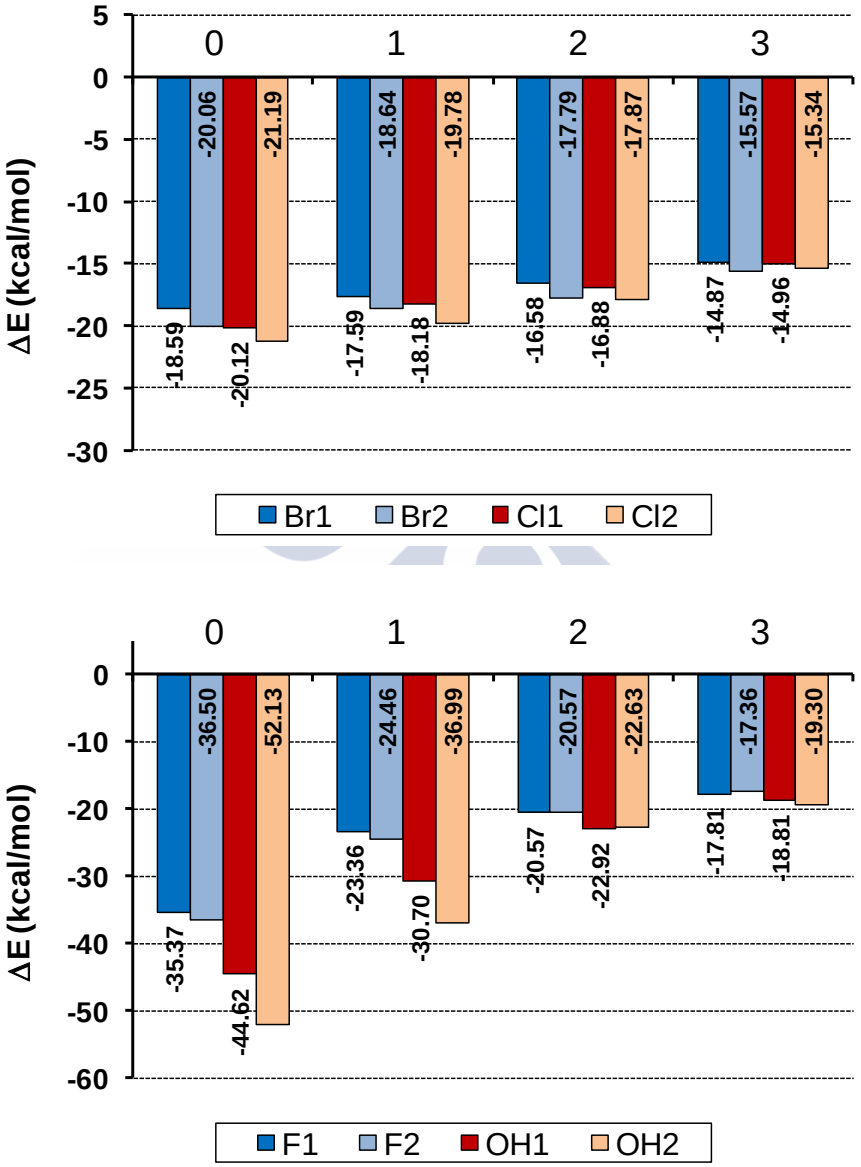


Figure 6.9. Complexation energy between NDI and the hydrated anions containing up to three water molecules at the BLYP-D/pVTZ level.

In any case, even when the process of anion transport is a very complex one, a simplified view of the problem as that presented in this work allows giving hints on the importance of water molecules attached to the anion inside the channel. The channel is wide enough to allow several water molecules to accompany the anion through the channel. Our results suggest that these water molecules are crucial both reducing the dehydration cost and contributing with stabilizing interactions with the NDI unit.

6.4. Conclusions

The interaction of anions with naphthalendiimides which constitute the basic structural motif of a recently proposed synthetic anion channel based in anion···π interactions have been studied computationally. The geometries of the complexes were obtained by employing the BLYP functional empirically corrected for taking into account dispersion (BLYP-D) together with the pVTZ basis set.

Different stable structures were found for the complexes formed with the anions studied. Some of these structures present strong anion···π interactions in the gas phase, amounting to around -20 kcal/mol for bromide and chloride complexes, -35 kcal/mol for fluoride and more than -50 kcal/mol for hydroxide.

Clusters including up to three water molecules were studied to assess the role of water molecules in these systems. The presence of water molecules strongly affects the interaction of fluoride and hydroxide with NDI, whereas its effect is less remarkable in the case of bromide and chloride complexes. As a consequence, the intensity of the interaction becomes similar among the different anions, with differences below 4 kcal/mol (in gas phase these differences reach more than 20 kcal/mol). The results suggest that a limited number of water molecules attached to the anion seems crucial to overcome dehydration costs, also contributing to the stabilization of the complex by means of favorable water···NDI contacts.

In summary, though anion transport is a very complex process, an analysis in simple systems as that carried out in this work helps revealing the crucial role water molecules attached to the anion into the channel have on the energetics of these systems.

6.5. References

[1] E. A. Meyer, R. K. Castellano, F. Diederich. *Angew. Chem. Int. Ed.* **2003**, *42*, 1210-1250.
[2] M. L. Waters. *Biopolymers (Peptide Sci.)* **2004**, *76*, 435-445.
[3] J. C. Ma, D. A. Dougherty. *Chem. Rev.* **1997**, *97*, 1303-1324.
[4] D. A. Dougherty. *J. Nutr.* **2007**, *137*, 1504S-1508S.
[5] J. P. Gallivan, D. A. Dougherty. *Proc. Natl. Acad. Sci. USA* **1999**, *96*, 9459-9464.
[6] N. Zacharias, D. A. Dougherty. *Trends Pharmacol. Sci.* **2002**, *23*, 281-287.

[7] J. P. Gallivan, D. A. Dougherty. *J. Am. Chem. Soc.* **2000**, *122*, 870-874.
[8] M. A. Anderson, B. Ogbay, R. Arimoto, W. Sha, O. G. Kisselev, D. P. Cistola, G. R. Marshall. *J. Am. Chem. Soc.* **2006**, *128*, 7531-7541.
[9] B. W. Berry, M. M. Elvekrog, C. Tommos. *J. Am. Chem. Soc.* **2007**, *129*, 5308-5309.
[10] C. Adamo, G. Berthier, R. Savinelli. *Theor. Chem. Acc.* **2004**, *111*, 176-181.
[11] N. J. Singh, S. K. Min, D. Y. Kim, K. S. Kim. *J. Chem. Theory Comput.* **2009**, *5*, 515-529.
[12] Y. Xu, J. Shen, W. Zhu, X. Luo, K. Chen, H. Jiang. *J. Phys. Chem. B* **2005**, *109*, 5945-5949.
[13] P. A. Gale, S. E. Garcia-Garrido, J. Garric. *Chem. Soc. Rev.* **2008**, *37*, 151-190.
[14] H.-J. Schneider, A. Yatsimirski, Principles and Methods in Supramolecular Chemistry, Wiley, New York, **2000**.
[15] A. Frontera, D. Quiñonero, P. M. Deyà. *WIREs Comput. Mol. Sci.* **2011**, *1*, 440-459.
[16] B. L. Schottel, H. T. Chifotides, K. R. Dunbar. *Chem. Soc. Rev.* **2008**, *37*, 68-83.
[17] D. Quiñonero, C. Garau, C. Rotger, A. Frontera, P. Ballester, A. Costa, P. M. Deyà. *Angew. Chem. Int. Ed.* **2002**, *41*, 3389-3392.
[18] C. Garau, D. Quiñonero, A. Frontera, P. Ballester, A. Costa, P. M. Deya. *New J. Chem.* **2003**, *27*, 211-214.
[19] C. Garau, A. Frontera, D. Quiñonero, P. Ballester, A. Costa, P. M. Deyà. *ChemPhysChem* **2003**, *4*, 1344-1348.
[20] C. Garau, D. Quiñonero, A. Frontera, P. Ballester, A. Costa, P. M. Deyà. *J. Phys. Chem. A* **2005**, *109*, 9341-9345.
[21] O. B. Berryman, D. W. Johnson. *Chem. Commun.* **2009**, 3143-3153.
[22] J. Rodríguez-Otero, E. M. Cabaleiro-Lago, A. Peña-Gallego. *Chem. Phys. Lett.* **2008**, *452*, 49-53.
[23] O. B. Berryman, V. S. Bryantsev, D. P. St7ay, D. W. Johnson, B. P. Hay. *J. Am. Chem. Soc.* **2006**, *129*, 48-58.
[24] J. M. Hermida-Ramón, C. M. Estévez. *Chem. Eur. J.* **2007**, *13*, 4743-4749.
[25] J. M. Hermida-Ramon, M. Mandado, M. Sanchez-Lozano, C. M. Estevez. *Phys. Chem. Chem. Phys.* **2010**, *12*, 164-169.
[26] M. Mandado, J. M. Hermida-Ramón, C. M. Estévez. *J. Mol. Struct. (THEOCHEM)* **2008**, *854*, 1-9.
[27] M. Sánchez-Lozano, N. s. Otero, J. M. Hermida-Ramón, C. M. Estévez, M. Mandado. *J. Phys. Chem. A* **2011**, *115*, 2016-2025.
[28] O. B. Berryman, F. Hof, M. J. Hynes, D. W. Johnson. *Chem. Commun.* **2006**, 506-508.
[29] N. Sakai, J. Mareda, E. Vauthey, S. Matile. *Chem. Commun.* **2010**, *46*, 4225-4237.
[30] J. Mareda, S. Matile. *Chem. Eur. J.* **2009**, *15*, 28-37.
[31] N. Sakai, J. Mareda, S. Matile. *Mol. BioSyst.* **2007**, *3*, 658-666.
[32] V. Gorteau, G. Bollot, J. Mareda, S. Matile. *Org. Biomol. Chem.* **2007**, *5*, 3000-3012.
[33] V. Gorteau, G. Bollot, J. Mareda, A. Perez-Velasco, S. Matile. *J. Am. Chem. Soc.* **2006**, *128*, 14788-14789.
[34] Y. S. Rosokha, S. V. Lindeman, S. V. Rosokha, J. K. Kochi. *Angew. Chem. Int. Ed.* **2004**, *43*, 4650-4652.
[35] F. Neese, ORCA. An Ab initio, DFT, and Semiempirical Electronic Structure Package, Version 2.6-35, University of Bonn, Germany, **2007**.

[36] D. Kim, P. Tarakeshwar, K. S. Kim. *J. Phys. Chem. A* **2004**, *108*, 1250-1258.
[37] S. Grimme. *J. Comput. Chem.* **2006**, *27*, 1787-1799.
[38] S. Grimme. *J. Comput. Chem.* **2004**, *25*, 1463-1473.
[39] C. Morgado, M. A. Vincent, I. H. Hillier, X. Shan. *Phys. Chem. Chem. Phys.* **2007**, *9*, 448-451.
[40] E. M. Cabaleiro-Lago, J. A. Carrazana-García, J. Rodríguez-Otero. *J. Chem. Phys.* **2009**, *130*, 234307/1-234307/11.
[41] F. Weigend. *Phys. Chem. Chem. Phys.* **2006**, *8*, 1057-1065.
[42] S. F. Boys, F. Bernardi. *Mol. Phys.* **1970**, *19*, 553-566.
[43] G. Chałasiński, M. M. Szczęśniak. *Chem. Rev.* **2000**, *100*, 4227-4252.
[44] E. Cabaleiro-Lago, J. Rodríguez-Otero, Á. Peña-Gallego. *Theor. Chem. Acc.* **2011**, *128*, 531-539.
[45] S. Grimme, J. Antony, S. Ehrlich, H. Krieg. *J. Chem. Phys.* **2010**, *132*, 154104/1-154104/19.

USC UNIVERSIDADE DE SANTIAGO DE COMPOSTELA

USC
UNIVERSIDADE
DE SANTIAGO
DE COMPOSTELA

7. Interaction between anions and substituted corannulene

USC
UNIVERSIDADE
DE SANTIAGO
DE COMPOSTELA

7.1. Introduction

Noncovalent intermolecular interactions are of great importance in modern chemical research, particularly in the area of molecular recognition, supramolecular chemistry, materials science and biochemistry.[1-5]

Klärner et al. showed that for certain molecular tweezers, the electrostatic potential is significantly more negative inside the tweezer than outside, so it could be possible to employ such systems as appropriate receptors for electron-deficient molecules.[6] This behavior was not only observed in this kind of molecular tweezers. During the last years, an interest has aroused with respect to the characteristics of the interactions involving aromatic systems presenting curved surfaces, especially those related to fullerenes, which lead to different properties depending on the face considered.[7-11] These molecular bowls are aromatic systems formed by joining six- and five-carbon rings in a similar way as in fullerenes, the five-carbon rings introducing curvature on the delocalized system.[7-9] These so-called buckybowls exhibit differences in the electrostatic potential depending on whether the concave or convex face is considered.[6, 12-14] So, for the simplest of these bowls, corannulene, $C_{20}H_{10}$, the electrostatic potential is different depending on whether the concave or the convex side of the bowl is considered[12-14] and, in fact, cations usually bind corannulene by the convex face.[9-13, 15-21]

Anion receptors are of great interest in different chemical and biological applications.[22-24] Recently, the possibility of stabilizing interactions between anions and electron-deficient aromatic systems in the so-called anion···π interaction has also aroused interest.[22, 25, 26] The extensive work of Deyá et al. has already shown that the interaction is mainly electrostatic in nature, so one must have an electron deficient aromatic system with positive quadrupole moment, such as hexafluorobenzene or triazine.[22, 25, 27-31] The attractive interaction between this quadrupole and the negative charge of the anion is mainly responsible of the stabilizing interaction, with strengths similar to those observed for cation···π interactions.

Most studies in this field have been carried out employing benzene as a model for the aromatic system, so these works have mostly considered hexafluorobenzene, trifluorobenzene or triazine complexes with halogen anions.[22, 23, 25, 32] However, there is a lack of studies on the interaction with more complex anions or with more extended aromatic systems. Recently, Hermida-Ramón et al. have performed studies on the interaction of anions with substituted molecular tweezers, showing a significant interaction and suggesting the possibility of complexation of the anion by the tweezers.[33-36] It can be expected that for more extended aromatic systems, the contribution of inductive forces will be larger than in benzene derivatives. Also, as indicated by Kim et al.,[32] the anion···π interaction presents a more dispersive character

than the cation···π contact, so in complexes formed by large aromatic systems and more complex anions the dispersion contribution could be significant.

In the present work, a computational study of complexes formed by several anions and substituted molecular bowls is presented. The systems studied are shown in Figure 7.1. The buckybowls are constructed from corannulene by substituting several hydrogen atoms by the electron-withdrawing chloride, fluoride or cyano groups, pretending to produce an inversion of the molecular electrostatic potential (MEP) thus allowing a stabilizing interaction with anions. To the best of our knowledge only the chlorinated derivatives have been already synthesized to date.[7] As anions, chloride and bromide were employed as representative of the simplest halogen anions. Fluoride was not considered since it binds to the molecular bowl in an almost covalent way as shown in other anion···π interactions.[23] Finally, a more structured anion as BF_4^- was employed to estimate the effect of including larger anions on the dispersive component of the interaction.

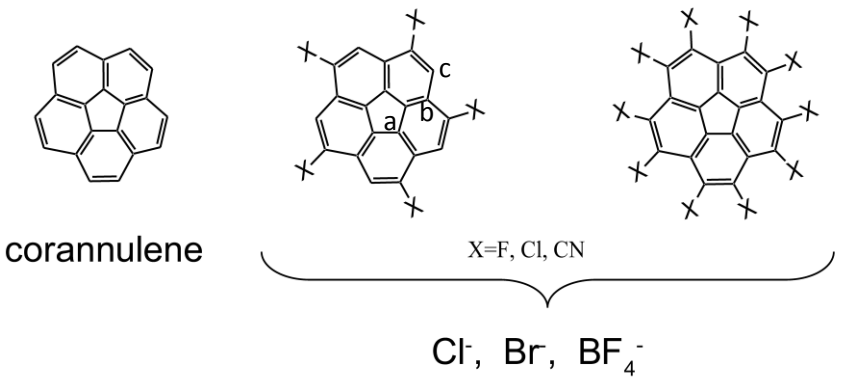


Figure 7.1. Molecular bowls and anions employed in the present study.

By studying these systems information can be obtained regarding the characteristics of the anion interaction with an extended curved π system. By comparing the different bowls it will be possible to assess the effect produced by changing the molecular electrostatic potential of the bowl on the interaction strength. Also, the minimum energy structures of the complexes will be obtained, giving information about the preference of concave/convex complexation and about the role of dispersion interactions in this kind of systems.

7.2. Computational Details

Clusters formed by substituted corannulenes and the anions indicated in Figure 7.1 were computationally studied by using density functional theory and MP2 methods. Starting structures were constructed by placing each of the anions over the different hexagonal or pentagonal faces of the substituted corannulenes, both in the concave and the convex sides. These initial structures were fully optimized employing the BLYP functional corrected by an empirical dispersion term as designed by Grimme (BLYP-D)[37, 38] together with the aug-cc-pVDZ basis set. Symmetry was only employed for complexes where chloride and bromide anions are located on the symmetry axis of the bowl. Numerical frequency calculations were performed in selected complexes to characterize them as minima in the potential energy surface.

The reason of employing a dispersion corrected functional comes from the possibility of dispersion being more important in these systems than in cation···π interactions.[32, 39] It can be expected that the combination of a large, curved system, together with the presence of anions, will lead to a larger contribution of dispersion which should be almost completely lost with common functionals. BLYP-D was chosen since in previous work has shown to give improved results for the interaction in systems containing aromatic units.[39, 40] Computational effort has been saved by applying the resolution of the identity (RI) approach, the def2-TZVPP basis set being used as auxiliary basis set.[41]

After locating the stationary points of the potential energy surface of each cluster, the interaction energies were calculated by means of the counterpoise method to avoid basis set superposition error.[42-44] Besides BLYP-D, the MP2 method together with the aug-cc-pVDZ basis set was also employed for obtaining interaction energies. MP2 single point calculations were performed at the optimized BLYP-D geometry, applying the resolution of the identity approach with the corresponding auxiliary basis set as implemented in Turbomole.[41]

It has already been noted that MP2 tends to produce overestimated interaction energies when applied to systems containing aromatic units.[4, 45-47] Different empirical scalings of the MP2 energies have been proposed to overcome this problem.[48-50] In the present work, the parameterization of Hill and Platts (SCSN-MP2) was employed,[50] developed employing the aug-cc-pVTZ basis set in local MP2 calculations.

Symmetry Adapted Perturbation Theory calculations (SAPT) were carried out for selected complexes in order to obtain more information about the characteristics of the interaction.[51, 52] Thus, the interaction energy was decomposed in several contributions as repulsion, dispersion, induction and electrostatic. In order to include intramonomer correlation effects SAPT(DFT) was used by employing the BLYP functional together with the aug-cc-pVDZ basis set and density fitting to save computation time. Grüning asymptotic correction was applied,[53] ionization potentials being obtained at the BLYP/aug-cc-pVDZ level.

Finally, an estimation of the complexation energies in solvents with different dielectric constants has been carried out by employing the COSMO model as implemented in Turbomole.[41, 54, 55] All calculations were performed with the Orca[56] and Turbomole[41, 55] programs. SAPT(DFT) calculations were done with Molpro2009.1.[57]

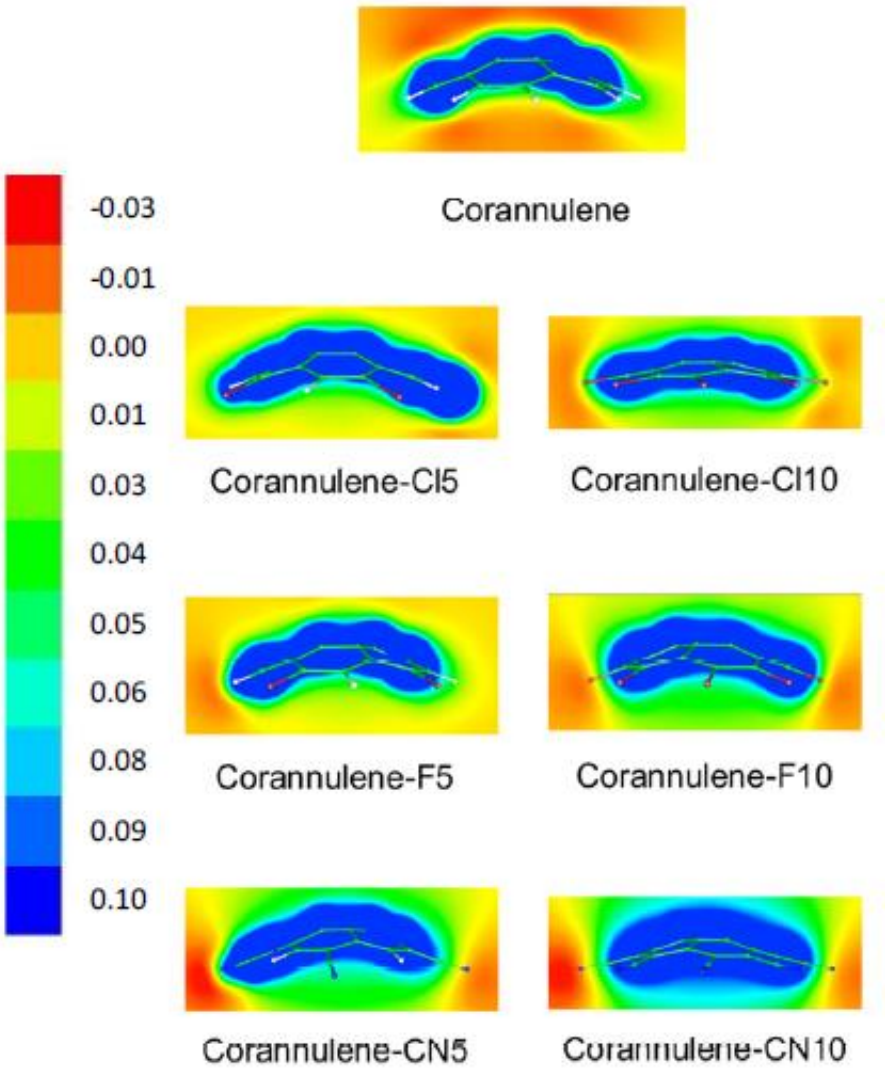


Figure 7.2. Molecular electrostatic potential of the molecular bowls employed in this study obtained at the BLYP-D/aug-cc-pVDZ level of calculation. The scale is shown in atomic units.

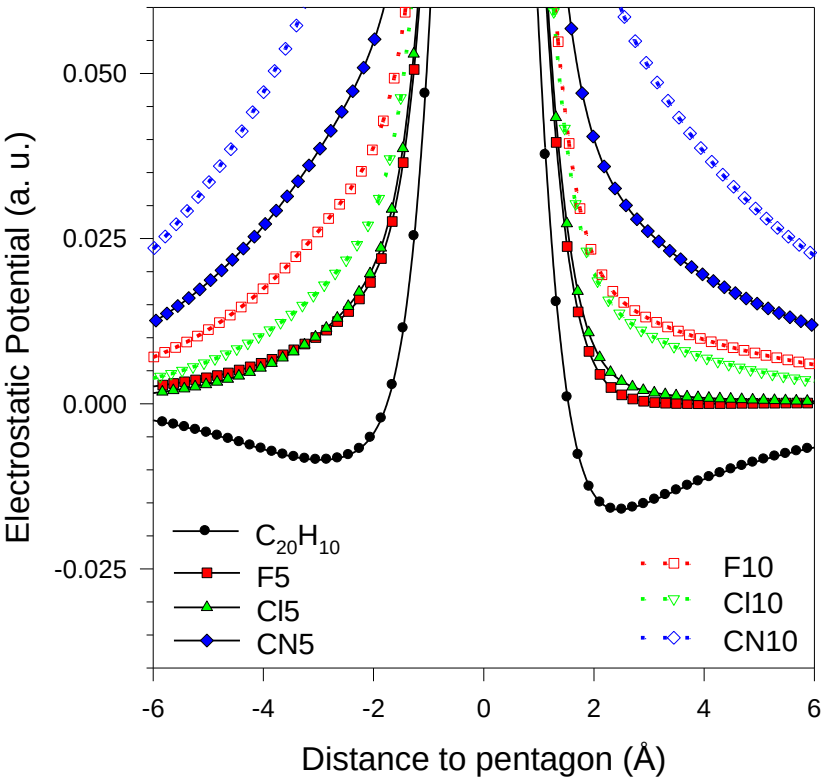


Figure 7.3. Molecular electrostatic potential of the molecular bowls studied in this work as obtained along the C5 symmetry axis with the BLYP-D/aug-cc-pVDZ level of calculation. Positive distances correspond to the convex face.

Table 7.1. Selected geometric parameters of the substituted bowls considered in the present study as obtained at the BLYP-D/aug-cc-pVDZ level. Distances in Å and angles in degrees. Carbons *a*, *b*, *c* as in Figure 7.1.

	Coran.	Cl5	F5	CN5	Cl10	F10	CN10
Depth	0.939	0.909	0.933	0.924	0.553	0.886	0.731
R_{pc} [(a)]	3.409	3.404	3.399	3.413	3.412	3.397	3.420
Diameter	6.554	6.561	6.538	6.570	6.733	6.560	6.682
POAV*a*	8.6	8.4	8.5	8.5	5.4	8.1	6.9
POAV*b*	4.2	4.0	4.4	4.0	1.8	4.3	2.7
POAV*c*	1.8	1.6	1.8	1.7	0.0	1.4	0.6

(a) R_{pc} is the distance from carbon *c* to the center of the pentagonal ring.

7.3. Results

7.3.1. Substituted Molecular Bowls

Table 7.1 lists selected geometrical parameters obtained for the substituted corannulenes at the BLYP-D/aug-cc-pVDZ level of calculation. Among these parameters there are some characteristic distances such as the depth of the bowl measured from the carbon atoms in the rim of the bowl (carbons labelled as *c* in Figure 7.1) to the plane of the pentagonal ring, the distance from these carbon atoms to the center of the pentagonal ring (R_{pc}) and the diameter of the bowl. Values for corannulene were also included as reference. Comparing with other results in literature the geometry of corannulene is well reproduced.[7, 16, 18, 58] As observed, corannulene is a molecular bowl which presents a depth of 0.94 Å and a diameter of 6.55 Å. Also, carbon atoms present some degree of pyramidalization as indicated by the π-orbital axis vector (POAV) values (the vector which makes equal angles ($\theta_{\sigma\pi}$) to the three σ-bonds at a conjugated carbon atom, the pyramidalization angle being obtained as $\theta_P = (\theta_{\sigma\pi} - 90)$).[59, 60] In any case, it can be observed that deviations from the planarity decrease as the rim of the bowl is approached. The carbons on the pentagonal ring are the most deviated from planarity presenting POAV values of 8.6 degrees.

It can be observed from the data in Table 7.1 that substitution in five alternating positions hardly affects the geometric characteristics of the bowl. A slight flattening of the bowl is observed as indicated by the values obtained for the bowl depth, which are slightly smaller than for corannulene. The largest deviation corresponds to the chlorinated compound, since this is the most bulky substituent and therefore there is more steric hindrance leading to an opening of the bowl. This effect is also observed for Coran-CN5 whereas for Coran-F5 almost no change is observed. These changes correlate with an increment in the bowl's diameter, though for Coran-F5 there is in fact a small reduction in diameter. POAV values show no significant change.

When the bowls are substituted in the ten available positions of corannulene, more dramatic changes are observed because the substituents are now closer. As expected, the most striking effect corresponds to Coran-Cl10, where the bowl depth is reduced to only 0.55 Å. Therefore, for this species, the bowl is flatter and there will be smaller differences between the concave and convex faces of the bowl. For Coran-CN10 the bowl also flattens, with a depth of 0.73 Å, whereas for Coran-F10 almost no changes are observed though the bowl depth decreases to 0.89 Å. So, any of the decasubstituted bowls is more planar than all the pentasubstituted ones, though the effect is only remarkable with chloride and cyano substituents. Also, POAV values are affected by substitution, with reductions of about 2-3 degrees for *a* and *b* carbon atoms.

Therefore, it cannot be expected the substituted bowls to introduce large geometrical effects as compared with the corannulene molecule, with the exception of Coran-Cl10 and maybe Coran-CN10. Though substitution does not significantly alter the geometry of the carbon skeleton, it can be expected the electronic distribution to be largely affected by the presence of electron-withdrawing substituents, thus favoring interaction with anions.

Figure 7.2 shows the Molecular Electrostatic Potential (MEP) of the substituted bowls together with that for corannulene on a plane which cuts the bowl following the C5 symmetry axis to visualize differences between the concave and convex sides of the bowls. In agreement with results already reported, the corannulene molecule presents negative MEP by both the convex and concave sides, the only positive regions corresponding to the CH groups in the rim of the bowl. However, though both sides of the molecule have negative MEP, the value is more negative in the convex face that in the concave one, so cations interact preferentially with corannulene by the convex side of the bowl.[9, 12, 18] This effect can be easily observed in Figure 7.3, where the MEP is represented along the C5 symmetry axis. Corannulene presents negative values, but more negative in the convex side.

When substituents are incorporated the MEP undergoes significant changes. Already for Coran-Cl5 the MEP is much less negative than for corannulene, starting to show positive or almost zero MEP regions. In fact, as observed in Figure 7.3, already for Coran-Cl5, the MEP along the symmetry axis always presents positive values, though in the convex side the values are almost zero. Along the axis the MEP is more positive in the concave side of the bowl. An almost identical pattern is obtained for Coran-F5, but the change is larger for Coran-CN5. In this latter case, the MEP is clearly positive in both sides of the bowl, and as observed in Figure 7.3 much more positive than either corannulene or any of the other pentasubstituted bowls. Therefore, on a purely electrostatic basis, the Coran-CN5 bowl will interact very favorably with anions, whereas for Coran-F5 and Coran-Cl5, the interaction will be favorable, but not very strong. In decasubstituted bowls the patterns are similar, though in this case the MEPs are clearly positive, and more positive than any of the pentasubstituted bowls with the exception of Coran-CN5. Again, Coran-Cl10 and Coran-F10 behave in a similar manner, though in the concave side the MEP is more positive for the fluorinated compound. For Coran-CN10, the MEP is clearly positive in either side of the bowl, and it will be the most favorable bowl for interacting with anions. This is in agreement with previous observations of Hermida-Ramón et al. in tweezer complexes.[34] Therefore, considering only electrostatics the complexation energies with anions should behave as CN10 >> CN5 > F10 ≈ Cl10 > F5 ≈ Cl5 >>> Corannulene.

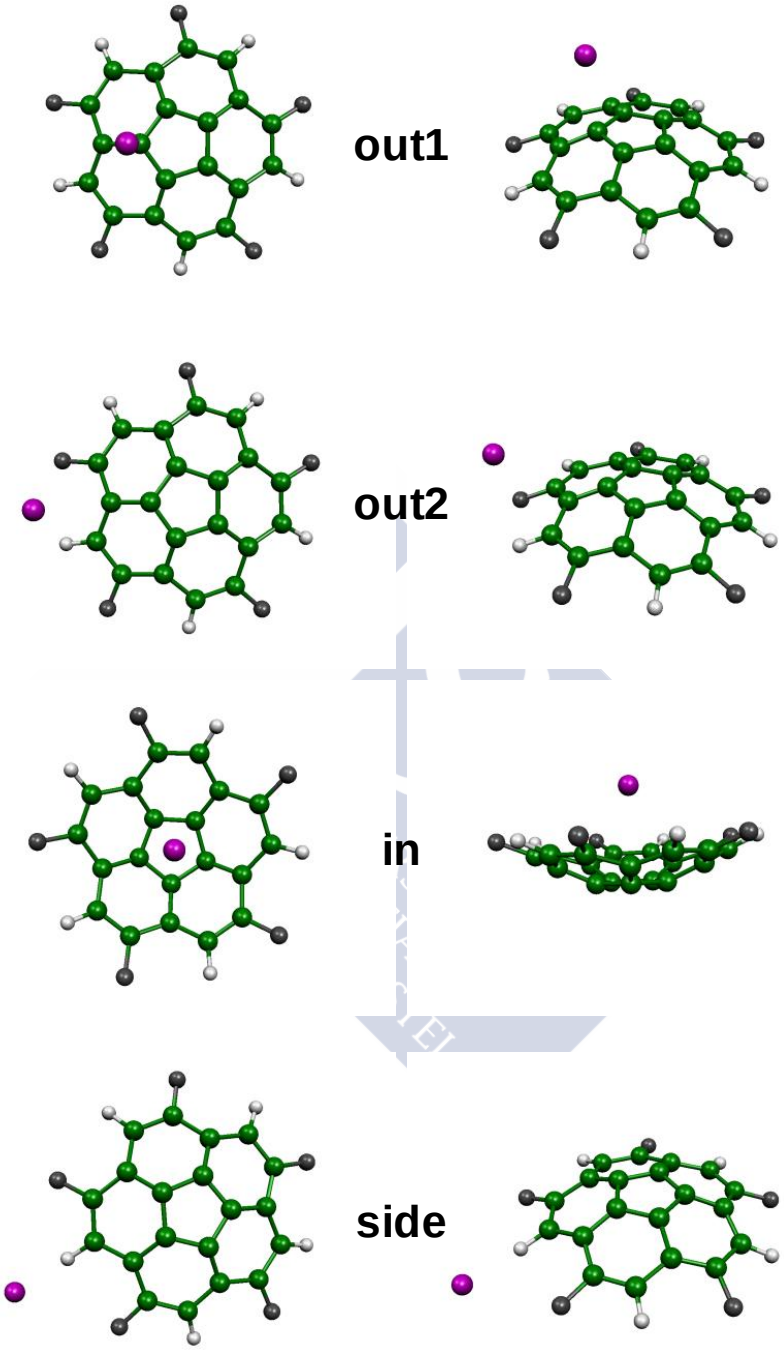


Figure 7.4. Structural arrangements found after optimization of the complexes formed by pentasubstituted bowls and anions.

7.3.2. Complexes between anions and molecular bowls

7.3.2.1. Complexes with pentasubstituted corannulene

The structures of the complexes formed by substituted corannulene and the different anions were optimized at the BLYP-D/aug-cc-pVDZ level. Several starting structures were employed for optimizations, but basically four different structural arrangements were found when employing pentasubstituted corannulenes, as shown in Figure 7.4. Two of the minima correspond to structures with the cation placed on the convex side, whereas only one structure was found with the interaction taking place by the concave side. Finally, a fourth structure was found where the anions interact with the C-H groups in the rim of the bowl.

As shown in Figure 7.4, in one of the structures of the convex side (**out1**) the anion is roughly over one of the carbon atoms of the pentagonal ring. In the other minimum of the convex face (**out2**) the anion is in a more outer position, interacting with one carbon atom in the rim of the bowl, but also with the hydrogen atom attached to it. As observed in Figure 7.4 the difference between structures **out2** and **side** comes from the anion interacting only with the C-H hydrogen in the **side** structure, establishing a hydrogen bond. Finally, the **in** structure presents the anion over the symmetry axis and interacting with the concave side of the bowl. The complexes formed with the BF_4^- anion are not as easily described because the anion is not monoatomic, but the position of the boron atom roughly corresponds to those shown in Figure 7.4, with the fluorine atoms contacting with different parts of the bowl. It is also worth noting that for Coran-CN5 no **side** structures were found, the optimizations going to the **out2** minima.

Table 7.2 lists several values for the distances between the anion and the nearest carbon atom for the complexes shown in Figure 7.4. Complexes formed by unsubstituted corannulene and the anions are included as reference, though in this case the **out2** structure has not been found. Overall, corannulene substitution results in shorter intermolecular distances to the anions. It can be observed that chloride anion is located at about 2.8-2.9 Å in the complexes formed by the outer side with Coran-Cl5. The behavior for the fluorinated bowl is similar, though in the **out2** structure the chloride anion is located nearer the bowl center, and the nearest carbon atom is of *b* type. In the complexes formed with Coran-CN5 distances are shorter in the convex face whereas the anion is located at similar distances in the concave side of the bowl. The complexes with bromine anion exhibit a similar behavior, though the distances are larger due to the larger size of the anion. The behavior is more complex for complexes with BF_4^-, but the location of the anion is similar to that observed in other complexes, though in the **out2** structure the anion is located nearer the bowl center, avoiding positions on the edge of the bowl.

Complexation energies were obtained for the clusters studied with the BLYP-D functional and employing the MP2 and the scaled SCSN-MP2 methods (the scaling

parameters are 0.00 an 1.76 for different-spin and same-spin electron pairs),[49, 50] all together with the aug-cc-pVDZ basis set. The results obtained are shown in Table 7.3, together with values for the complexes formed with corannulene. As expected, complexes formed with corannulene by the convex side are by large the least stable among the complexes studied in this work, in concordance with the MEP data shown in Figures 7.2 and 7.3. **In** complexes are more stable, but far from the values obtained for any of the complexes formed with substituted corannulenes. Only in the case of the **side** complexes, where the anions interact with hydrogen atoms on the rim of the bowl, the complexation energies are as large as those found in pentachlorinated of pentafluorinated corannulenes.

Table 7.2. Distances (Å) between the anions and the nearest carbon atom in the complexes formed with pentasubstituted corannulenes as obtained at the BLYP-D/aug-cc-pVDZ level. In italics the nearest carbon atom is C_c; underlined the nearest atom is C_b; plain text the nearest atom is C_a.

		Coran	Cl5	F5	CN5
Cl^-	**side**	*3.564*	*3.366*	*3.332*	
	out1	3.034	2.806	2.872	2.555
	out2		*2.861*	<u>3.043</u>	*2.416*
	in	3.539	3.403	3.425	3.501
Br^-	**side**	*3.751*	*3.626*	*3.568*	
	out1	3.205	3.028	3.091	2.785
	out2		*3.062*	<u>3.246</u>	*2.704*
	in	3.678	3.539	3.560	3.501
BF_4^-	**side**	*3.203*	*3.209*	*3.141*	
	out1	3.007	2.916	2.972	2.986
	out2		<u>3.105</u>	<u>2.857</u>	<u>2.764</u>
	in	2.991	2.888	2.923	2.841

Though the actual values differ among the different methods employed, the observed trends are fairly similar in all cases. As expected, the scaled SCSN-MP2 method corrects for a possible overestimation of the MP2 energies leading to less negative complexation energies in most cases (it should be taken into account that the parameterization of the SCSN-MP2 method also tries to include basis enlargement effects).[50] The **side** complexes are the less affected by the empirical scaling whereas larger changes with respect to the original MP2 method are observed for the other structures. On the other hand, the BLYP-D method produces less negative values for the **in** complexes (with the exception of BF_4^- complexes) and somewhat more stable complexes for the **out1** and **out2** structures. In the following the SCSN-MP2 results will be considered though the

same conclusions would be reached with the MP2 values. SCSN-MP2 complexation energies of complexes formed with the pentasubstituted corannulenes are shown in Figure 7.5.

Starting with complexes formed with the pentachlorinated corannulene, it can be observed that all anions form quite stable complexes. The two structures considered by the convex face present very similar complexation energies, which are less negative than the **side** structure at the SCSN-MP2 level (though the contrary happens with BLYP-D). Therefore, these three structures present similar stability, but are less stable than the complex formed by the concave side which is significantly more stable, especially with the SCSN-MP2 method (though less than with the original MP2 method). The complexation energies decrease in the order Cl^- > Br^- > BF_4^- following the polarizing power of the anion. Changing to the pentafluorinated bowl, the results are almost the same as those for the Coran-Cl5 bowl, in correlation with the behavior observed for the MEP. In Coran-CN5 however, the complexation energies dramatically increase leading to complexes stabilized by up to -40 kcal/mol (twice more than with other bowls). Taking into account the MEPs in Figures 7.2 and 7.3, this enhancement of the intensity of the interaction should be mainly electrostatic. As observed in Figure 7.5 and Table 7.3, the SCSN-MP2 method predicts much more stable coordination via the concave side of the bowl, with energy differences reaching 5-10 kcal/mol with respect to complexes formed by the convex face. Therefore, complexation in substituted bowls is clearly favored by the concave side of the bowl, a behavior quite the opposite to that observed in the complexation of corannulene with cations, which preferentially bind with the convex face.[9, 12, 18]

7.3.2.2. Complexes with decasubstituted corannulene

After optimization of complexes formed by the anions with the decasubstituted molecular bowls, similar structures as those shown in Figure 7.4 were found, with the obvious exception of the **side** complexes, which cannot be formed when all hydrogen atoms are substituted. Selected geometrical parameters for these complexes are shown in Table 7.4, showing similar characteristics as those observed in pentasubstituted corannulene, though in general distances tend to be somewhat shorter due to the expected larger interaction as a consequence of the more positive MEPs of the bowls. Also, it can be expected that as the planarity of the bowl increases the differences between concave and convex sides decrease, thus favoring **in** complexes to a smaller extent.

Table 7.5 and Figure 7.6 show the values obtained for the complexation energies of the complexes formed with decasubstituted corannulenes. Comparing the results in Tables 7.3 and 7.5 it is clear that decasubstitution leads to more stable clusters as a consequence of more electron-withdrawing groups being included in the molecular bowl.

Table 7.3. Complexation energies (kcal/mol) obtained for the complexes formed with pentasubstituted bowls.

		ΔE_{BLYP-D}	ΔE_{MP2}	$\Delta E_{SCSN-MP2}$			ΔE_{BLYP-D}	ΔE_{MP2}	$\Delta E_{SCSN-MP2}$
Coran···Cl	**side**	-13.40	-14.38	-14.42	**F5···Cl**	**side**	-12.55	-12.40	-12.00
	out1	-2.36	-2.10	0.16		**out1**	-12.50	-11.78	-8.94
	in	-4.86	-8.84	-6.71		**out2**	-13.86	-12.38	-10.61
Coran···Br	**side**	-12.07	-12.70	-12.61		**in**	-15.94	-20.53	-18.40
	out1	-2.02	-1.66	0.61	**F5···Br**	**side**	-10.92	-10.56	-10.06
	in	-5.09	-8.75	-6.49		**out1**	-11.74	-10.73	-7.93
Coran···BF_4	**side**	-10.95	-10.54	-10.93		**out2**	-12.88	-10.90	-9.13
	out1	-2.64	-1.02	0.56		**in**	-15.68	-19.77	-17.47
	in	-8.94	-6.64	-5.22	**F5···BF_4**	**side**	-9.99	-9.06	-9.08
Cl5···Cl	**side**	-13.70	-13.81	-13.50		**out1**	-11.59	-9.92	-8.29
	out1	-15.22	-13.55	-11.38		**out2**	-11.74	-10.13	-8.80
	out2	-15.77	-13.36	-12.09		**in**	-17.85	-15.49	-14.10
	in	-17.16	-21.75	-20.20	**CN5···Cl**	**out1**	-34.70	-31.07	-29.37
Cl5···Br	**side**	-12.19	-11.97	-11.50		**out2**	-34.82	-29.40	-28.61
	out1	-14.32	-12.36	-10.23		**in**	-35.16	-39.44	-39.24
	out2	-14.77	-12.05	-10.64	**CN5···Br**	**out1**	-33.20	-28.92	-27.20
	in	-16.80	-21.03	-19.24		**out2**	-32.84	-26.91	-25.91
Cl5···BF_4	**side**	-11.93	-10.95	-10.90		**in**	-34.54	-38.12	-37.45
	out1	-13.31	-11.04	-10.11	**CN5···BF_4**	**out1**	-28.04	-25.17	-25.57
	out2	-13.15	-11.19	-10.33		**out2**	-27.25	-24.62	-24.98
	in	-18.64	-16.18	-15.18		**in**	-34.51	-31.50	-31.79

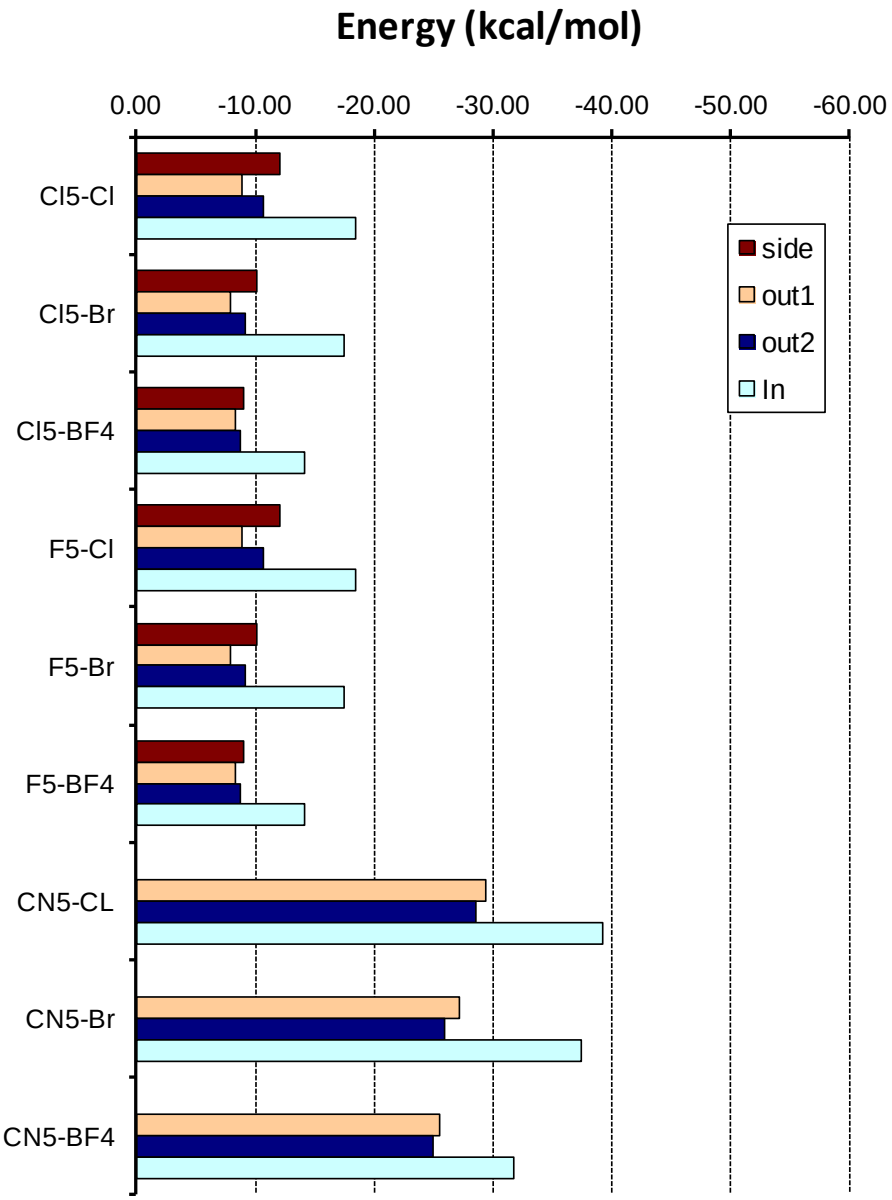


Figure 7.5. Complexation energy for the complexes with pentasubstituted corannulenes as obtained at the SCSN-MP2/aug-cc-pVDZ level.

The stability increases with respect to the pentasubstituted bowls around 5-10 kcal/mol for Coran-Cl10 and Coran-F10, whereas for Coran-CN10 the energy changes around 15-20 kcal/mol. In the case of Coran-Cl10 and Coran-CN10 complexes (with the exception of Coran-CN10···BF_4^-), the smaller energy gains are observed for the **in** complexes. On the other hand, Coran-F10 complexes show the opposite behavior, the **in** complexes being the most stabilized by the presence of more electron-withdrawing groups. This behavior could be related to the changes in the curvature of the bowl observed in Coran-Cl10 and Coran-CN10, leading to smaller differences between the concave and convex sides of the bowl.

Table 7.4. Distances (Å) between the anions and the nearest carbon atom in the complexes formed with decasubstituted corannulenes as obtained at the BLYP-D/aug-cc-pVDZ level. In italics the nearest carbon atom is C_c; underlined the nearest atom is C_b; plain text the nearest atom is C_a.

		Cl10	F10	CN10
Cl^-	out1	2.834	2.784	2.394
	out2	2.867	2.792	2.606
	in	3.302	3.348	2.241
Br^-	out1	3.056	3.005	2.655
	out2	3.077	2.998	2.833
	in	3.449	3.486	3.394
BF_4^-	out1	3.154	3.082	3.033
	out2	2.694	2.778	2.694
	in	2.855	2.843	2.746

In any case, the preference for complex formation with the concave side of the bowl is kept, exhibiting values surpassing -25 kcal/mol in complexes with Coran-Cl10 or Coran-F10, and reaching almost -60 kcal/mol in the case of Coran-CN10. As in the case of pentasubstituted bowls, the interaction loses intensity as the anion becomes less polarizing. Complexes formed with the concave side of Coran-Cl10 are less stable than the corresponding Coran-F10 ones, whereas the opposite was observed in complexes with pentasubstituted bowls.

This is a consequence of Coran-F10 having a significantly more positive MEP than Coran-Cl10 as shown in Figure 7.3, though the smaller bowl depth of Coran-Cl10 can also contribute to the weakening of the interaction.

Table 7.5. Complexation energies (kcal/mol) obtained for the complexes formed with decasubstituted bowls.

		ΔE_{BLYP-D}	ΔE_{MP2}	$\Delta E_{SCSN-MP2}$			ΔE_{BLYP-D}	ΔE_{MP2}	$\Delta E_{SCSN-MP2}$
Coran···Cl	**side**	-13.40	-14.38	-14.42	**F10···Cl**	**out1**	-21.30	-21.68	-17.50
	out1	-2.36	-2.10	0.16		**out2**	-21.49	-21.18	-17.69
	in	-4.86	-8.84	-6.71		**in**	-25.79	-31.60	-29.33
Coran···Br	**side**	-12.07	-12.70	-12.61	**F10···Br**	**out1**	-20.22	-19.98	-16.09
	out1	-2.02	-1.66	0.61		**out2**	-20.03	-18.93	-15.58
	in	-5.09	-8.75	-6.49		**in**	-25.17	-30.35	-27.94
Coran···BF_4	**side**	-10.95	-10.54	-10.93	**F10···BF_4**	**out1**	-19.72	-18.86	-16.87
	out1	-2.64	-1.02	0.56		**out2**	-19.26	-18.21	-16.54
	in	-8.94	-6.64	-5.22		**in**	-26.53	-25.05	-23.40
Cl10···Cl	**out1**	-21.68	-21.01	-18.26	**CN10···Cl**	**out1**	-56.91	-58.13	-53.08
	out2	-19.65	-19.57	-16.95		**out2**	-53.08	-50.69	-48.26
	in	-22.28	-26.58	-24.95		**in**	-54.78	-59.15	-59.61
Cl10···Br	**out1**	-20.67	-19.48	-16.85	**CN10···Br**	**out1**	-55.14	-53.44	-49.78
	out2	-18.40	-17.71	-15.15		**out2**	-51.46	-46.77	-44.53
	in	-21.44	-25.69	-23.90		**in**	-53.44	-57.15	-57.12
Cl10···BF_4	**out1**	-19.93	-18.43	-16.63	**CN10···BF_4**	**out1**	-45.48	-43.98	-44.46
	out2	-18.95	-17.40	-16.13		**out2**	-43.86	-42.40	-42.83
	in	-24.19	-22.49	-21.30		**in**	-53.20	-52.03	-52.77

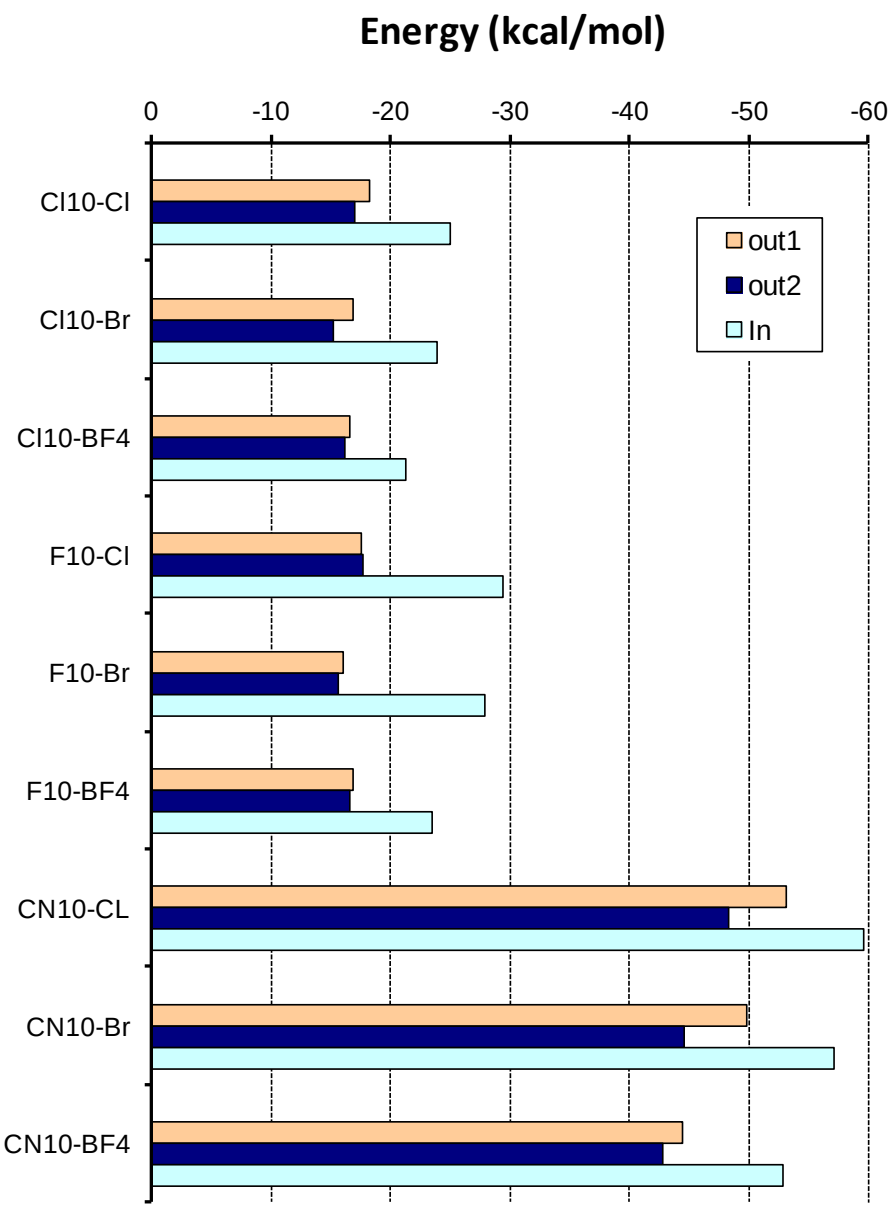


Figure 7.6. Complexation energy for the complexes with decasubstituted corannulenes as obtained at the SCSN-MP2/aug-cc-pVDZ level.

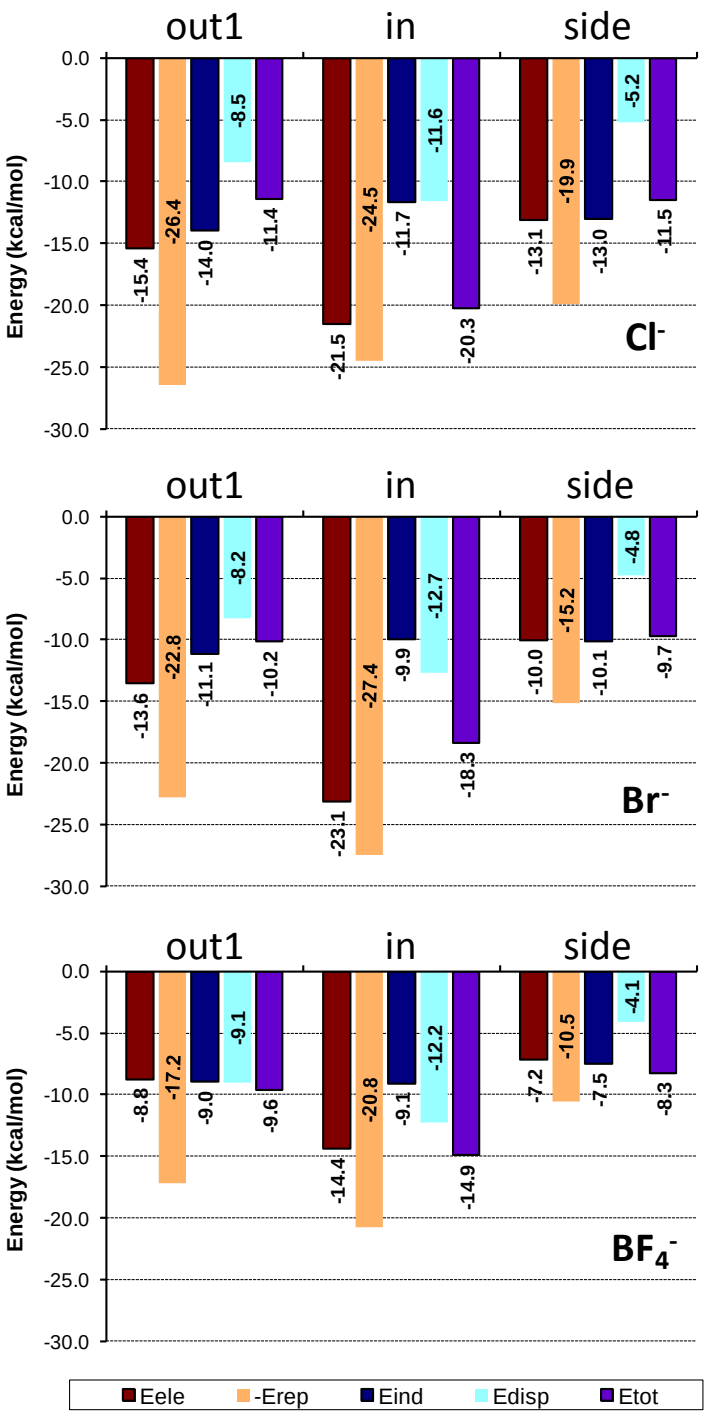


Figure 7.7. SAPT(DFT) results for complexes formed with Coran-F5. E_{disp} includes E_{disp} + $E_{exch\text{-}disp}$; E_{ind} includes E_{ind} + $E_{exch\text{-}ind}$ + δHF.

7.3.2.3. Energy decomposition

More detailed information about the nature of the interaction can be obtained by means of the SAPT(DFT) method,[51, 52] where a partition of the interaction energy in its various contributions is performed. The results of these calculations are shown in Figure 7.7 for complexes formed with the pentafluorinated corannulene.

It becomes apparent that the stabilization of the complexes with chloride anion comes mainly from the electrostatic term together with the induction contribution, which is of similar magnitude. The main difference between **side** and **out1** contributions comes from a smaller repulsion term in the **side** structure, in part compensated by a smaller dispersion contribution than in the **out1** structure. The interaction pattern for the **in** structure is different, presenting the largest electrostatic interaction, whereas induction presents values similar to those observed in other structures. Also, dispersion contribution is significantly larger than for structures formed by the convex side of the bowl. Therefore, the main reason for the **in** complex to be the most stable is a combination of larger electrostatic and dispersion contributions, which are only partially compensated by a larger repulsion term.

In the case of complexes with bromide, the behavior is similar but, as expected, electrostatic contribution with the convex side of the bowl is smaller, though increases in the concave face. Again, the interaction is controlled by electrostatic plus induction contributions, but dispersion contribution in the **in** structure is the second most important stabilizing effect. In the case of complexes with boron tetrafluoride, the electrostatic contribution drops significantly, as also does the induction term, as corresponds to a larger, less polarizing anion. However, dispersion contributes significantly in the **out1** structure, also becoming the second most stabilizing contribution in the **in** structure.

The results shown in Figure 7.7 allow understanding the effect of the anion on the interaction. In Figure 7.8 results are shown for the complexes formed with bromide and all substituted corannulenes, allowing determining the effect of bowl substitution on the interaction. As regards pentasubstituted bowls it can be appreciated that Coran-Cl5 and Coran-F5 behave in a very similar way, leading to fairly similar energy contributions, though Coran-Cl5 forms slightly more stable complexes due to larger induction and electrostatic contributions. Coran-CN5 presents a different pattern, with much larger electrostatic contributions, which are the main responsible of the larger stability or Coran-CN5 complexes. Decasubstituted complexes behave in a very similar way. All complexes present larger electrostatic contributions than their pentasubstituted counterparts, whereas induction only grows significantly in Coran-CN10 complexes.

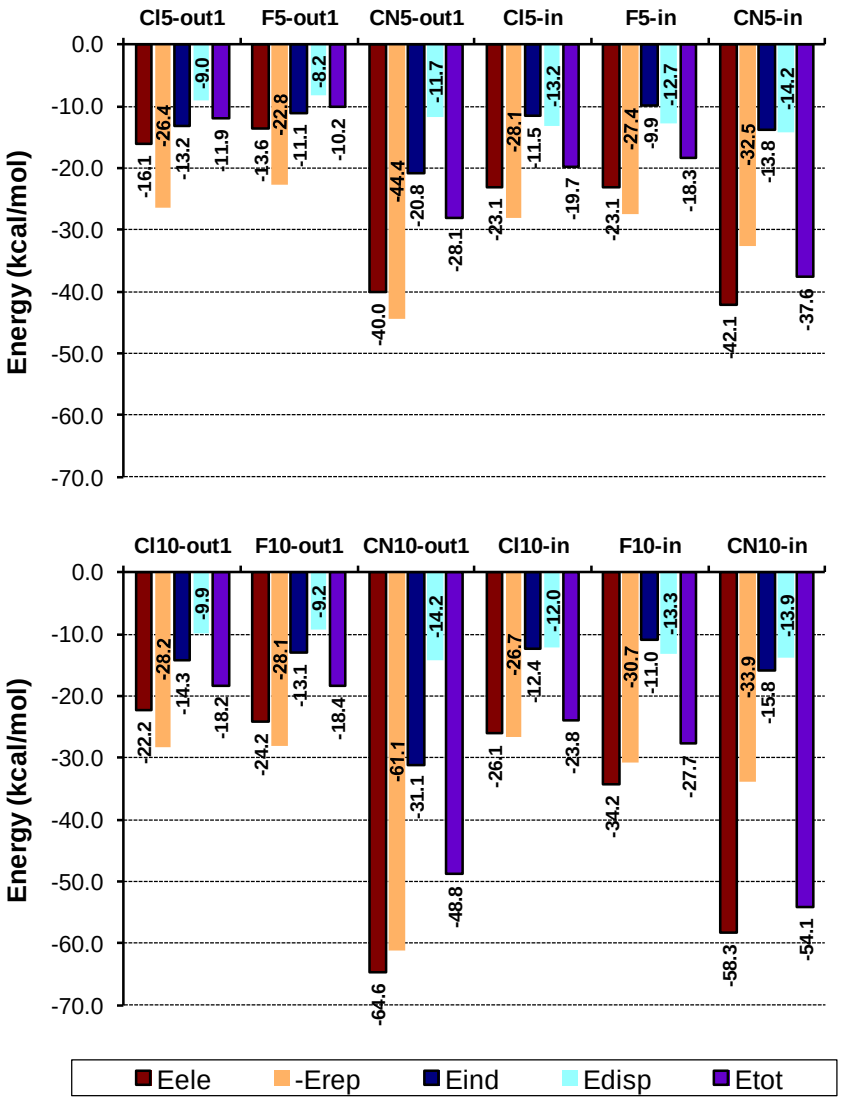


Figure 7.8. SAPT(DFT) results for complexes formed with bromide. E_{disp} includes E_{disp} + $E_{exch\text{-}disp}$; E_{ind} includes E_{ind} + $E_{exch\text{-}ind}$ + δHF.

Larger differences are observed between Coran-Cl10 and Coran-F10 complexes than in the corresponding pentasubstituded bowls, especially for the **in** structures as a consequence of the larger planarity of Coran-Cl10. However, though dispersion contribution slightly decreases in Coran-Cl10 complex as a consequence of its smaller curvature, the main responsible of the larger stability of the Coran-F10 complex is a significantly larger electrostatic contribution. In summary, the interaction of anions with substituted molecular bowls is mainly controlled by electrostatics, which roughly determines the intensity of the interaction. Also, larger electrostatic and dispersion interactions favor the formation of complexes with the concave side of the bowl.

7.3.2.4. Solvent Effect

Solvent effects on the stability of the complexes have been estimated by means of COSMO calculations at the BLYP-D/aug-cc-pVDZ level employing the optimized gas-phase structures, the results being shown in Table 7.6 for selected complexes. It can be observed that though the complexes are all stable in the gas phase, already in the presence of chloroform there is a huge change with respect to gas phase results. Of course, the presence of the anion implies a large desolvation cost, so the effect of the solvent is destabilizing the complex. Complexes formed by bromide and Coran-F5 or Coran-Cl5 are already unstable in chloroform when formed with the convex side of the bowl. **in** complexes are slightly more favorable though complexation energies are not large. Only in the case of the larger BF_4^- anion significant stabilization energies are observed for the complexes in chloroform. Complexes with Coran-CN5 are even more stable, reaching -12.6 kcal/mol for the **in** complex with BF_4^-. As the dielectric constant increases from chloroform to water, the formation of the complexes is less favorable. As a consequence, in water only stable complexes are formed with BF_4^- anion, with complexation energies spanning from -2 to -4 kcal/mol. In any case, there seems that despite the destabilization due to the solvent, there is still preference for complexation with the concave side of the bowls. In the case of decasubstituted corannulenes the formation of the complexes is more favorable, but not as much as in the gas phase. More complexes are stable since the larger gas-phase interactions are more difficult to overcome by solvent effects. In any case, only the complexes formed by BF_4^- present significant negative complexation energies in water amounting between -4 to -7 kcal/mol for **in** complexes.

Therefore, the results indicate that no stable complex is formed with chloride or bromide anion in water. This behavior is a consequence of the larger desolvation costs of the smaller, more polarizing anions. However, all substituted bowls considered in this work are predicted to form stable complexes with the BF_4^- anion in water, especially with the concave side of the bowl.

Table 7.6. Complexation energies (kcal/mol) for selected bowl···anion complexes in different solvents as obtained at the BLYP-D/aug-cc-pVDZ level and applying the COSMO model. Energies corrected with the BSSE obtained from gas-phase calculations.

		$CHCl_3$	THF	Ethanol	Water
Cl5···Br	**out1**	2.70	4.04	5.64	6.05
	in	-0.22	1.31	3.27	3.82
Cl5···BF_4	**out1**	-2.72	-1.67	-0.29	0.12
	in	-6.00	-4.64	-2.72	-2.15
F5···Br	**out1**	3.01	4.11	5.38	5.71
	in	0.17	1.65	3.61	4.16
F5···BF_4	**out1**	-2.01	-1.08	0.17	0.53
	in	-5.76	-4.42	-2.56	-2.01
CN5···Br	**out1**	-2.70	0.74	5.57	7.05
	in	-6.64	-3.47	1.08	2.49
CN5···BF_4	**out1**	-8.60	-6.17	-2.53	-1.39
	in	-12.64	-9.87	-5.76	-4.45
Cl10···Br	**out1**	0.17	2.06	4.49	5.19
	in	-2.46	-0.65	1.79	2.51
Cl10···BF_4	**out1**	-5.76	-4.18	-1.98	-1.31
	in	-8.77	-7.03	-4.59	-3.85
F10···Br	**out1**	0.60	2.56	5.16	5.93
	in	-3.85	-1.63	1.41	2.32
F10···BF_4	**out1**	-5.38	-3.75	-1.43	-0.72
	in	-9.58	-7.62	-4.80	-3.94
CN10···Br	**out1**	-13.26	-7.72	0.62	3.35
	in	-14.03	-9.08	-1.67	0.74
CN10··· BF_4	**out1**	-16.32	-12.19	-5.81	-3.70
	in	-21.06	-16.56	-9.63	-7.34

7.4. Conclusions

The interaction of anions with a series of corannulenes substituted with five and ten electron-withdrawing groups has been studied by means of the BLYP-D and MP2 methods together with the aug-cc-pVDZ basis set. Different structures for the complexes were optimized leading to several geometrical arrangements with the anions located over the concave or the convex faces of the bowls, as well as over the rim of the pentasubstituted corannulenes.

Substitution of hydrogen atoms of corannulene by Cl, F or CN groups does not introduce changes on the basic structure of corannulene. Only when ten substituents are included some flattening of the bowl is observed, especially for Coran-Cl10. However, great changes are produced on the MEP of the bowl, which becomes positive, in a similar degree for F and Cl derivatives, but markedly more positive for the CN substituted bowls. Therefore, all substituted bowls present positive MEP regions on the faces of the bowls that allow them to interact favorably with anions via the conjugated system.

Complexes with the anion inside the bowl (concave side) are the most stable, in contrast with cation complexes with corannulene. The complexation energies roughly follow the series of MEPs, being the most stable complexes those formed with corannulene substituted with CN groups.

A SAPT(DFT) energy decomposition allows recognizing the electrostatic contribution as the main stabilizing contribution to complexation. The combination of a larger electrostatic term together with important dispersion contributions results in structures formed with the concave side of the bowl to be the most stable.

Finally, though very stable in the gas phase, complexes are dramatically destabilized by the presence of the solvent. The results obtained show that complexes become much less stable as the dielectric constant increase, to the point that in water only complexes formed with BF_4^- are stable. In any case, the results point out the possibility of using substituted corannulenes as a means of interacting with anions via the concave side of the bowl, with a preference for large anions where desolvation costs are smaller.

7.5. References

[1] P. Hobza, R. Zaradnik, Intermolecular complexes: the role of van der Waals systems in physical chemistry and the biodisciplines, Elsevier, Amsterdam, **1988**.

[2] E. A. Meyer, R. K. Castellano, F. Diederich. *Angew. Chem. Int. Ed.* **2003**, *42*, 1210-1250.

[3] K. E. Riley, P. Hobza. *WIREs Comput. Mol. Sci.* **2011**, *1*, 3-17.

[4] S. Tsuzuki, T. Uchimaru. *Curr. Org. Chem.* **2006**, *10*, 745-762.

[5] M. L. Waters. *Biopolymers (Peptide Sci.)* **2004**, *76*, 435-445.

[6] F.-G. Klarner, J. Panitzky, D. Preda, L. T. Scott. *J. Mol. Model.* **2000**, *6*, 318-327

[7] Y.-T. Wu, J. S. Siegel. *Chem. Rev.* **2006**, *106*, 4843-4867.

[8] T. Kawase, H. Kurata. *Chem. Rev.* **2006**, *106*, 5250-5273.

[9] A. S. Filatov, M. A. Petrukhina. *Coord. Chem. Rev.* **2010**, *254*, 2234-2246.

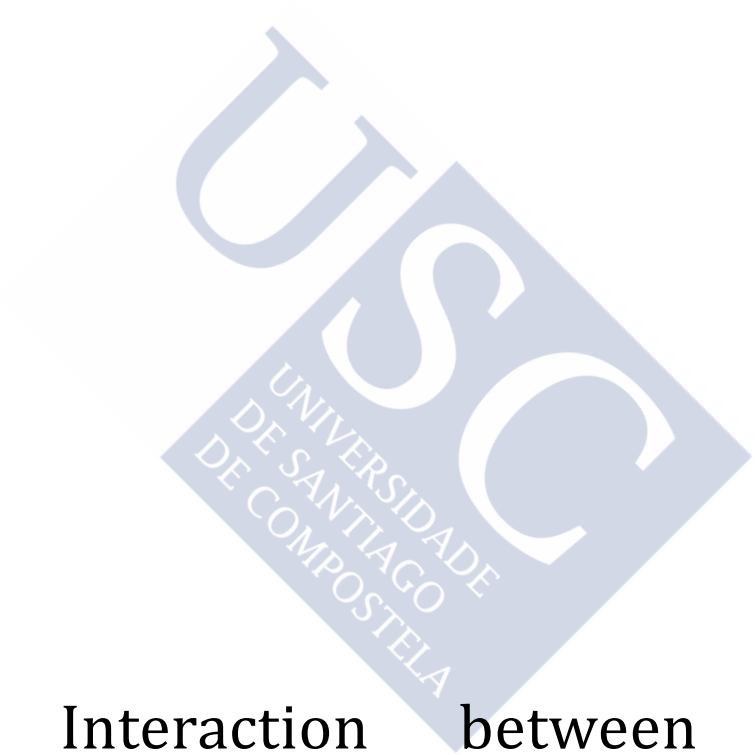
[10] M. A. Petrukhina, L. T. Scott. *Dalton Trans.* **2005**, 2969-2975.

[11] M. A. Petrukhina, Y. Sevryugina, A. Y. Rogachev, E. A. Jackson, L. T. Scott. *Organometallics* **2006**, *25*, 5492-5495.

[12] J. A. Carrazana-García, J. s. Rodríguez-Otero, E. M. Cabaleiro-Lago. *J. Phys. Chem. B* **2011**, *115*, 2774-2782.

[13] A. K. Kandalam, B. K. Rao, P. Jena. *J. Phys. Chem. A* **2005**, *109*, 9220-9225.
[14] L. T. Scott, H. E. Bronstein, D. V. Preda, R. B. M. Ansems, M. S. Bratcher, S. Hagen. *Pure & Applied Chemistry* **1999**, *71*, 209-219.
[15] M. V. Frash, A. C. Hopkinson, D. K. Bohme. *J. Am. Chem. Soc.* **2001**, *123*, 6687-6695.
[16] U. D. Priyakumar, G. N. Sastry. *Tetrahedron Lett.* **2003**, *44*, 6043-6046.
[17] U. D. Priyakumar, M. Punnagai, G. P. Krishna Mohan, G. N. Sastry. *Tetrahedron* **2004**, *60*, 3037-3043.
[18] R. C. Dunbar. *J. Phys. Chem. A* **2002**, *106*, 9809-9819.
[19] T. J. Seiders, K. K. Baldridge, J. M. O'Connor, J. S. Siegel. *Chem. Commun.* **2004**, 950-951.
[20] T. J. Seiders, K. K. Baldridge, J. M. O'Connor, J. S. Siegel. *J. Am. Chem. Soc.* **1997**, *119*, 4781-4782.
[21] R. B. M. Ansems, L. T. Scott. *J. Phys. Org. Chem.* **2004**, *17*, 819-823.
[22] B. L. Schottel, H. T. Chifotides, K. R. Dunbar. *Chem. Soc. Rev.* **2008**, *37*, 68-83.
[23] O. B. Berryman, V. S. Bryantsev, D. P. Stay, D. W. Johnson, B. P. Hay. *J. Am. Chem. Soc.* **2006**, *129*, 48-58.
[24] P. A. Gale, S. E. Garcia-Garrido, J. Garric. *Chem. Soc. Rev.* **2008**, *37*, 151-190.
[25] A. Frontera, D. Quiñonero, P. M. Deyà. *WIREs Comput. Mol. Sci.* **2011**, *1*, 440-459.
[26] H.-J. Schneider, A. Yatsimirski, Principles and Methods in Supramolecular Chemistry, New York, **2000**.
[27] D. Quiñonero, C. Garau, C. Rotger, A. Frontera, P. Ballester, A. Costa, P. M. Deyà. *Angew. Chem. Int. Ed.* **2002**, *41*, 3389-3392.
[28] C. Garau, D. Quiñonero, A. Frontera, P. Ballester, A. Costa, P. M. Deya. *New J. Chem.* **2003**, *27*, 211-214.
[29] C. Garau, A. Frontera, D. Quiñonero, P. Ballester, A. Costa, P. M. Deyà. *ChemPhysChem* **2003**, *4*, 1344-1348.
[30] C. Garau, D. Quiñonero, A. Frontera, P. Ballester, A. Costa, P. M. Deyà. *J. Phys. Chem. A* **2005**, *109*, 9341-9345.
[31] J. Rodríguez-Otero, E. M. Cabaleiro-Lago, A. Peña-Gallego. *Chem. Phys. Lett.* **2008**, *452*, 49-53.
[32] D. Kim, P. Tarakeshwar, K. S. Kim. *J. Phys. Chem. A* **2004**, *108*, 1250-1258.
[33] J. M. Hermida-Ramón, C. M. Estévez. *Chem. Eur. J.* **2007**, *13*, 4743-4749.
[34] J. M. Hermida-Ramon, M. Mandado, M. Sanchez-Lozano, C. M. Estevez. *Phys. Chem. Chem. Phys.* **2010**, *12*, 164-169.
[35] M. Mandado, J. M. Hermida-Ramón, C. M. Estévez. *J. Mol. Struct. (THEOCHEM)* **2008**, *854*, 1-9.
[36] M. Sánchez-Lozano, N. s. Otero, J. M. Hermida-Ramón, C. M. Estévez, M. Mandado. *J. Phys. Chem. A* **2011**, *115*, 2016-2025.
[37] S. Grimme. *J. Comput. Chem.* **2004**, *25*, 1463-1473.
[38] S. Grimme. *J. Comput. Chem.* **2006**, *27*, 1787-1799.
[39] E. M. Cabaleiro-Lago, J. A. Carrazana-García, J. Rodríguez-Otero. *J. Chem. Phys.* **2009**, *130*, 234307/1-234307/11.
[40] C. Morgado, M. A. Vincent, I. H. Hillier, X. Shan. *Phys. Chem. Chem. Phys.* **2007**, *9*, 448-451.
[41] R. Ahlrichs, M. Bär, M. Häser, H. Horn, C. Kölmel. *Chem. Phys. Lett.* **1989**, *162*, 165-169.

[42] S. F. Boys, F. Bernardi. *Mol. Phys.* **1970**, *19*, 553-566.
[43] G. Chałasiński, M. M. Szczęśniak. *Chem. Rev.* **2000**, *100*, 4227-4252.
[44] E. Cabaleiro-Lago, J. Rodríguez-Otero, Á. Peña-Gallego. *Theor. Chem. Acc.* **2011**, *128*, 531-539.
[45] E. M. Cabaleiro-Lago, J. Rodríguez-Otero, Á. Peña-Gallego. *J. Phys. Chem. A* **2008**, *112*, 6344-6350.
[46] E. M. Cabaleiro-Lago, J. Rodríguez-Otero, Á. Peña-Gallego. *J. Chem. Phys.* **2008**, *129*, 084305/1- 084305/8.
[47] C. D. Sherrill *Computations of Noncovalent π Interactions,* in Reviews in Computational Chemistry *Vol. 26*, John Wiley & Sons, New York, **2009**.
[48] R. A. Distasio Jr, M. Head-Gordon. *Mol. Phys.* **2007**, *105*, 1073-1083.
[49] S. Grimme. *J. Chem. Phys.* **2003**, *118*, 9095-9102.
[50] J. G. Hill, J. A. Platts. *J. Chem. Theory Comput.* **2006**, *3*, 80-85.
[51] B. Jeziorski, R. Moszynski, K. Szalewicz. *Chem. Rev.* **1994**, *94*, 1887-1930.
[52] A. J. Misquitta, R. Podeszwa, B. Jeziorski, K. Szalewicz. *J. Chem. Phys.* **2005**, *123*, 214103/1-214103/14.
[53] M. Grüning, O. V. Gritsenko, S. J. A. van Gisbergen, E. J. Baerends. *J. Chem. Phys.* **2001**, *114*, 652-660.
[54] A. Klamt, G. Schuurmann. *J. Chem. Soc. Perkin Trans. 2* **1993**, 799-805.
[55] TURBOMOLE V5.10 , a development of University of Karlsruhe and Forschungszentrum Karlsruhe GmbH, 1989-2007, TURBOMOLE GmbH, since 2007; available from http://www.turbomole.com, **2008**.
[56] F. Neese, ORCA. An Ab initio, DFT, and Semiempirical Electronic Structure Package, Version 2.6-35, University of Bonn, Germany, **2007**.
[57] H. J. Werner, P. J. Knowles, G. Knizia, F. R. Manby, M. Schütz, P. Celani, T. Korona, R. Lindh, A. Mitrushenkov, G. Rauhut, K. R. Shamasundar, T. B. Adler, R. D. Amos, A. Bernhardsson, A. Berning, D. L. Cooper, M. J. O. Deegan, A. J. Dobbyn, F. Eckert, E. Goll, C. Hampel, A. Hesselmann, G. Hetzer, T. Hrenar, G. Jansen, C. Kö, Y. Liu, A. W. Lloyd, R. A. Mata, A. J. May, S. J. McNicholas, W. Meyer, M. E. Mura, A. Nicklaß, D. P. O'Neill, P. Palmieri, D. Peng, K. P. Pitzer, M. Reiher, T. Shiozaki, H. Stoll, A. J. Stone, R. Tarroni, T. Thorsteinsson, M. Wang, Molpro version 2009.1, a package of ab initio programs, see http://www.molpro.net., **2009**.
[58] M. A. Petrukhina, K. W. Andreini, J. Mack, L. T. Scott. *J. Org. Chem.* **2005**, *70*, 5713-5716.
[59] R. C. Haddon. *J. Am. Chem. Soc.* **1986**, *108*, 2837-2842.
[60] R. C. Haddon. *J. Phys. Chem.* **1987**, *91*, 3719-3720.



8. Interaction between ions and substituted buckybowls: A comprehensive computational study

USC
UNIVERSIDADE
DE SANTIAGO
DE COMPOSTELA

8.1. Introduction

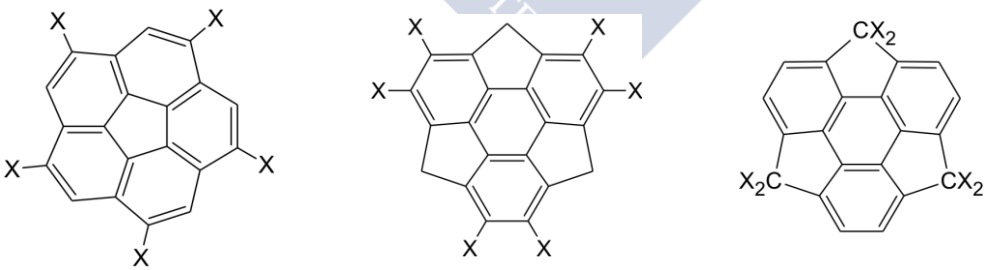
Non-covalent interactions play a key role in many areas of modern chemistry, especially in the field of supramolecular chemistry and molecular recognition, as well as in biochemistry.[1-4] A deep knowledge of the characteristics of these non-covalent interactions is necessary in order to understand cluster formation processes as for designing new supramolecular materials.[4-6] More specifically, the interactions involving aromatic species are known to be crucial as to determine the structures of molecular crystals, the stability of biological systems and molecular recognition processes.[3, 7-9] For instance, aromatic groups interact in a different manner than aliphatic units in the side chains of amino acids, so they can provide specificity in protein folding. [3, 7, 10-13]

When the interaction involves an aromatic unit, it usually corresponds to one of the following three types: π···π, XH···π or ion···π interactions.[3, 9] Both the π···π and the XH···π interactions are usually weak interactions in the gas phase, so their contribution to the stability of the system is often small. However, the combination of a large number of these weak interactions can have a deep impact on the structure and properties of large systems.[3, 8] On the other hand ion···π contacts are strong interactions in the gas phase. Cation···π interactions have been widely studied and are now recognized as one key motif controlling the interactions between amino acid side chains in proteins.[2, 3, 11, 12, 14] Also, anion···π interactions between an anion and an electron-deficient aromatic system have recently aroused interest.[15-18, 19] In both ion···π complexes, there seems that the interaction is mainly controlled by the electrostatic contribution coming from the interaction of the ion and the quadrupole moment of the aromatic system.[20, 21] However, it has been shown that in cation···π systems, the role played by polarization can be important, especially in extended aromatic systems,[22-24] where it can be the main responsible of the stability of a cation···π complex.[23, 24] As regards anion···π complexes, the weaker polarizing power of anions makes the polarization contribution less significant.[20, 25] It has also been shown that aromaticity can change upon ion complexation by aromatic species.[26-28] In any case, it has been observed that both ion···π interactions can show similar strength depending on the aromatic system considered.[18, 20, 24, 25]

Polycyclic aromatic hydrocarbons (PAHs) have attracted much interest related to possible application to materials science.[29-31] Knowing the characteristics of the interaction in these systems is crucial for understanding the behavior of nanotubes or fullerenes in view of their potential applications. Most PAHs present planar structures similar to graphene-like fragments, with an equivalent delocalized electron cloud both above and below the carbon plane. However, there are species that possess curved surfaces, which therefore lead to different behavior and properties depending on the face considered for the interaction. Klärner showed that for certain molecular tweezers,

the electrostatic potential is significantly more negative inside the tweezer than by the outer face, so it could be possible to employ such systems as appropriate receptors for electron deficient molecules.[32, 33] Recently, Hermida-Ramón et al. have performed a series of studies on the interaction of anions with substituted molecular tweezers resulting in large complexation energies.[34-38] Not only these tweezers exhibit different concave/convex faces. In fact, this is what happens in nanotubes or fullerenes, which show two distinct surfaces exhibiting different physical and chemical characteristics.

The so-called buckybowls are aromatic curved systems formed by joining six and five carbon rings in a similar way as in fullerenes, the five carbon rings introducing the curvature on the delocalized system.[39, 40] The simplest of these bowls, corannulene $C_{20}H_{10}$, has already been considered in different studies in order to determine its structure, barrier for inversion and also its capability for coordinating cations.[24, 39, 41-51] The curvature of corannulene produces different molecular electrostatic potential (MEP) by the convex and the concave face. The MEP of corannulene is more negative by the convex face so coordination of cations is mostly favored by this face.[24, 25] The other smallest bowl that can be mapped onto C_{60} is sumanene $C_{21}H_{12}$, quite recently synthesized and which corresponds to a bowl with a six-carbon ring at the bottom.[52] The coordination of metals to this bowl has also been considered showing similar characteristics as those observed for corannulene.[45, 51] To the best of our knowledge, most studies in literature deal with the interaction of cations and these unsubstituted bowls.[24, 39-41, 44, 45, 47-49, 51] However, in a previous work by our group, it has been shown that corannulene substituted with electron-withdrawing groups is able to form stable complexes with anions.[25]



X= H, CH_3, F, CN

Figure 8.1. Buckybowls employed in this work.

Even though this kind of ion···π complex is expected to be stabilized mainly by electrostatics, the interaction in these systems is quite difficult to describe. In a recent study dealing with complexes of cations and bowls of increasing size it has been observed that polarization plays a major role, its contribution being larger than the electrostatic one.[24] This is in line with results from other authors stressing the importance of polarization in cation···π interactions.[22, 23, 51] On the other hand, anion···buckybowl complexes show coordination preferentially by the concave face, with larger contributions from dispersion than in cationic complexes.[25] Therefore, quite rigorous methods should be applied in order to obtain a good description of these systems.

In the present work, a computational study of complexes formed by sodium cation and chloride anion with a series of buckybowls is presented. The systems studied are shown in Figure 8.1. The buckybowls are constructed from corannulene and sumanene by substituting half the hydrogen atoms by CH_3, F and CN in order to promote changes in the molecular electrostatic potential of the bowls leading to different interaction strengths. In the case of sumanene derivatives two substitution patterns have been considered depending on whether the hydrogen atoms are substituted on the C-H aromatic groups or on the CH_2 ones (see Figure 8.1). Employing these substituents, bowls are included which are expected to interact strongly with the ions, whereas the interaction will be weak or even repulsive with others. On the other hand, there could be bowls interacting favorably with both anions and cations.

By studying these systems, information can be obtained regarding the characteristics of the interaction of ions with an extended curved π system. The results will allow a direct comparison of the nature, characteristics and peculiarities of the interaction of the bowls with anions and cations. By comparing the different bowls it will be possible to assess the effect produced by substitution of the bowl on the strength of the interaction. Also, information will be obtained about the preference of concave/convex complexation. The variety of methods employed will also allow checking the performance of cheaper methods the use of which becomes necessary when considering even larger bowls.

8.2. Methods

The interaction energies of complexes formed by the bowls studied and sodium and chloride ions have been obtained along a line passing through the center of the ring at the bottom of the bowl. Other arrangements of the cation over the bowl can lead to even more stable minima, but the central ring has been chosen in order to allow a more direct comparison between anion and cation complexes.[24, 25, 51]

The ions are located at different distances from the bottom of each bowl, the bowl's geometry kept frozen at the values obtained by optimization at the BLYP/aug-cc-pVDZ level. Other levels of calculation would produce slightly different geometries for the bowls though the impact on the interaction energies is marginal. The interaction energies are obtained by applying the supermolecule method, using the counterpoise procedure to avoid basis set superposition error.[53, 54] Therefore, interaction energies are obtained as:

$$\Delta E_{int} = E_{AB}^{complex}(AB) - E_{A}^{complex}(AB) - E_{B}^{complex}(AB) . \quad \text{(eq. 8.1)}$$

Terms in parentheses indicate the basis set while the superscripts refer to the geometry employed in the calculations.

In the region close to the minima of the different complexes, the interaction energies have been obtained with a variety of different methods. Since no reference values for the complexation energies are available for these systems, high-level calculations have been carried out. Taking into account that CCSD(T) calculations are too expensive, an alternative approach has been employed as suggested by Hobza in the so-called MP2.X method.[55, 56] The MP2 correlation contribution to the interaction energy is obtained at the complete basis set limit (CBS) following an extrapolation procedure using the aug-cc-pVDZ and aug-cc-pVTZ basis sets.[57]

$$\Delta E_{corr,MP2}^{CBS} = \frac{X^3}{X^3-(X-1)^3}\Delta E_{corr,MP2}^{AVXZ} - \frac{(X-1)^3}{X^3-(X-1)^3}\Delta E_{corr,MP2}^{AV(X-1)Z}; X = 3 \quad \text{(eq. 8.2)}$$

.

The MP2 interaction energy to basis limit is then estimated combining the extrapolated correlation contribution with the HF/aug-cc-pVTZ interaction energy:

$$\Delta E_{MP2}^{CBS} = \Delta E_{HF}^{AVTZ} + \Delta E_{corr,MP2}^{CBS} . \quad \text{(eq. 8.3)}$$

Finally, the deficiencies in the *N*-electron model are corrected by using MP3 results obtained with a small basis set and adequately scaled in order to reproduce CCSD(T) values:

$$\Delta E_{MP2.X}^{CBS} = \Delta E_{MP2}^{CBS} + C\left(\Delta E_{MP3}^{smallbasis} - \Delta E_{MP2}^{smallbasis}\right) . \quad \text{(eq. 8.4)}$$

The empirical coefficient *C* depends on the basis set employed (in this work 6-31G*, 6-31G(0.25) and 6-31+G*).[56] The values obtained at the MP2.X level have been employed as reference for estimating the performance of cheaper methods.

Several empirical variants of MP2 have also been used; namely SCS-MP2 and SCSN-MP2.[58-61] In these methods the contributions to correlation energies from same-spin and different-spin electron pairs are empirically scaled in order to improve the performance of the native MP2. In SCS-MP2 the scaling factors are 1.20 and 0.33 for opposite-spin and same-spin components,[58] whereas in SCSN-MP2 the factors are 0.00 and 1.76.[60] In both cases, extrapolation to the basis set limit has been performed.

Among the possible DFT method to be tested, two popular approaches have been considered. First, Truhlar's M06-2X functional,[62] designed for intermolecular interactions, has been considered together with the 6-31+G* basis set as a compromise between accuracy and computational cost. Also, the dispersion corrected BLYP-D3 functional has been employed, where an empirical term is included in order to describe dispersion interactions.[63-65] The Becke-Johnson damping factor is employed in these calculations as recommended by Grimme.[66]

In order to obtain more information about the characteristics of the interaction, the interaction energies have been decomposed by applying the Symmetry Adapted Perturbation Theory (SAPT) method with intramonomer correlation effects described at the DFT level (SAPT(DFT)).[67-71] Density fitted SAPT(DFT) calculations were carried out, which provide information on the individual physical components of the interaction energy. For these calculations the PBE functional was used, involving a shift parameter obtained as the difference between the energy of the highest occupied molecular orbital and the negative ionization potential. Orbital energies and ionization potentials have been obtained by using the PBE functional with the aug-cc-pVDZ basis set. The SAPT(DFT) calculations were performed with the aug-cc-pVDZ basis set, employing the aug-cc-pVDZ/JKFIT for Hartree–Fock and aug-cc-pVDZ/MP2FIT for the second-order dispersion terms. In order to provide a more accurate description, the dispersion contribution has been scaled by a factor of 1.193 as suggested by Hobza.[72]

SAPT calculations have been performed with Molpro 2010.1.[73] M06-2X and MP3 calculations have been done with Gaussian09,[74] whereas BLYP-D3 and MP2 calculations have been performed with Turbomole 6.3.[75] In order to save computational time in MP2 calculations, the resolution of the identity approach has been employed both for the HF and correlation energies. That is; RI-JK-MP2 calculations have been performed using the aug-cc-pVXZ auxiliary basis set for correlation and the def2-TZVPP auxiliary basis set for both coulomb and exchange in the calculation of HF energies.[76, 77]

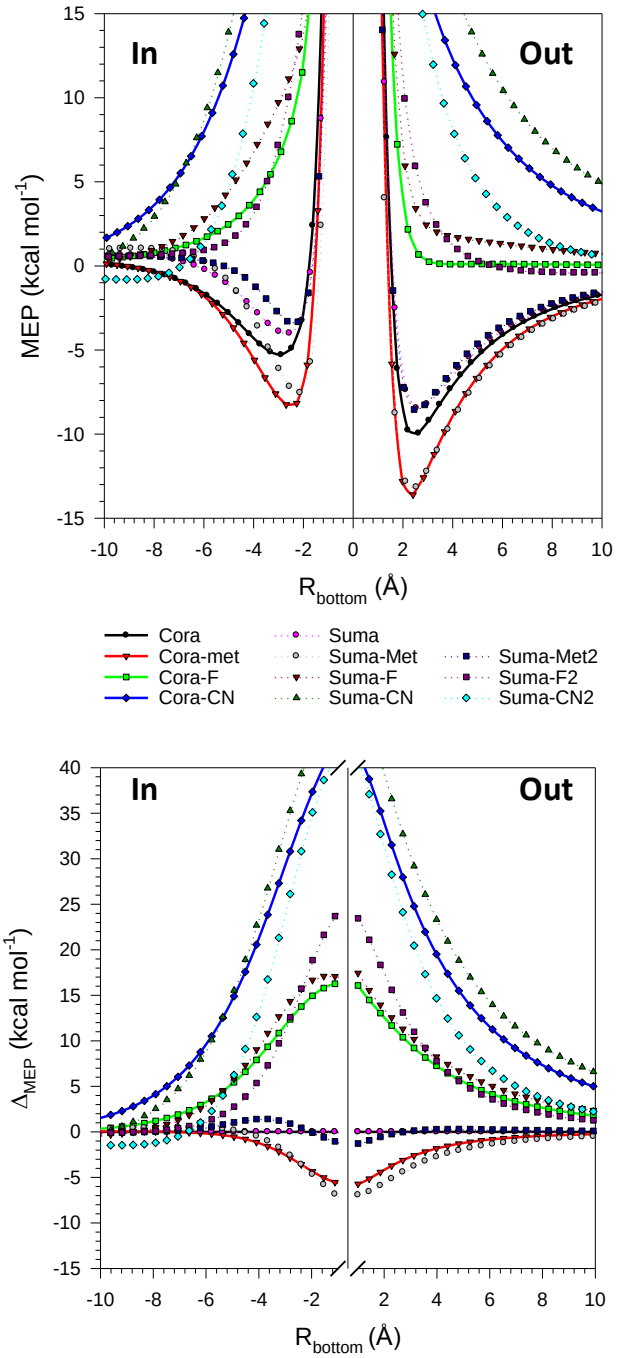


Figure 8.2. Molecular electrostatic potential of the bowls studied along a line following the symmetry axis (top) obtained at the BLYP/aug-cc-pVDZ level. Differences on MEPs due to substitution, relative to corannulene and sumanene (bottom).

8.3. Results

8.3.1. Molecular Electrostatic Potentials

Figure 8.2 shows the molecular electrostatic potentials (MEPs) along the symmetry axis of the bowls and their changes upon substitution. As observed in previous work, corannulene presents a more negative MEP by its convex face.[24, 25, 51] The same behavior is observed for sumanene, but the MEP is less negative than that observed for corannulene.

Methylation in Cora-Met and Suma-Met produces slightly more negative (up to 5 kcal/mol) MEPs than in the original bowls. On the other hand, methylation in Suma-Met2 hardly produces any change in the MEP of sumanene. Only a slightly more positive MEP is observed in the concave face as a consequence of the hydrogen atoms of the methyl groups pointing towards the center of the bowl. Fluorinated bowls show similar MEPs, being clearly more positive than unsubstituted bowls in both faces. Finally, CN derivatives exhibit very positive MEPs in both faces, with similar effects in Cora-CN and Suma-CN, whereas the change is smaller for Suma-CN2. Previous work suggests that changes observed in electronic properties of Suma-X2 can be related to homoconjugation exerted by the substituents.[78, 79] Therefore, as intended, substitution provides bowls with varying MEPs, ranging from moderately negative to moderately positive, which will allow comparing the characteristics of the interaction with ions of different charge. Thus, chloride and sodium ions will electrostatically interact favorably with some of the bowls whereas the interaction could be clearly repulsive in other cases.

8.3.2. Method Performance

8.3.2.1. Chloride Complexes

Even though the interaction between an ion and an aromatic cloud is expected to be mainly governed by electrostatics, the presence of a complex aromatic system as those represented by the molecular bowls can introduce some peculiarities in the interaction which could be hard to describe. In fact, it has been shown that inductive effects can be even more important than electrostatics in order to understand this kind of complexes.[24, 51] Since no high level calculations have been performed in these systems to our knowledge, a series of test calculations have been carried out in order to check the performance of commonly used methods, as well as to obtain information useful in future work regarding the best choice between cost and accuracy. Figure 8.3 shows the results obtained for the complexes formed with the fluorinated bowls with a variety of methods. The reference line in red corresponds to the MP2.X method where the correction of the correlation energy has been performed with the 6-31G(0.25) basis set (this is a 6-31G* basis set with the exponents in polarization functions replaced by 0.25 following Hobza).[80] It is worth indicating that several points have been obtained employing the 6-31+G* basis set, which correspond to almost identical values as those

obtained with the 6-31G(0.25) method. However, when the MP3 correction is obtained with the 6-31G* basis set it departs by 1 kcal/mol or even more from the values obtained with the 6-31+G* basis set. This behavior is probably related with the lack of diffuse functions in the basis set, needed for a correct description of the anion and the highly conjugated bowl. Results obtained for model systems formed by trifluorobenzene and chloride also point out a better behavior of 6-31G(0.25) over 6-31G*in MP2.X (0.5 kcal/mol deviation for the latter with respect to CCSD(T)/aug-cc-pVDZ, whereas negligible deviations for the former one). Also, CCSD(T) calculations in corannulene and sumanene complexes with chloride anion at 3.25 Å (near the minimum) corroborate this trend (error of around 1 kcal/mol with 6-31G*). Therefore, 6-31G(0.25) has been adopted as the reference method.

Considering the rest of the methods represented in Figure 8.3 it is clearly seen that MP2/CBS values are too negative, but the behavior improves significantly with the spin scaled versions of MP2. The results obtained at the SCS-MP2/CBS level match almost exactly those of the MP2.X variants with diffuse functions. SCSN-MP2 shows worse behavior, overestimating the interaction energy by the concave face. As regards the two DFT functionals tested, BLYP-D3 method underestimates the interaction by the concave face giving a better prediction for complexes with the convex face of the bowl, whereas M06-2X give values much closer to the reference ones. On the other hand, SAPT(DFT) scaled[72] results are quite close to the reference ones, though somewhat underestimated by both faces of the bowls. The interaction with the concave face is much harder to describe than the convex one, so the different methods span a range of around 6 kcal/mol near the minimum, which reduces to around 2-4 kcal/mol for the convex face. The behavior observed in Suma-F complexes is totally similar to that observed in Cora-F ones, and the same can be applied to Suma-F2 complexes, though differences are somewhat larger due to the fluorine atoms pointing out of the rim of the bowl. The behavior is pretty similar in unsubstituted, CN, and Met bowls, as can be consulted in Appendix C. Thus, there are three methods: MP2.X/6-31+G*, MP2.X/6-31G(0.25) and SCS-MP2/CBS which give almost the same values for the interaction with both faces of the bowl. The other methods depart to different extents from these values, several of them depending on the face of the bowl considered.

Focusing on the concave/convex energy difference, SCS-MP2/CBS closely follows the values obtained at the MP2.X level of calculation. Though M06-2X/6-31+G* seems to underestimate the interaction energy both by the concave and convex faces of the bowl, the relative energies of the complexes are better predicted. A similar behavior can be observed for the SAPT/scaled values. On the other hand, the MP2/CBS, SCSN-MP2/CBS or BLYP-D3 results are not so well balanced. These trends are observed in all systems considered, as shown in Appendix C (Figure C.3).

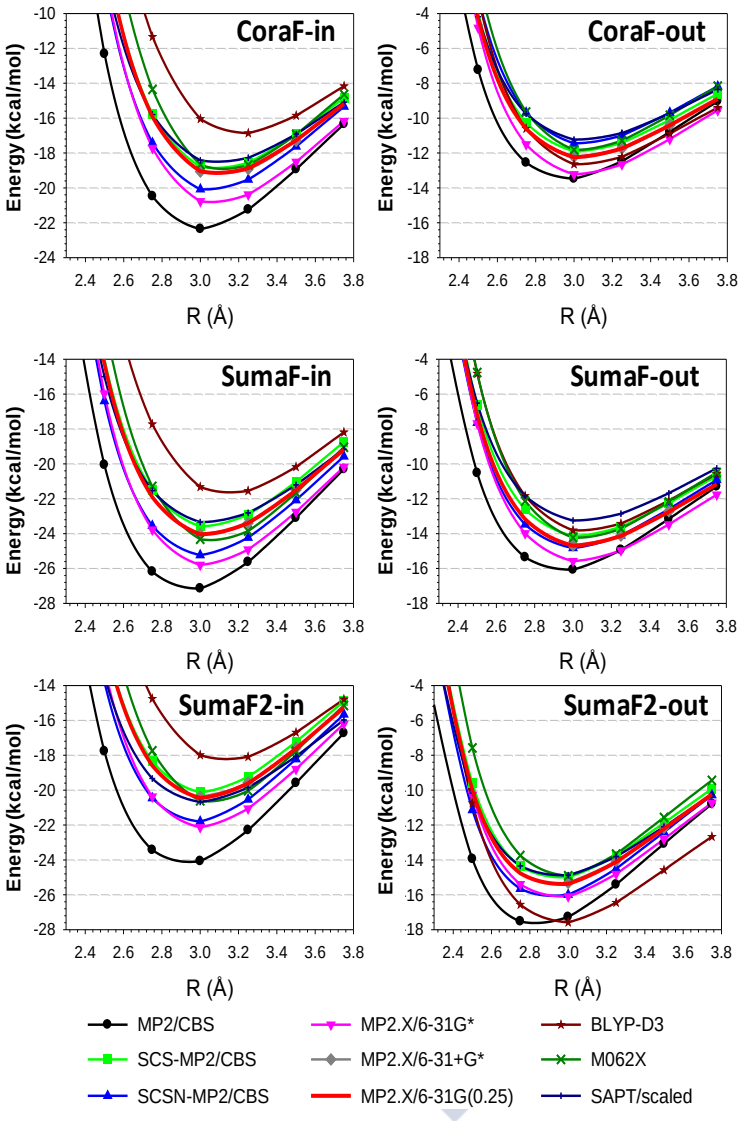


Figure 8.3. Interaction energies obtained for complexes formed by fluorinated bowls with chloride anion by the concave (left) and convex (right) faces of the bowls.

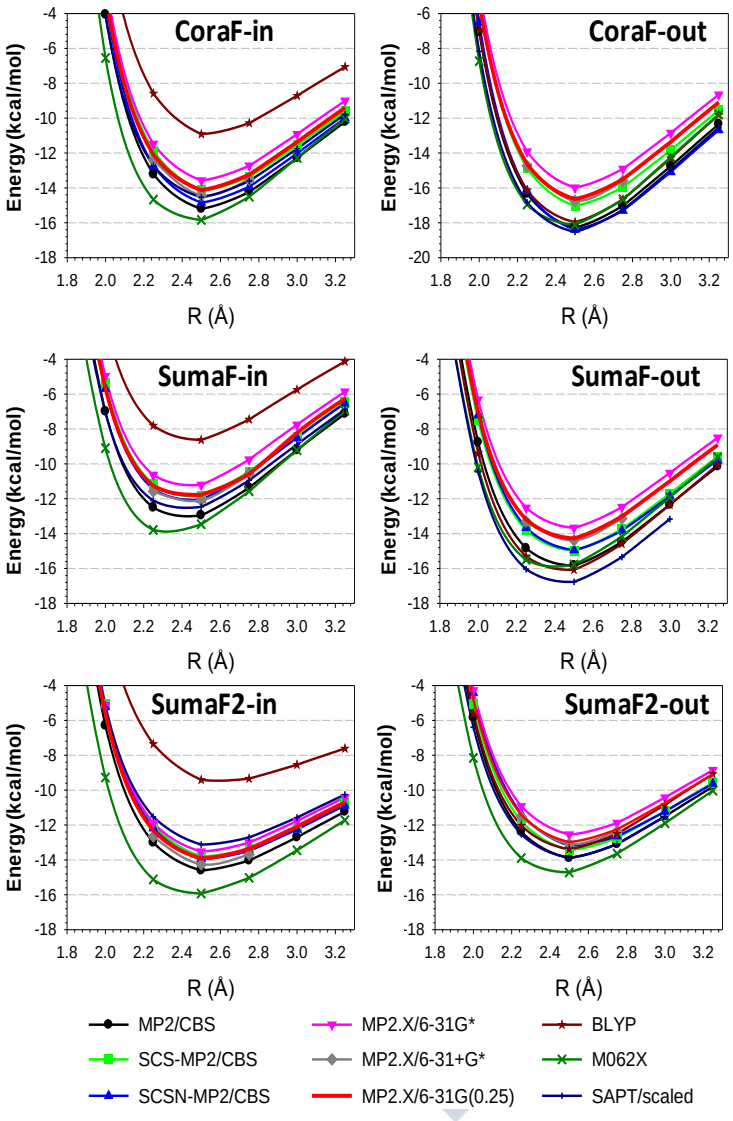


Figure 8.4. Interaction energies obtained for complexes formed by fluorinated bowls with sodium cation by the concave (left) and convex (right) faces of the bowls.

8.3.2.2. Sodium Complexes

Method performance has also been analysed in the case of sodium complexes. Figure 8.4 shows the results obtained for the complexes formed with fluorinated corannulene and sumanene, with a similar behavior to that observed in chloride complexes. Thus, MP2.X results are all pretty close, and even in this case the results obtained at the MP2.X level are independent of the basis set employed in the MP3 correction, suggesting that the differences found above are indeed related to the lack of diffuse functions for the description of the anion.

The SCS-MP2/CBS values are very close to the MP2.X ones. Overall, there seems that cation complexes are more easily described by any of the methods, with several exceptions. First, BLYP results underestimate to a large extent the results by the concave face (BLYP-D3 leads to bad results at intermediate distances as a consequence of changes in the C_6 coefficients, so it has not been included for sodium complexes).[63] M06-2X clearly overestimates the interaction by any of the faces of the bowl. It seems that the smaller contribution of dispersion in these complexes makes all methods come closer (for example MP2/CBS). Therefore, all methods perform reasonably well by the concave face, whereas most of them tend to overestimate the interaction by the convex face. As regards concave/convex energy differences, any of the MP2-based methods describes properly the interaction in this kind of systems, almost matching the highest-level values. In the case of the M06-2X results, there is a larger overestimation by the concave face but the behavior follows almost parallel the results obtained at the MP2.X level (Figure C.4).

In summary, taking into account the results obtained with the different methods, there seems that the SCS-MP2/CBS method is the optimal choice, with results very close to the reference ones and a still moderate computational cost. On the other hand, a method demanding less computational time, especially if optimizations are required, could be the M06-2X functional, which gives a quite balanced description of the complexes, especially regarding the concave/convex relative energies. On the following the discussion of the behavior of the complexes will be performed by using the MP2.X/6-31G(0.25) results, which are those used as reference in this study. In larger systems, the options commented above could be a suitable choice.

8.3.3. Influence of the Bowl

In this section, the influence of substitution of the bowl on the interaction energies will be analysed. Figure 8.5 shows the results obtained for the complexes formed with chloride anion as obtained at the MP2.X/6-31G(0.25) level of calculation. Table 8.1 lists the values obtained for the equilibrium geometry and interaction energy at the minimum of each of the complexes studied. These values have been obtained by applying a spline cubic interpolation procedure to the data shown in Figure 8.5.

Starting with complexes by the concave face (top left in Figure 8.5), it can be observed that the interaction between chloride anion and corannulene or sumanene is quite weak, though not repulsive as expected taking into account the negative values observed for the electrostatic potential. The minima of the curves are located around 3.2 Å in both cases (a bit shorter in the case of sumanene), whereas the interaction energies reach -6.8 and -9.5 kcal/mol for corannulene and sumanene, respectively. That is, even though these are among the weakest interactions between anions and the bowls studied, the interaction is quite strong if it is taken into account that a typical hydrogen bond amounts to barely 5 kcal/mol. As regards complexes by the convex face of the bowls (top right in Figure 8.5), equilibrium distances are somewhat shorter, while the interaction energy decreases significantly, reaching around -1.5 and -2.9 kcal/mol with corannulene and sumanene, respectively. It has to be considered that at around 3.1 Å, the MEP has values of -5 and -9 kcal/mol for corannulene (in/out), and -4 and -8 kcal/mol for sumanene. Therefore, the interaction clearly departs from the MEP values, which would lead to clearly repulsive structures.

Table 8.1. Equilibrium distance and interaction energy as obtained for the different complexes with chloride anion at the MP2.X/6-31G(0.25) level of calculation.

	In		Out	
	R_{min} (Å)	ΔE (kcal/mol)	R_{min}(Å)	ΔE (kcal/mol)
Cora	3.221	-6.77	3.157	-1.52
Cora-Met	3.253	-6.16	3.186	0.07
Cora-F	3.098	-19.26	3.042	-12.27
Cora-CN	3.018	-37.13	2.862	-29.65
Suma	3.187	-9.45	3.130	-2.93
Suma-Met	3.238	-9.59	3.175	-0.26
Suma-F	3.045	-24.08	3.034	-14.71
Suma-CN	2.944	-45.03	2.833	-36.29
Suma-Met2	3.249	-14.06	3.129	-4.15
Suma-F2	3.023	-20.46	2.938	-15.44
Suma-CN2	2.941	-36.06	2.844	-26.48

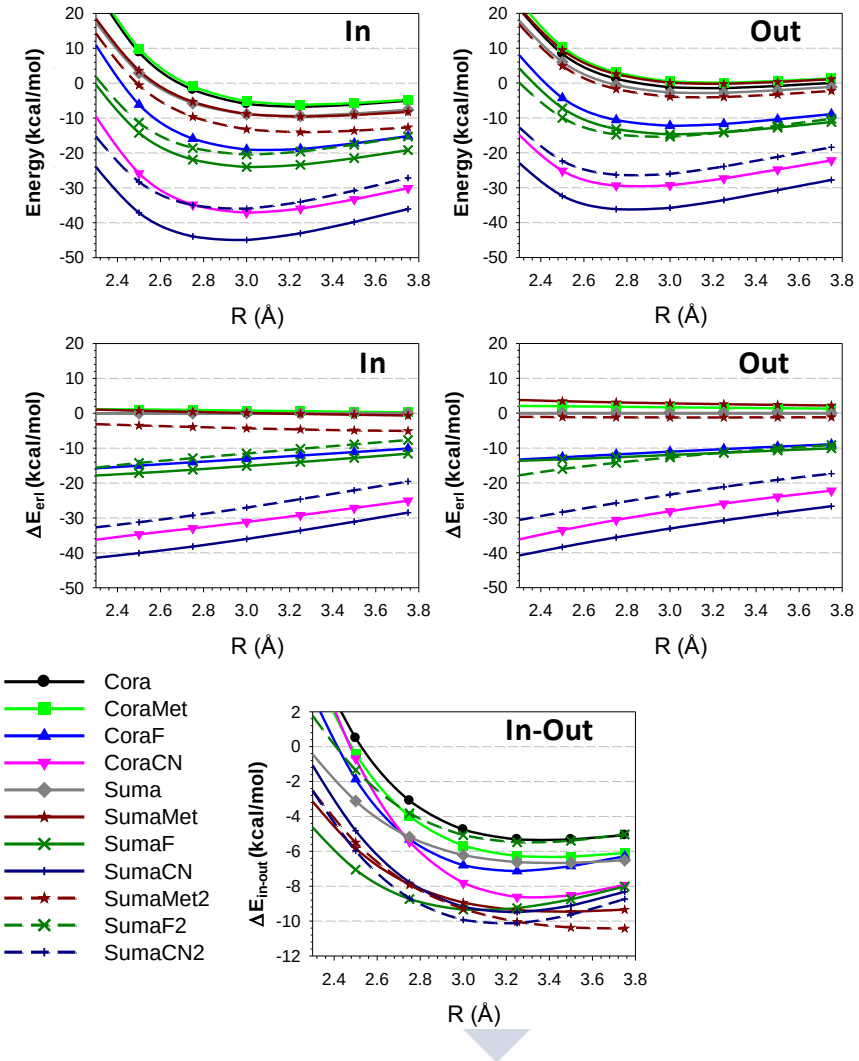


Figure 8.5. Interaction energy of chloride complexes with the different bowls considered in this work as obtained at the MP2.X/6-31G(0.25) level. Top: interaction energies; Middle: interaction energies relative to corannulene and sumanene. Bottom: differences between concave and convex (in-out) faces of the bowl.

When X=Met the interaction with the anion is even weaker, as expected, though changes with respect to unsubstituted bowls are marginal. In complexes with Suma-Met2, the changes are more significant, so the interaction energy is increased by -4.6 kcal/mol with respect to that observed in sumanene. This is a consequence of the presence of the bulky CH_3 groups protruding from the bowl's rim and partially occupying the concave face of the bowl. The methyl groups offer a series of positively charged hydrogen atoms, which can interact with the anion when located by the concave side of the bowl. Fluorination produces larger changes leading to more positive MEPs, so the interaction with chloride becomes more favorable. The equilibrium distances are shortened by 0.1-0.2 Å, whereas the interaction energies become more negative. Therefore, in the case of the Cora-F and Suma-F complexes by the concave face, the interaction energies increase as a consequence of substitution with an electron-withdrawing group, reaching -19.3 and -24.1 kcal/mol, respectively. In Suma-F2, the interaction energy of the complex reaches -20.5 kcal/mol by the concave face, in accordance with the less positive MEPs observed when substitution takes place on the CH_2 groups. Finally, in CN substituted bowls, the behavior is similar, but with even shorter equilibrium distances and larger interaction energies. Equilibrium distances by the concave face are around 3.0 Å or even shorter, while interaction energies reach values of -45 kcal/mol. By the convex face the interaction is also strong, reaching -29.7 and -36.3 kcal/mol for Cora-CN and Suma-CN. Suma-CN2 shows significantly smaller interaction energies than Suma-CN, with values more similar to those observed in Cora-CN. This can be related to the fact that CN is a π-acceptor group showing less electron-withdrawing character when bonded to sp^3 carbon atoms.

The changes in interaction energies upon substitution can be clearly seen in Figure 8.5, medium section, where the interaction energies appear grouped by substituent, with the X2 derivative always showing less negative interaction energies, and with the only deviation of Suma-Met2 by the concave face due to interaction with the methyl groups. Figure 8.5 also shows in its bottom section the relative energy differences between concave and convex complexes. In all cases complexation by the concave face is favored over the convex one. Thus, corannulene complexation by the concave face is favored by -5.3 kcal/mol, whereas in the case of sumanene the difference reaches -6.5 kcal/mol. Substitution increases the differences to around -7 kcal/mol in corannulene derivatives, whereas values of around -9 kcal/mol are obtained for sumanene ones. Substitution favors concave complexation, and this is more strongly favored in sumanene derivatives than in corannulene ones. So, independently of the strength of the interaction a good in-out selectivity could be obtained in all cases considered, favoring the location of the anion inside the bowl.

Figure 8.6 and Table 8.2 show the results obtained for sodium complexes. As expected, the behavior is opposite to that found for chloride complexes, since now the electrostatic interaction becomes repulsive upon substitution with electron-withdrawing groups. Therefore, the interaction of sodium cation with corannulene and sumanene amounts to around -30 kcal/mol by both faces. Equilibrium distances show values around 2.4 Å in corannulene complexes whereas in sumanene complexes are somewhat shorter. Methylation reinforces the interaction, reaching -35.4 kcal/mol with Cora-Met and -36.5 kcal/mol with Suma-Met, corresponding to increases in the strength of the interaction of around -5 to -6 kcal/mol. Fluorination significantly weakens the interaction, which still remains favorable, reaching between -12 to -14 kcal/mol for the different bowls. Finally, substitution with CN produces a dramatic change in the behavior of the complexes, so they are barely attractive or not stable at all, with interaction energies hardly reaching a couple of kcal/mol.

As regards the energy differences between complexes by the two faces of the bowl (Figure 8.6, bottom section), they are smaller in the case of sodium complexes. As electron-withdrawing groups are introduced complexes by the convex face are favored over those with the concave face. In any case the energy differences are quite small, reaching 3 kcal/mol at most. It is worth noting that fluorinated compounds are able to interact with significant strength with both cations and anions, though the interaction is stronger with chloride than with sodium. The stability differences are not large by the convex face but very important by the concave face, clearly favoring interaction with anions.

Table 8.2. Equilibrium distance and interaction energy as obtained for the different complexes with sodium cation at the MP2.X/6-31G(0.25) level of calculation.

	In		Out	
	R_{min} (Å)	ΔE (kcal/mol)	R_{min} (Å)	ΔE (kcal/mol)
Cora	2.412	-29.95	2.410	-29.73
Cora-Met	2.382	-35.35	2.392	-34.50
Cora-F	2.475	-14.14	2.465	-16.67
Cora-CN	2.598	2.02	2.565	-1.39
Suma	2.345	-30.21	2.370	-28.73
Suma-Met	2.312	-36.52	2.346	-35.19
Suma-F	2.391	-12.01	2.432	-14.37
Suma-CN	2.524	7.23	2.563	4.73
Suma-Met2	2.338	-33.31	2.362	-30.47
Suma-F2	2.496	-13.92	2.483	-12.98
Suma-CN2	2.702	-2.39	2.615	-3.33

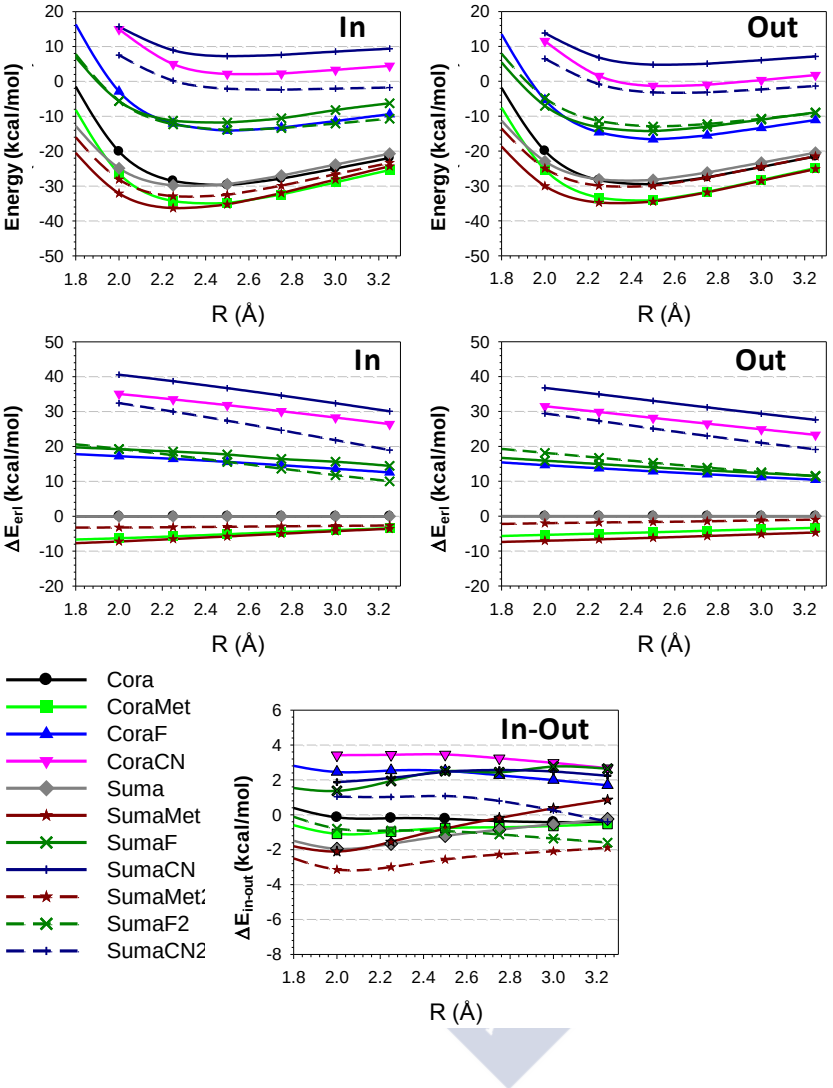


Figure 8.6. Interaction energy of sodium complexes with the different bowls considered in this work as obtained at the MP2.X/6-31G(0.25) level. Top: interaction energies; Middle: interaction energies relative to corannulene and sumanene; Bottom: differences between concave and convex (in-out) faces of the bowl.

8.3.4. SAPT(DFT) Analysis

As commented in Computational Details, SAPT(DFT) calculations have been carried out in order to understand the physical origins of the interaction in the complexes studied. So, SAPT(DFT) calculations have been performed following a line on the symmetry axis of the bowls as already commented in previous sections. In the following, $E_{ele}= E_{1pol}$; $E_{rep}= E_{1exch}$; $E_{ind}= E_{2ind-exch} + E_{2ind} + \delta HF$; $E_{disp}= E_{2disp-exch} + E_{2disp}$. In the systems studied herein, apart from the electrostatic interaction strong orbital interactions could be expected, which can be related to the induction term in SAPT(DFT).[81] For the sake of brevity, only results for fluorinated compounds will be shown, the rest of the complexes being reported in Appendix C. Figure 8.7 shows the energy decomposition for complexes with chloride anion. As expected, all attractive contributions to the interaction energy become more negative as the distance from the anion to the bowl is shortened, whereas repulsion increases quickly. Cora-F complex with chloride by the concave face shows that the most important contribution to the stabilization of the complex is electrostatic, as it could be expected from the MEP values. It is worth noting however, that a great part of the electrostatic contribution comes from penetration and therefore cannot be properly described by the multipole expansion or the MEP value.[6] This behavior is observed in all complexes with chloride, and reflects the interpenetration of the electron clouds of the anion and the bowl, which is significant for all distances shown in Figure 8.7, but especially by the concave face. It can be appreciated that the electrostatic contribution changes more slowly by the convex face where penetration is less important. Repulsion contribution behaves in a similar manner, increasing steeply by the concave face and more slowly by the convex one. On the other hand, induction and dispersion contribute to a smaller extent to the stability of the complexes. As expected, dispersion contribution is larger by the concave face, where a larger number of atoms are close to the anion, whereas induction is the smallest contribution in complexes by the concave face. However, this behavior is the contrary by the convex face and induction contribution is slightly more negative than dispersion, both contributions evolving in a parallel way. In summary, all contributions to the stability of the complex are larger by the concave face, so favoring formation of the complexes by this side of the bowl.

Figure 8.8 shows the behavior of sodium complexes with the fluorinated bowls, exhibiting a totally different pattern. Most significant is that the electrostatic contribution is quite small and repulsive. Therefore, these complexes are not bound by electrostatics, as expected taking into account the positive MEP. Therefore, if the complexes are stable, they must be held by other contributions. It can be observed that dispersion is small in all cases, both by the convex or the concave face, so the contribution responsible of the stability of the complex must be induction. It can be appreciated that induction contribution is larger than that observed in chloride complexes. The smaller and more polarizing sodium cation combined with the

polarizable aromatic cloud of the bowls are responsible of induction playing a major role in this kind of complexes. This behavior is extensible to the other bowls considered.

Figure 8.9 shows the results of the SAPT(DFT) partitioning at the MP2.X/6-31G(0.25) minima for all complexes considered. It can be observed how substitution produces changes mainly in the electrostatic component of the interaction. Overall, complexes with chloride anion are stabilized by large electrostatic contributions when X = F or CN. The increase in electrostatic contribution is partially cancelled out by increases in repulsion, which reflect the shortening in the equilibrium distances of the complexes as the interaction becomes stronger. On the other hand, induction and dispersion remain almost unchanged upon substitution, though small increments can be observed when going to more stable complexes.

As regards sodium complexes, the behavior is totally different. Of course, large changes in electrostatic contribution are observed as the MEPs are changed due to substitution, but the main contribution to the stability of the complexes is induction, whereas dispersion remains almost constant and contributes marginally to the interaction. Repulsion is significantly smaller due to the smaller size and extent of the electron cloud of sodium cation. The balance between a strong induction attraction (always larger than -20 kcal/mol) with a moderate repulsion and an increasingly repulsive electrostatic contribution as electron-withdrawing groups are included, results in the final stability of a given complex.

These results are quite in line with those already obtained for sodium complexes with sumanene and corannulene using the Local Molecular Orbital- Energy Decomposition Analysis (LMO-EDA).[51, 82] The differences observed are related to the different partitioning methods employed as well as to differences on the level of calculation. Comparing the results obtained for the complexes studied in this work with prototypical π···π or CH···π contacts in benzene clusters, the main difference comes of course from the larger electrostatic contribution and the secondary role of dispersion.[83, 84] Previous results in ion··· π systems are more similar to those found in the present work,[20, 85, 86] though induction is significantly larger in bowl complexes as a consequence of the more extended aromatic cloud.

It is worth noting that the electrostatic contribution is similar in sumanene complexes with sodium and chloride as a consequence of the significant penetration in chloride complexes. A priori, sumanene should interact repulsively by electrostatics with chloride, but penetration makes this contribution attractive and of similar size as that observed in sodium complexes. It can also be observed in sodium complexes that the increase in electrostatic repulsion upon substitution is not matched by a significant change in repulsion. Induction exhibits moderate changes upon substitution, though in all cases constitutes a highly attractive contribution.

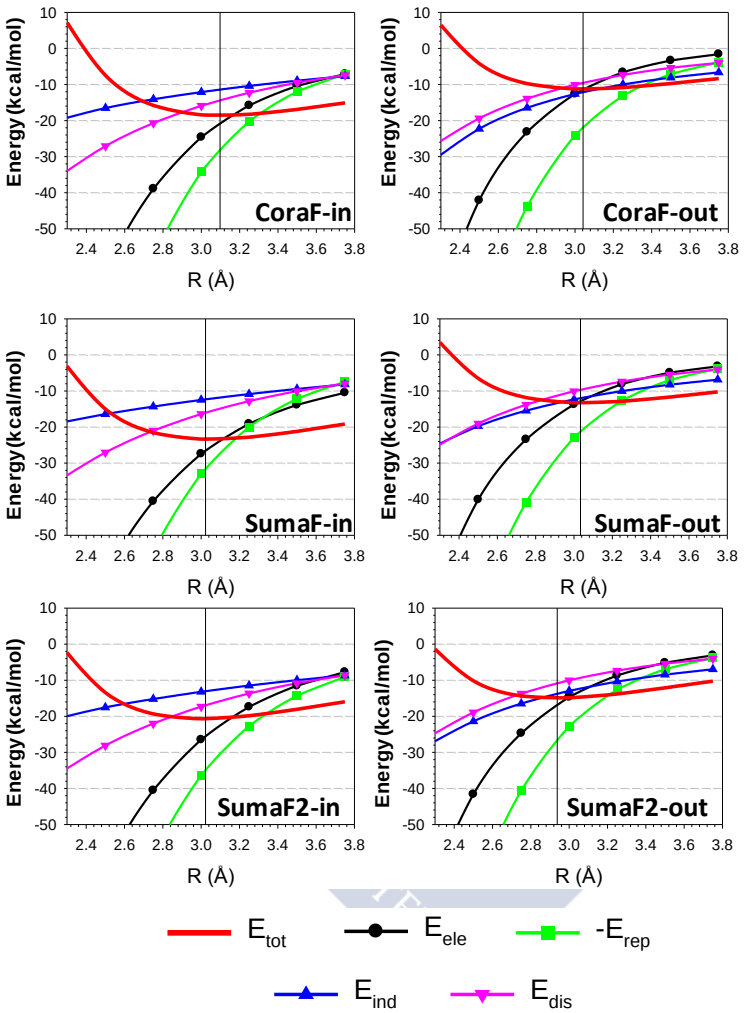


Figure 8.7. SAPT(DFT) energy decomposition for complexes formed by chloride anion and fluorinated bowls. The vertical line indicates the position of the minimum obtained at the MP2.X/6-31G(0.25) level of calculation.

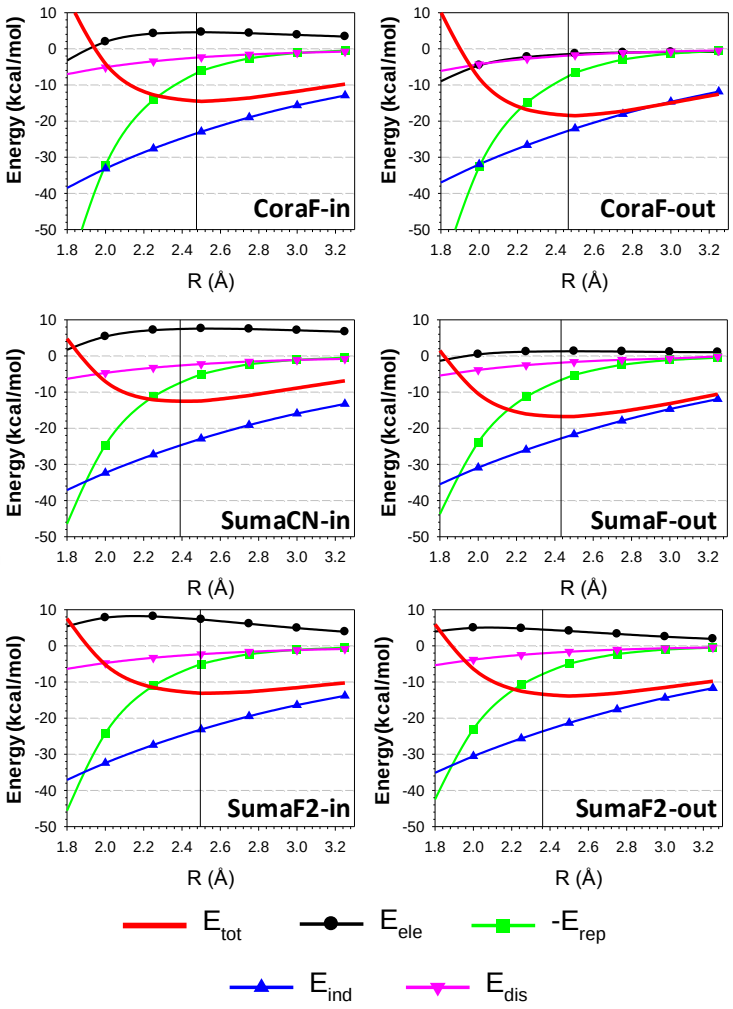


Figure 8.8. SAPT(DFT) energy decomposition for complexes formed by sodium cation and fluorinated bowls. The vertical line indicates the position of the minimum obtained at the MP2.X/6-31G(0.25) level of calculation.

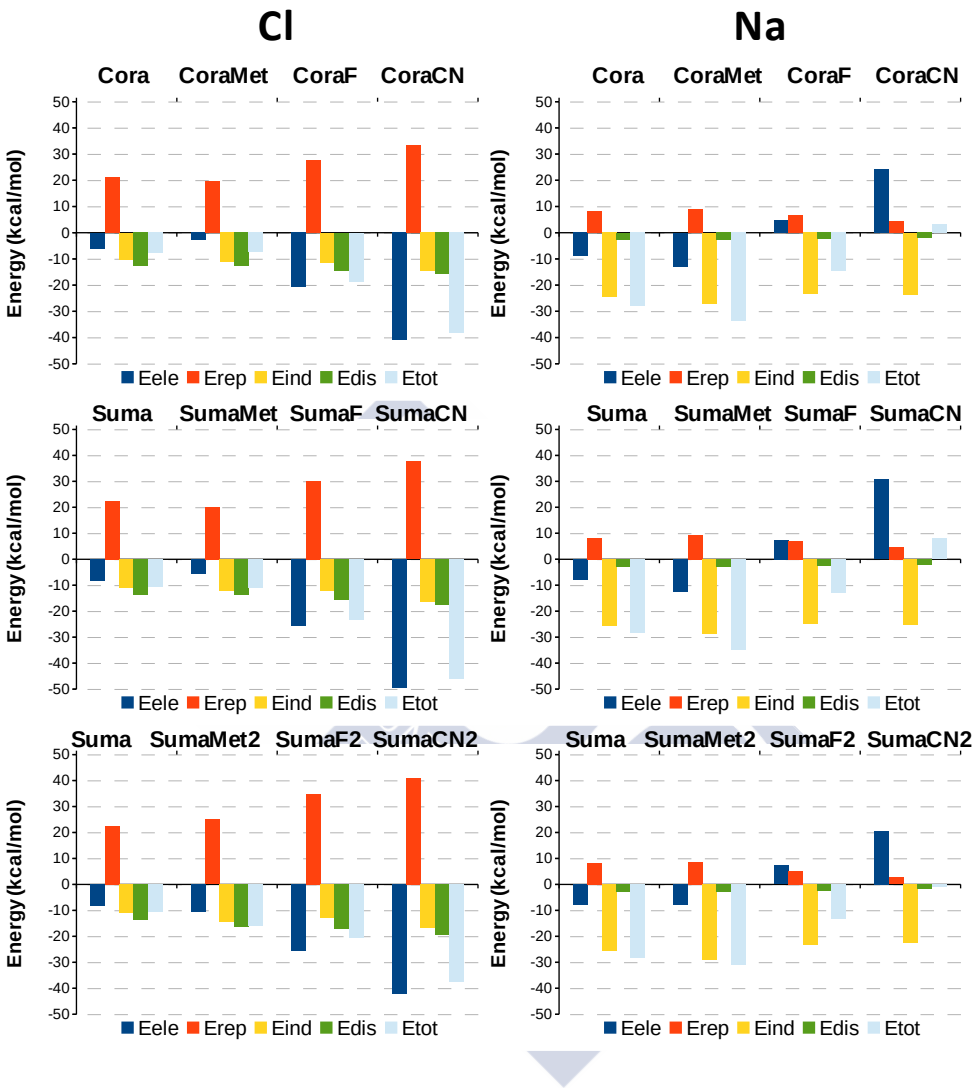


Figure 8.9. SAPT(DFT) decomposition for complexes formed by the concave side of the bowls.

It is worth noting, however, that changes in induction and dispersion are mainly a consequence of changes in the equilibrium distances. That is, if dispersion and induction contributions are compared at the same intermolecular distance in different bowls, there is almost no change to be observed.

This is the basis of some approximate methods estimating the strength of ion···π interactions.[87-91] If all contributions are the same as in the unsubstituted complexes except electrostatics, the interaction can be predicted checking only changes in electrostatics. However, these approximate methods face several problems. First, in complexes with chloride, penetration is an important contribution to the stability of the complex, so there is a part of the electrostatic contribution which cannot be recovered by simplified models based in the electrostatic potential or multipole expansion, or even simpler atomic dipole or partial charge contributions. On the other hand, the variations in electrostatic contribution change the equilibrium distances, which also reflect in changes in the rest of the contributions. Therefore, the interaction energy could also contain contributions from changes in induction and dispersion due to the variations in equilibrium distances. Even though these changes are not large they can affect significantly to the energetics of the complex. In any case, these contributions due to changes in induction and dispersion will be more significant when larger changes in electrostatic contribution take place, so they are expected in complexes with X = CN, as it can be corroborated from Figure 8.9.

8.4. Conclusions

A computational study has been carried out in order to get insight into the interaction of molecular bowls with ions. Complexes formed by substituted buckybowls based on corannulene and sumanene and chloride anion or sodium cation have been considered. The choice of substituents, going from electron-withdrawing groups to slightly donating groups, allows knowing how changing the MEP of the bowls affects to the interaction.

A selection of different computational methods has been employed for obtaining the interaction energies of the complexes. Overall, the global behavior of the complexes with the different bowls by the concave and convex faces and ranging from very attractive complexes to slightly repulsive ones, is quite difficult to reproduce for most of the methods employed. The best performance is given by the SCS-MP2 method extrapolated to basis limit, which matches almost perfectly the values obtained at the MP2.X/6-31G(0.25) level of calculation. As regards DFT methods, M06-2X/6-31+G* seems to be able to provide a quite balanced description of the concave/convex energy differences despite the errors introduced in the interaction energies.

As regards the effect of bowl substitution the following conclusions can be drawn. Sumanene interacts more strongly than corannulene with both anions and cations. In

substituted bowls, the effect of the substituent is more pronounced in sumanene derivatives when the substitution takes place on the CH groups of the aromatic rings, whereas substitution on the CH_2 groups introduces smaller changes. As the substituent becomes more electron-withdrawing, the interaction with the anion becomes stronger, closely following the changes in the MEPs of the bowls. It is worth noting that chloride complexes are stable with all bowls, even when substituted with a donating group as methyl. Cation complexes also follow the changes in the MEPs of the bowls, leading to unstable complexes with CN-substituted bowls.

SAPT(DFT) decomposition shows the large differences in the nature of the interaction for the ion complexes studied. Cation complexes are dominated by a large induction component, even larger than the electrostatic contribution, together with negligible dispersion effects. In anion complexes, however, the role of induction is less significant, being electrostatics and dispersion the main stabilizing components. Even though the largest effect of the substituents comes from modulation of the MEP of the bowl, there are also changes affecting to the induction and dispersion contributions which may introduce deviations over the behavior expected from a purely electrostatics point of view.

8.5. References

[1] H.-J. Schneider, A. Yatsimirski, Principles and Methods in Supramolecular Chemistry, Wiley, New York, **2000**.

[2] A. S. Mahadevi, G. N. Sastry. *Chem. Rev.* **2013**, *113*, 2100-2138.

[3] L. M. Salonen, M. Ellermann, F. Diederich. *Angew. Chem. Int. Ed.* **2011**, *50*, 4808-4842.

[4] N. J. Singh, H. M. Lee, I.-C. Hwang, K. S. Kim. *Supramol. Chem.* **2007**, *19*, 321-332.

[5] I. Kaplan, Intermolecular Interactions : Physical Picture , Computational Methods, John Wiley & Sons, Chichester, **2006**.

[6] A. J. Stone, The theory of intermolecular forces, Oxford University Press, Oxford, **2013**.

[7] E. A. Meyer, R. K. Castellano, F. Diederich. *Angew. Chem. Int. Ed.* **2003**, *42*, 1210-1250.

[8] M. Nishio. *Phys. Chem. Chem. Phys.* **2011**, *13*, 13873-13900.

[9] S. Tsuzuki, T. Uchimaru. *Curr. Org. Chem.* **2006**, *10*, 745-762.

[10] M. L. Waters. *Biopolymers (Peptide Sci.)* **2004**, *76*, 435-445.

[11] D. A. Dougherty. *J. Nutr.* **2007**, *137*, 1504S-1508S.

[12] N. Zacharias, D. A. Dougherty. *Trends Pharm. Sci.* **2002**, *23*, 281-287.

[13] K. E. Riley, P. Hobza. *Acc. Chem. Res.* **2013**, *46*, 927-936.

[14] K. D. Daze, F. Hof. *Acc. Chem. Res.* **2013**, *46*, 937-945.

[15] H. T. Chifotides, K. I. M. R. Dunbar. *Acc. Chem. Res.* **2013**, *46*, 894-906.

[16] C. Estarellas, A. Frontera, D. Quiñonero, P. M. Deya. *Chem. Phys. Lett.* **2009**, *479*, 316-320.

[17] D. Quiñonero, A. Frontera, C. Garau, P. Ballester, A. Costa, P. M. Deya. *ChemPhysChem* **2006**, *7*, 2487-2491.
[18] A. Frontera, D. Quiñonero, P. M. Deyà. *WIRES: Comput. Mol. Sci.* **2011**, *1*, 440-459.
[19] B. L. Schottel, H. T. Chifotides, K. R. Dunbar. *Chem. Soc. Rev.* **2008**, *37*, 68-83.
[20] D. Kim, E. C. Lee, K. S. Kim, P. Tarakeshwar. *J. Phys. Chem. A* **2007**, *111*, 7980-7986.
[21] N. J. Singh, S. K. Min, D. Y. Kim, K. S. Kim. *J. Chem. Theory Comput.* **2009**, *5*, 515-529.
[22] I. Soteras, M. Orozco, F. J. Luque. *Phys. Chem. Chem. Phys.* **2008**, *10*, 2616-2624.
[23] C. D. Sherrill. *Acc. Chem. Res.* **2013**, *46*, 1020-1028.
[24] J. A. Carrazana-Garcia, J. Rodriguez-Otero, E. M. Cabaleiro-Lago. *J. Phys. Chem. B* **2011**, *115*, 2774-2782.
[25] P. Garcia-Novo, A. Campo-Cacharron, E. M. Cabaleiro-Lago, J. Rodriguez-Otero. *Phys. Chem. Chem. Phys.* **2012**, *14*, 104-112.
[26] M. Güell, J. Poater, J. M. Luis, O. Mó, M. Yáñez, M. Solà. *ChemPhysChem* **2005**, *6*, 2552-2561.
[27] J.-F. Gal, P.-C. Maria, M. Decouzon, O. Mó, M. Yáñez, J. L. M. Abboud. *J. Am. Chem. Soc.* **2003**, *125*, 10394-10401.
[28] J. Rodríguez-Otero, E. M. Cabaleiro-Lago, A. Peña-Gallego. *Chem. Phys. Lett.* **2008**, *452*, 49-53.
[29] R. G. Harvey, Polycyclic aromatic hydrocarbons, Wiley-VCH, New York, **1997**.
[30] S. Reich, C. Thomsen, J. Maultzsch, Carbon Nanotubes: Basic Concepts and Physical Properties, Wiley-VCH, Weiheim, **2004**.
[31] A. Hirsch, M. Brettreich, Fullerenes: chemistry and reactions Wiley-VCH, Weiheim, **2005**.
[32] F.-G. Klärner, T. Schrader. *Acc. Chem. Res.* **2013**, *46*, 967-978.
[33] F.-G. Klarner, J. Panitzky, D. Preda, L. T. Scott. *J. Mol. Model.* **2000**, *6*, 318-327.
[34] J. M. Hermida-Ramon, C. M. Estevez. *Chem. Eur. J.* **2007**, *13*, 4743-4749.
[35] J. M. Hermida-Ramon, M. Mandado, M. Sanchez-Lozano, C. M. Estevez. *Phys. Chem. Chem. Phys.* **2010**, *12*, 164-169.
[36] M. Mandado, J. M. Hermida-Ramon, C. M. Estevez. *J. Mol. Struct. (THEOCHEM)* **2008**, *854*, 1-9.
[37] M. Sanchez-Lozano, N. Otero, J. M. Hermida-Ramon, C. M. Estevez, M. Mandado. *J. Phys. Chem. A* **2011**, *115*, 2016-2025.
[38] J. M. Hermida-Ramon, M. Sanchez-Lozano, C. M. Estevez. *Phys. Chem. Chem. Phys.* **2013**, *15*, 18204-18216.
[39] M. A. Petrukhina, L. A. Scott, Fragments of fullerenes and carbon nanotubes, John Wiley & Sons, Inc., Hoboken, New Jersey, **2012**.
[40] M. A. Petrukhina, L. T. Scott. *Dalton T.* **2005**, 2969-2975.
[41] A. S. Filatov, M. A. Petrukhina. *Coord. Chem. Rev.* **2010**, *254*, 2234-2246.
[42] A. Sygula, P. W. Rabideau. *J. Mol. Struct. (THEOCHEM)* **1995**, *333*, 215-226.
[43] U. D. Priyakumar, G. N. Sastry. *J. Org. Chem.* **2001**, *66*, 6523-6530.
[44] R. C. Dunbar. *J. Phys. Chem. A* **2002**, *106*, 9809-9819.
[45] U. D. Priyakumar, G. N. Sastry. *Tetrahedron Lett.* **2003**, *44*, 6043-6046.
[46] M. W. Stoddart, J. H. Brownie, M. C. Baird, H. L. Schmider. *J. Organomet. Chem.* **2005**, *690*, 3440-3450.
[47] K. H. Lee, C. Lee, J. Kang, S. S. Park, J. Lee, S. K. Lee, D. K. Bohme. *J. Phys. Chem. A* **2006**, *110*, 11730-11733.

[48] J. R. Green, R. C. Dunbar. *J. Phys. Chem. A* **2011**, *115*, 4968-4975.
[49] S. N. Spisak, A. V. Zabula, A. S. Filatov, A. Y. Rogachev, M. A. Petrukhina. *Angew. Chem., Int. Ed.* **2011**, *50*, 8090-8094.
[50] M. R. Kennedy, L. A. Burns, C. D. Sherrill. *J. Phys. Chem. A* **2012**, *116*, 11920-11926.
[51] D. Vijay, H. Sakurai, V. Subramanian, G. N. Sastry. *Phys. Chem. Chem. Phys.* **2012**, *14*, 3057-3065.
[52] H. Sakurai, T. Daiko, H. Sakane, T. Amaya, T. Hirao. *J. Am. Chem. Soc.* **2005**, *127*, 11580-11581.
[53] S. F. Boys, F. Bernardi. *Mol. Phys.* **1970**, *19*, 553-566.
[54] G. Chalasinski, M. M. Szczesniak. *Chem. Rev.* **2000**, *100*, 4227-4252.
[55] K. E. Riley, J. Řezáč, P. Hobza. *Phys. Chem. Chem. Phys.* **2011**, *13*, 21121-21125.
[56] K. E. Riley, J. Rezac, P. Hobza. *Phys. Chem. Chem. Phys.* **2012**, *14*, 13187-13193.
[57] T. Helgaker, W. Klopper, H. Koch, J. Noga. *J. Chem. Phys.* **1997**, *106*, 9639-9646.
[58] S. Grimme. *J. Chem. Phys.* **2003**, *118*, 9095-9102.
[59] J. Antony, S. Grimme. *J. Phys. Chem. A* **2007**, *111*, 4862–4868.
[60] J. C. Hill, J. A. Patts. *J. Chem. Theory Comput.* **2007**, *3*, 80-85.
[61] R. Distasio Jr., M. Head-Gordon. *Mol. Phys.* **2007**, *105*, 1073-1083.
[62] Y. Zhao, D. G. Truhlar. *Theor. Chem. Acc.* **2007**, *120*, 215-241.
[63] S. Grimme. *J. Comput. Chem.* **2006**, *27*, 1787–1799.
[64] S. Grimme, J. Antony, S. Ehrlich, H. Krieg. *J. Chem. Phys.* **2010**, *132*, 214301/1-214301/19.
[65] S. Ehrlich, J. Moellmann, S. Grimme. *Acc. Chem. Res.* **2013**, *46*, 916-926.
[66] S. Grimme, S. Ehrlich, L. Goerigk. *J. Comput. Chem.* **2011**, *32*, 1456-1465.
[67] B. Jeziorski, R. Moszynski, K. Szalewicz. *Chem. Rev.* **1994**, *94*, 1887-1930.
[68] A. J. Misquitta, K. Szalewicz. *J. Chem. Phys.* **2005**, *122*, 214109/1-214109/19.
[69] A. Hesselmann, G. Jansen, M. Schütz. *J. Chem. Phys.* **2005**, *122*, 014103/1-014103/17.
[70] E. G. Hohenstein, C. D. Sherrill. *WIRES: Comput. Mol. Sci.* **2012**, *2*, 304-326.
[71] K. Szalewicz. *WIRES: Comput. Mol. Sci.* **2012**, *2*, 254-272.
[72] J. Řezáč, P. Hobza. *J. Chem. Theory Comput.* **2011**, *7*, 685-689.
[73] H. J. Werner, P. J. Knowles, G. Knizia, F. R. Manby, M. Schütz, P. Celani, T. Korona, R. Lindh, A. Mitrushenkov, G. Rauhut, K. R. Shamasundar, T. B. Adler, R. D. Amos, A. Bernhardsson, A. Berning, D. L. Cooper, M. J. O. Deegan, A. J. Dobbyn, F. Eckert, E. Goll, C. Hampel, A. Hesselmann, G. Hetzer, T. Hrenar, G. Jansen, C. Kö, Y. Liu, A. W. Lloyd, R. A. Mata, A. J. May, S. J. McNicholas, W. Meyer, M. E. Mura, A. Nicklaß, D. P. O'Neill, P. Palmieri, D. Peng, K. P. Pitzer, M. Reiher, T. Shiozaki, H. Stoll, A. J. Stone, R. Tarroni, T. Thorsteinsson, M. Wang, Molpro version 2010.1, a package of ab initio programs, see http://www.molpro.net, **2010**.
[74] M. J. Frisch, G. W. Trucks, H. B. Schlegel, G. E. Scuseria, M. A. Robb, J. R. Cheeseman, G. Scalmani, V. Barone, B. Mennucci, G. A. Petersson, H. Nakatsuji, M. Caricato, X. Li, H. P. Hratchian, A. F. Izmaylov, J. Bloino, G. Zheng, J. L. Sonnenberg, M. Hada, M. Ehara, K. Toyota, R. Fukuda, J. Hasegawa, M. Ishida, T. Nakajima, Y. Honda, O. Kitao, H. Nakai, T. Vreven, J. M. J. A, J. E. Peralta, F. Ogliaro, M. Bearpark, J. J. Heyd, E. Brothers, K. N. Kudin, V. N. Staroverov, R. Kobayashi, J. Normand, K. Raghavachari, A. Rendell, J. C. Burant, S. S. Iyengar, J. Tomasi, M. Cossi, N. Rega, N. J. Millam, M. Klene, J. E. Knox, J. B. Cross, V. Bakken, C. Adamo, J. Jaramillo, R. Gomperts, R. E. Stratmann, O. Yazyev, A. J. Austin, R.

Cammi, C. Pomelli, J. W. Ochterski, R. L. Martin, K. Morokuma, V. G. Zakrzewski, G. A. Voth, P. Salvador, J. J. Dannenberg, S. Dapprich, A. D. Daniels, Ö. Farkas, J. B. Foresman, J. V. Ortiz, J. Cioslowski, D. J. Fox. Gaussian 09, revision B.01, Gaussian, Inc., Wallingford CT, **2009**.

[75] TURBOMOLE V6.3 , a development of University of Karlsruhe and Forschungszentrum Karlsruhe GmbH, 1989-2007, TURBOMOLE GmbH, since 2007; available from http://www.turbomole.com, **2011**.

[76] F. Weigend. *Phys. Chem. Chem. Phys.* **2002**, *4*, 4285-4291.

[77] F. Weigend, A. Köhn, C. Hättig. *J. Chem. Phys.* **2002**, *116*, 3175-3183.

[78] D. A. Lawlor, D. E. Bean, P. W. Fowler, J. R. Keeffe, J. S. Kudavalli, R. A. More O'Ferrall, S. N. Rao. *J. Am. Chem. Soc.* **2011**, *133*, 19729-19742.

[79] I. Fernández, J. I. Wu, P. von Ragué Schleyer. *Org. Lett.* **2013**, *15*, 2990-2993.

[80] J. Šponer, J. Leszczyński, P. Hobza. *J. Phys. Chem.* **1996**, *100*, 5590-5596.

[81] M. V. Hopffgarten, G. Frenking. *WIRES: Comput. Mol. Sci.* **2012**, *2*, 43-62.

[82] P. Su, H. Li. *J. Chem. Phys.* **2009**, *131*, 014102/1-014102/15.

[83] Y. Cho, S. K. Min, J. Yun, W. Y. Kim, A. Tkatchenko, K. S. Kim. *J. Chem. Theory Comput.* **2013**, *9*, 2090-2096.

[84] E. C. Lee, D. Kim, P. Jurečka, P. Tarakeshwar, P. Hobza, K. S. Kim. *J. Phys. Chem. A* **2007**, *111*, 3446-3457.

[85] E. M. Cabaleiro-Lago, J. Rodríguez-Otero, Á. Peña-Gallego. *J. Chem. Phys.* **2011**, *135*, 214301/1-214301/9.

[86] A. A. Rodríguez-Sanz, E. M. Cabaleiro-Lago, J. Rodríguez-Otero. *Org. Biomol. Chem.* **2014**, *12*, 2938-2949.

[87] S. E. Wheeler, K. N. Houk. *J. Am. Chem. Soc.* **2009**, *131*, 3126-3127.

[88] S. E. Wheeler, K. N. Houk. *J. Phys. Chem. A* **2010**, *114*, 8658-8664.

[89] S. E. Wheeler. *Acc. Chem. Res.* **2013**, *46*, 1029-1038.

[90] F. B. Sayyed, C. H. Suresh. *J. Phys. Chem. A* **2012**, *116*, 5723-5732.

[91] A. Bauzá, P. M. Deyà, A. Frontera, D. Quiñonero. *Phys. Chem. Chem. Phys.* **2014**, *16*, 1322-1326.

9. Interaction of anions with substituted buckybowls. Anion's nature and solvent effects.

USC
UNIVERSIDADE
DE SANTIAGO
DE COMPOSTELA

9.1. Introduction

Traditionally, polycyclic aromatic hydrocarbons have been considered as planar structures similar in most cases to graphene-like fragments.[1] However, with the discovery of fullerenes and carbon nanotubes, a full family of aromatic hydrocarbons with curved surfaces has aroused, attracting the interest of the scientific community.[2, 3] Part of the interest devoted to this kind of systems has been oriented towards understanding the different properties of concave and convex surfaces, especially regarding to how other species interact with each of the faces on a curved hydrocarbon.

Klärner showed that for certain molecular clips and tweezers, there is a different behavior depending on the face considered.[4, 5] The Molecular Electrostatic Potential (MEP) is more negative inside the tweezers than in their outer face, suggesting the possibility of employing them as effective receptors for electron-deficient molecules.[4-9] Carbon nanotubes and fullerenes also exhibit different behavior depending on the face considered. The so-called buckybowls are aromatic curved systems that can be mapped onto the surface of fullerenes.[10, 11] These buckybowls are formed by joining six and five carbon rings, the presence of the latter introducing the structural strain leading to the curvature of the system. Buckybowls offer easy access for interaction of a given species with both different faces, so different works have been devoted to determine their characteristics. The simplest buckybowl, corannulene $C_{20}H_{10}$, as well as its derivatives, has been the subject of different studies in order to determine its curvature,[12-14] barrier for inversion of the bowl and also its ability for coordinating different species.[11, 15-24] The curvature of corannulene gives rise to more negative MEP by the convex face, so most cations prefer coordinating to the convex face of the bowl.[4, 21, 23, 24] Also, corannulene has been employed as the basic unit for constructing fullerene receptors, as in the buckycatcher devised by Sygula.[25-28] The other smallest bowl which can be mapped onto C_{60} is sumanene $C_{21}H_{12}$, recently synthesized and showing a six carbon ring in the bottom of the bowl.[29] The coordination of cations to this bowl has also been considered, exhibiting similar characteristics as those found in corannulene-containing systems. In any case, there seems that interaction with sumanene is usually stronger than with corannulene.[17, 18, 23, 24]

Most studies in literature deal with the interaction of these unsubstituted bowls and cations. However, Hermida-Ramón et al. have already shown that the molecular tweezers devised by Klärner can be appropriately modified in order to interact favorably with electron-rich species, and more specifically with anions. In a series of works, these authors have explored the effect on substitution on molecular tweezers in order to make them amenable for interacting with anions.[30-32] The results indicate that substitution with CN groups is an effective route for inverting the MEP of the tweezer leading to stable complexes with anions. Other structural modifications have been

considered by these authors, which lead to even more intense interaction with anions.[33, 34] Very recently, host molecules based on subphthalocyanines have been presented, forming complexes with anions that are suggested to be stable even in water solution.[34]

Following this line, buckybowls can be conveniently modified in order to make them to interact favorably with anions, as already shown in previous work by our group.[23, 24] Different substituents have been considered with the purpose of tuning the MEP of the bowls so they can interact both with anions and cations, CN substitution emerging as the most appropriate way of obtaining a bowl that interacts favorably with anions (see chapters 7 and 8). Previous work indicates that anions interact preferentially with these substituted buckybowls by the concave face.[23, 24] Therefore, anion receptors based on substituted buckybowls can be devised relying on anion···π interactions, which can constitute an interesting option for encapsulating anions selectively.[35-37] This kind of anion···π complexes is mainly stabilized by electrostatics, though the interaction in these systems is quite difficult to describe, with important contributions from polarization and dispersion.[23, 24]

The effect of substitution upon the interaction with chloride anion and sodium cation has already been thoroughly studied.[23] However, the effect of the anions' nature upon the interaction with substituted buckybowls has not been treated in detail yet. Therefore, in the present work, the interaction of CN-substituted buckybowls based on corannulene and sumanene with a series of anions is studied. Different monovalent anions have been considered as indicated in Figure 9.1, comprising monatomic (Cl^- and Br^-), planar trigonal (NO_3^- and CO_2H^-) and tetrahedral (BF_4^- and ClO_4^-) ones. The results obtained from this set of anions will provide information about specific effects associated to more complex anions, which can interact with different regions of the bowl. Another aspect of the interaction which deserves attention in these systems is how these complexes behave when immersed in solvent. To the best of our knowledge, few works have been devoted to analyze this effect, but their results clearly indicate that the role played by the solvent is crucial, leading to large destabilizations of the complexes relative to the gas phase.[24, 32] Therefore, the effect of different solvents upon the characteristics of the complexes considered in this work has also been studied. It can be expected that the results would help to understand the properties of these systems and to provide hints in order to consider them as possible anion receptors in future work.

9.2. Computational Details

As indicated above, complexes formed by a series of anions and buckybowls have been studied employing different orientations. Therefore, for a given bowl, the central atom of the anion has been located at several distances relative to the bowl in order to

obtain interaction energy profiles. Four approaching lines have been employed for studying the complexes as summarized in Figure 9.2. Two approaching lines correspond to points over the symmetry axis of the bowl by the concave (**I**) and convex (**O**) faces of the bowl. Besides, an approaching line passing through the center of the hexagonal external rings of the bowl (**H**), as well as a line following a C-H bond on the rim of the bowls (**R**) has been studied. In each of these lines, several intermolecular distances between the central atom of the anion and the center of the rings have been employed (in **R** the distances are measured to the hydrogen atom). Finally, several orientations have been considered for the polyatomic anions as indicated in Figure 9.2. The geometries of the anions and the bowls are kept frozen to the values obtained in isolation at the M06-2X/6-31+G* level.[38]

In the systems constructed as explained above, the interaction energy has been obtained at the M06-2X/6-31+G* level, in order to obtain energy profiles for the different approaching lines. All interaction energies have been calculated by using the counterpoise correction in order to avoid the basis set superposition error (BSSE).[39, 40] The equilibrium geometries of the complexes have been determined from these curves by interpolation, the interaction energies at the minima being also obtained at the SCS-MP2/CBS level of calculation.[41, 42] It has been found in previous work that the values obtained at this level of calculation are pretty similar to benchmark values.[23] SCS-MP2 is a variant of MP2 where the contributions to the correlation energy from electron pairs with different and equal spins are empirically scaled in order to improve the performance of MP2.[41, 42] SCS-MP2 interaction energies have been obtained with the aug-cc-pVDZ and aug-cc-pVTZ, these values being employed in a two-point extrapolation scheme in order to obtain values extrapolated to the complete basis set limit.[43]

In order to obtain more information about the characteristics of the interaction, interaction energies have been decomposed by applying the Symmetry Adapted Perturbation Theory (SAPT) method[44] with intramonomer correlation effects described at the DFT level (SAPT(DFT)).[45-48] Density fitted SAPT(DFT) calculations were carried out, providing information on the individual physical components of the interaction energy. For these calculations the PBE functional was used, involving a shift parameter obtained as the difference between the energy of the highest occupied molecular orbital and the negative ionization potential of each fragment. Orbital energies and ionization potentials have been obtained by using the PBE functional with the aug-cc-pVDZ basis set. The SAPT(DFT) calculations were performed with the aug-cc-pVDZ basis set, employing the aug-cc-pVDZ/JKFIT for Hartree–Fock and aug-cc-pVDZ/MP2FIT for the second-order dispersion terms.

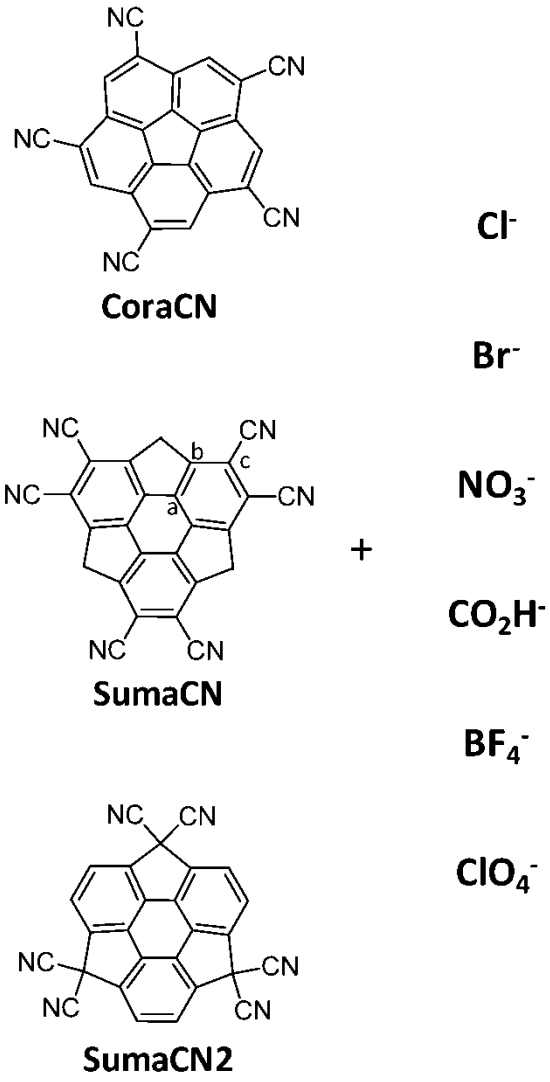


Figure 9.1. Combination of buckybowls and anions forming the complexes studied in this work.

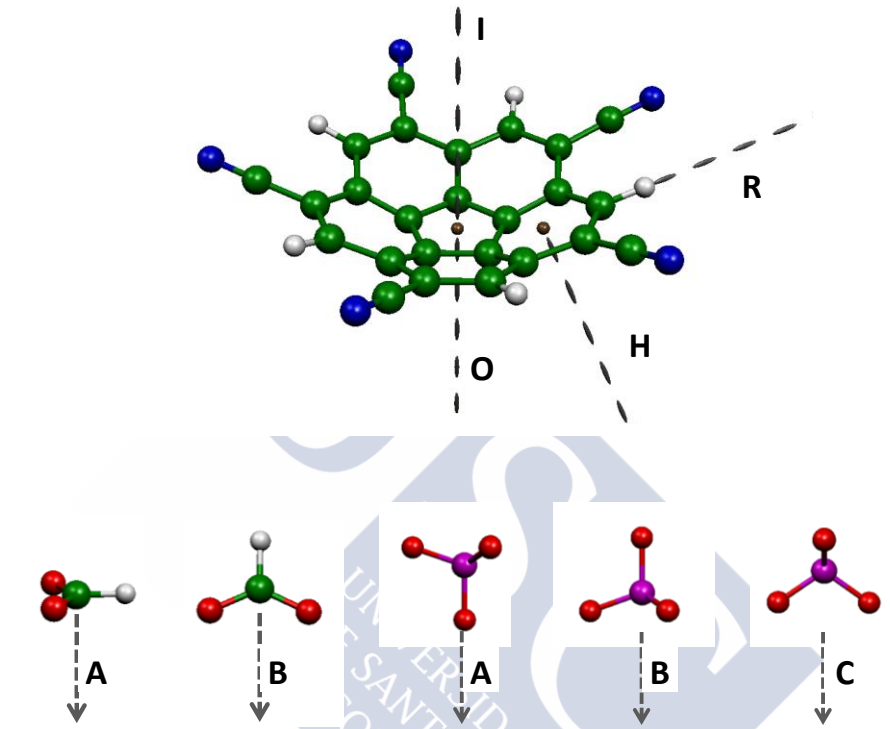


Figure 9.2. Representation of the set of different approaching lines (top) to the bowl and different orientations (bottom) of the anions employed in this work. Similar approaching lines are also used in the other buckybowls.

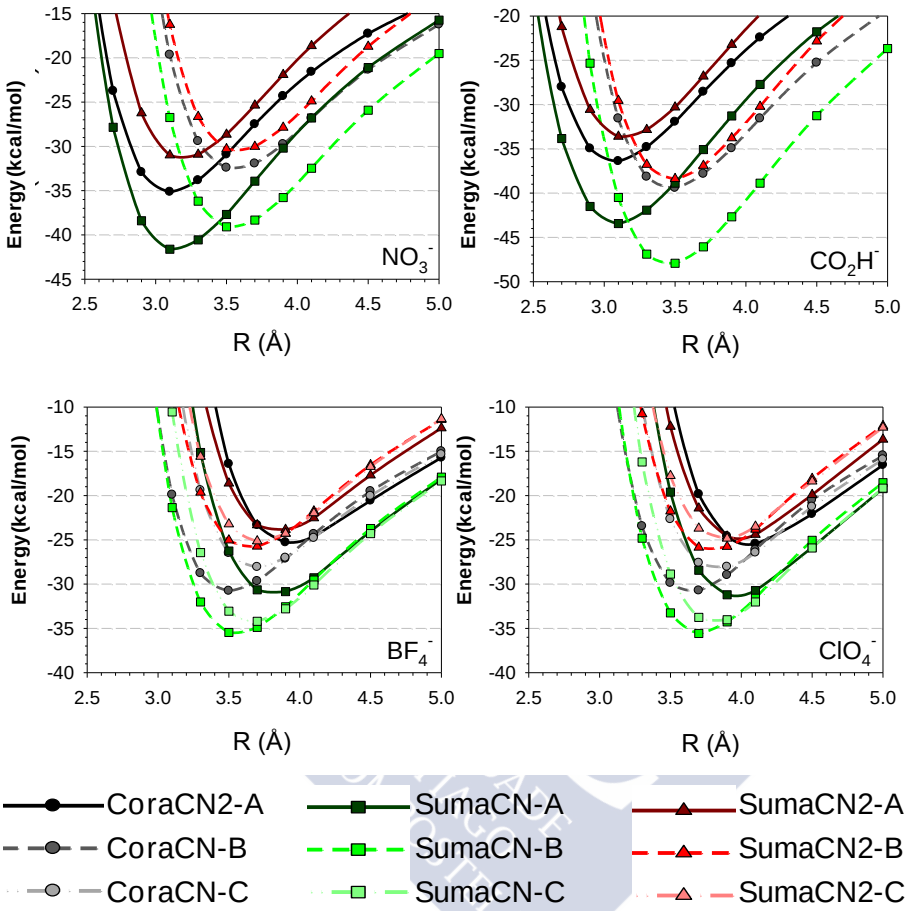


Figure 9.3. Effect of the orientation of the anion upon the interaction energy profiles in complexes formed employing the **I** approaching line obtained at the M06-2X/6-31+G* level of calculation.

An analysis of the electron density has been carried out by using the non-covalent interaction index (NCI).[49] NCI is an index based on the analysis of the reduced density gradient that can be employed to visualize both favorable and unfavorable interactions. These interactions can be graphically displayed as a plot of the product of the second eigenvalue of the hessian of the density times the density (sign(λ_2) ρ), mapped onto an isosurface of reduced density gradient.[49, 50]

In order to estimate solvent effects upon the characteristics of the complexes studied, the interaction energies for the complexes have been obtained by using a polarizable continuum model (C-PCM), within the framework of the conductor-like screening model,[51] as implemented in Gaussian09.[52-54] Thus, employing gas-phase equilibrium geometries, the interaction energies are obtained in a series of solvents with varying dielectric constant. The BSSE is corrected by assuming that its value is the same obtained in a gas-phase calculation.[32, 34]

All SAPT calculations have been performed with Molpro 2010.1.[55] M06-2X calculations have been done with Gaussian09,[54] whereas MP2 calculations have been performed with Turbomole 6.3.[56] In order to save computational time in MP2 calculations, the resolution of the identity approach has been employed both for the HF and correlation energies. That is; RI-JK-MP2 calculations have been performed using the aug-cc-pVXZ auxiliary basis set for correlation and the def2-TZVPP auxiliary basis set for both coulomb and exchange in the calculation of HF energies.[57, 58]

9.3. Results

As commented above, the interaction energy of the different buckybowl···anion complexes has been obtained by using a variety of approaching lines, as well as different orientations of the polyatomic anions. In the following sections, the effect of these variables upon the characteristics of the interaction will be analyzed.

9.3.1. Orientation dependence

Figure 9.3 shows the energy profiles obtained when the anions approach the buckybowls employing different orientations of the anions (of course only polyatomic ones are considered). For the sake of brevity, only results for the **I** line are shown; that is, for complexes formed with the anion following the symmetry axis of the bowl by the concave face. It can be observed in Figure 9.3 that in nitrate complexes the most stable orientation corresponds to the anion parallel to the bottom of the bowl (**A** in Figure 9.2) for any of the bowls considered. As it can be observed in Table 9.1, that lists the interaction energy values for all complexes studied with trigonal anions at the M06-2X/6-31+G* and SCS-MP2/CBS levels, the interaction of nitrate anion with CoraCN and SumaCN in orientation **A** is stronger by around 2.5 kcal/mol with respect to complexes with nitrate in orientation **B**. On the other hand, complexes with SumaCN2 show similar

interaction energies (0.5 kcal/mol difference) irrespective of the orientation of the anion. The preference for nitrate to interact parallel to the bottom of the bowl can be understood considering that, in that way, the three negatively charged oxygen atoms can contact with the positively charged phenyl rings of the bowls. In orientation **B** only two such contacts are possible. In SumaCN2, the presence of the CN groups pointing to the concave face of the bowl introduces some repulsion with the negative oxygen atoms, so the energy differences between the two orientations decrease.

Formate complexes behave differently, being more stable when approaching with orientation **B** (see Table 9.1 and Figure 9.3). When the anion approaches parallel to the bottom of the bowl, the interaction energy is around 3 to 6 kcal/mol less negative. This behavior can be explained considering that the hydrogen atom in formate anion bears positive charge, whereas the oxygens carry larger negative charge than in nitrate. Therefore, in parallel orientation, the hydrogen atom is oriented towards regions of positive electrostatic potential, destabilizing the complex. When the anion is oriented perpendicular to the bowl (**B**) both oxygen atoms point towards the positive regions of the bowl. Since oxygen atoms are more negative in formate than in nitrate, the interaction is stronger with the former one, as clearly observed in Figure 9.3. As a consequence of the larger interaction, formate anion goes deeper into the bowl as indicated by the equilibrium distances in Table 9.1.

In the case of the two tetrahedral anions considered in this study, the results are also shown in Figure 9.3, with the full set of energies and equilibrium distances listed in Table 9.2. Considering the data shown in Figure 9.3, it can be observed that the most stable orientation is **B**, with the three equivalent B-F or Cl-O groups pointing to the bowl (see Figure 9.2). Complexes with the anion in orientation **C**, with two B-F or C-O groups towards the bowl are slightly less stable (1-2 kcal/mol), whereas orientation **A**, with one B-F or Cl-O bond pointing toward the bowl is clearly less stable, with differences reaching 3-4 kcal/mol. Therefore, as more negatively charged atoms are close to the inner surface of the bowl, the interaction becomes stronger. In SumaCN2 the three orientations considered provide very similar interaction energies due to the steric hindrance of the CN groups, which is smallest in orientation **A**, with only one bond pointing toward the bottom of the bowl. The same behavior is observed by the outer face of the bowls, though when the anion contacts with the rim of the bowl (**R**), orientation **C** is favored because the hydrogen bond is more effectively formed. Summarizing, the orientation of the anion as approaches the bowl moderately affects the complex stability, so tetrahedral anions will orientate as in **B**, whereas the preference for parallel or perpendicular approach in trigonal anions depends on its nature. Formate prefers orientation **B**, whereas nitrate is more stable in orientation **A**. In the following, only the most stable orientation for each complex will be considered for discussion.

Table 9.1. Equilibrium distances and interaction energies, in kcal/mol, for complexes formed with trigonal anions employing different approaching lines.

			NO_3^-			CO_2H^-		
			R (Å)[(a)]	M062X/ 6-31+G*	SCS-MP2/ CBS	R (Å)[(a)]	M062X/ 6-31+G*	SCS-MP2/ CBS
CoraCN	**I**	**A**	3.103	-35.15	-35.30	3.074	-36.43	-35.50
		B	3.557	-32.53	-32.80	3.467	-39.47	-38.54
	O	**A**	2.816	-26.76	-27.50	2.808	-27.63	-27.36
		B	3.340	-25.95	-25.88	3.186	-31.81	-30.94
	H	**A**	2.851	-25.88	-26.30	2.790	-27.45	-26.66
		B	3.391	-22.55	-22.65	3.287	-29.39	-28.41
	R	**A**	2.246	-8.36	-8.15	2.256	-9.83	-8.90
		B	2.354	-16.28	-15.70	2.302	-22.03	-20.43
SumaCN	**I**	**A**	3.130	-41.66	-41.66	3.094	-43.44	-42.30
		B	3.540	-39.16	-39.23	3.45	-48.02	-46.63
	O	**A**	2.862	-31.09	-32.15	2.809	-32.89	-32.88
		B	3.341	-31.68	-31.81	3.181	-38.60	-37.71
	H	**A**	2.917	-27.76	-28.56	2.875	-28.20	-28.05
		B	3.389	-25.41	-25.73	3.291	-32.06	-31.59
	R	**A**	2.165	-12.76	-13.73	2.185	-14.52	-14.79
		B	2.338	-18.87	-19.00	2.286	-25.70	-24.76
SumaCN2	**I**	**A**	3.188	-31.38	-30.81	3.143	-33.69	-31.91
		B	3.575	-30.53	-30.23	3.482	-38.40	-36.70
	O	**A**	2.872	-20.57	-22.17	2.818	-22.47	-22.99
		B	3.347	-21.86	-22.49	3.184	-28.26	-27.94
	H	**A**	2.938	-18.24	-19.24	2.889	-19.26	-19.18
		B	3.423	-16.82	-17.27	3.323	-22.82	-22.55
	R	**A**	2.114	-14.46	-15.26	2.198	-14.81	-15.03
		B	2.405	-16.55	-16.49	2.351	-21.77	-20.81

(a) Interpolated from M06-2X/6-31+G* curves

Table 9.2. Equilibrium distances and interaction energies, in kcal/mol, for complexes formed with tetrahedral anions employing different approaching lines.

			BF_4^-			ClO_4^-		
			R (Å)[(a)]	M062X/ 6-31+G*	SCS-MP2/ CBS	R (Å)[(a)]	M062X/ 6-31+G*	SCS-MP2/ CBS
CoraCN	I	A	3.928	-25.30	-25.32	4.064	-25.50	-27.29
		B	3.500	-30.77	-29.12	3.641	-30.86	-31.46
		C	3.694	-28.08	-27.28	3.823	-28.24	-29.44
	O	A	3.954	-19.04	-18.67	4.085	-18.80	-19.47
		B	3.215	-23.87	-23.04	3.374	-23.07	-24.11
		C	3.494	-21.83	-21.43	3.612	-21.52	-22.53
	H	A	3.972	-17.66	-17.49	4.112	-17.28	-18.00
		B	3.250	-23.08	-22.02	3.410	-22.38	-23.00
		C	3.585	-20.01	-19.75	3.713	-19.59	-20.55
	R	A	3.256	-8.86	-8.57	3.405	-8.16	-8.29
		B	2.430	-8.90	-7.31	2.755	-6.98	-6.92
		C	2.581	-11.67	-10.55	2.733	-11.28	-10.75
SumaCN	I	A	3.805	-31.10	-30.95	3.956	-31.31	-33.31
		B	3.554	-35.59	-33.85	3.706	-35.57	-36.30
		C	3.660	-34.26	-33.01	3.809	-34.31	-35.35
	O	A	3.825	-25.01	-24.49	3.998	-24.48	-25.12
		B	3.244	-28.75	-28.19	3.415	-27.65	-28.90
		C	3.481	-27.42	-27.04	3.608	-26.95	-27.99
	H	A	3.987	-20.29	-20.13	4.132	-19.83	-20.58
		B	3.300	-25.25	-24.69	3.467	-24.42	-25.38
		C	3.572	-23.18	-23.01	3.699	-22.67	-23.76
	R	A	3.245	-10.36	-10.73	3.384	-9.65	-10.68
		B	2.343	-14.68	-13.63	2.541	-12.76	-13.29
		C	2.496	-14.82	-14.40	2.658	-14.35	-15.02

(a) Interpolated from M06-2X/6-31+G* curves

Table 9.2 (continuation). Equilibrium distances and interaction energies, in kcal/mol, for complexes formed with tetrahedral anions employing different approaching lines.

			BF_4^-			ClO_4^-		
			R (Å)[(a)]	M062X/ 6-31+G*	SCS-MP2/ CBS	R (Å)[(a)]	M062X/ 6-31+G*	SCS-MP2/ CBS
SumaCN2	I	A	3.830	-23.97	-23.30	3.978	-24.83	-25.95
		B	3.640	-25.85	-24.01	3.787	-26.18	-26.36
		C	3.715	-25.15	-23.51	3.866	-24.88	-25.38
	O	A	3.839	-15.55	-15.50	4.012	-15.13	-16.19
		B	3.254	-18.75	-18.74	3.428	-17.68	-19.49
		C	3.491	-17.60	-17.71	3.618	-17.16	-18.71
	H	A	4.028	-11.80	-11.93	4.174	-11.47	-12.42
		B	3.326	-16.19	-15.91	3.491	-15.53	-16.62
		C	3.609	-14.15	-14.26	3.739	-13.81	-15.05
	R	A	3.274	-12.11	-12.19	3.426	-11.31	-11.87
		B	2.317	-16.24	-15.30	2.482	-14.40	-14.76
		C	2.589	-14.30	-13.96	2.739	-13.49	-13.90

(a) Interpolated from M06-2X/6-31+G* curves

Table 9.3. Equilibrium distances and interaction energies, in kcal/mol, for complexes formed with monoatomic anions employing different approaching lines.

		Cl^-			Br^-		
		R (Å)[(a)]	M062X/ 6-31+G*	SCS-MP2/ CBS	R (Å)[(a)]	M062X/ 6-31+G*	SCS-MP2/ CBS
CoraCN	I	3.048	-36.97	-37.61	3.218	-35.39	-35.96
	O	2.895	-29.53	-29.30	3.083	-27.71	-27.29
	H	3.004	-26.32	-26.37	3.183	-24.71	-24.58
	R	2.212	-16.38	-16.22	2.374	-13.83	-13.09
SumaCN	I	2.971	-45.29	-45.62	3.157	-43.46	-43.70
	O	2.887	-35.55	-35.74	3.076	-33.54	-33.48
	H	3.067	-28.18	-28.72	3.248	-26.57	-27.01
	R	2.075	-20.72	-21.23	2.298	-18.38	-18.29
SumaCN2	I	2.976	-37.33	-37.13	3.164	-35.40	-34.85
	O	2.886	-25.66	-26.22	3.076	-23.66	-24.03
	H	3.112	-18.63	-19.30	3.291	-17.26	-17.80
	R	2.215	-20.34	-20.76	2.357	-18.26	-18.25

(a) Interpolated from M06-2X/6-31+G* curves

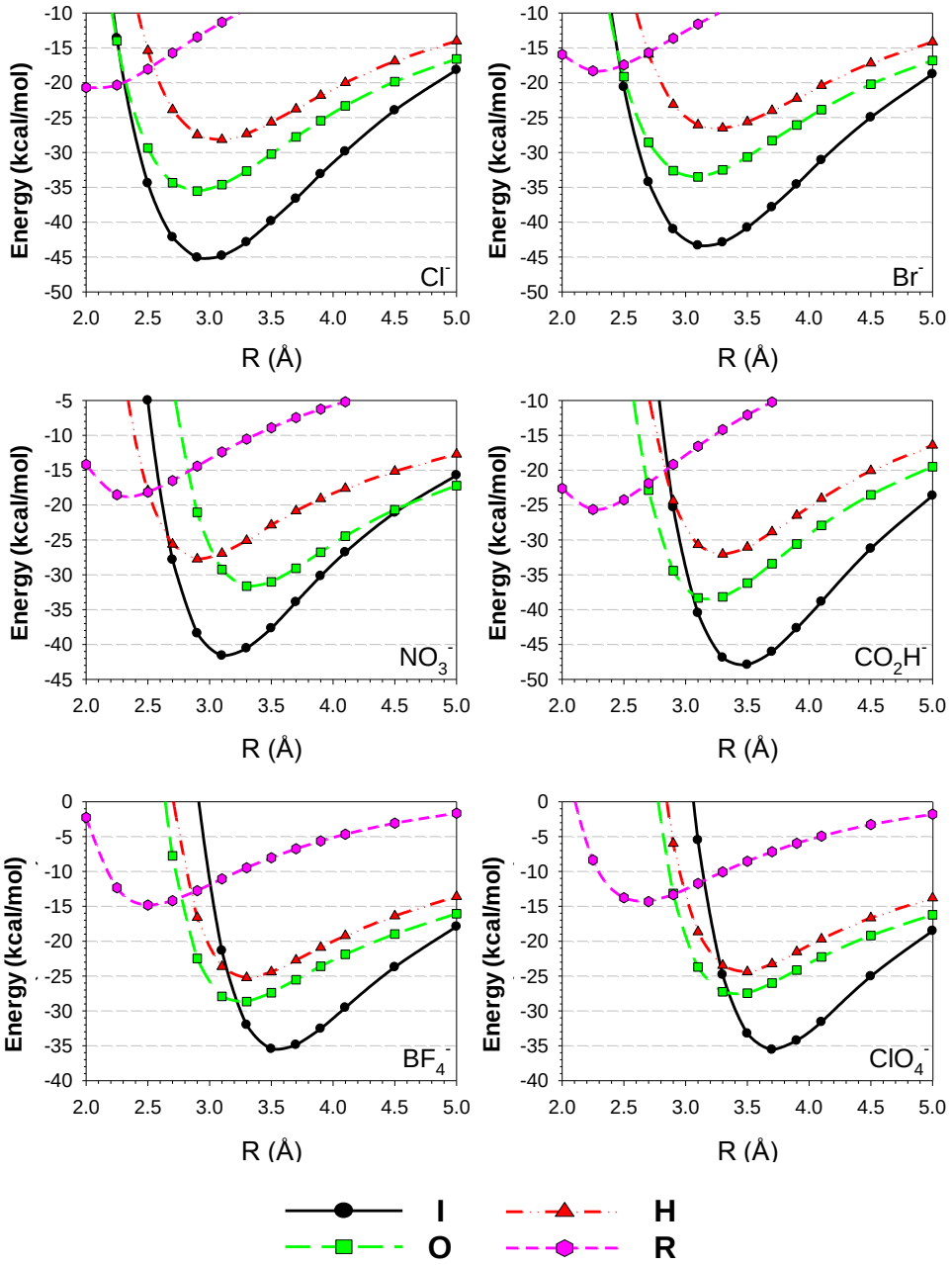


Figure 9.4. Effect of the approaching line upon the interaction energy profiles in complexes formed by SumaCN bowl and the most stable orientation obtained at the M06-2X/6-31+G* level of calculation.

9.3.2. Effect of the approaching line

Figure 9.4 shows how the interaction energy changes depending on the line employed for getting the bowl and the anion closer (Data in Tables 9.1, 9.2 and 9.3). In agreement with previous work with Cl^-,[23] complexes are more stable by the concave face of the bowl than by the convex side. The same behavior is observed with all anions considered. It has to be taken into account that the interaction is electrostatically favored by the concave face, which exhibits more positive molecular electrostatic potential.[23, 24] Besides, the proximity of a larger number of atoms makes dispersion grow, also favoring concave complexation. When the anion approaches by the convex face of the bowl following the symmetry axis (**O**), the interaction energy decreases noticeably, with changes around 10 kcal/mol in most cases. The only exceptions are the bulkiest BF_4^- and ClO_4^- anions, which show somewhat smaller energy differences (5-7 kcal/mol). This is probably related to the difficulties found for these anions for approaching more closely to the bowl face, thus leading to less negative interaction energies. Approaching the anions by the center of the hexagonal faces on the rim of the bowls decreases even more the interaction energy of the complexes in all cases, as observed in Figure 9.4. Again, as the anion becomes bulkier the interaction energy becomes more insensitive to the specific approaching line employed. Finally, when the anions approach the rim of the bowl, so a hydrogen bond between a C-H group and the anion can be formed (**R**), the stabilization is the smallest observed among the lines employed. Therefore, even though the electrostatic interaction with the positively charged hydrogen atoms should be favorable, there seems that the lack of contact with the surface of the bowl avoids a larger stabilization. This happens even for complexes with the most polarizing anions as Cl^- or CO_2H^-, where the hydrogen bond is expected to be strongest. Therefore, it can be assumed that in all cases, effective encapsulation of the anion by the concave side of the bowl is achieved, other possible rearrangements being not competitive.

9.3.3. Anion and bowl dependence

Figure 9.5 shows the energy profile for complexes formed by the buckybowls and the anions studied. Only the most stable orientation of the anion and the **I** approaching line (the most stable one) are presented. Considering monoatomic anions, chloride complexes are always more stable than bromide ones, as expected taking into account the smaller size and larger polarizing power of the former. Thus, at the SCS-MP2/CBS level of calculation Cl^- complexes show interaction energies of -37.6, -45.2 and -37.3 kcal/mol for CoraCN, SumaCN and SumaCN2, respectively, whereas in the case of Br^- complexes, the interaction energies amount to -36.0, -43.7 and -34.9 kcal/mol. On the other hand, tetrahedral anions form the least stable complexes, in line with their larger size. Thus, complexes with ClO_4^- show interaction energies of -36.3 and -31.5 kcal/mol with SumaCN and CoraCN, respectively. Complexes formed with BF_4^- show a similar behavior, with interaction energies slightly less negative (around 2 kcal/mol). Contrary

to what it has been observed in monoatomic anion complexes, complexes with BF_4^- and ClO_4^- are significantly less stable when formed with SumaCN2 as compared with CoraCN, so the interaction energies round -26 and -24 kcal/mol for ClO_4^- and BF_4^-, respectively. This decrease in the interaction is also observed in other approaching lines and seems related to steric hindrance.

As regards NO_3^- complexes, they show an intermediate stability, though closer to Br^- complexes than to tetrahedral ones. The most striking behavior corresponds to CO_2H^- anion, which forms the most stable complexes among the systems studied, being clearly more stable than chloride ones by around 2 kcal/mol. In fact, at the SCS-MP2/CBS level the interaction of CO_2H^- with the bowls considered in this study amounts to -38.5, -46.6, and -36.7 kcal/mol for CoraCN, SumaCN, and SumaCN2, respectively. The structurally similar NO_3^- anion forms complexes around 5 kcal/mol less stable with sumanene derivatives, whereas for corannulene ones, the energy differences amount to about 3 kcal/mol.

Therefore, the interaction strength changes with the anion nature in the following sequence: $CO_2H^- > Cl^- > Br^- > NO_3^- >> ClO_4^- > BF_4^-$. This is as expected taking into account the size and polarizing power of the anions. The behavior of CO_2H^- should be related to the large negative charge carried by the two oxygen atoms, which allows establishing two strong contacts with the positively charged regions of the bowl (CO_2H^- has the larger basic character).

The effect of the nature of the bowl upon the interaction is also reflected in Figure 9.5. In agreement with previous results obtained for chloride complexes, the interaction is strongest with SumaCN, followed by CoraCN, and SumaCN2 forming the least stable complexes. This trend follows the values of the Molecular Electrostatic Potential of the bowls, which are more positive in SumaCN.[23] It is worth noting that only BF_4^-, ClO_4^- and NO_3^- exhibit significant differences in the stability of complexes formed with CoraCN and SumaCN2 (6 kcal/mol more stable with CoraCN for tetrahedral anions; around 2 kcal/mol for NO_3^-). The results seem to indicate that apart from the MEP value (which is similar in both bowls), steric effects are also important. Therefore, in complexes formed with the bulkier anions, steric repulsion with the CN groups in SumaCN2 destabilizes the complexes, whereas for smaller anions there is no such effect.

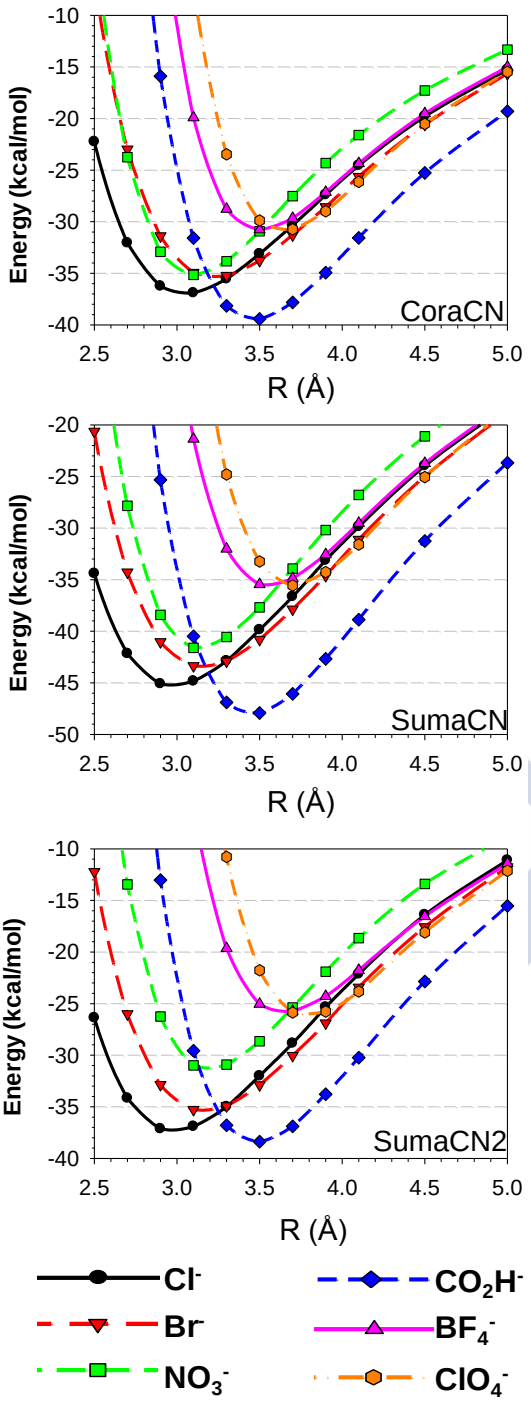


Figure 9.5. Effect of the anion upon the interaction energy profiles in complexes formed employing the **I** approaching line and the most stable orientation obtained at the M06-2X/6-31+G* level of calculation.

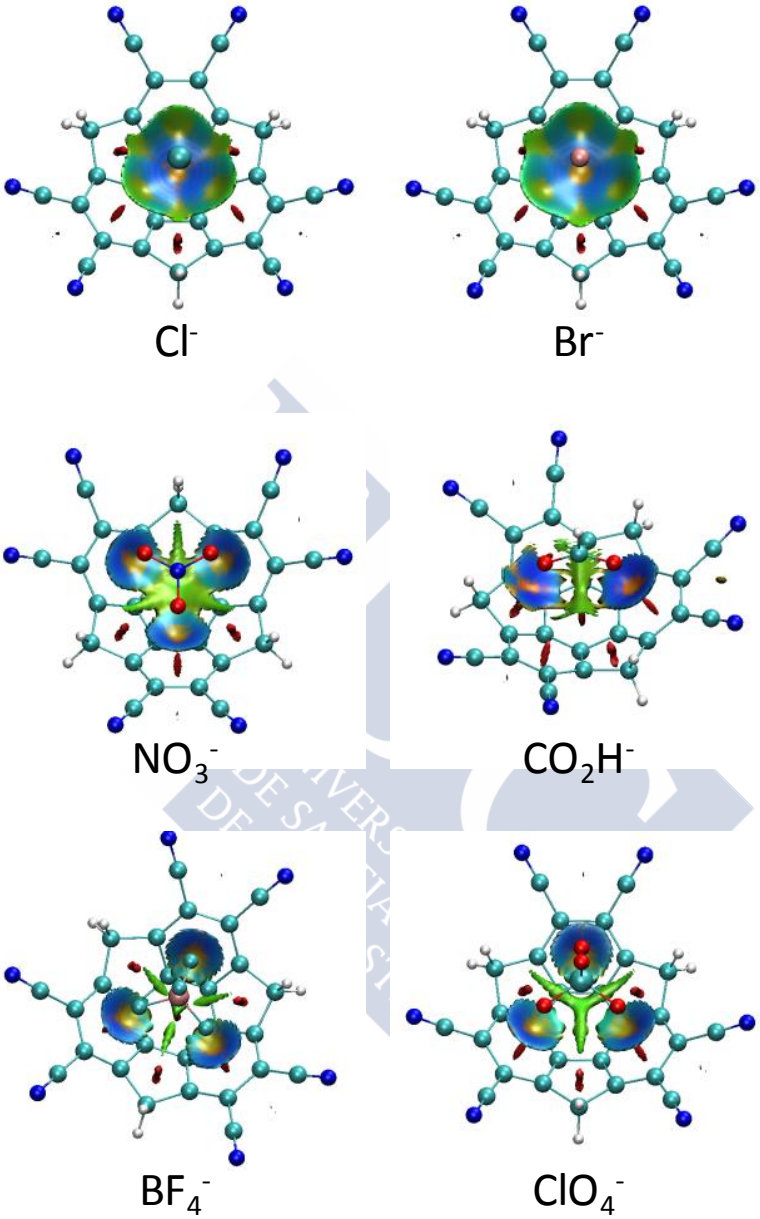


Figure 9.6. NCI plots for the complexes formed by SumaCN and the anions studied. Only complexes by the **I** line and the most stable orientation are shown. The product of the density times the sign of the second eigenvalue of its hessian is mapped onto an isosurface of reduced density gradient with value 0.5 a.u. The color scale goes from -0.015 a.u. (blue) to 0.015 a.u. (red).

9.3.4. NCI Analysis

Figure 9.6 shows the non-covalent interaction NCI plots for complexes formed with SumaCN. NCI maps the product of the sign of the second eigenvalue of the hessian of the density times the density onto an isosurface of reduced density gradient, allowing a graphical display of the most relevant stabilizing (blue) and destabilizing (red) interaction in a system.[49, 50] Considering the plots in Figure 9.6, a region of stabilizing interactions can be observed for Cl^- complexes, corresponding to the six interactions of the anion with the central carbons of the sumanene derivative. This attractive region extends over the six C_a atoms (see Figure 9.1), corresponding to six equivalent bond critical points with density of 0.0106 a.u. according to Atoms in Molecules theory.[59] Bromide complex shows a similar plot, though it can be already appreciated in Figure 9.6 that the interaction is slightly weaker (lighter blue), in accordance with the smaller values of the critical points (0.0098 a.u.). The plot is more complex for trigonal anions which, in addition, show two different orientations. NO_3^- complex shows three attractive regions roughly corresponding to contacts with the three phenyl rings in SumaCN. These three regions are associated to a set of six bond critical points with density of 0.0111 a.u. The different orientation of the most stable complex with CO_2H^- anion (**B**) gives rise to a different pattern, with two pairs of bond critical points connecting the anion with the C_b atoms of the pentagonal (0.0124 a.u.) and hexagonal (0.0125 a.u.) rings. An attractive interaction between the anion and the hydrogen atom of the CH_2 group can also be observed in the NCI plot. Finally, for BF_4^- and ClO_4^- complexes the behavior is similar. In the most stable orientation three oxygen atoms point to three different phenyl rings, so three attractive regions are displayed in the NCI plot. These attractive regions are related to a set of six bond critical points connected to the C_c atoms, with densities of 0.0114 a.u. for BF_4^- and 0.0113 a.u. for ClO_4^-.

CoraCN and SumaCN2 complexes show similar NCI plots (Appendix D). The largest qualitative difference is observed for SumaCN2 complexes which also display areas of weak interaction which extend towards the CN groups. These regions are already observed in Cl^- complex, becoming larger as the size of the anion increases, and they are probably associated to the steric hindrance experienced by the anions due to the disposition of the CN groups, as commented above. Therefore, these plots allow identifying the main attractive interactions established and qualitatively obtaining information about the intensity of the interaction.

9.3.5. SAPT(DFT) Energy Analysis

Figure 9.7 summarizes the results of the Symmetry Adapted Perturbation Theory calculations for the most stable complexes formed by each bowl with the anions considered in this study. In agreement with previous work,[23] in the complex formed by Cl^- anion and CoraCN the largest contribution to the interaction energy is the electrostatic one, reaching -41 kcal/mol, with contributions from induction and

dispersion reaching -14 and -13 kcal/mol, respectively. Due to the large cancellation of electrostatic and repulsion contribution, the stability of the complex mainly comes from the combined effect of dispersion and induction. When bromide is coordinated to CoraCN, there is an increase in repulsion relative to Cl^- complex as a consequence of the larger size of the anion. Dispersion slightly increases due to the same reason, whereas induction decreases by a similar amount (this could be related with the slightly larger equilibrium distance in Br^- complex). On the other hand, the electrostatic contribution increases with respect to that observed in chloride complex. A priori, the opposite effect would be expected, due to the longer equilibrium distance but, as indicated in previous work,[23] the electrostatic contribution comes to a significant extent from penetration effects and this could be the reason of the larger electrostatic contribution in bromide complex. Chloride and bromide complexes with SumaCN and SumaCN2 show the same behavior already described for CoraCN. Therefore, in all cases there are increments in the electrostatic, induction and dispersion contributions, though partially cancelled out by the increment in repulsion.

Nitrate complexes with CoraCN and SumaCN show a large electrostatic contribution together with significant repulsion, though it must be taken into account that the balance of these two contributions is less favorable than for both Cl^- and Br^- complexes. Induction is of similar magnitude as in complexes with monatomic anions, whereas dispersion exhibits a significant increase as a consequence of the larger size of nitrate anion and the close proximity to the walls of the bowl in orientation **A**. In the complex with SumaCN2 the repulsion contribution undergoes a large increase together with a small decrease in electrostatic contribution, so the combination of these first-order terms gives an overall balance of +7 kcal/mol (-6 kcal/mol in SumaCN). Dispersion and induction contributions partially cancel this effect showing increments of around 1-2 kcal/mol each with respect to SumaCN complex. The large repulsion contribution has its origins in the unfavorable interaction with the CN groups close to the oxygen atoms of the nitrate anion in orientation **A**. CO_2H^- anion forms the most stable complexes among all anions studied as a consequence of the large electrostatic contribution observed, just a bit smaller than in Br^- complexes. This, together with a significant increase in the induction contribution and also large dispersion, overcomes the larger repulsion consequence of the short distances between the oxygen atoms of the anion in orientation **B** and the carbon atoms of the bowl.

Tetrahedral anion complexes exhibit almost the same characteristics for a given buckybowl. Thus, the energy contributions are almost the same for both anions, though dispersion is always larger for ClO_4^-, being the reason of the larger stability of its complexes as compared with BF_4^- ones. Electrostatic contributions are the smallest ones observed among the different complexes, as also happens to induction.

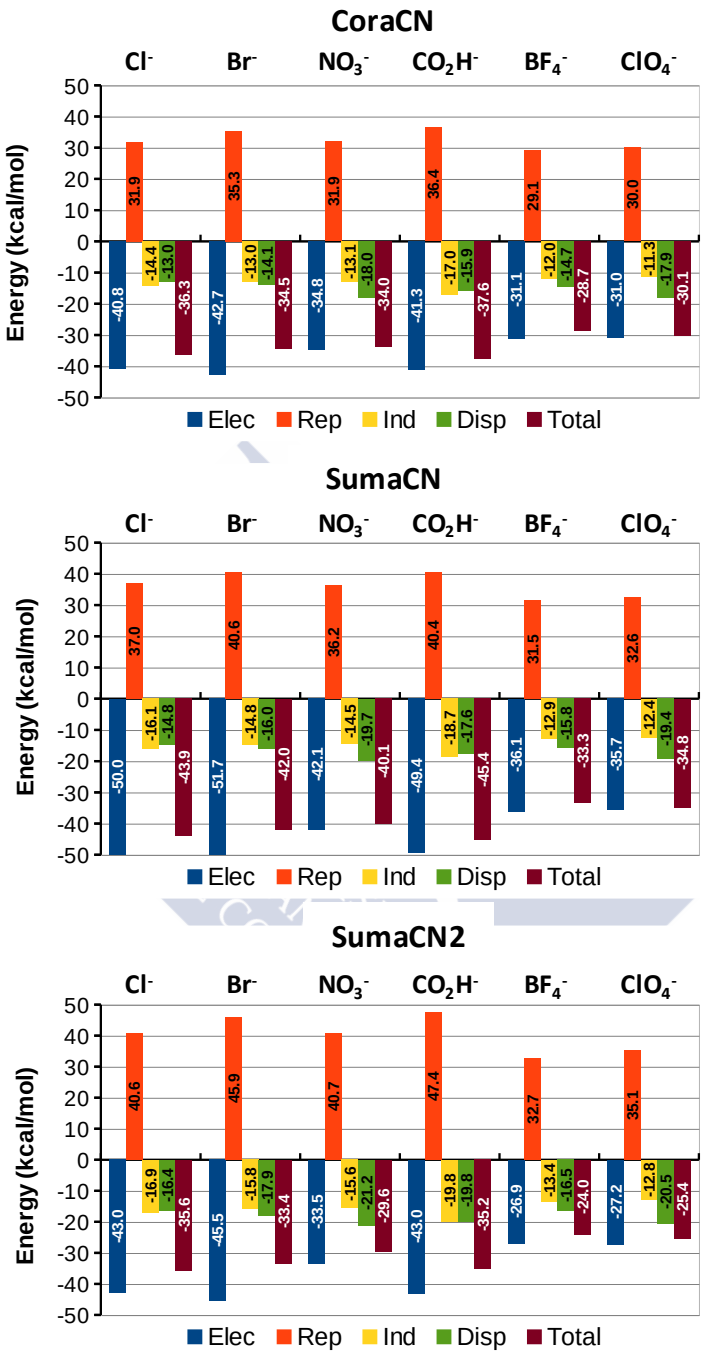


Figure 9.7. SAPT(DFT) decomposition of complexes formed employing the **I** approaching line and the most stable orientation.

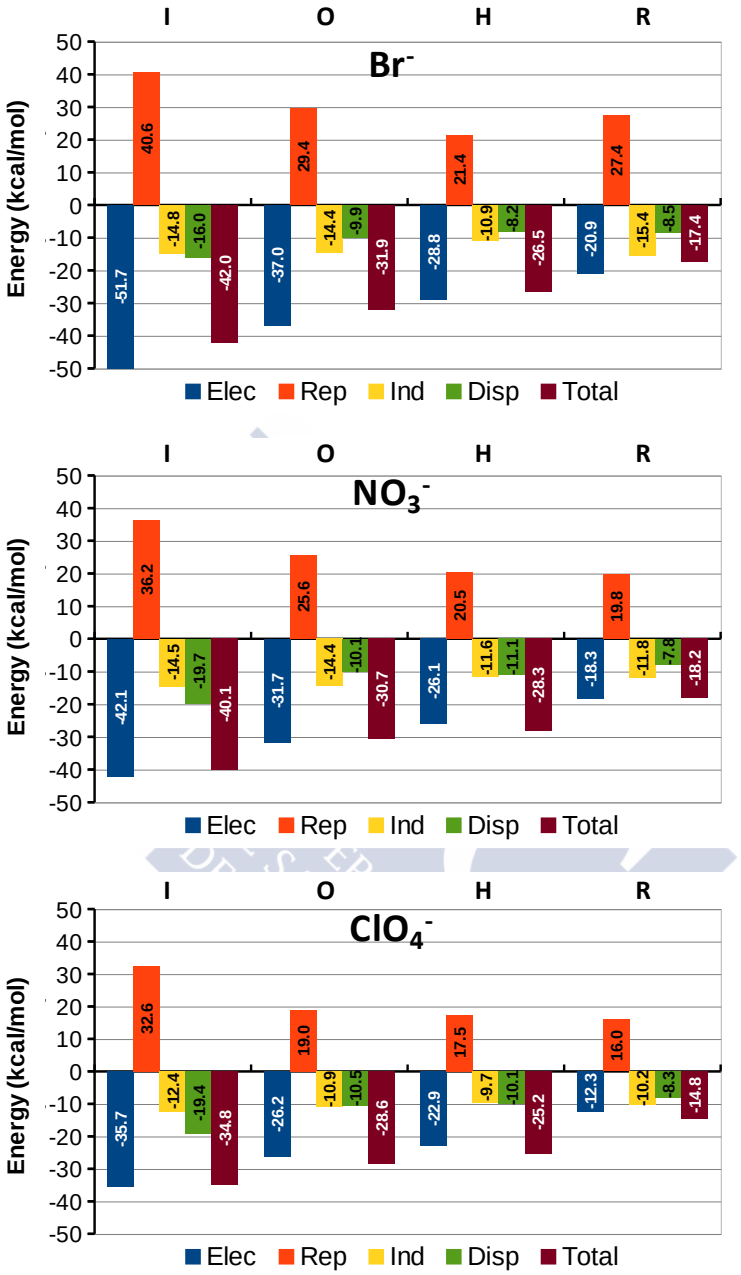


Figure 9.8. SAPT(DFT) decomposition of complexes formed with Br^-, NO_3^-, ClO_4^- and SumaCN along different approaching lines employing the most stable orientation.

On the other hand, for these bulky anions dispersion is large, only nitrate complexes showing larger dispersion contributions. Even though large repulsion contributions could be expected, these anions are located further away than smaller ones so repulsion is not as large as for other anions. Thus, repulsion contribution is the smallest among complexes studied, but its relative weight is the largest.

Figure 9.8 explains the preference for **I** orientation over other possibilities. When the anion approaches the bowl by the central ring of the convex face of the bowl (**O**), there is a sharp decrease on electrostatic contribution relative to **I**, since the MEP by the convex face of the bowls is less positive. Repulsion also decreases since there are few atoms close by, but the combination of both contributions already favors by 3 kcal/mol the formation of the Br^- complex by the concave side. However, as the size of the anion grows, the combination of electrostatic plus repulsion becomes more favorable to the **O** complex (see results for ClO_4^-). Induction shows similar contributions by both faces of the bowl (**I** and **O**), while dispersion decreases by 6-10 kcal/mol for the **O** structures. Complexes by the **H** line are even less stable since all contributions diminish, especially the electrostatic (and induction) one. When the anion interacts directly with a C-H group (**R**) forming a hydrogen bond to the rim of the bowl, the electrostatic contribution is the smallest one observed for the different attacking lines. Dispersion also decreases, as expected taking into account the larger distances to other atoms. This, combined with a repulsion larger than the electrostatic contribution makes these complexes the least stable ones among those considered in this work.

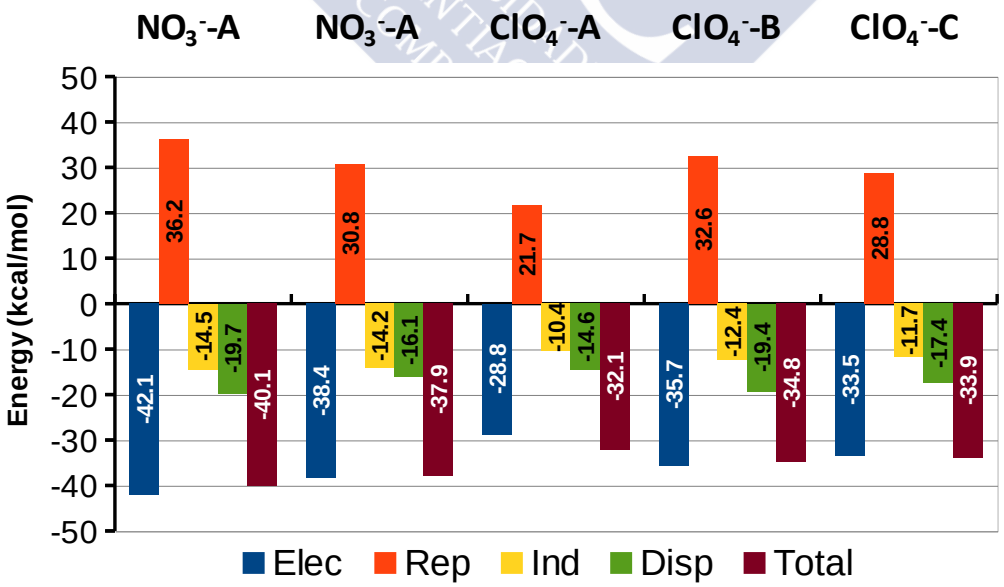


Figure 9.9. SAPT(DFT) decomposition of complexes formed with NO_3^-, ClO_4^- and SumaCN employing different anion orientation and the **I** approaching line.

The source of the orientation dependence of the interaction energy can be analyzed in Figure 9.9**,** which shows the effect of the orientation of the anion on the interaction when approaching SumaCN by the **I** line. In the case of nitrate complexes, orientation **A** introduces more repulsion since the three oxygen atoms are closer to the bowl (only two in **B**). The larger repulsion in **A** is compensated by larger dispersion and electrostatic contributions, the result being that minimum **A** is favored. In fact, it is the larger contribution from dispersion which makes the formation of the **A** complex more favorable (in the case of CO_2H^- induction is what makes **B** more stable). In ClO_4^- complexes orientation **B** is the most stable one because, despite the larger repulsion contribution, it maximizes the stabilizing contributions, reaching the largest values for electrostatic, dispersion and induction.

9.3.6. Solvent Effect

The interaction energies for the complexes studied have been obtained in different solvents by applying the C-PCM method at the M062X/6-31+G* level. The presence of a dielectric medium has a deep impact onto the energetics of the complexes, but in all cases the most stable structures still correspond to complexes formed by the **I** line and, overall, the stability order obtained for the different attacking lines is the same as observed in the gas phase. Solvent effect is larger in complexes formed with the concave face of the bowl, where the anion has to desolvate to a larger extent since part of its surface is contacting with the bowl. On the other hand, **R** complexes are the least penalized since almost the whole anion surface is still exposed to the solvent. Despite this, the stability differences observed in the gas phase are so large that no changes in the stability order due to the solvent depending on the attacking line have been observed. Therefore, Table 9.4 only shows **I** complexes in a series of solvents with varying dielectric constant for the most stable orientation of the anion.

Complexes formed with CoraCN in toluene already exhibit significant changes with respect to the values obtained in the gas phase despite the low dielectric constant of the solvent. Thus, complexation energies decrease by around one half in all cases with respect to the gas phase, so the most stable complexes barely reach -19 kcal/mol. Further decreases are observed as the dielectric constant of the solvent increases, and already in chloroform the interaction energies are around one third of the gas phase values. In dimethylchloride and solvents with larger dielectric constants the interaction energies stabilize in values around 20-15 % of the original gas phase values.

Thus, in water, complexation energies hardly reach -7 kcal/mol for any of the complexes with CoraCN. SumaCN complexes also show similar changes as the solvent becomes more polar. However, as in the gas phase, complexes formed with SumaCN are more stable than those formed with CoraCN. In chloroform, the most favorable complexes exhibit complexation energies around -15 to -16 kcal/mol, which reduce even more and hardly reach -9 kcal/mol at most in water. Complexes of Br^- and Cl^- with

SumaCN2 show similar values to those obtained in SumaCN as the dielectric constant of the solvent increases. Polyatomic anions exhibit smaller stabilities as a consequence of the reduced size of the cavity due to the presence of the CN groups in the concave side of the bowl.

Table 9.4. M06-2X/6-31+G* interaction energies, in kcal/mol, for complexes formed employing **I** approaching line, the most stable orientations and different solvents modeled with C-PCM, as obtained at the minima of the M06-2X/6-31+G* gas-phase curves.

	Gas-phase	Toluene	$CHCl_3$	THF	$Cl_2C_2H_4$	Ethanol	DMSO	H_2O
ε	1.00	2.37	4.71	7.43	10.13	24.85	46.82	78.36
				CoraCN				
Cl^-	-36.97	-18.16	-11.46	-9.00	-7.87	-6.03	-5.44	-5.17
Br^-	-35.39	-18.42	-12.37	-10.15	-9.13	-7.47	-6.93	-6.69
NO_3^-	-35.15	-17.90	-11.68	-9.38	-8.32	-6.58	-6.03	-5.77
CO_2H^-	-39.47	-18.62	-10.88	-7.98	-6.62	-4.41	-3.70	-3.37
BF_4^-	-30.77	-15.18	-9.55	-7.45	-6.49	-4.90	-4.39	-4.16
ClO_4^-	-30.86	-16.22	-10.99	-9.06	-8.16	-6.71	-6.24	-6.03
				SumaCN				
Cl^-	-45.29	-22.96	-14.91	-11.93	-10.55	-8.31	-7.59	-7.26
Br^-	-43.46	-23.21	-15.92	-13.21	-11.97	-9.94	-9.28	-8.99
NO_3^-	-41.66	-21.62	-14.34	-11.63	-10.38	-8.34	-7.68	-7.38
CO_2H^-	-48.02	-24.16	-15.24	-11.88	-10.31	-7.74	-6.91	-6.53
BF_4^-	-35.59	-17.92	-11.51	-9.12	-8.02	-6.21	-5.63	-5.37
ClO_4^-	-35.57	-18.90	-12.96	-10.75	-9.74	-8.08	-7.55	-7.30
				SumaCN2				
Cl^-	-37.33	-18.83	-12.60	-10.36	-9.35	-7.72	-7.20	-6.96
Br^-	-35.40	-19.06	-13.57	-11.61	-10.72	-9.30	-8.85	-8.64
NO_3^-	-31.38	-14.94	-9.24	-7.17	-6.22	-4.69	-4.20	-3.98
CO_2H^-	-38.40	-17.92	-10.53	-7.78	-6.52	-4.45	-3.79	-3.48
BF_4^-	-25.85	-11.77	-6.96	-5.21	-4.41	-3.12	-2.71	-2.52
ClO_4^-	-26.18	-13.02	-8.59	-7.00	-6.27	-5.11	-4.74	-4.57

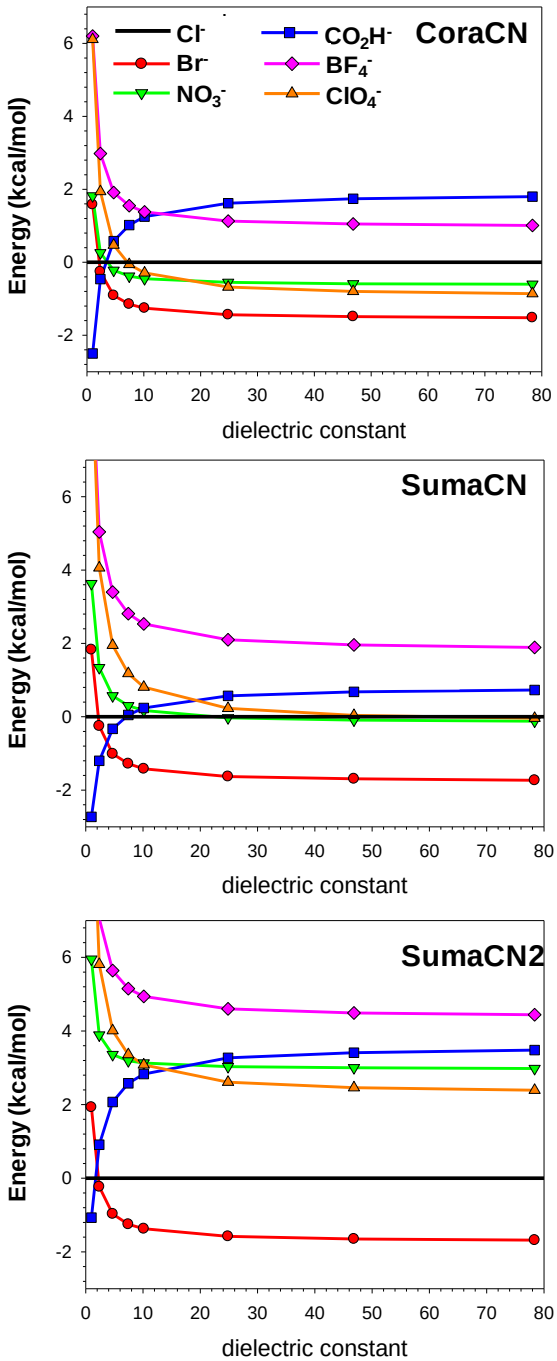


Figure 9.10. Variations in interaction energies relative to Cl^- complexes as the dielectric constant of the solvent is changed. C-PCM results obtained at the M06-2X/6-31+G* level.

However, the effect of the solvent upon the stability of a given complex is remarkably different for each anion. While bromide complex becomes the most stable complex with CoraCN as the dielectric constant grows, CO_2H^- complex is penalized to a larger extent, becoming one of the least stable complexes obtained.

Chloride and NO_3^- complexes exhibit similar interaction energies, whereas ClO_4^- complexes are relatively favored, reaching interaction energies similar to those of NO_3^- complexes. These trends are more easily seen in Figure 9.10, which shows the changes in interaction energy of the complexes as the dielectric constant changes relative to chloride complexes. As commented above, stability differences in the gas phase are quite large, spanning an energy range of around 8-12 kcal/mol. However, the incorporation of the solvent quickly decreases this range and already in chloroform it only amounts to around 4 kcal/mol. It can be observed that all anion complexes with CoraCN gain stability relative to chloride ones, except in the case of CO_2H^-, which is the most destabilized by the solvent as commented above. For dielectric constants around 10 or larger, only BF_4^- and CO_2H^- complexes are less stable than Cl^- ones; NO_3^- and ClO_4^- exhibit similar stabilities, whereas Br^- complexes are clearly the most stable ones. The same behavior is observed for SumaCN complexes, even though in this case Cl^- complexes are equally stable as NO_3^- and ClO_4^-. SumaCN2 complexes show a different behavior, and in this case only Br^- complexes are more stable than Cl^- ones, independently of the dielectric constant of the solvent.

Considering the decreases in interaction energies relative to gas phase, it becomes clear that the most destabilized complexes are CO_2H^- ones, followed by Cl^- and BF_4^- ones. On the other hand, Br^- and ClO_4^- complexes are the least affected by the presence of the solvent, while NO_3^- occupies an intermediate position. These trends are the consequence of two main factors. First, the larger the intensity of the interaction between bowl and anion in the gas phase, the larger would be the stability in solvent, as already indicated by the fact that the stability order depending on the attacking line is preserved from the gas phase. Second, the desolvation cost of the anion has the larger impact on the final energy differences. In this case, the larger the interaction in the gas phase the larger the interaction with the solvent molecules and the larger the desolvation cost. Thus, polarizing anions such as Cl^- and CO_2H^- are clearly disfavored by desolvation, whereas bulkier anions as Br^- and ClO_4^- are the ones taking the larger benefit. Overall, it can be observed that complexes formed with Br^- anion are the most stable ones, whereas the least stable are the BF_4^- ones. As regards the rest of the anions, there are changes in the order of stability depending on the solvent and the bowl considered. Overall, the presence of the solvent clearly favors complexes with Br^-, while CO_2H^- undergoes the largest destabilization becoming one of the least stable complexes

9.4. Conclusions

The characteristics of complexes formed by CN-substituted buckybowls derived from corannulene and sumanene with a set of different anions have been computationally studied by using the M06-2X/6-31+G* and SCS-MP2/CBS levels of calculation.

Despite employing different lines approaching the anions to the bowl and several orientations of the polyatomic anions, in all cases the most stable complexes correspond to the anion located on the symmetry axis of the bowl by the concave face. The interaction of the anions with the convex face of the bowl or with the hydrogen atoms of the rim of the bowl is significantly less favorable. The interaction energy does not show a significant dependence on the orientations employed for polyatomic anions though, overall, there is a preference for the largest number of atoms carrying negative charge to be oriented towards the surface of the concave face of the bowls. Thus, tetrahedral anions orient themselves with three bonds towards the bottom of the bowl. Nitrate complexes are more stable with the anion parallel to the bottom of the bowl, the oxygen atoms oriented towards the positively charged six-carbon rings. On the other hand formate complexes are more stable with the anion perpendicular to the bottom of the bowl, avoiding the interaction of the hydrogen atom with the walls of the bowl. The order of stability obtained for the different anions is the following independently of the bowl considered: $CO_2H^- > Cl^- > Br^- > NO_3^- >> ClO_4^- > BF_4^-$. Slight variations of this trend can be observed, especially in complexes formed with SumaCN2 as a consequence of the smaller size of the concave cavity of the bowl due to the presence of the CN groups.

SAPT(DFT) energy analysis indicates that in all cases the interaction is clearly dominated by the electrostatic contribution, as expected taking into account the highly positive MEP of the CN-substituted bowls. The preference for the anions to coordinate by the concave face of the bowl is a combination of more favorable electrostatic, induction and dispersion contributions. Overall, all these attractive contributions decrease as other possible approaching lines are considered.

The presence of solvent has a deep impact on the properties of the complexes, and already in solvents with low dielectric constant as chloroform, the interaction energies decrease to one third of the values in the gas phase. Solvent affects the different anions to distinct extents, so the more polarizing ones are the most affected whereas the bulkier ones register smaller decreases. Therefore, in solvents of moderate to large dielectric constant, the most stable complexes are those formed with Br^- whereas CO_2H^- is among the least favorable complexes formed.

Overall, these results help understanding the characteristics of these systems and how they could be employed for selectively catching anions playing with anion's nature and solvent effects.

9.5. References

[1] R. G. Harvey, Polycyclic aromatic hydrocarbons, Wiley-VCH, New York, **1997**.

[2] A. Hirsch, M. Brettreich, Fullerenes: chemistry and reactions Wiley-VCH, Weiheim, **2005**.

[3] S. Reich, C. Thomsen, J. Maultzsch, Carbon Nanotubes: Basic Concepts and Physical Properties, Wiley-VCH, Weiheim, **2004**.

[4] F.-G. Klarner, J. Panitzky, D. Preda, L. T. Scott. *J. Mol. Model.* **2000**, *6*, 318-327.

[5] F.-G. Klärner, T. Schrader. *Acc. Chem. Res.* **2013**, *46*, 967-978.

[6] S. Dutt, C. Wilch, T. Gersthagen, P. Talbiersky, K. Bravo-Rodriguez, M. Hanni, E. Sanchez-Garcia, C. Ochsenfeld, F.-G. Klaerner, T. Schrader. *J. Org. Chem.* **2013**, *78*, 6721-6734.

[7] R. Gomes, A. J. Parola, F. Bastkowski, J. Polkowska, F.-G. Klaerner. *J. Am. Chem. Soc.* **2009**, *131*, 8922-8938.

[8] B. Branchi, V. Balzani, P. Ceroni, M. Campana Kuchenbrandt, F.-G. Klarner, D. Blaser, R. Boese. *J. Org. Chem.* **2008**, *73*, 5839-5851.

[9] M. Fokkens, T. Schrader, F.-G. Klaerner. *J. Am. Chem. Soc.* **2005**, *127*, 14415-14421.

[10] M. A. Petrukhina, L. A. Scott, Fragments of fullerenes and carbon nanotubes, John Wiley & Sons, Inc., Hoboken, New Jersey, **2012**.

[11] M. A. Petrukhina, L. T. Scott. *Dalton Trans.* **2005**, 2969-2975.

[12] U. D. Priyakumar, G. N. Sastry. *J. Org. Chem.* **2001**, *66*, 6523-6530.

[13] A. Sygula, P. W. Rabideau. *J. Mol. Struct. (THEOCHEM)* **1995**, *333*, 215-26.

[14] M. R. Kennedy, L. A. Burns, C. D. Sherrill. *J. Phys. Chem. A* **2012**, *116*, 11920-11926.

[15] A. S. Filatov, M. A. Petrukhina. *Coord. Chem. Rev.* **2010**, *254*, 2234-2246.

[16] S. N. Spisak, A. V. Zabula, A. S. Filatov, A. Y. Rogachev, M. A. Petrukhina. *Angew. Chem., Int. Ed.* **2011**, *50*, 8090-8094.

[17] U. D. Priyakumar, G. N. Sastry. *Tetrahedron Lett.* **2003**, *44*, 6043-6046.

[18] D. Vijay, H. Sakurai, V. Subramanian, G. N. Sastry. *Phys. Chem. Chem. Phys.* **2012**, *14*, 3057-3065.

[19] R. C. Dunbar. *J. Phys. Chem. A* **2002**, *106*, 9809-9819.

[20] J. R. Green, R. C. Dunbar. *J. Phys. Chem. A* **2011**, *115*, 4968-4975.

[21] J. A. Carrazana-Garcia, J. Rodriguez-Otero, E. M. Cabaleiro-Lago. *J. Phys. Chem. B* **2011**, *115*, 2774-2782.

[22] M. W. Stoddart, J. H. Brownie, M. C. Baird, H. L. Schmider. *J. Organomet. Chem.* **2005**, *690*, 3440-3450.

[23] A. Campo-Cacharrón, E. M. Cabaleiro-Lago, J. Rodriguez-Otero. *J. Comput. Chem.* **2014**, *35,* 1533-1544.

[24] P. Garcia-Novo, A. Campo-Cacharron, E. M. Cabaleiro-Lago, J. Rodriguez-Otero. *Phys. Chem. Chem. Phys.* **2012**, *14*, 104-112.

[25] A. Sygula, F. R. Fronczek, R. Sygula, P. W. Rabideau, M. M. Olmstead. *J. Am. Chem. Soc.* **2007**, *129*, 3842-3843.

[26] L. Kobryn, W. P. Henry, F. R. Fronczek, R. Sygula, A. Sygula. *Tetrahedron Lett.* **2009**, *50*, 7124-7127.

[27] C. Mueck-Lichtenfeld, S. Grimme, L. Kobryn, A. Sygula. *Phys. Chem. Chem. Phys.* **2010**, *12*, 7091-7097.

[28] M. Yanney, A. Sygula. *Tetrahedron Lett.* **2013**, *54*, 2604-2607.

[29] H. Sakurai, T. Daiko, H. Sakane, T. Amaya, T. Hirao. *J. Am. Chem. Soc.* **2005**, *127*, 11580-11581.
[30] J. M. Hermida-Ramon, C. M. Estevez. *Chem. Eur. J.* **2007**, *13*, 4743-4749.
[31] M. Mandado, J. M. Hermida-Ramon, C. M. Estevez. *J. Mol. Struct. (THEOCHEM)* **2008**, *854*, 1-9.
[32] M. Sanchez-Lozano, N. Otero, J. M. Hermida-Ramon, C. M. Estevez, M. Mandado. *J. Phys. Chem. A* **2011**, *115*, 2016-2025.
[33] J. M. Hermida-Ramon, M. Mandado, M. Sanchez-Lozano, C. M. Estevez. *Phys. Chem. Chem. Phys.* **2010**, *12*, 164-169.
[34] J. M. Hermida-Ramon, M. Sanchez-Lozano, C. M. Estevez. *Phys. Chem. Chem. Phys.* **2014**, 16, 6108-6117.
[35] B. L. Schottel, H. T. Chifotides, K. R. Dunbar. *Chem. Soc. Rev.* **2008**, *37*, 68-83.
[36] H. T. Chifotides, K. I. M. R. Dunbar. *Acc. Chem. Res.* **2013**, *46*, 894-906.
[37] A. Frontera, D. Quiñonero, P. M. Deyà. *WIREs Comput. Mol. Sci.* **2011**, *1*, 440-459.
[38] Y. Zhao, D. G. Truhlar. *Theor. Chem. Acc.* **2007**, *120*, 215-241.
[39] S. F. Boys, F. Bernardi. *Mol. Phys.* **1970**, *19*, 553-566.
[40] G. Chalasinski, M. M. Szczesniak. *Chem. Rev.* **2000**, *100*, 4227-4252.
[41] S. Grimme. *J. Chem. Phys.* **2003**, *118*, 9095-9102.
[42] J. Antony, S. Grimme. *J. Phys. Chem. A* **2007**, *111*, 4862–4868.
[43] T. Helgaker, W. Klopper, H. Koch, J. Noga. *J. Chem. Phys.* **1997**, *106*, 9639-9646.
[44] B. Jeziorski, R. Moszynski, K. Szalewicz. *Chem. Rev.* **1994**, *94*, 1887-1930.
[45] A. J. Misquitta, K. Szalewicz. *J. Chem. Phys.* **2005**, *122*, 214109/1-214109/19.
[46] A. Hesselmann, G. Jansen, M. Schütz. *J. Chem. Phys.* **2005**, *122*, 014103/1-014103/17.
[47] G. Jansen. *WIREs Comput. Mol. Sci.* **2014**, *4*, 127-144.
[48] K. Szalewicz. *WIREs Comput. Mol. Sci.* **2012**, *2*, 254-272.
[49] E. R. Johnson, S. Keinan, P. Mori-Sánchez, J. Contreras-García, A. J. Cohen, W. Yang. *J. Am. Chem. Soc.* **2010**, *132*, 6498-6506.
[50] J. Contreras-García, E. R. Johnson, S. Keinan, R. Chaudret, J.-P. Piquemal, D. N. Beratan, W. Yang. *J. Chem. Theory Comput.* **2011**, *7*, 625-632.
[51] A. Klamt, G. Schuurmann. *J. Chem. Soc. Perkin Trans. 2* **1993**, 799-805.
[52] V. Barone, M. Cossi. *J. Phys. Chem. A* **1998**, *102*, 1995-2001.
[53] M. Cossi, N. Rega, G. Scalmani, V. Barone. *J. Comput. Chem.* **2003**, *24*, 669-681.
[54] M. J. Frisch, G. W. Trucks, H. B. Schlegel, G. E. Scuseria, M. A. Robb, J. R. Cheeseman, G. Scalmani, V. Barone, B. Mennucci, G. A. Petersson, H. Nakatsuji, M. Caricato, X. Li, H. P. Hratchian, A. F. Izmaylov, J. Bloino, G. Zheng, J. L. Sonnenberg, M. Hada, M. Ehara, K. Toyota, R. Fukuda, J. Hasegawa, M. Ishida, T. Nakajima, Y. Honda, O. Kitao, H. Nakai, T. Vreven, J. M. J. A, J. E. Peralta, F. Ogliaro, M. Bearpark, J. J. Heyd, E. Brothers, K. N. Kudin, V. N. Staroverov, R. Kobayashi, J. Normand, K. Raghavachari, A. Rendell, J. C. Burant, S. S. Iyengar, J. Tomasi, M. Cossi, N. Rega, N. J. Millam, M. Klene, J. E. Knox, J. B. Cross, V. Bakken, C. Adamo, J. Jaramillo, R. Gomperts, R. E. Stratmann, O. Yazyev, A. J. Austin, R. Cammi, C. Pomelli, J. W. Ochterski, R. L. Martin, K. Morokuma, V. G. Zakrzewski, G. A. Voth, P. Salvador, J. J. Dannenberg, S. Dapprich, A. D. Daniels, Ö. Farkas, J. B. Foresman, J. V. Ortiz, J. Cioslowski, D. J. Fox, Gaussian 09, revision B.01, Gaussian, Inc., Wallingford CT, **2009**.

[55] H. J. Werner, P. J. Knowles, G. Knizia, F. R. Manby, M. Schütz, P. Celani, T. Korona, R. Lindh, A. Mitrushenkov, G. Rauhut, K. R. Shamasundar, T. B. Adler, R. D. Amos, A. Bernhardsson, A. Berning, D. L. Cooper, M. J. O. Deegan, A. J. Dobbyn, F. Eckert, E. Goll, C. Hampel, A. Hesselmann, G. Hetzer, T. Hrenar, G. Jansen, C. Kö, Y. Liu, A. W. Lloyd, R. A. Mata, A. J. May, S. J. McNicholas, W. Meyer, M. E. Mura, A. Nicklaß, D. P. O'Neill, P. Palmieri, D. Peng, K. P. Pitzer, M. Reiher, T. Shiozaki, H. Stoll, A. J. Stone, R. Tarroni, T. Thorsteinsson, M. Wang, Molpro version 2010.1, a package of ab initio programs, see http://www.molpro.net, **2010**.

[56] TURBOMOLE V6.3 , a development of University of Karlsruhe and Forschungszentrum Karlsruhe GmbH, 1989-2007, TURBOMOLE GmbH, since 2007; available from http://www.turbomole.com, **2011**.

[57] F. Weigend. *Phys. Chem. Chem. Phys.* **2002**, *4*, 4285-4291.

[58] F. Weigend, A. Köhn, C. Hättig. *J. Chem. Phys.* **2002**, *116*, 3175-3183.

[59] R. F. W. Bader, Atoms in Molecules: A Quantum Theory, Clarendon Press, Oxford **1990**.

USC UNIVERSIDADE DE SANTIAGO DE COMPOSTELA

USC
UNIVERSIDADE
DE SANTIAGO
DE COMPOSTELA

10. Conclusions

USC
UNIVERSIDADE
DE SANTIAGO
DE COMPOSTELA

Complexes involving ion···π interactions have been computationally studied in order to gain insight about the characteristics and factors controlling the interactions. A variety of systems have been considered ranging from cation···π contacts in simple aromatic moieties to ion···π interactions in more complex structures as buckybowls. Below, the main conclusions reached in these studies are listed.

- The incorporation of water molecules to phenol···cation complexes leads to a great variety of similarly stable structures differing on the topology of the hydrogen bond network. The behavior is more complex than in benzene analogues because the hydroxyl group of phenol starts participating in hydrogen bonds when three and four water molecules are included.
- Li^+ and Mg^{2+} complexes show structures with water and phenol surrounding the ions without forming hydrogen bonds among themselves. Otherwise Na^+ and K^+ interact more weakly with water and phenol so hydrogen bonds start being competitive, leading to minima with hydrogen bonds between water molecules or between water and phenol.
- Vibrational spectra in the region of the O-H stretching mode are quite simple in Li^+ and Mg^{2+} complexes, with shifts associated to hydrogen bonds being only observed when the fourth water molecule is located in the second solvation shell. Na^+ and K^+ complexes show more complex spectra, with important red shifts associated to O-H···O hydrogen bonds between water molecules but also with participation of phenol in ϕ-OH···O hydrogen bonds.

✓ Ternary complexes formed between guanidinium cation and aromatic units from amino acids show a variety of minima which can be roughly grouped as parallel stacked (two parallel rings), T-shaped (perpendicular rings) and doubly T-shaped (cation between both rings). Most stable structures are doubly T-shaped ones, followed by T-shaped and parallel stacked minima

✓ The interaction is mostly controlled by the intensity of the cation···aromatic contacts in the cluster. Guanidinium prefers interacting with indole than with phenol and benzene. The formation of hydrogen bonds in complexes containing phenol or indole introduces extra stability in T-shaped structures.

✓ Three-body effects are only cooperative in T-shaped minima containing indole or phenol when hydrogen bonds are formed. Though the interaction is dominated by electrostatics, contributions from dispersion and induction are also relevant.

❖ The study of the interaction of anions in simplified models for a synthetic anion channel based in naphthalendiimide (NDI) units shows that anion···π interactions are highly favorable in the gas phase, with minima connecting a path that allows the anions to move along the aromatic surface.

❖ The presence of water molecules strongly affects the interaction of fluoride and hydroxide anions with NDI, whereas the effect is less remarkable in the case of bromide and chloride complexes. As a consequence, the intensity of the interaction becomes similar among the different anions, with differences below 4 kcal/mol (in gas phase these differences reach more than 20 kcal/mol).

❖ The results suggest that a limited number of water molecules attached to the anion could be crucial to overcome dehydration costs, also contributing to the stabilization of the complex by means of favorable water···NDI contacts.

➢ Substitution of corannulene and sumanene is an effective method to promote great changes in the electric properties of the bowls, hardly changing their geometry and keeping their characteristic bowl shape.

➢ Substitution allows modulating the molecular electrostatic potential (MEP) of the bowls so they can be tuned for favorable interaction with anions or cations. Electron-withdrawing groups as nitrile create positive MEP regions on both faces of the bowl; electron-donating groups as methyl and unsubstituted bowls exhibit negative MEP regions on both faces; other groups as fluoride produce almost zero MEP allowing favorable interaction with both anions and cations.

➢ The interaction in these systems is hard to describe with accuracy. Testing a variety of methods it has been found that the best performance is given by the SCS-MP2 method extrapolated to basis limit, which matches almost perfectly the reference values obtained at the MP2.X/6-31G(0.25) level of calculation. M06-2X/6-31+G* also seems to be able to provide a quite balanced description of the concave/convex energy differences despite the errors introduced in the interaction energies.

➢ Sumanene and its derivatives interact more favorably than corannulene with anions and cations. Substitution effects in sumanene are stronger if applied in the CH aromatic groups than in the CH_2 groups of pentagonal rings. Cation complexes are dominated by a large induction component that can be even larger than the electrostatic contribution, whereas in anion complexes electrostatics and dispersion are the main stabilizing components.

- Complexation energies roughly follow the series of MEPs, being the most stable complexes those formed with corannulene substituted with CN groups. However, there are also changes affecting to the induction and dispersion contributions which may introduce deviations over the behavior expected from a purely electrostatics point of view.

- Anions are oriented so the largest negative regions point towards the positively charged surfaces of the bowl. Tetrahedral anions orient themselves with three bonds towards the bottom of the bowl. Nitrate complexes are more stable with the anion parallel to the bottom of the bowl, the oxygen atoms oriented towards the positively charged six-carbon rings. Formate complexes are more stable with the anion perpendicular to the bottom of the bowl, avoiding the interaction of the hydrogen atom with the walls of the bowl.

- The most stable complexes correspond to the anion located on the symmetry axis of the bowl by the concave face. The interaction of the anions with the convex face of the bowl or with the hydrogen atoms on the rim of the bowl is significantly less favorable. The order of stability of the complexes formed with CN-substituted bowls in the gas phase as obtained for the different anions is the following: CO_2H^- > Cl^- > Br^- > NO_3^- >> ClO_4^- > BF_4^-.

- The presence of solvent has a deep impact on the properties of the complexes, and already in solvents with low dielectric constant the interaction strength decreases dramatically. Solvent affects the different anions to distinct extents, so the more polarizing ones are the most affected whereas the bulkier ones register smaller decreases. Therefore, in solvents of moderate to large dielectric constant, the most stable complexes are those formed with Br^- whereas CO_2H^- is among the least favorable complexes formed.

- Overall, the results obtained for ion complexes formed with properly substituted buckybowls encourage to follow this topic, since this strategy promises to be suitable for designing selective anion receptors.

USC
UNIVERSIDADE
DE SANTIAGO
DE COMPOSTELA

Appendices

USC
UNIVERSIDADE
DE SANTIAGO
DE COMPOSTELA

Appendix A

Table A.1. Complexation energies (kcal/mol) for monohydrated cation···phenol clusters as obtained with different levels of calculation.

		Phe-X1-1H_2O	Phe-X2-1H_2O	Phe-X3-1H_2O	Phe-X4-1H_2O	Phe-X5-1H_2O	Phe-X6-1H_2O
B3LYP[a]		-31.03	-28.16	-30.90	-30.77	-27.61	-32.35
MP2-A[b]		-31.12	-29.39	-33.18	-32.38	-29.14	-34.98
MP2-B[c]	K^+	-31.87	-30.24	-33.30	-33.07	-29.94	-35.72
MP2-C[d]		-31.91	-29.29	-33.19	-32.18	-29.10	-34.87
MP2-D[e]		-32.33	-30.01	-33.94	-32.99	-30.20	-36.13
MP2-E[f]		-32.28	-30.26	-34.08	-33.30	-30.78	-36.62
B3LYP[a]		-44.89	-37.57	-44.89	-45.01	-37.40	-44.72
MP2-A[b]		-41.45	-35.23	-41.46	-41.52	-34.80	-42.94
MP2-B[c]	Na^+	-41.80	-36.13	-42.41	-42.35	-35.56	-43.70
MP2-C[d]		-41.94	-35.65	-42.55	-41.88	-35.09	-43.23
MP2-D[e]		-41.25	-35.32	-42.10	-40.95	-34.48	-42.45
MP2-E[f]		-41.05	-35.35	-41.99	-40.95	-34.73	-42.63
B3LYP[a]		-64.60	-51.59		-65.71	-53.44	
MP2-A[b]		-61.00	-48.67		-62.14	-49.74	
MP2-B[c]	Li^+	-61.01	-48.99		-62.23	-50.02	
MP2-C[d]		-61.17	-48.98		-62.27	-50.02	
MP2-D[e]		-60.73	-49.10		-61.82	-49.93	
MP2-E[f]		-60.63	-49.04		-61.77	-49.99	
B3LYP[a]		-183.04	-153.00		-185.71	-151.48	
MP2-A[b]		-171.18	-139.90		-174.86	-140.31	
MP2-B[c]	Mg^{+2}	-171.40	-140.45		-174.91	-140.61	
MP2-C[d]		-171.55	-140.50		-175.00	-140.62	
MP2-D[e]		-170.32	-139.71		-173.15	-139.05	
MP2-E[f]		-170.98	-140.37		-174.03	-139.85	

a) B3LYP/6-31+G(2d,p); b) MP2/6-31+G(2d,p)//B3LYP/6-31+G(2d,p);
c) MP2/6-31+G(2d,p)//MP2/6-31+G(d); d) MP2/631+G(2d,p);
e) MP2/6-311++G(2d,2p)//MP2/6-31+G(d); f) MP2/6-311++G(3d,2p) //MP2/6-31+G(d).

Table A.2. OH stretching frequencies for selected complexes with sodium as obtained at the MP2/6-31+G(2d,p) level. Values obtained with the harmonic approximation and corrected from anharmonicity are presented.

	Harmonic	Anharmonic
Factor(*)	0.9797	1.0321
Phenol	3657.0	3657.0
Water	3672.9	3688.3
Phe-Na-O	3646.9	3649.2
Phe-Na-π	3631.2	3631.8
Phe-Na1-1H2O	3758.3	3816.0
Phe-Na1-1H2O	3653.9	3685.2
Phe-Na1-1H2O	3648.9	3650.5
Phe-Na2-1H2O	3772.6	3778.8
Phe-Na2-1H2O	3650.7	3661.7
Phe-Na2-1H2O	3326.5	3251.6
Phe-Na3-1H2O	3750.0	3744.0
Phe-Na3-1H2O	3646.7	3647.0
Phe-Na3-1H2O	3629.3	3635.7
Phe-Na4-1H2O	3758.3	3829.1
Phe-Na4-1H2O	3654.0	3688.4
Phe-Na4-1H2O	3634.5	3635.7
Phe-Na5-1H2O	3766.0	3763.4
Phe-Na5-1H2O	3644.8	3654.3
Phe-Na5-1H2O	3372.9	3327.6
Phe-Na6-1H2O	3739.4	3736.8
Phe-Na6-1H2O	3626.3	3627.1
Phe-Na6-1H2O	3571.4	3570.7

(*) As commented in the text, a correction factor is applied in order to reproduce the experimental OH stretching frequency of phenol.

Appendix B

Table B.1. LMO-EDA partition (kcal/mol) of the interaction energy for complexes in the manuscript with equal aromatic units, as obtained at the M06-2X/aug-cc-pVDZ level.

	Electrostatic	Exchange	Repulsion	Polarization	Dispersion
Bz-Bz-1	-15.05	-12.19	41.04	-9.69	-23.66
Bz-Bz-2	-15.89	-10.85	39.41	-10.19	-24.52
Bz-Bz-3	-16.09	-11.76	42.76	-9.13	-27.31
Bz-Bz-4	-19.61	-10.63	38.75	-12.78	-22.71
Ph-Ph-1	-35.71	-20.37	68.35	-16.88	-28.96
Ph-Ph-2	-33.56	-19.94	69.29	-16.11	-32.16
Ph-Ph-3	-32.52	-20.05	64.61	-19.78	-23.11
Ph-Ph-4	-29.29	-17.47	62.49	-12.44	-34.64
Ph-Ph-5	-34.16	-19.41	65.84	-15.35	-29.98
Ph-Ph-6	-30.16	-14.78	51.85	-15.85	-24.49
Ph-Ph-7	-34.13	-16.37	55.26	-16.20	-21.12
In-In-1	-24.12	-20.04	66.30	-14.00	-38.78
In-In-2	-26.13	-17.82	59.87	-14.72	-33.97
In-In-3	-26.70	-17.60	58.99	-15.93	-32.34
In-In-4	-26.89	-17.48	58.98	-15.72	-32.99
In-In-5	-29.66	-15.16	54.88	-16.34	-32.72

USC UNIVERSIDADE DE SANTIAGO DE COMPOSTELA

Table B.2. LMO-EDA partition (kcal/mol) of the interaction energy for complexes in the manuscript with different aromatic units, as obtained at the M06-2X/aug-cc-pVDZ level.

		Electrostatic	Exchange	Repulsion	Polarization	Dispersion
Stacked	B-Ph-P	-17.23	-14.37	47.76	-10.51	-26.70
	Ph-B-P	-20.87	-14.69	48.78	-11.73	-22.80
T-shaped	B-Ph-T	-27.79	-15.48	55.14	-13.13	-29.86
	Ph-B-T	-24.47	-15.53	52.34	-14.80	-25.36
Double T-shaped	B-Ph-DT	-24.96	-12.76	45.55	-14.35	-23.95
Stacked	B-In-P	-18.42	-16.47	53.77	-11.37	-30.41
	In-B-P	-21.55	-16.22	55.02	-12.30	-32.66
T-shaped	B-In-T	-19.94	-13.31	47.75	-11.16	-30.41
	In-B-T	-22.70	-14.24	49.27	-14.23	-27.97
Double T-shaped	B-In-DT	-23.92	-13.10	47.84	-13.93	-28.36
Stacked	Ph-In-P	-37.00	-21.36	72.36	-16.08	-34.69
	In-Ph-P	-22.92	-17.02	58.26	-12.72	-34.55
T-shaped	Ph-In-T	-28.84	-19.49	63.73	-16.96	-30.88
	In-Ph-T	-24.52	-16.53	56.25	-13.65	-32.10
Doubly T-shaped	Ph-In-DT	-30.57	-17.60	62.65	-16.31	-34.68

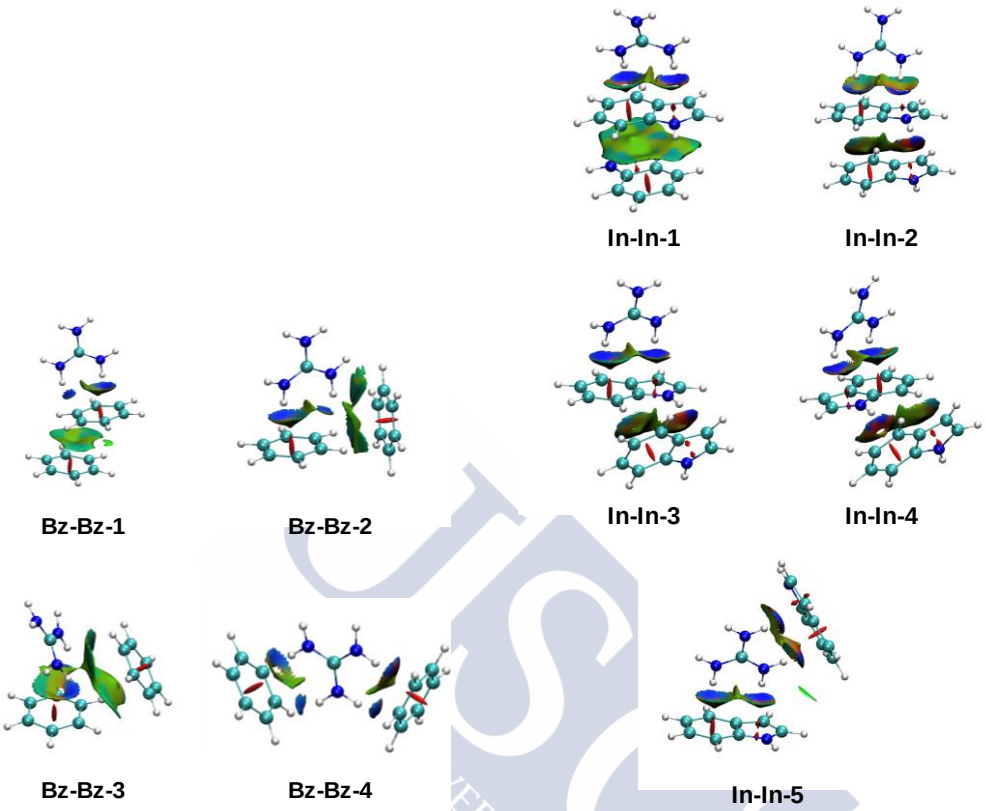


Figure B.1. NCI surfaces corresponding to the bencene-bencene (left) and indole-indole (right) complexes. A reduced density gradient isosurface of 0.5 a.u. and a color scale of −0.015 (blue) to 0.015 (red) a.u. are employed.

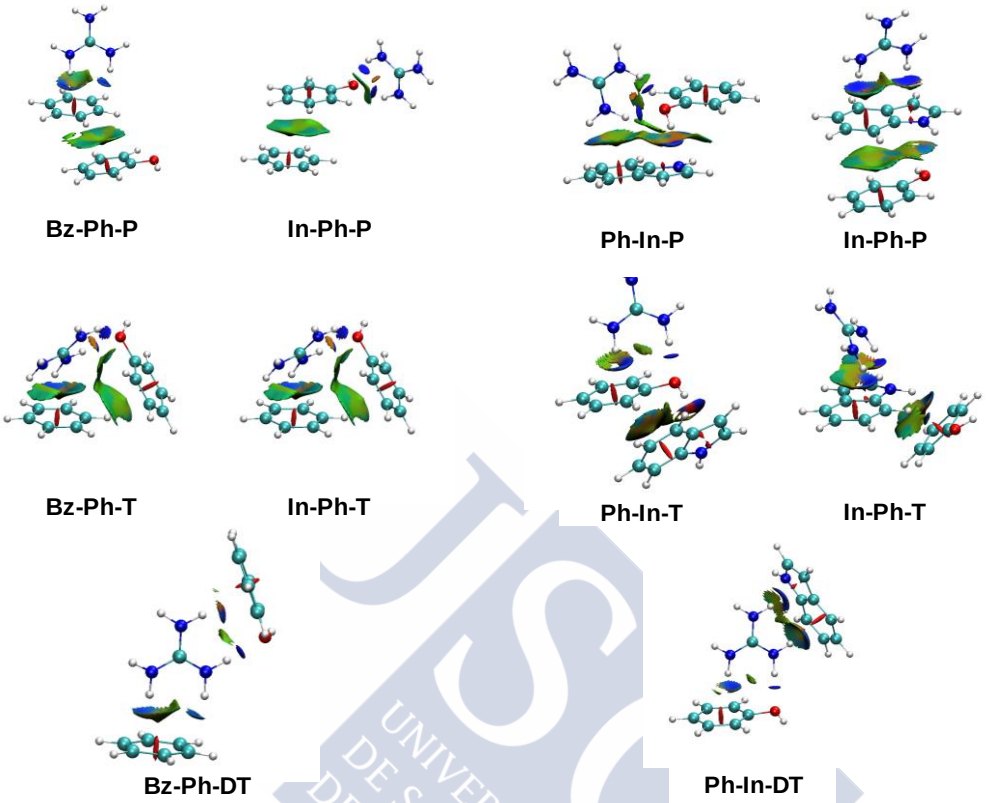


Figure B.2. NCI surfaces corresponding to the bencene-phenol (left) and phenol-indole (right) complexes. A reduced density gradient isosurface of 0.5 a.u. and a color scale of −0.015 (blue) to 0.015 (red) a.u. are employed.

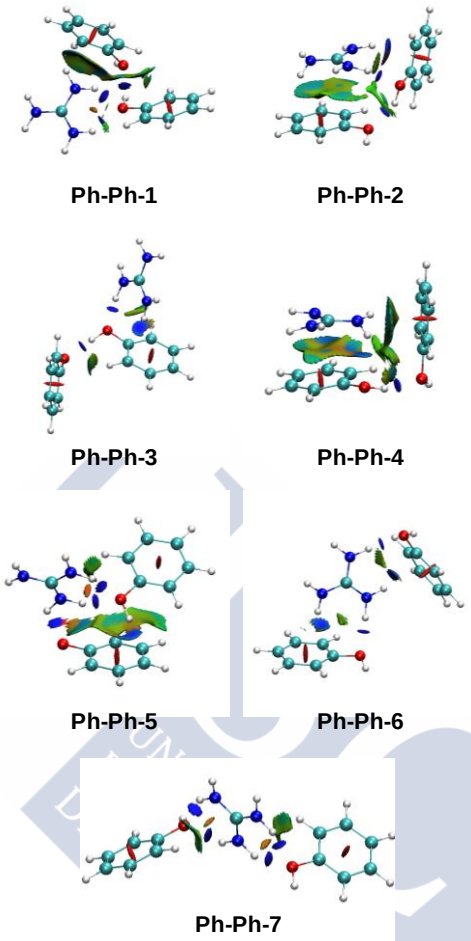


Figure B.3. NCI surfaces corresponding to the phenol-phenol complexes complexes containing phenol and indole. A reduced density gradient isosurface of 0.5 a.u. and a color scale of −0.015 (blue) to 0.015 (red) a.u. are employed.

USC
UNIVERSIDADE
DE SANTIAGO
DE COMPOSTELA

Appendix C

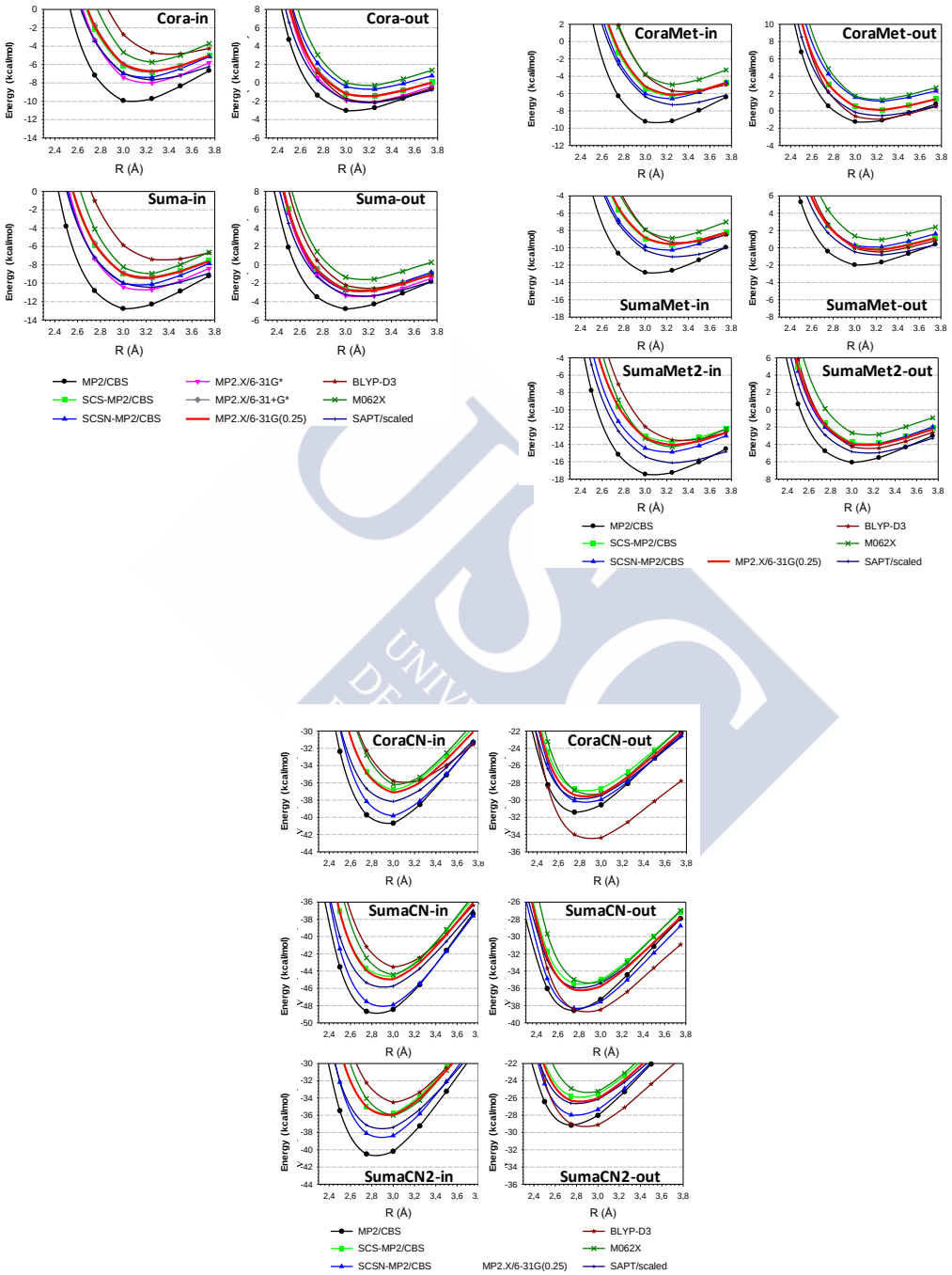


Figure C.1. Interaction energies obtained for complexes formed by unsubstituted, CH_3-substituted amd CN-substituted corannulene and sumanene with chloride anion by the concave (left) and convex (right) faces of the bowls.

.

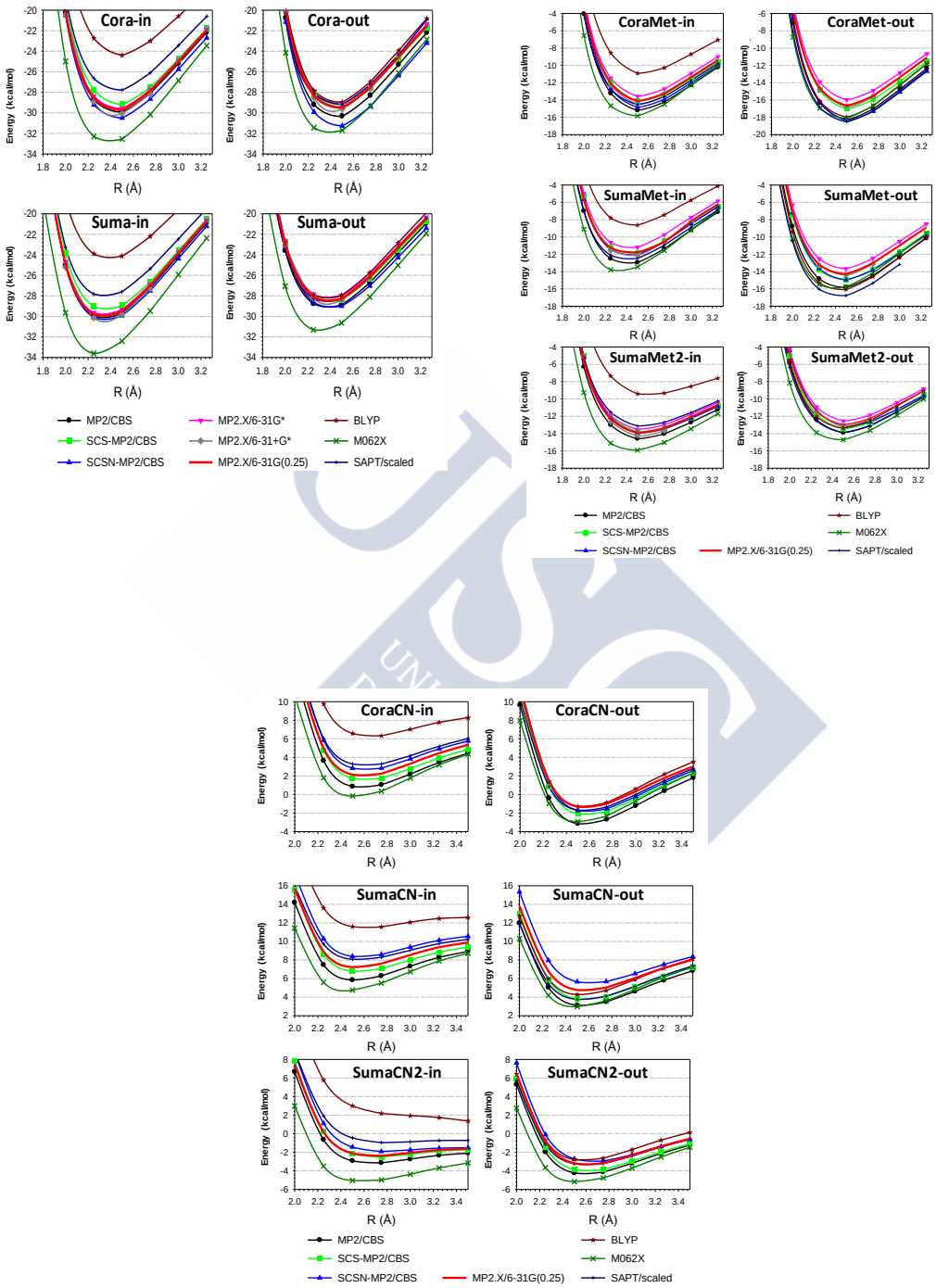


Figure C.2. Interaction energies obtained for complexes formed by unsubstituted, CH_3-substituted and CN-substituted corannulene and sumanene with sodium cation by the concave (left) and convex (right) faces of the bowls.

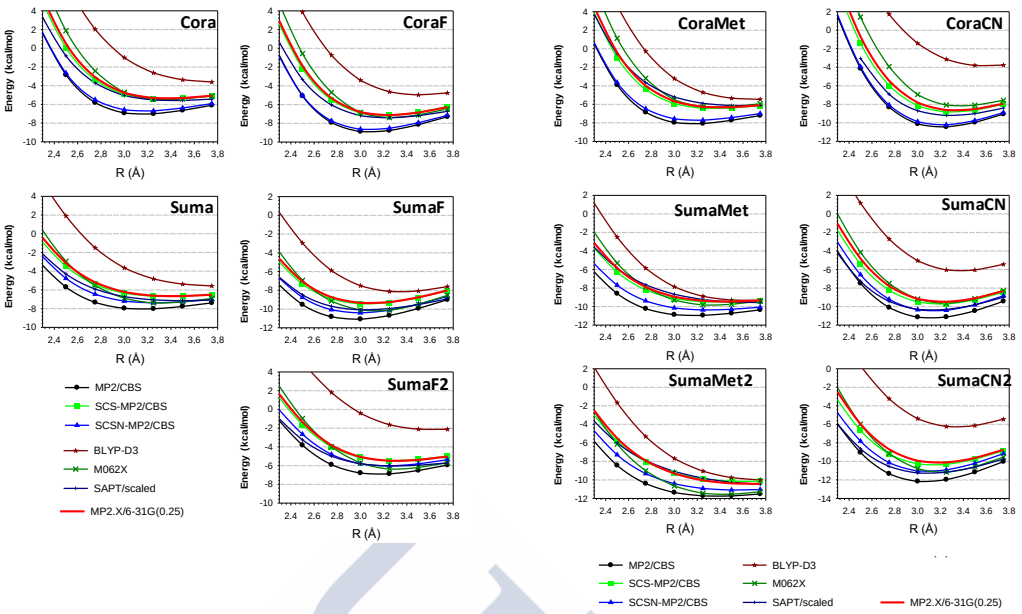


Figure C.3. Relative energy (in-out) of complexes formed by chloride anion with the different bowls.

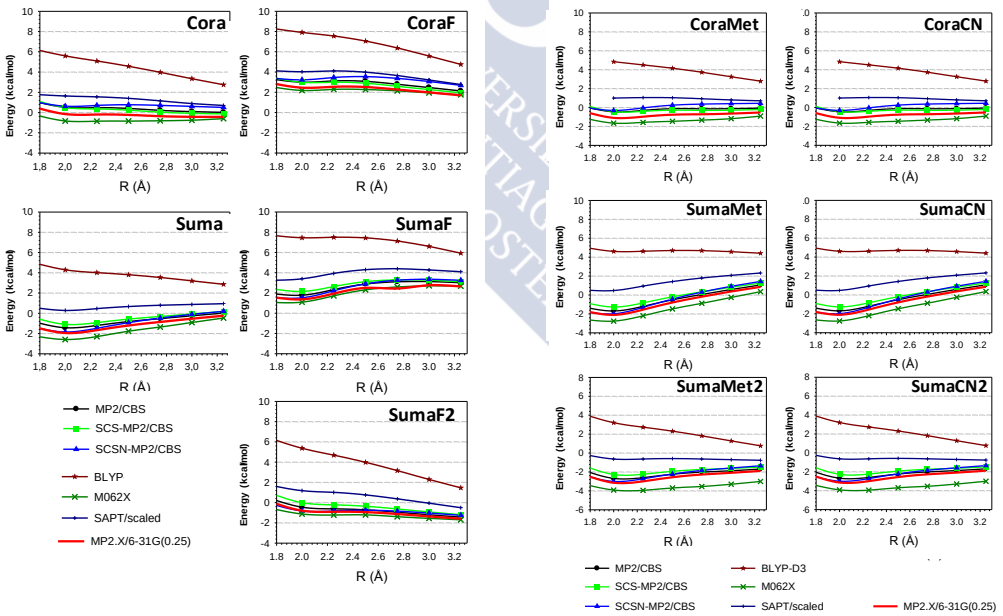


Figure C.4. Relative energy (in-out) of complexes formed by sodium cation with the different bowls.

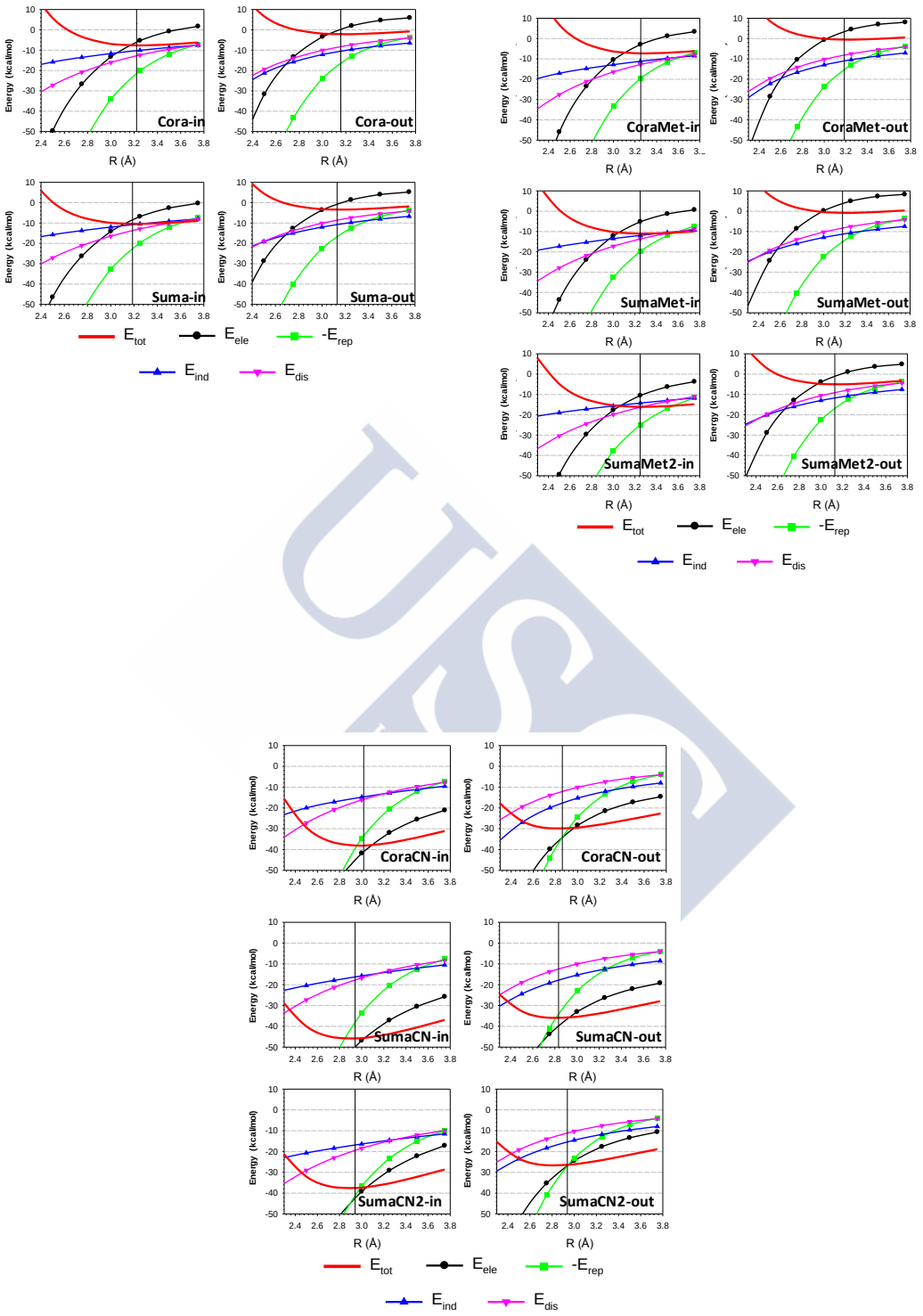


Figure C.5. SAPT(DFT) energy decomposition for complexes formed by chloride anion and unsubstituted, CH_3-substituted and CN-substituted bowls. The vertical line indicates the position of the minimum obtained at the MP2.X level of calculation.

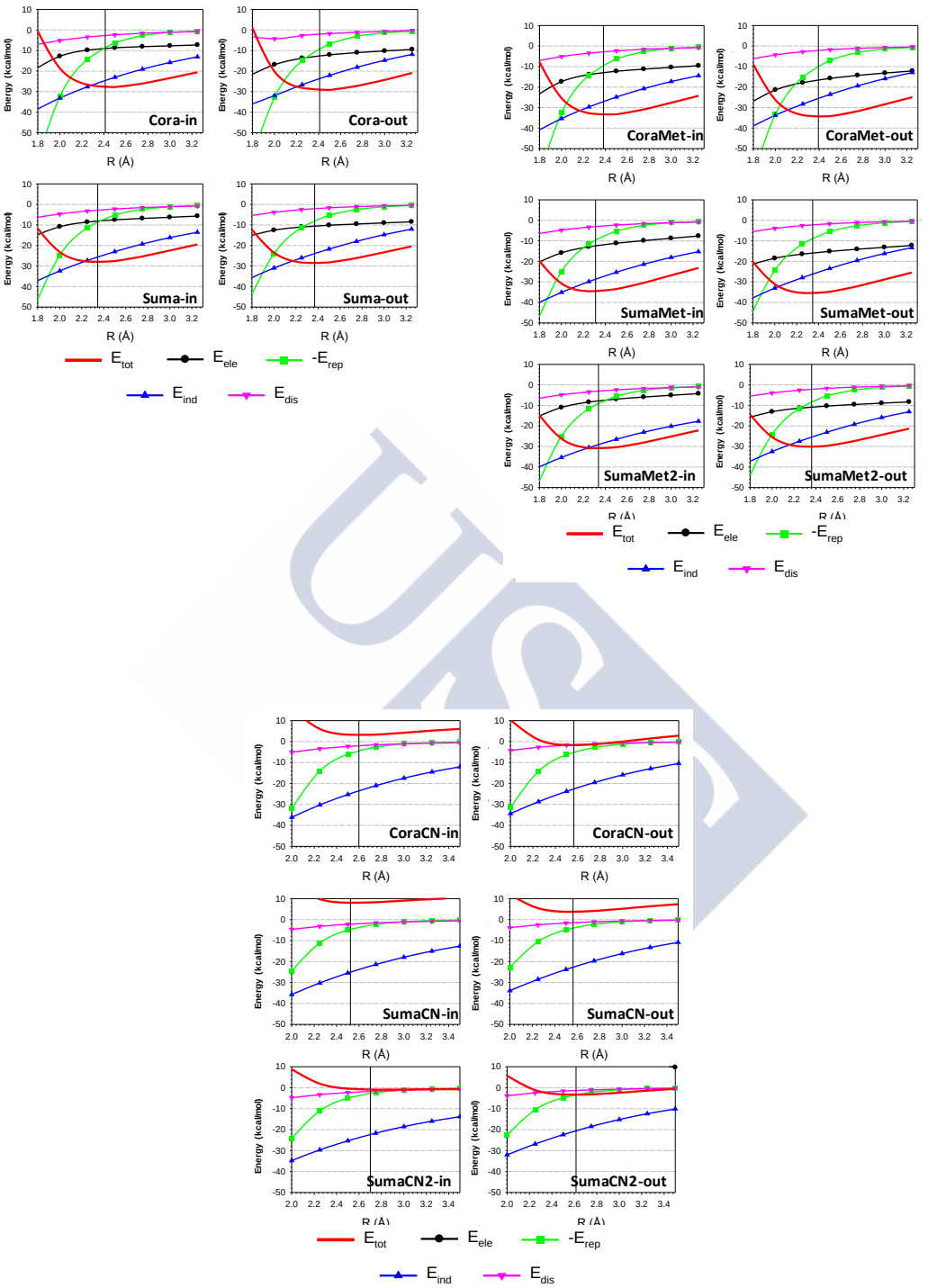


Figure C.6. SAPT(DFT) energy decomposition for complexes formed by sodium cation and unsubstituted, CH_3-substituted and CN-substituted bowls. The vertical line indicates the position of the minimum obtained at the MP2.X level of calculation.

Table C.1. SAPT(DFT) values (kcal/mol) for complexes formed by the bowls and chloride anion. The values are obtained by interpolation of the SAPT(DFT) curves at the equilibrium geometry obtained at the MP2.X/6-31G(0.25) level (Table 8.1). Dispersion and dispersion-exchange contributions are scaled by 1.193 as indicated in the text.

	Eele	Erep	Eind	Edis	Etot
			CONCAVE/IN		
cora	-6.01	21.32	-10.24	-12.76	-7.68
coraMet	-2.87	19.49	-11.17	-12.75	-7.31
CoraF	-20.62	27.80	-11.40	-14.37	-18.60
coraCN	-40.95	33.26	-14.66	-15.81	-38.16
suma	-8.33	22.41	-10.84	-13.71	-10.47
sumaMet	-5.46	20.21	-11.98	-13.82	-11.05
sumaF	-25.63	30.12	-12.17	-15.68	-23.38
sumaCN	-49.61	37.59	-16.23	-17.66	-45.91
suma	-8.33	22.41	-10.84	-13.71	-10.47
sumaMet2	-10.55	24.96	-14.25	-16.29	-16.14
sumaF2	-25.46	34.77	-13.04	-16.94	-20.68
sumaCN2	-42.29	40.98	-16.86	-19.44	-37.61
			CONVEX/OUT		
cora	0.38	16.16	-10.48	-8.26	-2.20
coraMet	3.50	15.06	-11.00	-8.14	-0.57
CoraF	-11.34	21.72	-12.11	-9.54	-11.27
coraCN	-34.04	33.83	-17.61	-12.08	-29.90
suma	-0.64	16.52	-10.77	-8.59	-3.47
sumaMet	3.86	14.86	-11.28	-8.29	-0.85
sumaF	-12.76	21.13	-11.99	-9.66	-13.28
sumaCN	-39.72	33.96	-17.79	-12.43	-35.98
suma	-0.64	16.52	-10.77	-8.59	-3.47
sumaMet2	-0.92	16.64	-11.72	-9.08	-5.07
sumaF2	-16.73	26.37	-13.73	-10.83	-14.92
sumaCN2	-30.67	33.23	-16.77	-12.46	-26.67

Table C.2. SAPT(DFT) values (kcal/mol) for complexes formed by the bowls and sodium cation. The values are obtained by interpolation of the SAPT(DFT) curves at the equilibrium geometry obtained at the MP2.X/6-31G(0.25) level (Table 8.2). Dispersion and dispersion-exchange contributions are scaled by 1.193 as indicated in the text.

	Eele	Erep	Eind	Edis	Etot
			CONCAVE/IN		
cora	-8.90	8.13	-24.56	-2.66	-27.99
coraMet	-12.89	9.02	-27.03	-2.83	-33.72
CoraF	4.62	6.59	-23.36	-2.41	-14.56
coraCN	24.26	4.40	-23.53	-1.99	3.15
suma	-8.06	8.24	-25.62	-2.80	-28.24
sumaMet	-12.36	9.33	-28.67	-3.01	-34.71
sumaF	7.53	7.04	-24.72	-2.62	-12.77
sumaCN	30.65	4.65	-25.08	-2.15	8.05
suma	-8.06	8.24	-25.62	-2.80	-28.24
sumaMet2	-7.74	8.71	-29.05	-3.02	-31.10
sumaF2	7.32	5.08	-23.20	-2.31	-13.12
sumaCN2	20.53	2.69	-22.36	-1.78	-0.92
			CONVEX/OUT		
cora	-12.55	8.81	-23.66	-2.05	-29.46
coraMet	-16.52	9.51	-25.52	-2.15	-34.67
CoraF	-1.44	7.37	-22.65	-1.86	-18.58
coraCN	17.29	5.13	-22.61	-1.54	-1.73
suma	-10.54	7.73	-23.92	-2.06	-28.78
sumaMet	-15.88	8.56	-26.16	-2.18	-35.67
sumaF	1.31	6.39	-22.79	-1.85	-16.93
sumaCN	23.89	4.00	-22.70	-1.45	3.74
suma	-10.54	7.73	-23.92	-2.06	-28.78
sumaMet2	-10.81	8.01	-25.42	-2.13	-30.35
sumaF2	4.16	5.21	-21.60	-1.67	-13.89
sumaCN2	15.16	3.37	-20.56	-1.34	-3.36

USC
UNIVERSIDADE
DE SANTIAGO
DE COMPOSTELA

Appendix D

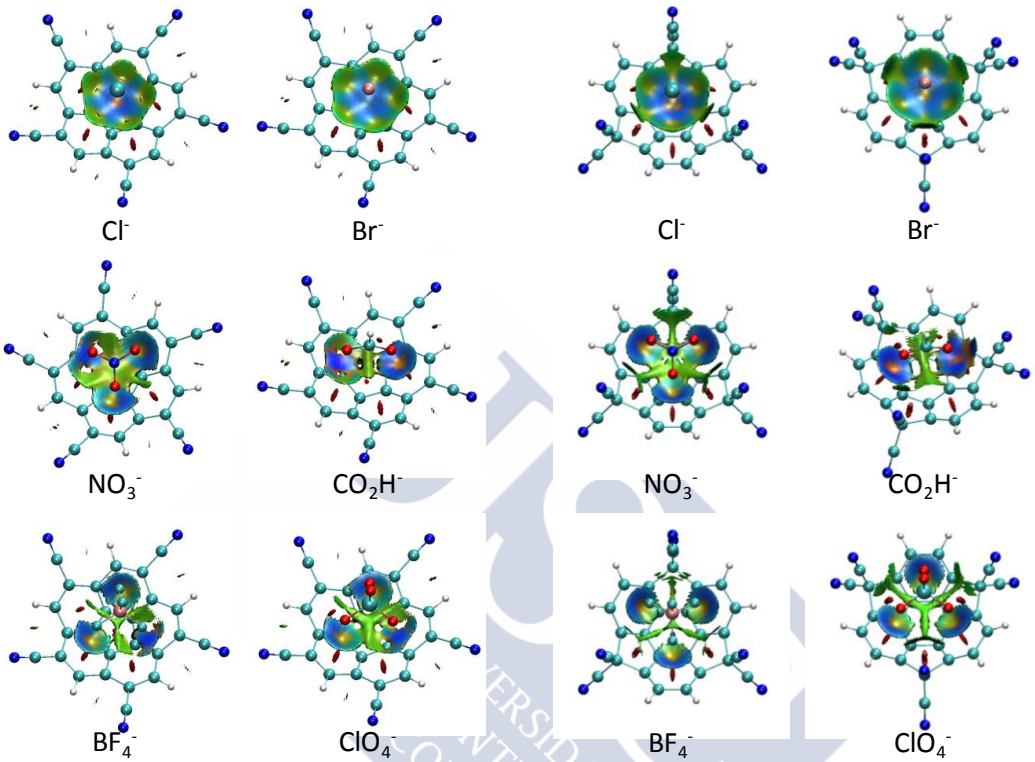


Figure D.1. NCI plots for the complexes formed by CoraCN (left) and SumaCN2 (right) and the anions studied. Only complexes by the **I** line and the most stable orientation are shown. The product of the density times the sign of the second eigenvalue of its hessian is mapped onto an isosurface of reduced density gradient with value 0.5 a.u. The color scale goes from -0.015 a.u. (blue) to 0.015 a.u. (red).

USC
UNIVERSIDADE
DE SANTIAGO
DE COMPOSTELA

USC
UNIVERSIDADE
DE SANTIAGO
DE COMPOSTELA

USC
UNIVERSIDADE
DE SANTIAGO
DE COMPOSTELA